Detailed formulation of SCALE-RM

Seiya Nishizawa, Hirofumi Tomita, and Team SCALE

December 25, 2024

Contents

Chapter 1

Introduction

1.1 What is SCALE

SCALE (Scalable Computing for Advanced Library and Environment)is a basic library of weather and climate models of the earth and planets intended for widespread use. The SCALE library was co-designed by computational science and computer science researchers.

Chapter 2

Governing equations

Corresponding author : Hirofumi Tomita

2.1 Continuity equations

The continuity equations for each material can be described as the flux form:

$$\frac{\partial \rho q_d}{\partial t} + \nabla \cdot (\rho q_d \mathbf{u}) = \text{DIFF}\,[q_d] \tag{2.1}$$

$$\frac{\partial \rho q_v}{\partial t} + \nabla \cdot (\rho q_v \mathbf{u}) = S_v + \text{DIFF}\,[q_v] \tag{2.2}$$

$$\frac{\partial \rho q_l}{\partial t} + \nabla \cdot (\rho q_l \mathbf{u}) + \frac{\partial \rho q_l w_l}{\partial z} = S_l + \text{DIFF}\,[q_l] \tag{2.3}$$

$$\frac{\partial \rho q_s}{\partial t} + \nabla \cdot (\rho q_s \mathbf{u}) + \frac{\partial \rho q_s w_s}{\partial z} = S_s + \text{DIFF}\,[q_s] \tag{2.4}$$

The summation of the mass concentrations should be unit:

$$q_d + q_v + q_l + q_s = 1. \tag{2.5}$$

The source terms of water substances should satisfy the following relation:

$$S_v + S_l + S_s = 0. \tag{2.6}$$

The summation of Eqs.(2.1)-(2.4) gives the continuity equation of total density:

$$\frac{\partial \rho}{\partial t} + \nabla \cdot (\rho \mathbf{u}) + \frac{\partial \rho q_l w_l}{\partial z} + \frac{\partial \rho q_s w_s}{\partial z} = 0, \tag{2.7}$$

For this derivation, we assume that the operator DIFF $[]$ is distributive. Using Eq.(2.5),

$$\begin{aligned} &\text{DIFF}\,[q_d] + \text{DIFF}\,[q_v] + \text{DIFF}\,[q_l] + \text{DIFF}\,[q_s] \\ = \ &\text{DIFF}\,[q_d + q_v + q_l + q_s] = \text{DIFF}\,[1] = 0 \end{aligned} \tag{2.8}$$

2.2 Momentum equations

The momentum equations for the gas, liquid, and solid material are described as

$$\frac{\partial \rho (q_d + q_v) \mathbf{u}}{\partial t} + \nabla \cdot [\rho (q_d + q_v) \mathbf{u} \otimes \mathbf{u}] \tag{2.9}$$

$$= -\nabla p - [\rho (q_d + q_v) g + (f_l + f_s)] \mathbf{e_z}$$

$$+ \mathbf{u} S_v + \mathrm{DIFF} \left[(q_d + q_v) \mathbf{u} \right] \tag{2.10}$$

$$\frac{\partial \rho q_l \mathbf{u}}{\partial t} + \nabla \cdot (\rho q_l \mathbf{u} \otimes \mathbf{u}) + \frac{\partial \rho q_l \mathbf{u} w_l}{\partial z} = -(\rho q_l g - f_l) \mathbf{e_z}$$

$$+ \mathbf{u} S_l + \mathrm{DIFF} \left[q_l \mathbf{u} \right] \tag{2.11}$$

$$\frac{\partial \rho q_s \mathbf{u}}{\partial t} + \nabla \cdot (\rho q_s \mathbf{u} \otimes \mathbf{u}) + \frac{\partial \rho q_s \mathbf{u} w_s}{\partial z} = -(\rho q_s g - f_s) \mathbf{e_z}$$

$$+ \mathbf{u} S_s + \mathrm{DIFF} \left[q_s \mathbf{u} \right] \tag{2.12}$$

The pressure is derived from the equation of state as

$$p = \rho (q_d R_d + q_v R_v) T. \tag{2.13}$$

The summation of Eqs.(2.10)-(2.12) gives the total momentum equation as

$$\frac{\partial \rho \mathbf{u}}{\partial t} + \nabla \cdot (\rho \mathbf{u} \otimes \mathbf{u}) + \left(\frac{\partial \rho q_l w_l}{\partial z} + \frac{\partial \rho q_s w_s}{\partial z} \right) \mathbf{e_z}$$

$$= -\nabla p - \rho g \mathbf{e_z} + \mathrm{DIFF} \left[\mathbf{u} \right] \tag{2.14}$$

Note that the drag forces by water loading does not appear in Eq.(2.14), because those terms are cancelled out through the summation.

2.3 Thermodynamics equations

The equations of the internal energies are described as

$$\frac{\partial \rho (q_d e_d + q_v e_v)}{\partial t} + \nabla \cdot [\rho (q_d e_d + q_v e_v) \mathbf{u}]$$

$$= -p \nabla \cdot \mathbf{u} + Q_d + Q_v + \mathrm{DIFF} \left[(q_d + q_v) T^* \right] \tag{2.15}$$

$$\frac{\partial \rho q_l e_l}{\partial t} + \nabla \cdot (\rho q_l e_l \mathbf{u}) + \frac{\partial \rho q_l e_l w_l}{\partial z} = Q_l + \mathrm{DIFF} \left[q_l T^* \right] \tag{2.16}$$

$$\frac{\partial \rho q_l e_s}{\partial t} + \nabla \cdot (\rho q_s e_s \mathbf{u}) + \frac{\partial \rho q_s e_s w_s}{\partial z} = Q_s + \mathrm{DIFF} \left[q_s T^* \right] \tag{2.17}$$

where T^* is some kind of potential temperature, discussed later. The internal energies are defined as

$$e_d = c_{vd} T \tag{2.18}$$

$$e_v = c_{vv} T \tag{2.19}$$

$$e_l = c_l T \tag{2.20}$$

$$e_s = c_s T, \tag{2.21}$$

The summation of Eqs.(2.15)-(2.17) gives the following internal energy equations:

$$\frac{\partial \rho e}{\partial t} + \nabla \cdot (\rho e \mathbf{u}) + \frac{\partial \rho q_l e_l w_l}{\partial z} + \frac{\partial \rho q_s e_s w_s}{\partial z} + p\nabla \cdot \mathbf{u}$$
$$= Q + \text{DIFF}\,[T^*] \tag{2.22}$$

where

$$e = q_d e_d + q_v e_v + q_l e_l + q_s e_s, \tag{2.23}$$

and the total diabatic heating is described as

$$Q = Q_d + Q_v + Q_l + Q_s. \tag{2.24}$$

2.4 Conceptual separation for solving the set of equations

Eqs.(2.2)-(2.4),(2.7),(2.14), and (2.13) with Eq.(2.22) are the complete set of equations. For solving them easily, we separate the set of equations conceptually as

$$\frac{\partial \phi}{\partial t} = \left(\frac{\partial \phi}{\partial t}\right)_{dynamics} + \left(\frac{\partial \phi}{\partial t}\right)_{physics} \tag{2.25}$$

The falling process of liquid and solid waters, the source and sink process of water vapor, and the diabatic heating process for energy equations are treated as physical process, the others are treated as dynamical process.

According to this scheme, the dynamical process can be written as

$$\frac{\partial \rho q_v}{\partial t} + \nabla \cdot (\rho q_v \mathbf{u}) = 0 \tag{2.26}$$

$$\frac{\partial \rho q_l}{\partial t} + \nabla \cdot (\rho q_l \mathbf{u}) = 0 \tag{2.27}$$

$$\frac{\partial \rho q_s}{\partial t} + \nabla \cdot (\rho q_s \mathbf{u}) = 0 \tag{2.28}$$

$$\frac{\partial \rho}{\partial t} + \nabla \cdot (\rho \mathbf{u}) = 0 \tag{2.29}$$

$$\frac{\partial \rho \mathbf{u}}{\partial t} + \nabla \cdot (\rho \mathbf{u} \otimes \mathbf{u}) = -\nabla p - \rho g \mathbf{e_z} \tag{2.30}$$

$$\frac{\partial \rho e}{\partial t} + \nabla \cdot (\rho e \mathbf{u}) + p\nabla \cdot \mathbf{u} = 0 \tag{2.31}$$

On the other hand, the physical processes are as follows:

$$\frac{\partial \rho q_v}{\partial t} = S_v + \text{DIFF}\,[q_v] \tag{2.32}$$

$$\frac{\partial \rho q_l}{\partial t} + \frac{\partial \rho q_l w_l}{\partial z} = S_l + \text{DIFF}\,[q_l] \tag{2.33}$$

$$\frac{\partial \rho q_s}{\partial t} + \frac{\partial \rho q_s w_s}{\partial z} = S_s + \text{DIFF}\,[q_s] \tag{2.34}$$

$$\frac{\partial \rho}{\partial t} + \frac{\partial \rho q_l w_l}{\partial z} + \frac{\partial \rho q_s w_s}{\partial z} = 0 \tag{2.35}$$

$$\frac{\partial \rho \mathbf{u}}{\partial t} + \frac{\partial \rho q_l \mathbf{u} w_l}{\partial z} + \frac{\partial \rho q_s \mathbf{u} w_s}{\partial z} = \text{DIFF}\,[\mathbf{u}] \tag{2.36}$$

$$\frac{\partial \rho e}{\partial t} + \frac{\partial \rho q_l e_l w_l}{\partial z} + \frac{\partial \rho q_s e_s w_s}{\partial z} = Q + \text{DIFF}\,[T^*] \tag{2.37}$$

2.5 Conservation of thermodynamics in the dynamical process

Equation (2.31) is not a complete flux form, because the internal energy itself is not conserved both in the Euler sense and in the Lagrangian sense. In this section, we consider the conservative quantity for thermodynamics equation.

In the dry atmosphere, the potential temperature for dry air, which is defined as

$$\theta_d \;=\; T \left(\frac{p_{00}}{p} \right)^{R_d/c_{pd}}, \tag{2.38}$$

is used as a conserved quantity it is conserved along the Lagrange trajectory c_{pd} R_d are the specific heats at constant pressure and However, it is no longer satisfied when the water substances are included.

Since Eq.(2.29) is equivallent to

$$\frac{d\rho}{dt} + \rho \nabla \cdot \mathbf{u} = 0, \tag{2.39}$$

Equation (2.31) is

$$\rho \frac{de}{dt} - \frac{p}{\rho} \frac{d\rho}{dt} = 0. \tag{2.40}$$

Dividing by ρ, this equation can be written as

$$\frac{de}{dt} + p \frac{d}{dt} \left(\frac{1}{\rho} \right) = 0. \tag{2.41}$$

Substiting Eq.(2.13) into Eq.(2.41),

$$\frac{dq_d c_{vd} T}{dt} + p \frac{d}{dt} \left[\frac{q_d R_d T}{p} \right] + \frac{dq_v c_{vv} T}{dt} + p \frac{d}{dt} \left[\frac{q_v R_v T}{p} \right]$$
$$+ \frac{dq_l c_l T}{dt} + \frac{dq_s c_s T}{dt} = 0 \tag{2.42}$$

8

Since Eqs.(2.26)-(2.29) give

$$\frac{dq_d}{dt} = \frac{dq_v}{dt} = \frac{dq_l}{dt} = \frac{dq_s}{dt} = 0, \tag{2.43}$$

Equation (2.42) gives the following form:

$$q_d \left[\frac{dc_{vd}T}{dt} + p\frac{d}{dt}\left[\frac{R_dT}{p} \right] \right] + q_v \left[\frac{dc_{vv}T}{dt} + p\frac{d}{dt}\left[\frac{R_vT}{p} \right] \right]$$
$$+q_l\frac{dc_lT}{dt} + q_s\frac{dc_sT}{dt} = 0 \tag{2.44}$$

Dividing this equation by T,

$$q_d \left[c_{pd}\frac{1}{T}\frac{dT}{dt} + R_dp\frac{d}{dt}\left(\frac{1}{p} \right) \right] + q_v \left[c_{pv}\frac{1}{T}\frac{dT}{dt} + R_vp\frac{d}{dt}\left(\frac{1}{p} \right) \right]$$
$$+q_lc_l\frac{1}{T}\frac{dT}{dt} + q_sc_s\frac{1}{T}\frac{dT}{dt} = 0 \tag{2.45}$$

$$q_dc_{pd} \left[\frac{d\ln T}{dt} + \frac{R_d}{c_{pd}}\frac{d}{dt}\left[\ln\left(\frac{1}{p} \right) \right] \right] + q_vc_{pv} \left[\frac{d\ln T}{dt} + \frac{R_v}{c_{pv}}\frac{d}{dt}\left[\ln\left(\frac{1}{p} \right) \right] \right]$$
$$+q_lc_l\frac{d\ln T}{dt} + q_sc_s\frac{d\ln T}{dt} = 0 \tag{2.46}$$

$$q_dc_{pd}\frac{d\ln\theta_d}{dt} + q_vc_{pv}\frac{d\ln\theta_v}{dt} + q_lc_l\frac{d\ln T}{dt} + q_sc_s\frac{d\ln T}{dt} = 0 \tag{2.47}$$

$$\frac{d}{dt}\left[\ln\left(\theta_d^{q_dc_{pd}}\theta_v^{q_vc_{pv}}T^{q_lc_l}T^{q_sc_s} \right) \right] = 0 \tag{2.48}$$

Thus,

$$\frac{d}{dt}\left[\theta_d^{q_dc_{pd}}\theta_v^{q_vc_{pv}}T^{q_lc_l}T^{q_sc_s} \right] = 0 \tag{2.49}$$

Thus, the following quantity is conserved along the flow trajectory;

$$\Theta = \theta_d^{q_dc_{pd}}\theta_v^{q_vc_{pv}}T^{q_lc_l}T^{q_sc_s} \tag{2.50}$$

where θ_v is the potential temperature for water vapor, defined as

$$\theta_v = T\left(\frac{p_{00}}{p} \right)^{R_v/c_{pv}} \tag{2.51}$$

The equation of state has the following expression using Θ.

$$\Theta = T^{q_dc_{pd}}\left(\frac{p_{00}}{p} \right)^{q_dR_d}T^{q_vc_{pv}}\left(\frac{p_{00}}{p} \right)^{q_vR_v}T^{q_lc_l} + T^{q_sc_s} \tag{2.52}$$

$$= T^{q_dc_{pd}+q_vc_{pv}+q_lc_l+q_sc_s}\left(\frac{p_{00}}{p} \right)^{q_dR_d+q_vR_v} \tag{2.53}$$

$$= T^{c_p^*}\left(\frac{p_{00}}{p} \right)^{R^*}, \tag{2.54}$$

where

$$c_p^* \equiv q_dc_{pd} + q_vc_{pv} + q_lc_l + q_sc_s \tag{2.55}$$
$$R^* \equiv q_dR_d + q_vR_v \tag{2.56}$$

9

We define a new potential temperature

$$\theta \equiv \Theta^{1/c_p^*} \quad = \quad T \left(\frac{p_{00}}{p} \right)^{R^*/c_p^*} \tag{2.57}$$

The pressure expression is derived diagnostically as follows:

$$p \quad = \quad \rho(q_d R_d + q_v R_v)\theta \left(\frac{p}{p_{00}} \right)^{\frac{R^*}{c_p^*}} \tag{2.58}$$

$$p^{1-\frac{R^*}{c_p^*}} \quad = \quad \rho R^* \theta \left(\frac{1}{p_{00}} \right)^{\frac{R^*}{c_p^*}} \tag{2.59}$$

$$p \quad = \quad p_{00} \left(\frac{\rho \theta R^*}{p_{00}} \right)^{\frac{c_p^*}{c_p^* - R^*}} \tag{2.60}$$

Note that

$$\frac{d\theta}{dt} = \frac{1}{a} \Theta^{1/a - 1} \frac{d\Theta}{dt} = 0 \tag{2.61}$$

Therefore, $\rho\theta$ can be employed for the prognostic varaiable!

Figure 2.1(a) gives the vertical profile of the temperature in the U.S.standard atmosphere and Fig.2.1(b) shows the vertical profiles of θ/θ_d under this temperature condition when we assume that q_v is mass concentration of water vapor at the saturation, $q_l + q_s$ gives 0.0, 0.01, 0.02, and 0.04. The difference between θ and θ_d becomes larger with the height and it may not be negligible.

2.6 Diabatic heating in the physical process

If the prognostic variable for thermodynamics is changed from the internal energy to the newly defined potential temperature θ, the diabatic heating in Eq.(2.37) should be modified. Through the manupulation from Eq.(2.40) to Eq.(2.48), Eq.(2.37) without turbulence term can be written as

$$\frac{d \ln \Theta}{dt} = \frac{Q}{\rho T} \tag{2.62}$$

On the other hand, Eq.(2.61) gives

$$\frac{d\theta}{dt} = \frac{1}{c_p^*} \Theta^{1/a} \frac{d \ln \Theta}{dt} \tag{2.63}$$

Substituting Eq.(2.62) into Eq.(2.63),

$$\frac{d\theta}{dt} = \frac{1}{c_p^*} \left(\frac{p_{00}}{p} \right)^{\frac{R^*}{c_p^*}} \frac{Q}{\rho} \tag{2.64}$$

2.7 Summary of equations in the dynamical process and physical process

2.7.1 The dynamical process

$$\frac{\partial \rho q_v}{\partial t} + \nabla \cdot (\rho q_v \mathbf{u}) = \left(\frac{\partial \rho q_v}{\partial t} \right)_{physics} \tag{2.65}$$

$$\frac{\partial \rho q_l}{\partial t} + \nabla \cdot (\rho q_l \mathbf{u}) = \left(\frac{\partial \rho q_l}{\partial t} \right)_{physics} \tag{2.66}$$

$$\frac{\partial \rho q_s}{\partial t} + \nabla \cdot (\rho q_s \mathbf{u}) = \left(\frac{\partial \rho q_s}{\partial t} \right)_{physics} \tag{2.67}$$

$$\frac{\partial \rho}{\partial t} + \nabla \cdot (\rho \mathbf{u}) = \left(\frac{\partial \rho}{\partial t} \right)_{physics} \tag{2.68}$$

$$\frac{\partial \rho \mathbf{u}}{\partial t} + \nabla \cdot (\rho \mathbf{u} \otimes \mathbf{u}) = -\nabla p - \rho g \mathbf{e_z} + \left(\frac{\partial \rho \mathbf{u}}{\partial t} \right)_{physics} \tag{2.69}$$

$$\frac{\partial \rho \theta}{\partial t} + \nabla \cdot (\rho \theta \mathbf{u}) = \left(\frac{\partial \rho \theta}{\partial t} \right)_{physics} \tag{2.70}$$

$$p = p_{00} \left(\frac{\rho \theta R^*}{p_{00}} \right)^{\frac{c_p^*}{c_p^* - R^*}} \tag{2.71}$$

where

$$c_p^* \equiv q_d c_{pd} + q_v c_{pv} + q_l c_l + q_s c_s \tag{2.72}$$
$$R^* \equiv q_d R_d + q_v R_v \tag{2.73}$$

2.7.2 The physical process

$$\left(\frac{\partial \rho q_v}{\partial t} \right)_{physics} = S_v + \text{DIFF}\left[q_v \right] \tag{2.74}$$

$$\left(\frac{\partial \rho q_l}{\partial t} \right)_{physics} = -\frac{\partial \rho q_l w_l}{\partial z} + S_l + \text{DIFF}\left[q_l \right] \tag{2.75}$$

$$\left(\frac{\partial \rho q_s}{\partial t} \right)_{physics} = -\frac{\partial \rho q_s w_s}{\partial z} + S_s + \text{DIFF}\left[q_s \right] \tag{2.76}$$

$$\left(\frac{\partial \rho}{\partial t} \right)_{physics} = -\frac{\partial \rho q_l w_l}{\partial z} - \frac{\partial \rho q_s w_s}{\partial z} \tag{2.77}$$

$$\left(\frac{\partial \rho \mathbf{u}}{\partial t} \right)_{physics} = -\frac{\partial \rho q_l \mathbf{u} w_l}{\partial z} - \frac{\partial \rho q_s \mathbf{u} w_s}{\partial z} + \text{DIFF}\left[\mathbf{u} \right] \tag{2.78}$$

$$\left(\frac{\partial \rho \theta}{\partial t} \right)_{physics} = \frac{1}{c_p^*} \left(\frac{p_{00}}{p} \right)^{\frac{R^*}{c_p^*}} \left[Q - \frac{\partial \rho q_l e_l w_l}{\partial z} - \frac{\partial \rho q_s e_s w_s}{\partial z} \right] + \text{DIFF}\left[\theta \right] \tag{2.79}$$

(a)

(b)
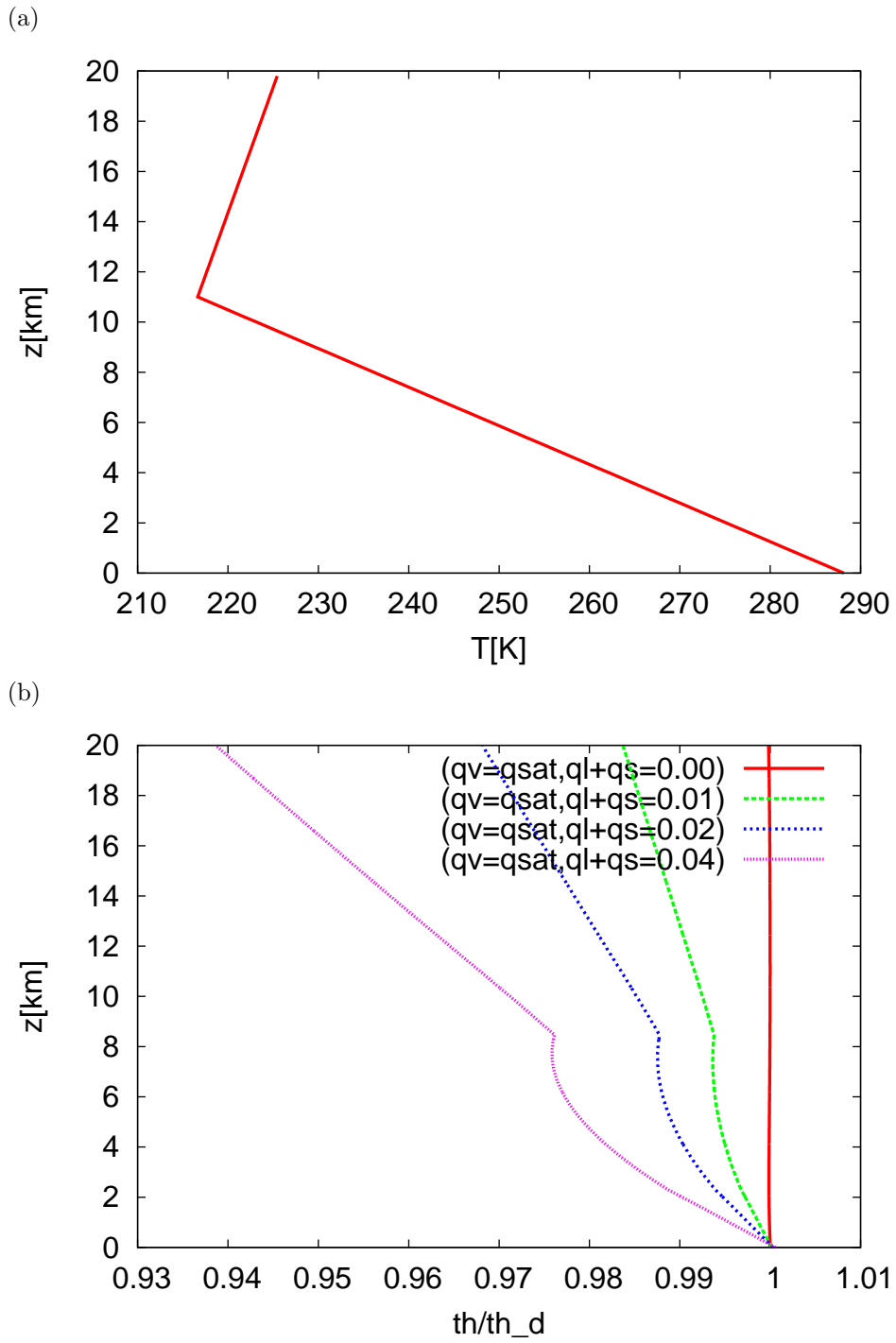
Figure 2.1: The vertical profile of (a) U.S. standard atmosphere, (b) Several profiles of θ/θ_d.

Chapter 3

Discretization of dynamics

Corresponding author : Seiya Nishizawa

3.1 Temporal integration scheme

3.1.1 Runge-Kutta schemes

For the time integration of Eqs.(2.68)-(2.40), we adopt the full explicit scheme with the p step Runge-Kutta scheme.

$$\phi_0^* = \phi^t \tag{3.1}$$

$$k_1 = f(\phi^t) \tag{3.2}$$

$$k_2 = f(\phi^t + k_1 \Delta t \alpha_1) \tag{3.3}$$

$$\cdots$$

$$k_p = f(\phi^t + k_{p-1} \Delta t \alpha_{p-1}) \tag{3.4}$$

$$\phi^{t+\Delta t} = \phi^t + \Delta t \sum_p \beta_p k_p. \tag{3.5}$$

The 3 and 4 step Runge-Kutta scheme are implemented.

The Heun's three step scheme

$$k_1 = f(\phi^n), \tag{3.6}$$

$$k_2 = f\left(\phi^n + \frac{1}{3}\Delta t k_1\right), \tag{3.7}$$

$$k_3 = f\left(\phi^n + \frac{2}{3}\Delta t k_2\right), \tag{3.8}$$

$$\phi^{n+1} = \phi^n + \frac{1}{4}\Delta t(k_1 + 3k_3). \tag{3.9}$$

The Kutta's three step scheme

$$k_1 = f(\phi^n), \tag{3.10}$$

$$k_2 = f\left(\phi^n + \frac{1}{2}\Delta t k_1\right), \tag{3.11}$$

$$k_3 = f\left(\phi^n - \Delta t k_1 + 2\Delta t k_2\right), \tag{3.12}$$

$$\phi^{n+1} = \phi^n + \frac{1}{6}\Delta t(k_1 + 4k_2 + k_3). \tag{3.13}$$

The Wicker and Skamarock (2002)'s three step scheme

$$k_1 = f(\phi^n), \tag{3.14}$$

$$k_2 = f\left(\phi^n + \frac{1}{3}\Delta t k_1\right), \tag{3.15}$$

$$k_3 = f\left(\phi^n + \frac{1}{2}\Delta t k_2\right), \tag{3.16}$$

$$\phi^{n+1} = \phi^n + \Delta t k_3. \tag{3.17}$$

The four step scheme

$$k_1 = f(\phi^n), \tag{3.18}$$

$$k_2 = f\left(\phi^n + \frac{1}{2}\Delta t k_1\right), \tag{3.19}$$

$$k_3 = f\left(\phi^n + \frac{1}{2}\Delta t k_2\right), \tag{3.20}$$

$$k_4 = f\left(\phi^n + \Delta t k_3\right), \tag{3.21}$$

$$\phi^{n+1} = \phi^n + \frac{1}{6}\Delta t(k_1 + 2k_2 + 2k_3 + k_4). \tag{3.22}$$

The forward-backward scheme

In the short time step, the momentums are updated first and then density is updated with the updated momentums.

$$\rho u_i^{n+1} = \rho u_i^n + \Delta t f_{\rho u_i}(\rho^n), \tag{3.23}$$

$$\rho^{n+1} = \rho^n + \Delta t f_\rho(\rho u_i^{n+1}). \tag{3.24}$$

3.1.2 Numerical stability

A fully compressive equations of a acoustic mode is considered. The continuous and momentum equations is the followings:

$$\frac{\partial \rho}{\partial t} = -\frac{\partial \rho u_i}{\partial x_i} \tag{3.25}$$

$$\frac{\partial \rho u_i}{\partial t} = -\frac{\partial p}{\partial x_i} \tag{3.26}$$

$$p = p_0 \left(\frac{R\rho\theta}{p_0} \right)^{c_p/c_v}, \tag{3.27}$$

here the potential temperature θ is assumed to be constant.

In order to analyze the numerical stability of equation, the equation of the state is linearized.

$$p \approx \bar{p} + c^2 \rho', \tag{3.28}$$

where c is the sound speed: $c^2 = \frac{c_p \bar{p}}{c_v \bar{\rho}}$.

We discritize the governing equation with the 2nd order central difference.

$$\left. \frac{\partial \rho}{\partial t} \right|_{i,j,k} = -\frac{U_{i+1/2} - U_{i-1/2}}{\Delta x} - \frac{V_{j+1/2} - V_{j-1/2}}{\Delta y} - \frac{W_{k+1/2} - W_{k-1/2}}{\Delta z} \tag{3.29}$$

$$\left. \frac{\partial U}{\partial t} \right|_{i+1/2} = -c^2 \frac{\rho_{i+1} - \rho_i}{\Delta x} \tag{3.30}$$

$$\left. \frac{\partial V}{\partial t} \right|_{j+1/2} = -c^2 \frac{\rho_{j+1} - \rho_j}{\Delta y} \tag{3.31}$$

$$\left. \frac{\partial W}{\partial t} \right|_{i+1/2} = -c^2 \frac{\rho_{k+1} - \rho_k}{\Delta z}, \tag{3.32}$$

where U, V, and W is the momentum at the staggared grid point in x, y, and z direction, respectively.

The error of the spatial difference of a wavenumber k component $\hat{\phi}_k$ is $\{\exp(ik\Delta x) - 1\} \hat{\phi}$, and the error of 2-grid mode is the largest: $\exp(i\pi) - 1 = -2$.

The temporal differential of the 2-grid mode is

$$\frac{\partial \rho}{\partial t} = -\frac{1 - \exp(-i\pi)}{\Delta x} U - \frac{1 - \exp(-i\pi)}{\Delta y} V - \frac{1 - \exp(-i\pi)}{\Delta z} W \tag{3.33}$$

$$\frac{\partial U}{\partial t} = -c^2 \frac{\exp(i\pi) - 1}{\Delta x} \rho \tag{3.34}$$

$$\frac{\partial V}{\partial t} = -c^2 \frac{\exp(i\pi) - 1}{\Delta y} \rho \tag{3.35}$$

$$\frac{\partial W}{\partial t} = -c^2 \frac{\exp(i\pi) - 1}{\Delta z} \rho. \tag{3.36}$$

The mode of which the U, V and W has the same phase is the most unstable:

$$\frac{\partial \rho}{\partial t} = -3\frac{1 - \exp(-i\pi)}{\Delta x} U \tag{3.37}$$

$$\frac{\partial U}{\partial t} = -c^2 \frac{\exp(i\pi) - 1}{\Delta x} \rho \tag{3.38}$$

Writing matrix form,

$$\begin{pmatrix} \frac{\partial \rho}{\partial t} \\ \frac{\partial U}{\partial t} \end{pmatrix} = D \begin{pmatrix} \rho \\ U \end{pmatrix}, \tag{3.39}$$

where

$$D = \begin{pmatrix} 0 & -\frac{6}{\Delta x} \\ \frac{2c^2}{\Delta x} & 0 \end{pmatrix}. \tag{3.40}$$

The Euler scheme

With the Euler scheme,

$$\phi^{n+1} = \phi^n + \Delta t f(\phi^n) \tag{3.41}$$

The A is the matrix representing the time step, then

$$A = I + dtD, \tag{3.42}$$

$$= \begin{pmatrix} 1 & -6\frac{\Delta t}{\Delta x} \\ \frac{2c^2 \Delta t}{\Delta x} & 1 \end{pmatrix}. \tag{3.43}$$

The eigen value of A is larger than 1, and the Euler scheme is unstable for any Δt.

The second step Runge-Kutta scheme

The Heun's second step Runge-Kutta scheme is

$$k_1 = f(\phi^n), \tag{3.44}$$
$$k_2 = f(\phi^n + \Delta t k_1), \tag{3.45}$$
$$\phi^{n+1} = \phi^n + \frac{\Delta t}{2}(k_1 + k_2). \tag{3.46}$$

$$A = I + \frac{\Delta t}{2}(K_1 + K_2), \tag{3.47}$$
$$K_1 = D, \tag{3.48}$$
$$K_2 = D(I + \Delta t K_1). \tag{3.49}$$

After all,

$$A = \begin{pmatrix} 1 - 6\nu^2 & -\frac{6\Delta t}{\Delta x} \\ \frac{2c^2 \Delta t}{\Delta x} & 1 - 6\nu^2 \end{pmatrix}, \tag{3.50}$$

where ν is the Courant number for the sound speed: $\frac{c\Delta t}{\Delta x}$. The eigen value of A is larger than 1, and the Euler scheme is unstable for any Δt.

The third step Runge-Kutta scheme

With the Heun's third step Runge-Kutta scheme, the matrix A is written by

$$A = I + \frac{\Delta t}{4}(K_1 + 4K_3), \tag{3.51}$$

$$= \begin{pmatrix} 1 - 6\nu^2 & -\frac{6\Delta t}{\Delta x}(1 - 2\nu^2) \\ \frac{2c^2 \Delta t}{\Delta x}(1 - 2\nu^2) & 1 - 6\nu^2 \end{pmatrix}, \tag{3.52}$$

where

$$K_1 = D, \tag{3.53}$$

$$K_2 = D(I + \frac{\Delta t}{3} K_1), \tag{3.54}$$

$$K_3 = D(I + \frac{2\Delta t}{3} K_2). \tag{3.55}$$

The condition that all the eigen values are less than or equal to 1 is

$$\nu \leq \frac{1}{2}. \tag{3.56}$$

In the Kutta's three step Runge-Kutta scheme, the matrix A is

$$A = I + \frac{\Delta t}{6}(K_1 + 4K_2 + K_3), \tag{3.57}$$

where

$$K_1 = D, \tag{3.58}$$

$$K_2 = D\left(I + \frac{\Delta t}{2} K_1\right), \tag{3.59}$$

$$K_3 = D\left(I - \Delta t K_1 + 2\Delta t K_2\right). \tag{3.60}$$

It is the idential as that in the Heun's scheme (eq. 3.52). Thus, the stable condition is the same (eq. 3.56).

The Wicker and Skamarock (2002)'s Runge-Kutta scheme is described as

$$A = I + \Delta t K_3, \tag{3.61}$$

$$K_1 = D, \tag{3.62}$$

$$K_2 = D\left(I + \frac{\Delta t}{3} K_1\right), \tag{3.63}$$

$$K_3 = D\left(I + \frac{\Delta t}{2} K_2\right). \tag{3.64}$$

The A and the consequent stable condition are the identical as the above two schemes.

The four step Runge-Kutta scheme

The matrix A is

$$A = I + \frac{\Delta t}{6}(K_1 + 2K_2 + 2K_3 + K_4), \tag{3.65}$$

$$= \begin{pmatrix} 1 - 6\nu^2 + 6\nu^4 & -\frac{6\Delta t}{\Delta x}(1 - 2\nu^2) \\ \frac{2c^2\Delta t}{\Delta x}(1 - 2\nu^2) & 1 - 6\nu^2 + 6^4 \end{pmatrix}, \tag{3.66}$$

where

$$K_1 = D, \tag{3.67}$$

$$K_2 = D\left(I + \frac{\Delta t}{2}K_1\right), \tag{3.68}$$

$$K_3 = D\left(I + \frac{\Delta t}{2}K_2\right), \tag{3.69}$$

$$K_4 = D(I + \Delta t K_3). \tag{3.70}$$

The condition for stability is

$$\nu \leq \frac{\sqrt{6}}{3}. \tag{3.71}$$

The number of floating point operations with the four step Runge-Kutta scheme is about 4/3 times larger than that with the three step scheme. However, the time step can be $2\sqrt{6}/3$ larger than that in the three step scheme. Since $2\sqrt{6}/3 > 4/3$, the four step Runge-Kutta scheme is more cost effective than the three step scheme in terms of numerical stability.

The forward-backward scheme

The stability condition is

$$\nu \leq \frac{1}{\sqrt{3}}. \tag{3.72}$$

The forward-backward scheme can be used in each step in the Runge-Kutta schemes. The stability conditions are the followings:

The second step RK scheme

$$\nu \leq \frac{1}{\sqrt{3}}. \tag{3.73}$$

The Heun's three step RK scheme

$$\nu \leq \frac{1}{2}. \tag{3.74}$$

The Kutta's three step RK scheme

$$\nu \leq \frac{1}{2}. \tag{3.75}$$

The Wicker and Skamarock (2002)'s three step RK scheme

$$\nu \leq \frac{\sqrt{6}}{4}. \tag{3.76}$$

The four step RK scheme

$$\nu \leq 0.66 \tag{3.77}$$

Corresponding author : Hirofumi Tomita

3.2 Spatial discretization

We employ the Arakawa-C staggered grid with the 3-dimensional momentum $(\rho u, \rho v, \rho w)$, density (ρ) and mass-weighted potential temperature$(\rho\theta)$ as the prognostic variables. Figure 3.1(a) shows the structure of the control volume for the mass, indicating the location of each of prognostic variables. Conceptually, we use the 4th order central difference scheme for the advection or convection terms and the 2nd order central difference scheme for the other terms. Before the discretization of differential equations, we should diagnose several quantities from the prognostic variables.

Full-level pressure and potential temperature

$$p_{i,j,k} = p_{00} \left[\frac{(\rho\theta)_{i,j,k} R^*}{p_{00}} \right]^{\frac{c_p^*}{c_p^* - R^*}} \tag{3.78}$$

$$\theta_{i,j,k} = \frac{(\rho\theta)_{i,j,k}}{\rho_{i,j,k}} \tag{3.79}$$

$$\tag{3.80}$$

Half-level density

$$\overline{\rho}_{i+\frac{1}{2},j,k} = \frac{\rho_{i+1,j,k} + \rho_{i,j,k}}{2} \tag{3.81}$$

$$\overline{\rho}_{i,j+\frac{1}{2},k} = \frac{\rho_{i,j+1,k} + \rho_{i,j,k}}{2} \tag{3.82}$$

$$\overline{\rho}_{i,j,k+\frac{1}{2}} = \frac{\Delta z_k \rho_{i,j,k+1} + \Delta z_{k+1} \rho_{i,j,k}}{\Delta z_k + \Delta z_{k+1}} \tag{3.83}$$

Half-level velocity

$$\overline{u}_{i+\frac{1}{2},j,k} = \frac{(\rho u)_{i+\frac{1}{2},j,k}}{\overline{\rho}_{i+\frac{1}{2},j,k}} \tag{3.84}$$

$$\overline{v}_{i,j+\frac{1}{2},k} = \frac{(\rho v)_{i,j+\frac{1}{2},k}}{\overline{\rho}_{i,j+\frac{1}{2},k}} \tag{3.85}$$

$$\overline{w}_{i,j,k+\frac{1}{2}} = \frac{(\rho w)_{i,j,k+\frac{1}{2}}}{\overline{\rho}_{i,j,k+\frac{1}{2}}} \tag{3.86}$$

Full-level velocity

$$\overline{u}_{i,j,k} = \frac{(\rho u)_{i+\frac{1}{2},j,k} + (\rho u)_{i-\frac{1}{2},j,k}}{2\rho_{i,j,k}} \tag{3.87}$$

$$\overline{v}_{i,j,k} = \frac{(\rho v)_{i,j+\frac{1}{2},k} + (\rho v)_{i,j-\frac{1}{2},k}}{2\rho_{i,j,k}} \tag{3.88}$$

$$\overline{w}_{i,j,k} = \frac{(\rho w)_{i,j,k+\frac{1}{2}} + (\rho w)_{i,j,k-\frac{1}{2}}}{2\rho_{i,j,k}} \tag{3.89}$$

3.2.1 Continuity equation

$$\left(\frac{\partial \rho}{\partial t}\right)_{i,j,k} = -\frac{(\rho u)_{i+\frac{1}{2},j,k} - (\rho u)_{i-\frac{1}{2},j,k}}{\Delta x}$$

$$-\frac{(\rho v)_{i,j+\frac{1}{2},k} - (\rho v)_{i,j-\frac{1}{2},k}}{\Delta y}$$

$$-\frac{(\rho w)_{i,j,k+\frac{1}{2}} - (\rho w)_{i,j,k-\frac{1}{2}}}{\Delta z} \tag{3.90}$$

3.2.2 Momentum equations

Figure 3.1(a) shows the structure of the control volume for the momentum in the x direction. The momentum equation is discretized as

$$\left(\frac{\partial \rho u}{\partial t}\right)_{i+\frac{1}{2},j,k} = -\frac{\overline{(\rho u)}_{i+1,j,k}\,\overline{u}_{i+1,j,k} - \overline{(\rho u)}_{i,j,k}\,\overline{u}_{i,j,k}}{\Delta x}$$

$$-\frac{\overline{(\rho u)}_{i+\frac{1}{2},j+\frac{1}{2},k}\,\overline{v}_{i+\frac{1}{2},j+\frac{1}{2},k} - \overline{(\rho u)}_{i+\frac{1}{2},j-\frac{1}{2},k}\,\overline{v}_{i+\frac{1}{2},j-\frac{1}{2},k}}{\Delta y}$$

$$-\frac{\overline{(\rho u)}_{i+\frac{1}{2},j,k+\frac{1}{2}}\,\overline{w}_{i+\frac{1}{2},j,k+\frac{1}{2}} - \overline{(\rho u)}_{i+\frac{1}{2},j,k-\frac{1}{2}}\,\overline{w}_{i+\frac{1}{2},j,k-\frac{1}{2}}}{\Delta z}$$

$$-\frac{p_{i+1,j,k} - p_{i,j,k}}{\Delta x}, \tag{3.91}$$

where

$$\overline{(\rho u)}_{i,j,k}$$
$$= \frac{-(\rho u)_{i+\frac{3}{2},j,k} + 7(\rho u)_{i+\frac{1}{2},j,k} + 7(\rho u)_{i-\frac{1}{2},j,k} - (\rho u)_{i-\frac{3}{2},j,k}}{12} \tag{3.92}$$

$$\overline{(\rho u)}_{i+\frac{1}{2},j+\frac{1}{2},k}$$
$$= \frac{-(\rho u)_{i+\frac{1}{2},j+2,k} + 7(\rho u)_{i+\frac{1}{2},j+1,k} + 7(\rho u)_{i+\frac{1}{2},j,k} - (\rho u)_{i+\frac{1}{2},j-1,k}}{12} \tag{3.93}$$

$$\overline{(\rho u)}_{i+\frac{1}{2},j,k+\frac{1}{2}}$$
$$= \frac{-(\rho u)_{i+\frac{1}{2},j,k+2} + 7(\rho u)_{i+\frac{1}{2},j,k+1} + 7(\rho u)_{i+\frac{1}{2},j,k} - (\rho u)_{i+\frac{1}{2},j,k-1}}{12} \tag{3.94}$$

and the velocities at the cell wall for the staggered control volume to x direction are defined as

$$\overline{u}_{i,j,k} = \frac{\overline{u}_{i+\frac{1}{2},j,k} + \overline{u}_{i-\frac{1}{2},j,k}}{2} \tag{3.95}$$

$$\overline{v}_{i+\frac{1}{2},j+\frac{1}{2},k} = \frac{\overline{v}_{i,j+\frac{1}{2},k} + \overline{v}_{i+1,j+\frac{1}{2},k}}{2} \tag{3.96}$$

$$\overline{w}_{i+\frac{1}{2},j,k+\frac{1}{2}} = \frac{\overline{w}_{i,j,k+\frac{1}{2}} + \overline{w}_{i+1,j,k+\frac{1}{2}}}{2} \tag{3.97}$$

In this form, the 4th order accuracy is guaranteed on the condition of the constant velocity.

The momentum equations in the y and z directions are descretized in the same way:

$$
\left(\frac{\partial \rho v}{\partial t}\right)_{i,j+\frac{1}{2},k} = -\frac{\overline{(\rho v)}_{i+\frac{1}{2},j+\frac{1}{2},k}\,\overline{u}_{i+\frac{1}{2},j+\frac{1}{2},k} - \overline{(\rho v)}_{i-\frac{1}{2},j+\frac{1}{2},k}\,\overline{u}_{i-\frac{1}{2},j+\frac{1}{2},k}}{\Delta x}
$$

$$
-\frac{\overline{(\rho v)}_{i,j+1,k}\,\overline{v}_{i,j+1,k} - \overline{(\rho v)}_{i,j,k}\,\overline{v}_{i,j,k}}{\Delta y}
$$

$$
-\frac{\overline{(\rho v)}_{i,j+\frac{1}{2},k+\frac{1}{2}}\,\overline{v}_{i,j+\frac{1}{2},k+\frac{1}{2}} - \overline{(\rho v)}_{i,j+\frac{1}{2},k-\frac{1}{2}}\,\overline{v}_{i,j+\frac{1}{2},k-\frac{1}{2}}}{\Delta z}
$$

$$
-\frac{p_{i,j+1,k} - p_{i,j,k}}{\Delta y}, \tag{3.98}
$$

$$
\left(\frac{\partial \rho w}{\partial t}\right)_{i,j,k+\frac{1}{2}} = -\frac{\overline{(\rho w)}_{i+\frac{1}{2},j,k+\frac{1}{2}}\,\overline{u}_{i+\frac{1}{2},j,k+\frac{1}{2}} - \overline{(\rho w)}_{i-\frac{1}{2},j,k+\frac{1}{2}}\,\overline{u}_{i-\frac{1}{2},j,k+\frac{1}{2}}}{\Delta x}
$$

$$
-\frac{\overline{(\rho w)}_{i,j+\frac{1}{2},k+\frac{1}{2}}\,\overline{w}_{i,j+\frac{1}{2},k+\frac{1}{2}} - \overline{(\rho w)}_{i,j-\frac{1}{2},k+\frac{1}{2}}\,\overline{w}_{i,j-\frac{1}{2},k+\frac{1}{2}}}{\Delta y}
$$

$$
-\frac{\overline{(\rho w)}_{i,j,k+1}\,\overline{w}_{i,j,k+1} - \overline{(\rho w)}_{i,j,k}\,\overline{w}_{i,j,k}}{\Delta z}
$$

$$
-\frac{p_{i,j,k+1} - p_{i,j,k}}{\Delta z} - \overline{\rho}_{i,j,k+\frac{1}{2}}\, g \tag{3.99}
$$

Pressure

Since the pressure perturbation is much smaller than the absolute value of the pressure, truncation error of floating point value is relatively large and its precision could become smaller. Therefore, the pressure gradient terms are calculated from the deviation from reference pressure field satisfying the hydrostatic balance. Additionally, the calculation of the pressure (Eq.2.60) is linearized avoiding a power calculation, which numerically costs expensive.

$$
p \approx \bar{p} + \frac{c_p^*}{R^* C_v^*} \left(\frac{\rho \theta R^*}{p_{00}}\right)^{\frac{R^*}{c_v^*}} \{\rho\theta - \overline{\rho\theta}\}
$$

$$
= \bar{p} + \frac{c_p^*}{c_v^*} \frac{\bar{p}}{\overline{\rho\theta}} (\rho\theta)' \tag{3.100}
$$

$$
p - p_{\text{ref}} = \bar{p} - p_{\text{ref}} + \frac{c_p^*}{c_v^*} \frac{\bar{p}}{\overline{\rho\theta}} (\rho\theta)' \tag{3.101}
$$

3.2.3 Energy equation

$$
\left(\frac{\partial \rho\theta}{\partial t}\right)_{i,j,k} = -\frac{(\rho u)_{i+\frac{1}{2},j,k}\,\overline{\theta}_{i+\frac{1}{2},j,k} - (\rho u)_{i-\frac{1}{2},j,k}\,\overline{\theta}_{i-\frac{1}{2},j,k}}{\Delta x}
$$

$$
-\frac{(\rho v)_{i,j+\frac{1}{2},k}\,\overline{\theta}_{i,j+\frac{1}{2},k} - (\rho v)_{i,j-\frac{1}{2},k}\,\overline{\theta}_{i,j-\frac{1}{2},k}}{\Delta y}
$$

$$
-\frac{(\rho w)_{i,j,k+\frac{1}{2}}\,\overline{\theta}_{i,j,k+\frac{1}{2}} - (\rho w)_{i,j,k-\frac{1}{2}}\,\overline{\theta}_{i,j,k-\frac{1}{2}}}{\Delta z}
$$

$$
\tag{3.102}
$$

where

$$\overline{\theta}_{i+\frac{1}{2},j,k} = \frac{-\theta_{i+2,j,k} + 7\theta_{i+1,j,k} + 7\theta_{i,j,k} - \theta_{i-1,j,k}}{12} \qquad (3.103)$$

$$\overline{\theta}_{i,j+\frac{1}{2},k} = \frac{-\theta_{i,j+2,k} + 7\theta_{i,j+1,k} + 7\theta_{i,j,k} - \theta_{i,j-1,k}}{12} \qquad (3.104)$$

$$\overline{\theta}_{i,j,k+\frac{1}{2}} = \frac{-\theta_{i,j,k+2} + 7\theta_{i,j,k+1} + 7\theta_{i,j,k} - \theta_{i,j,k-1}}{12} \qquad (3.105)$$

3.2.4 Tracer advection

The tracer advection process is done after the time integration of the dynamical variables (ρ, ρu, ρv, ρw, and $\rho \theta$). We impose two constraints to tracer advection:

Consistency With Continuity (CWC) On the condition without any source/sink, the mass concentration in the advection process should be conserved along the trajectory. It is, at least, necessary that the spatially constant mass concentration should be kept in any motion of fluid. In order to satisfy this condition, we need to mass flux consistent with that at the last Runge-Kutta process of Eq.(3.5) for integration of tracers:

$$\frac{(\rho q)^{n+1}_{i,j,k} - (\rho q)^{n}_{i,j,k}}{\Delta t} = -\frac{(\rho u)_{i+\frac{1}{2},j,k}\overline{q}_{i+\frac{1}{2},j,k} - (\rho u)_{i-\frac{1}{2},j,k}\overline{q}_{i-\frac{1}{2},j,k}}{\Delta x}$$
$$-\frac{(\rho v)_{i,j+\frac{1}{2},k}\overline{q}_{i,j+\frac{1}{2},k} - (\rho v)_{i,j-\frac{1}{2},k}\overline{q}_{i,j-\frac{1}{2},k}}{\Delta y}$$
$$-\frac{(\rho w)_{i,j,k+\frac{1}{2}}\overline{q}_{i,j,k+\frac{1}{2}} - (\rho w)_{i,j,k-\frac{1}{2}}\overline{q}_{i,j,k-\frac{1}{2}}}{\Delta z} \qquad (3.106)$$

Monotonicity In order to satisfy the monotonicity of tracer advection, we employ the Flux Corrected Transport scheme, which is a hybrid scheme with the 4th order central difference scheme and 1st order upwind scheme. If The 4th order central difference is applied, $\overline{q}$ is discretized as

$$\overline{q}^{high}_{i+\frac{1}{2},j,k} = \frac{-q_{i+2,j,k} + 7q_{i+1,j,k} + 7q_{i,j,k} - q_{i-1,j,k}}{12} \qquad (3.107)$$

$$\overline{q}^{high}_{i,j+\frac{1}{2},k} = \frac{-q_{i,j+2,k} + 7q_{i,j+1,k} + 7q_{i,j,k} - q_{i,j-1,k}}{12} \qquad (3.108)$$

$$\overline{q}^{high}_{i,j,k+\frac{1}{2}} = \frac{-q_{i,j,k+2} + 7q_{i,j,k+1} + 7q_{i,j,k} - q_{i,j,k-1}}{12}. \qquad (3.109)$$

On the other hand, in the 1st order upwind scheme $\overline{q}$ is described as

$$\overline{q}^{low}_{i+\frac{1}{2},j,k} = \begin{cases} q_{i,j,k} & ((\rho u)_{i+\frac{1}{2},j,k} > 0) \\ q_{i+1,j,k} & (\text{otherwise}) \end{cases} \qquad (3.110)$$

$$\overline{q}^{low}_{i,j+\frac{1}{2},k} = \begin{cases} q_{i,j,k} & ((\rho u)_{i,j+\frac{1}{2},k} > 0) \\ q_{i,j+1,k} & (\text{otherwise}) \end{cases} \qquad (3.111)$$

$$\overline{q}^{low}_{i,j,k+\frac{1}{2}} = \begin{cases} q_{i,j,k} & ((\rho u)_{i,j,k+\frac{1}{2}} > 0) \\ q_{i,j,k+1} & (\text{otherwise}) \end{cases} \qquad (3.112)$$

The actual $\overline{q}$ is described as

$$\overline{q}_{i+\frac{1}{2},j,k} = C_{i+\frac{1}{2},j,k}\overline{q}^{high}_{i+\frac{1}{2},j,k} + \left(1 - C_{i+\frac{1}{2},j,k}\right)\overline{q}^{low}_{i+\frac{1}{2},j,k} \quad (3.113)$$

$$\overline{q}_{i,j+\frac{1}{2},k} = C_{i,j+\frac{1}{2},k}\overline{q}^{high}_{i,j+\frac{1}{2},k} + \left(1 - C_{i,j+\frac{1}{2},k}\right)\overline{q}^{low}_{i,j+\frac{1}{2},k} \quad (3.114)$$

$$\overline{q}_{i,j,k+\frac{1}{2}} = C_{i,j,k+\frac{1}{2}}\overline{q}^{high}_{i,j,k+\frac{1}{2}} + \left(1 - C_{i,j,k+\frac{1}{2}}\right)\overline{q}^{low}_{i,j,k+\frac{1}{2}} \quad (3.115)$$

See the appendix for the method to determine the flux limiter.

3.3 Boundary condition

The boundary condition only for the vertical velocity at the top and bottom boundaries is needed:

$$w_{i,j,k_{max}+\frac{1}{2}} = 0 \quad (3.116)$$

$$w_{i,j,k_{min}-\frac{1}{2}} = 0 \quad (3.117)$$

This leads to the boundary condition of the prognostic variable as

$$(\rho w)_{i,j,k_{max}+\frac{1}{2}} = 0 \quad (3.118)$$

$$(\rho w)_{i,j,k_{min}-\frac{1}{2}} = 0 \quad (3.119)$$

3.4 Numerical filters

We impose an explicit numerical filter using the numerical viscosity and diffusion. Although the filter is necessary for numerical stability, too strong a filter could dampen any physically meaningful variability. In this subsection, we describe the numerical filters used in this model, and discuss the strength of the filter.

In order to damp the higher wavenumber component selectively, we adopt the hyperviscosity and diffusion in the traditional way. The hyperviscosity and diffusion of the nth order are defined as

$$\frac{\partial}{\partial x}\left[\nu\rho\frac{\partial^{n-1}f}{\partial x^{n-1}}\right] \quad (3.120)$$

for arbitrary variables ($f \in u, v, w, \theta, q$) except the density. For the density, it is defined as

$$\frac{\partial}{\partial x}\left[\nu\frac{\partial^{n-1}\rho}{\partial x^{n-1}}\right].$$

The Laplacian of f is discretized as

$$\Delta f_i = \frac{1}{\Delta x_i}\left[\frac{1}{\Delta x_{i+\frac{1}{2}}}f_{i+1} - \left(\frac{1}{\Delta x_{i+\frac{1}{2}}} + \frac{1}{\Delta x_{i-\frac{1}{2}}}\right)f_i + \frac{1}{\Delta x_{i-\frac{1}{2}}}f_{i-1}\right], \quad (3.121)$$

and

$$\Delta^{n/2}f_i = \frac{1}{\Delta x_i}\left[\frac{1}{\Delta x_{i+\frac{1}{2}}}\Delta^{n/2-1}f_{i+1} - \left(\frac{1}{\Delta x_{i+\frac{1}{2}}} + \frac{1}{\Delta x_{i-\frac{1}{2}}}\right)\Delta^{n/2-1}f_i \right.$$
$$\left. + \frac{1}{\Delta x_{i-\frac{1}{2}}}\Delta^{n/2-1}f_{i-1}\right]. \quad (3.122)$$

Here we consider spatially dependent grid interval in calculating the Laplacian. If it is calculated with constant Δx_i as

$$\Delta f_i = \frac{1}{\Delta x_i^2} \left(f_{i+1} - 2f_i + f_{i-1} \right), \tag{3.123}$$

$$\Delta^{n/2} f_i = \frac{1}{\Delta x_i^2} \left(\Delta^{n/2-1} f_{i+1} - 2\Delta^{n/2-1} f_i + \Delta^{n/2-1} f_{i-1} \right), \tag{3.124}$$

non-negligible numerical noise appears where the grid spacing varies (e.g., stretching layer near the top boundary).

The hyperviscosity and diffusion can be discretized as

$$\frac{\partial}{\partial x} \left[\nu \rho \frac{\partial^{n-1} f}{\partial^{n-1} x} \right] \sim \frac{F_{i+\frac{1}{2}} - F_{i-\frac{1}{2}}}{\Delta x_i}, \tag{3.125}$$

where

$$F_{i+\frac{1}{2}} \frac{\nu_{i+\frac{1}{2}} \rho_{i+\frac{1}{2}}}{\Delta x_{i+\frac{1}{2}}} \left(\Delta^{n/2-1} f_{i+1} - \Delta^{n/2-1} f_i \right). \tag{3.126}$$

The coefficient, ν, is written as

$$\nu_{i+\frac{1}{2}} = (-1)^{n/2+1} \gamma \frac{\Delta x_{i+\frac{1}{2}}^n}{2^n \Delta t}, \tag{3.127}$$

where γ is a non-dimensional coefficient. One-dimensional sinusoidal two-grid noise will decay to $1/e$ with $1/\gamma$ time steps. Note that the theoretical e-folding time is $\frac{2^n}{\pi^n} \frac{\Delta t}{\gamma}$. However, it is $\frac{\Delta t}{\gamma}$ with the fourth-order central scheme used in this model.

For the numerical stability of the numerical filter itself, it should satisfy

$$\gamma < 1 \tag{3.128}$$

for the one-dimensional two-grid noise, and

$$\gamma < \frac{1}{3} \tag{3.129}$$

for the three-dimensional two-grid noise. The conditions might be stricter for other types of noise.

The flux, F, for the numerical filter is added to the advective flux as

$$(\rho u f)_{i+\frac{1}{2}}^{\dagger} = (\rho u f)_{i+\frac{1}{2}} + F_{i+\frac{1}{2}}, \tag{3.130}$$

where the first term of the right-hand side is the flux calculated by the advection scheme. In the present model, the advection scheme is the fourth-order central difference scheme. This concept is very important for the CWC condition in the tracer equations. The modified mass flux of the numerical filter should be used in the tracer advection, otherwise the CWC condition is violated.

The numerical viscosity and diffusion in the y and z directions are formulated in the same way as in the x direction, although a special treatment for the z direction is needed. At the top and bottom boundaries, the flux must be zero, $F_{k_{\max}+\frac{1}{2}} = F_{k_{\min}-\frac{1}{2}} = 0$. In order to calculate the $F_{k_{\max}-\frac{1}{2}}$ and $F_{k_{\min}+\frac{1}{2}}$,

values beyond the boundaries, $f_{k_{\max}+1}$ and $f_{k_{\min}-1}$, are required, then the mirror boundary condition is assumed; $f_{k_{\max}+1} = -f_{k_{\max}}$ and $f_{k_{\min}-1} = -f_{k_{\min}}$. This condition is appropriate to cause the decay the vertical two-grid noise.

Vertical profiles of density, potential temperature, and water vapor usually have significant (e.g., logarithmic) dependencies on height. Eq. (3.125) has a non-zero value even for the steady state, and the numerical filter produces artificial motion. To reduce this artificial motion, we introduce a reference profile which is a function of height, and deviation from the reference is used as f instead of ρ, θ, and q_{v} in calculating the numerical filter. The reference profile can be chosen arbitrarily, but a profile under hydrostatic balance is usually chosen.

(a) Control volume for the mass
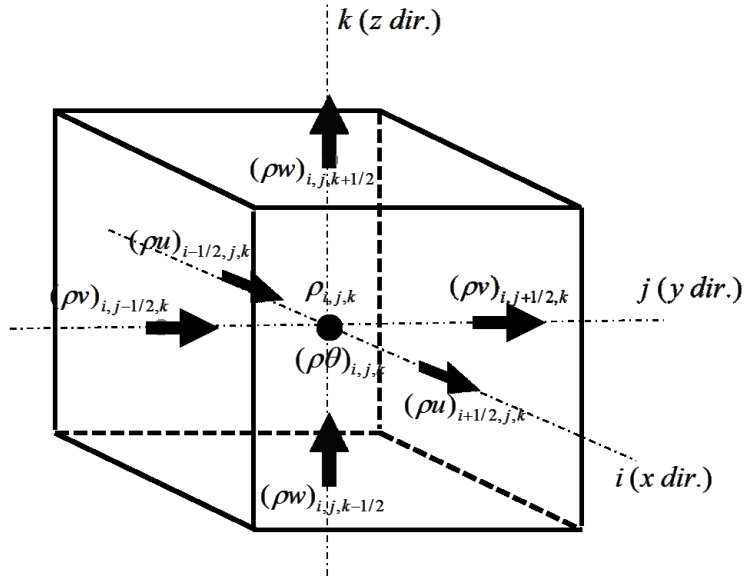
(b) Control volume for the momentum
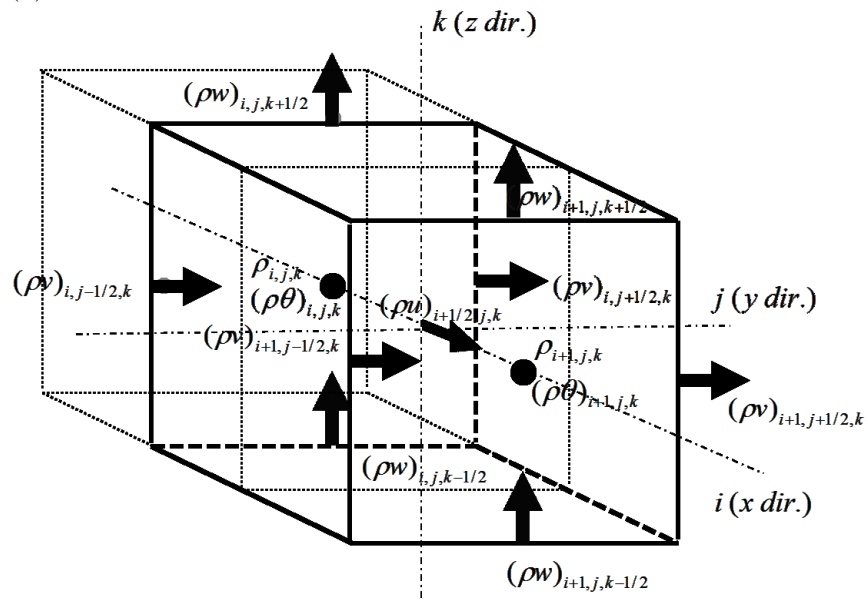
Figure 3.1: Control volume

Chapter 4

Terrain-following Coordinates

Corresponding author : Hisashi Yashiro

4.1 Geometry and Definitions

We introduce a terrain following coordinate system with a new vertical coordinate ξ. ξ-coordinate system is not deformable system. We use the relation between z and ξ as

$$\xi = \frac{z_{toa}(z - z_{sfc})}{z_{toa} - z_{sfc}},\tag{4.1}$$

Where z_{toa} is the top of the model domain and z_{sfc} is the surface height, which depends on the horizontal location.

The metrics are defined as

$$G^{\frac{1}{2}} = \frac{\partial z}{\partial \xi},\tag{4.2}$$

$$J_{13}^{\xi} = \left(\frac{\partial \xi}{\partial x}\right)_z = -\frac{J_{13}^z}{J_{33}^z},\tag{4.3}$$

$$J_{23}^{\xi} = \left(\frac{\partial \xi}{\partial y}\right)_z = -\frac{J_{23}^z}{J_{33}^z},\tag{4.4}$$

$$J_{33}^{\xi} = \frac{\partial \xi}{\partial z} = \frac{1}{J_{33}^z},\tag{4.5}$$

where

$$J_{13}^z = \left(\frac{\partial z}{\partial x}\right)_{\xi},\tag{4.6}$$

$$J_{23}^z = \left(\frac{\partial z}{\partial y}\right)_{\xi},\tag{4.7}$$

$$J_{33}^z = G^{\frac{1}{2}}\tag{4.8}$$

If we use the Eqs.(4.1)-(4.5), we obtain following equations:

$$G^{\frac{1}{2}}\nabla\phi = \left[\left(\frac{\partial G^{\frac{1}{2}}\phi}{\partial x}\right)_\xi + \frac{\partial J_{13}^\xi G^{\frac{1}{2}}\phi}{\partial \xi}\right]\hat{\boldsymbol{e}}_x + \left[\left(\frac{\partial G^{\frac{1}{2}}\phi}{\partial y}\right)_\xi + \frac{\partial J_{23}^\xi G^{\frac{1}{2}}\phi}{\partial \xi}\right]\hat{\boldsymbol{e}}_y$$
$$+ \left[\frac{\partial J_{33}^\xi G^{\frac{1}{2}}\phi}{\partial \xi}\right]\hat{\boldsymbol{e}}_z, \tag{4.9}$$

$$G^{\frac{1}{2}}\nabla\cdot(\phi\mathbf{u}) = \left(\frac{\partial G^{\frac{1}{2}}\phi u}{\partial x}\right)_\xi + \left(\frac{\partial G^{\frac{1}{2}}\phi v}{\partial y}\right)_\xi + \frac{\partial G^{\frac{1}{2}}\phi\dot{\xi}}{\partial \xi} \tag{4.10}$$

where $\{\hat{\boldsymbol{e}}_x, \hat{\boldsymbol{e}}_y, \hat{\boldsymbol{e}}_z\}$ are unit vectors in Cartesian coordinate, and $\dot{\xi}$ is the vertical velocity component in the terrain following coordinate, giving by

$$\dot{\xi} \equiv \frac{d\xi}{dt} = J_{13}^\xi u + J_{23}^\xi v + J_{33}^\xi w. \tag{4.11}$$

4.2 Summary of modified equations in the dynamical process

Prognostic variables by multiplying $G^{\frac{1}{2}}$ are defined as

$$(\rho Q_v)_{i,j,k} = G^{\frac{1}{2}}_{i,j,k}(\rho q_v)_{i,j,k}, \tag{4.12}$$

$$(\rho Q_l)_{i,j,k} = G^{\frac{1}{2}}_{i,j,k}(\rho q_l)_{i,j,k}, \tag{4.13}$$

$$(\rho Q_s)_{i,j,k} = G^{\frac{1}{2}}_{i,j,k}(\rho q_s)_{i,j,k}, \tag{4.14}$$

$$R_{i,j,k} = G^{\frac{1}{2}}_{i,j,k}\rho_{i,j,k}, \tag{4.15}$$

$$(\rho U)_{i+\frac{1}{2},j,k} = G^{\frac{1}{2}}_{i+\frac{1}{2},j,k}(\rho u)_{i+\frac{1}{2},j,k}, \tag{4.16}$$

$$(\rho V)_{i,j+\frac{1}{2},k} = G^{\frac{1}{2}}_{i,j+\frac{1}{2},k}(\rho v)_{i,j+\frac{1}{2},k}, \tag{4.17}$$

$$(\rho W)_{i,j,k+\frac{1}{2}} = G^{\frac{1}{2}}_{i,j,k+\frac{1}{2}}(\rho w)_{i,j,k+\frac{1}{2}}, \tag{4.18}$$

$$(\rho\Theta)_{i,j,k} = G^{\frac{1}{2}}_{i,j,k}(\rho\theta)_{i,j,k}, \tag{4.19}$$

$$P_{i,j,k} = G^{\frac{1}{2}}_{i,j,k}p_{i,j,k}. \tag{4.20}$$

Eqs.(2.67)-(2.72) are modified using Eqs.(4.9)-(4.11),

$$\frac{\partial \rho Q_v}{\partial t} + \frac{\partial}{\partial x_j}\left(\rho Q_v u_j\right) = 0, \tag{4.21}$$

$$\frac{\partial \rho Q_l}{\partial t} + \frac{\partial}{\partial x_j}\left(\rho Q_l u_j\right) = 0, \tag{4.22}$$

$$\frac{\partial \rho Q_s}{\partial t} + \frac{\partial}{\partial x_j}\left(\rho Q_s u_j\right) = 0, \tag{4.23}$$

$$\frac{\partial R}{\partial t} + \frac{\partial}{\partial x_j}\left(R u_j\right) = 0, \tag{4.24}$$

$$\frac{\partial \rho U}{\partial t} + \frac{\partial}{\partial x_j}\left(\rho U u_j\right) = -\left(\frac{\partial P}{\partial x}\right)_\xi - \frac{\partial J_{13}^\xi P}{\partial \xi}, \tag{4.25}$$

$$\frac{\partial \rho V}{\partial t} + \frac{\partial}{\partial x_j}\left(\rho V u_j\right) = -\left(\frac{\partial P}{\partial y}\right)_\xi - \frac{\partial J_{23}^\xi P}{\partial \xi}, \tag{4.26}$$

$$\frac{\partial \rho W}{\partial t} + \frac{\partial}{\partial x_j}\left(\rho W u_j\right) = -\frac{\partial J_{33}^\xi P}{\partial \xi} - Rg, \tag{4.27}$$

$$\frac{\partial \rho \Theta}{\partial t} + \frac{\partial}{\partial x_j}\left(\rho \Theta u_j\right) = 0, \tag{4.28}$$

where Einstein summation has been used to implicitly sum over repeated indices, and $(x_1, x_2, x_3) = (x, y, \xi)$, $(u_1, u_2, u_3) = (u, v, \dot{\xi})$.

4.3 Spatial descretization

4.3.1 Continuity equation

$$
\begin{aligned}
\left(\frac{\partial R}{\partial t}\right)_{i,j,k} = -\Bigg[& \frac{(\rho U)_{i+\frac{1}{2},j,k} - (\rho U)_{i-\frac{1}{2},j,k}}{\Delta x} \\
& + \frac{(\rho V)_{i,j+\frac{1}{2},k} - (\rho V)_{i,j-\frac{1}{2},k}}{\Delta y} \\
& + \frac{(J_{13}^\xi)_{i,j,k+\frac{1}{2}} \overline{\widetilde{(\rho U)}}^{xz}_{i,j,k+\frac{1}{2}} - (J_{13}^\xi)_{i,j,k-\frac{1}{2}} \overline{\widetilde{(\rho U)}}^{xz}_{i,j,k-\frac{1}{2}}}{\Delta \xi} \\
& + \frac{(J_{23}^\xi)_{i,j,k+\frac{1}{2}} \overline{\widetilde{(\rho V)}}^{yz}_{i,j,k+\frac{1}{2}} - (J_{23}^\xi)_{i,j,k-\frac{1}{2}} \overline{\widetilde{(\rho V)}}^{yz}_{i,j,k-\frac{1}{2}}}{\Delta \xi} \\
& + \frac{(J_{33}^\xi)_{i,j,k+\frac{1}{2}} (\rho W)_{i,j,k+\frac{1}{2}} - (J_{33}^\xi)_{i,j,k+\frac{1}{2}} (\rho W)_{i,j,k-\frac{1}{2}}}{\Delta \xi} \Bigg]
\end{aligned} \tag{4.29}
$$

where

$$\overline{\widetilde{(\rho U)}}^{xz}_{i,j,k+\frac{1}{2}} = G^{\frac{1}{2}}_{i,j,k+\frac{1}{2}} \frac{\widetilde{(\rho u)}^x_{i,j,k+1} + \widetilde{(\rho u)}^x_{i,j,k}}{2}, \tag{4.30}$$

$$\overline{\widetilde{(\rho V)}}^{yz}_{i,j,k+\frac{1}{2}} = G^{\frac{1}{2}}_{i,j,k+\frac{1}{2}} \frac{\widetilde{(\rho v)}^y_{i,j,k+1} + \widetilde{(\rho v)}^y_{i,j,k}}{2}, \tag{4.31}$$

$\widetilde{(\rho u)}^x_{i,j,k}$ and $\widetilde{(\rho v)}^y_{i,j,k}$ are obtained by same manner in eq.(3.20)

4.3.2 Momentum equations

$$
\left(\frac{\partial \rho U}{\partial t}\right)_{i+\frac{1}{2},j,k} = -\left[\frac{\widetilde{(\rho U)}^{x}_{i+1,j,k}\,\overline{u}_{i+1,j,k} - \widetilde{(\rho U)}^{x}_{i,j,k}\,\overline{u}_{i,j,k}}{\Delta x}\right.
$$

$$
+ \frac{\widetilde{(\rho U)}^{y}_{i+\frac{1}{2},j+\frac{1}{2},k}\,\overline{v}_{i+\frac{1}{2},j+\frac{1}{2},k} - \widetilde{(\rho U)}^{y}_{i+\frac{1}{2},j-\frac{1}{2},k}\,\overline{v}_{i+\frac{1}{2},j-\frac{1}{2},k}}{\Delta y}
$$

$$
+ \frac{(J^{\xi}_{13})_{i+\frac{1}{2},j,k+\frac{1}{2}}\,\widetilde{(\rho U)}^{z}_{i+\frac{1}{2},j,k+\frac{1}{2}}\,\overline{\overline{u}}^{z}_{i+\frac{1}{2},j,k+\frac{1}{2}} - (J^{\xi}_{13})_{i+\frac{1}{2},j,k-\frac{1}{2}}\,\widetilde{(\rho U)}^{z}_{i+\frac{1}{2},j,k-\frac{1}{2}}\,\overline{\overline{u}}^{z}_{i+\frac{1}{2},j,k-\frac{1}{2}}}{\Delta \xi}
$$

$$
+ \frac{(J^{\xi}_{23})_{i+\frac{1}{2},j,k+\frac{1}{2}}\,\widetilde{(\rho U)}^{z}_{i+\frac{1}{2},j,k+\frac{1}{2}}\,\overline{\overline{v}^{y}}^{xz}_{i+\frac{1}{2},j,k+\frac{1}{2}} - (J^{\xi}_{23})_{i+\frac{1}{2},j,k-\frac{1}{2}}\,\widetilde{(\rho U)}^{z}_{i+\frac{1}{2},j,k-\frac{1}{2}}\,\overline{\overline{v}^{y}}^{xz}_{i+\frac{1}{2},j,k-\frac{1}{2}}}{\Delta \xi}
$$

$$
+ \frac{(J^{\xi}_{33})_{i+\frac{1}{2},j,k+\frac{1}{2}}\,\widetilde{(\rho U)}^{z}_{i+\frac{1}{2},j,k+\frac{1}{2}}\,\overline{\overline{w}}^{x}_{i+\frac{1}{2},j,k+\frac{1}{2}} - (J^{\xi}_{33})_{i+\frac{1}{2},j,k-\frac{1}{2}}\,\widetilde{(\rho U)}^{z}_{i+\frac{1}{2},j,k-\frac{1}{2}}\,\overline{\overline{w}}^{x}_{i+\frac{1}{2},j,k-\frac{1}{2}}}{\Delta \xi}
$$

$$
+ \frac{P_{i+1,j,k} - P_{i,j,k}}{\Delta x}
$$

$$
\left.+ \frac{(J^{\xi}_{13})_{i+\frac{1}{2},j,k+\frac{1}{2}}\,\overline{P}^{xz}_{i+\frac{1}{2},j,k+\frac{1}{2}} - (J^{\xi}_{13})_{i+\frac{1}{2},j,k-\frac{1}{2}}\,\overline{P}^{xz}_{i+\frac{1}{2},j,k-\frac{1}{2}}}{\Delta \xi}\right],
\tag{4.32}
$$

where $\widetilde{(\rho U)}^{x}_{i,j,k}$, $\widetilde{(\rho U)}^{y}_{i+\frac{1}{2},j+\frac{1}{2},k}$ and $\widetilde{(\rho U)}^{z}_{i+\frac{1}{2},j,k+\frac{1}{2}}$ is obtained according to the method of eq(3.20)-(3.22). The velocities at the cell wall for the staggered control volume to x direction are defined by eq(3.23)-(3.25). $\overline{\overline{u}}^{z}$ and $\overline{\overline{v}^{y}}^{xz}$ are defined as

$$
\overline{\overline{u}}^{z}_{i+\frac{1}{2},j,k+\frac{1}{2}} = \frac{\overline{u}_{i+\frac{1}{2},j,k+1} + \overline{u}_{i+\frac{1}{2},j,k}}{2},
\tag{4.33}
$$

$$
\overline{\overline{v}^{y}}^{xz}_{i+\frac{1}{2},j,k+\frac{1}{2}} = \frac{\overline{v}^{y}_{i+1,j,k+1} + \overline{v}^{y}_{i+1,j,k} + \overline{v}^{y}_{i,j,k+1} + \overline{v}^{y}_{i,j,k}}{4}.
\tag{4.34}
$$

$\overline{P}^{xz}$ is defined as

$$
\overline{P}^{xz}_{i+\frac{1}{2},j,k+\frac{1}{2}} = G^{\frac{1}{2}}_{i+\frac{1}{2},j,k+\frac{1}{2}}\frac{p_{i+1,j,k+1} + p_{i+1,j,k} + p_{i,j,k+1} + p_{i,j,k}}{4}.
\tag{4.35}
$$

The momentum equations in the y and z directions are descretized in the

same way:

$$
\left(\frac{\partial \rho V}{\partial t}\right)_{i,j+\frac{1}{2},k} = -\left[\frac{\widetilde{(\rho V)}_{i+\frac{1}{2},j+\frac{1}{2},k}^{x}\,\overline{u}_{i+\frac{1}{2},j+\frac{1}{2},k} - \widetilde{(\rho V)}_{i-\frac{1}{2},j+\frac{1}{2},k}^{x}\,\overline{u}_{i-\frac{1}{2},j+\frac{1}{2},k}}{\Delta x}\right.
$$

$$
+\frac{\widetilde{(\rho V)}_{i,j+1,k}^{y}\,\overline{v}_{i,j+1,k} - \widetilde{(\rho V)}_{i,j,k}^{y}\,\overline{v}_{i,j,k}}{\Delta y}
$$

$$
+\frac{(J_{13}^{\xi})_{i,j+\frac{1}{2},k+\frac{1}{2}}\widetilde{(\rho V)}_{i,j+\frac{1}{2},k+\frac{1}{2}}^{z}\,\overline{\overline{u^x}}_{i,j+\frac{1}{2},k+\frac{1}{2}}^{yz} - (J_{13}^{\xi})_{i,j+\frac{1}{2},k-\frac{1}{2}}\widetilde{(\rho V)}_{i,j+\frac{1}{2},k-\frac{1}{2}}^{z}\,\overline{\overline{u^x}}_{i,j+\frac{1}{2},k-\frac{1}{2}}^{yz}}{\Delta \xi}
$$

$$
+\frac{(J_{23}^{\xi})_{i,j+\frac{1}{2},k+\frac{1}{2}}\widetilde{(\rho V)}_{i,j+\frac{1}{2},k+\frac{1}{2}}^{z}\,\overline{\overline{v}}_{i,j+\frac{1}{2},k+\frac{1}{2}}^{z} - (J_{23}^{\xi})_{i,j+\frac{1}{2},k-\frac{1}{2}}\widetilde{(\rho V)}_{i,j+\frac{1}{2},k-\frac{1}{2}}^{z}\,\overline{\overline{v}}_{i,j+\frac{1}{2},k-\frac{1}{2}}^{z}}{\Delta \xi}
$$

$$
+\frac{(J_{33}^{\xi})_{i,j+\frac{1}{2},k+\frac{1}{2}}\widetilde{(\rho V)}_{i,j+\frac{1}{2},k+\frac{1}{2}}^{z}\,\overline{\overline{w}}_{i,j+\frac{1}{2},k+\frac{1}{2}}^{y} - (J_{33}^{\xi})_{i,j+\frac{1}{2},k-\frac{1}{2}}\widetilde{(\rho V)}_{i,j+\frac{1}{2},k-\frac{1}{2}}^{z}\,\overline{\overline{w}}_{i,j+\frac{1}{2},k-\frac{1}{2}}^{y}}{\Delta \xi}
$$

$$
+\frac{P_{i,j+1,k} - P_{i,j,k}}{\Delta y}
$$

$$
\left.+\frac{(J_{23}^{\xi})_{i,j+\frac{1}{2},k+\frac{1}{2}}\overline{P}_{i,j+\frac{1}{2},k+\frac{1}{2}}^{yz} - (J_{23}^{\xi})_{i,j+\frac{1}{2},k-\frac{1}{2}}\overline{P}_{i,j+\frac{1}{2},k-\frac{1}{2}}^{yz}}{\Delta \xi}\right],
$$

$$(4.36)$$

$$
\left(\frac{\partial \rho W}{\partial t}\right)_{i,j,k+\frac{1}{2}} = -\left[\frac{\widetilde{(\rho W)}_{i+\frac{1}{2},j,k+\frac{1}{2}}^{x}\,\overline{u}_{i+\frac{1}{2},j,k+\frac{1}{2}} - \widetilde{(\rho W)}_{i-\frac{1}{2},j,k+\frac{1}{2}}^{x}\,\overline{u}_{i-\frac{1}{2},j,k+\frac{1}{2}}}{\Delta x}\right.
$$

$$
+\frac{\widetilde{(\rho W)}_{i,j+\frac{1}{2},k+\frac{1}{2}}^{y}\,\overline{v}_{i,j+\frac{1}{2},k+\frac{1}{2}} - \widetilde{(\rho W)}_{i,j-\frac{1}{2},k+\frac{1}{2}}^{y}\,\overline{v}_{i,j-\frac{1}{2},k+\frac{1}{2}}}{\Delta y}
$$

$$
+\frac{(J_{13}^{\xi})_{i,j,k+1}\widetilde{(\rho W)}_{i,j,k+1}^{z}\,\overline{u}_{i,j,k+1}^{x} - (J_{13}^{\xi})_{i,j,k}\widetilde{(\rho W)}_{i,j,k}^{z}\,\overline{u}_{i,j,k}^{x}}{\Delta \xi}
$$

$$
+\frac{(J_{23}^{\xi})_{i,j,k+1}\widetilde{(\rho W)}_{i,j,k+1}^{z}\,\overline{v}_{i,j,k+1}^{y} - (J_{23}^{\xi})_{i,j,k}\widetilde{(\rho W)}_{i,j,k}^{z}\,\overline{v}_{i,j,k}^{y}}{\Delta \xi}
$$

$$
+\frac{(J_{33}^{\xi})_{i,j,k+1}\widetilde{(\rho W)}_{i,j,k+1}^{z}\,\overline{w}_{i,j,k+1}^{z} - (J_{33}^{\xi})_{i,j,k}\widetilde{(\rho W)}_{i,j,k}^{z}\,\overline{w}_{i,j,k}^{z}}{\Delta \xi}
$$

$$
\left.+\frac{(J_{33}^{\xi})_{i,j,k+1}P_{i,j,k+1} - (J_{33}^{\xi})_{i,j,k}P_{i,j,k}}{\Delta \xi}\right].
$$

$$(4.37)$$

4.3.3 Energy equation

$$
\left(\frac{\partial \rho \Theta}{\partial t}\right)_{i,j,k} = -\Bigg[\frac{(\rho U)_{i+\frac{1}{2},j,k}\overline{\theta}_{i+\frac{1}{2},j,k} - (\rho U)_{i-\frac{1}{2},j,k}\overline{\theta}_{i-\frac{1}{2},j,k}}{\Delta x}
$$

$$
+ \frac{(\rho V)_{i,j+\frac{1}{2},k}\overline{\theta}_{i,j+\frac{1}{2},k} - (\rho V)_{i,j-\frac{1}{2},k}\overline{\theta}_{i,j-\frac{1}{2},k}}{\Delta y}
$$

$$
+ \frac{(J_{13}^{\xi})_{i,j,k+\frac{1}{2}}\overline{\widetilde{(\rho U)}}^{xz}_{i,j,k+\frac{1}{2}}\overline{\theta}_{i,j,k+\frac{1}{2}} - (J_{13}^{\xi})_{i,j,k-\frac{1}{2}}\overline{\widetilde{(\rho U)}}^{xz}_{i,j,k-\frac{1}{2}}\overline{\theta}_{i,j,k-\frac{1}{2}}}{\Delta \xi}
$$

$$
+ \frac{(J_{23}^{\xi})_{i,j,k+\frac{1}{2}}\overline{\widetilde{(\rho V)}}^{yz}_{i,j,k+\frac{1}{2}}\overline{\theta}_{i,j,k+\frac{1}{2}} - (J_{23}^{\xi})_{i,j,k-\frac{1}{2}}\overline{\widetilde{(\rho V)}}^{yz}_{i,j,k-\frac{1}{2}}\overline{\theta}_{i,j,k-\frac{1}{2}}}{\Delta \xi}
$$

$$
+ \frac{(J_{33}^{\xi})_{i,j,k+\frac{1}{2}}(\rho W)_{i,j,k+\frac{1}{2}}\overline{\theta}_{i,j,k+\frac{1}{2}} - (J_{33}^{\xi})_{i,j,k+\frac{1}{2}}(\rho W)_{i,j,k-\frac{1}{2}}\overline{\theta}_{i,j,k-\frac{1}{2}}}{\Delta \xi} \Bigg]
$$

$$(4.38)$$

where $\overline{\theta}_{i+\frac{1}{2},j,k}$, $\overline{\theta}_{i,j+\frac{1}{2},k}$ and $\overline{\theta}_{i,j,k+\frac{1}{2}}$ are obtained according to the method of eq(3.29)-(3.31).

Chapter 5

Map factor

Corresponding author : Seiya Nishizawa

5.1 Coordinate transform

A orthogonal rectangular coordinate (x, y, z). A orthogonal curvilinear coordinate (ξ, η, ζ).

The transform is defined by

$$\boldsymbol{e}_\xi = \frac{\partial x}{\partial \xi}\hat{\boldsymbol{e}}_x + \frac{\partial y}{\partial \xi}\hat{\boldsymbol{e}}_y + \frac{\partial z}{\partial \xi}\hat{\boldsymbol{e}}_z, \tag{5.1}$$

$$\boldsymbol{e}_\eta = \frac{\partial x}{\partial \eta}\hat{\boldsymbol{e}}_x + \frac{\partial y}{\partial \eta}\hat{\boldsymbol{e}}_y + \frac{\partial z}{\partial \eta}\hat{\boldsymbol{e}}_z, \tag{5.2}$$

$$\boldsymbol{e}_\zeta = \frac{\partial x}{\partial \zeta}\hat{\boldsymbol{e}}_x + \frac{\partial y}{\partial \zeta}\hat{\boldsymbol{e}}_y + \frac{\partial z}{\partial \zeta}\hat{\boldsymbol{e}}_z. \tag{5.3}$$

Reverse transform is

$$\hat{\boldsymbol{e}}_x = \frac{\partial \xi}{\partial x}\boldsymbol{e}_\xi + \frac{\partial \eta}{\partial x}\boldsymbol{e}_\eta + \frac{\partial \zeta}{\partial x}\boldsymbol{e}_\zeta, \tag{5.4}$$

$$\hat{\boldsymbol{e}}_y = \frac{\partial \eta}{\partial y}\boldsymbol{e}_\xi + \frac{\partial \eta}{\partial y}\boldsymbol{e}_\eta + \frac{\partial \zeta}{\partial y}\boldsymbol{e}_\zeta, \tag{5.5}$$

$$\hat{\boldsymbol{e}}_z = \frac{\partial \zeta}{\partial z}\boldsymbol{e}_\xi + \frac{\partial \eta}{\partial z}\boldsymbol{e}_\eta + \frac{\partial \zeta}{\partial z}\boldsymbol{e}_\zeta. \tag{5.6}$$

The Jacobian matrix is $\{\frac{\partial \xi^k}{\partial x^i}\}$.

The reverse transform after the transform of the transform after the reverse transform make a vector to the original vector;

$$\frac{\partial \xi^k}{\partial x^i}\frac{\partial x^i}{\partial \xi^l} = \delta_l^k, \tag{5.7}$$

$$\frac{\partial x^i}{\partial \xi^k}\frac{\partial \xi^k}{\partial x^j} = \delta_j^i, \tag{5.8}$$

where index which appares upper and lower suffix in a single term implies summation of the term over set $1, 2, 3$ (Einstein notation).

Spatial partial derivative is transformed with the Jacobian matrix (covariant transform);

$$\frac{\partial}{\partial \xi^k} = \frac{\partial x^i}{\partial \xi^k} \frac{\partial}{\partial x^i}, \qquad (5.9)$$

$$\frac{\partial}{\partial x^i} = \frac{\partial \xi^k}{\partial x^i} \frac{\partial}{\partial \xi^k}. \qquad (5.10)$$

Velocity is transformed with the inverse of the Jacobian matrix (contravariant transform);

$$d\xi^k = \frac{\partial \xi^k}{\partial x^i} dx^i, \qquad (5.11)$$

$$dx^i = \frac{\partial x^i}{\partial \xi^k} d\xi^k. \qquad (5.12)$$

The metric tensor, g_{kl} is defined by

$$g_{kl} = \boldsymbol{e}_k \cdot \boldsymbol{e}_l = \left(\frac{\partial x^i}{\partial \xi_k} \hat{\boldsymbol{e}}_i \right) \cdot \left(\frac{\partial x^j}{\partial \xi_l} \hat{\boldsymbol{e}}_j \right)$$

$$= \frac{\partial x^i}{\partial \xi_k} \frac{\partial x^i}{\partial \xi_l}. \qquad (5.13)$$

For orthogonal curvilinear coordinates, the matrix g_{kl} is diagonal. Metric factor, h_k is defined as

$$h_k^2 = g_{kk} = \sum_i \left(\frac{\partial x^i}{\partial \xi_k} \right)^2. \qquad (5.14)$$

Here we define the matrix, $\boldsymbol{E}_\xi$ is

$$\boldsymbol{E}_\xi = (\boldsymbol{e}_\xi \, \boldsymbol{e}_\eta \, \boldsymbol{e}_\zeta) \cdot \boldsymbol{H}^{-1} = \boldsymbol{E}_x \cdot \left\{ \frac{\partial x^i}{\partial \xi^k} \right\} \cdot \boldsymbol{H}^{-1}, \qquad (5.15)$$

where $\boldsymbol{E}_x = (\hat{\boldsymbol{e}}_x \, \hat{\boldsymbol{e}}_y \, \hat{\boldsymbol{e}}_z)$, and

$$\boldsymbol{H} = \begin{pmatrix} h_1 & 0 & 0 \\ 0 & h_2 & 0 \\ 0 & 0 & h_3 \end{pmatrix}. \qquad (5.16)$$

The vector $\frac{1}{h_k} \boldsymbol{e}_k$ is unit vector and orthogonal each other, so the inverse of the $\boldsymbol{E}_\xi$ is $\boldsymbol{E}_\xi^T$.

$$\left(\boldsymbol{E}_x \cdot \left\{ \frac{\partial x^i}{\partial \xi^k} \right\} \cdot \boldsymbol{H}^{-1} \right)^{-1} = \left(\boldsymbol{E}_x \cdot \left\{ \frac{\partial x^i}{\partial \xi^k} \right\} \cdot \boldsymbol{H}^{-1} \right)^T,$$

$$\boldsymbol{H} \cdot \left\{ \frac{\partial \xi^i}{\partial x^k} \right\} \cdot \boldsymbol{E}_x^{-1} = \boldsymbol{H}^{-1} \cdot \left\{ \frac{\partial x^i}{\partial \xi^k} \right\}^T \cdot \boldsymbol{E}_x^T,$$

$$\left\{ \frac{\partial \xi^i}{\partial x^k} \right\} = \boldsymbol{H}^{-2} \cdot \left\{ \frac{\partial x^i}{\partial \xi^k} \right\}^T \cdot \boldsymbol{E}_x^T \cdot \boldsymbol{E}_x$$

$$= \boldsymbol{H}^{-2} \cdot \left\{ \frac{\partial x^k}{\partial \xi^i} \right\}. \qquad (5.17)$$

34

That is

$$\frac{\partial \xi^k}{\partial x^i} = \frac{1}{h_k^2} \frac{\partial x^i}{\partial \xi^k}. \tag{5.18}$$

5.2 Governing equations

5.2.1 Continuous equation

Divergence of $\rho \boldsymbol{u}$ is

$$
\begin{aligned}
\frac{\partial}{\partial x^i}(\rho dx^i) &= \frac{\partial \xi^k}{\partial x^i} \frac{\partial}{\partial \xi^k} \left(\rho \frac{\partial x^i}{\partial \xi^l} d\xi^l \right) \\
&= \frac{\partial \xi^k}{\partial x^i} \frac{\partial x^i}{\partial \xi^l} \frac{\partial}{\partial \xi^k}(\rho d\xi^l) + \rho d\xi^l \frac{\partial \xi^k}{\partial x^i} \frac{\partial^2 x^i}{\partial \xi^k \partial \xi^l} \\
&= \frac{\partial}{\partial \xi^k}(\rho d\xi^k) + \sum_k \frac{1}{h_k^2} \rho d\xi^l \frac{\partial x^i}{\partial \xi^k} \frac{\partial^2 x^i}{\partial \xi^k \partial \xi^l} \\
&= \frac{\partial}{\partial \xi^k}(\rho d\xi^k) + \sum_k \frac{1}{2h_k^2} \rho d\xi^l \frac{\partial}{\partial \xi^l} \left(\frac{\partial x^i}{\partial \xi^k} \right)^2 \\
&= \frac{\partial}{\partial \xi^k}(\rho d\xi^k) + \sum_k \frac{1}{2h_k^2} \rho d\xi^l \frac{\partial}{\partial \xi^l} h_k^2 \\
&= \frac{\partial}{\partial \xi^k}(\rho d\xi^k) + \sum_k \frac{1}{2} \rho d\xi^l \frac{\partial}{\partial \xi^l} \ln h_k^2 \\
&= \frac{\partial}{\partial \xi^k}(\rho d\xi^k) + \rho d\xi^k \frac{\partial}{\partial \xi^k} \ln(\prod_l h_l) \\
&= J \left\{ J^{-1} \frac{\partial}{\partial \xi^k}(\rho d\xi^l) + \rho d\xi^k \frac{\partial}{\partial \xi^k} J^{-1} \right\} \\
&= J \frac{\partial}{\partial \xi^k}(J^{-1} \rho d\xi^k),
\end{aligned} \tag{5.19}
$$

where J is the Jacobian of the Jacobian matrix and

$$J = \frac{1}{\prod_k h_k}. \tag{5.20}$$

The continuous equation is

$$\frac{\partial \rho}{\partial t} + J \frac{\partial}{\partial \xi^k} \frac{\rho d\xi^k}{J} = 0. \tag{5.21}$$

5.2.2 Momentum equation

$$\frac{\partial \rho d\xi^k}{\partial t} = \frac{\partial \xi^k}{\partial x^i} \frac{\partial \rho dx^i}{\partial t}. \tag{5.22}$$

Advection term

$$\frac{\partial \xi^k}{\partial x^i}\frac{\partial \rho dx^i dx^j}{\partial x^j}$$

$$= \frac{\partial \xi^k}{\partial x^i}\left(dx^j \frac{\partial \rho dx^i}{\partial x^j} + \rho dx^i \frac{\partial dx^j}{\partial x^j}\right)$$

$$= \frac{\partial \xi^k}{\partial x^i}\left(\frac{\partial x^j}{\partial \xi^l}d\xi^l\right)\frac{\partial \xi^m}{\partial x^j}\frac{\partial}{\partial \xi^m}\left(\rho \frac{\partial x^i}{\partial \xi^n}d\xi^n\right) + \frac{\partial \xi^k}{\partial x^i}\rho\left(\frac{\partial x^i}{\partial \xi^l}d\xi^l\right)\frac{\partial \xi^m}{\partial x^j}\frac{\partial}{\partial \xi^m}\left(\frac{\partial x^j}{\partial \xi^n}d\xi^n\right)$$

$$= d\xi^l \frac{\partial \xi^k}{\partial x^i}\frac{\partial}{\partial \xi^l}\left(\rho \frac{\partial x^i}{\partial \xi^n}d\xi^n\right) + \rho d\xi^k \frac{\partial \xi^m}{\partial x^j}\frac{\partial}{\partial \xi^m}\left(\frac{\partial x^j}{\partial \xi^n}d\xi^n\right)$$

$$= d\xi^l \frac{\partial \xi^k}{\partial x^i}\left\{\frac{\partial x^i}{\partial \xi^n}\frac{\partial}{\partial \xi^l}\left(\rho d\xi^n\right) + \rho d\xi^n \frac{\partial^2 x^i}{\partial \xi^l \partial \xi^n}\right\} + \rho d\xi^k \frac{\partial \xi^m}{\partial x^j}\left(\frac{\partial x^j}{\partial \xi^n}\frac{\partial d\xi^n}{\partial \xi^m} + d\xi^n \frac{\partial^2 x^j}{\partial \xi^m \partial \xi^n}\right)$$

$$= d\xi^l \frac{\partial}{\partial \xi^l}\left(\rho d\xi^k\right) + \rho d\xi^l d\xi^n \frac{\partial \xi^k}{\partial x^i}\frac{\partial^2 x^i}{\partial \xi^l \partial \xi^n} + \rho d\xi^k \frac{\partial d\xi^m}{\partial \xi^m} + \rho d\xi^k d\xi^n \frac{\partial \xi^m}{\partial x^j}\frac{\partial^2 x^j}{\partial \xi^m \partial \xi^n}$$

$$= \frac{\partial}{\partial \xi^l}\left(\rho d\xi^k d\xi^l\right) + \rho d\xi^l d\xi^n \frac{\partial \xi^k}{\partial x^i}\frac{\partial^2 x^i}{\partial \xi^l \partial \xi^n} + \rho d\xi^k d\xi^l \frac{\partial \xi^m}{\partial x^i}\frac{\partial^2 x^i}{\partial \xi^l \partial \xi^m}$$

$$= J\left\{J^{-1}\frac{\partial}{\partial \xi^l}(\rho d\xi^k d\xi^l) + \rho d\xi^k d\xi^l \frac{\partial J^{-1}}{\partial \xi^l}\right\} + \rho d\xi^l d\xi^m \frac{\partial \xi^k}{\partial x^i}\frac{\partial^2 x^i}{\partial \xi^l \partial \xi^m}$$

$$= J\frac{\partial}{\partial \xi^l}J^{-1}\rho d\xi^k d\xi^l + \rho d\xi^l d\xi^m \Gamma^k_{lm}, \tag{5.23}$$

where Γ is the Christoffel symbols of the second kind, and

$$\Gamma^k_{lm} = \frac{\partial \xi^k}{\partial x^i}\frac{\partial^2 x^i}{\partial \xi^l \partial \xi^m}$$

$$= \frac{1}{2}g^{kn}\left(\frac{\partial g_{mn}}{\partial \xi^l} + \frac{\partial g_{ln}}{\partial \xi^m} - \frac{\partial g_{lm}}{\partial \xi^n}\right)$$

$$= \frac{1}{h_k^2}\left(h_k \frac{\partial h_k}{\partial \xi^l}\delta_{km} + h_k \frac{\partial h_k}{\partial \xi^m}\delta_{kl} - h_l \frac{\partial h_l}{\partial \xi^k}\delta_{lm}\right), \tag{5.24}$$

where $\{g^{kn}\}$ is inverse matrix of $\{g_{kn}\}$.

Coriolis term

$$\frac{\partial \xi^k}{\partial x^i}\epsilon^{ijp}f^j \rho dx^p = \epsilon^{klm}\frac{1}{h_k h_l h_m}\hat{f}^l d\xi^m, \tag{5.25}$$

where ϵ is the Levi-Civita symbol, and

$$\hat{f}^l = \frac{\partial \xi^l}{\partial x^j}f^j. \tag{5.26}$$

Pressure gradient term

$$\frac{\partial \xi^k}{\partial x^i}\frac{\partial p}{\partial x^i} = \frac{\partial \xi^k}{\partial x^i}\left(\frac{\partial \xi^l}{\partial x^i}\frac{\partial p}{\partial \xi^l}\right)$$

$$= \frac{1}{h_k^2}\frac{\partial x^i}{\partial \xi^k}\frac{\partial \xi^l}{\partial x^i}\frac{\partial p}{\partial \xi^l}$$

$$= \frac{1}{h_k^2}\frac{\partial p}{\partial \xi^k}. \tag{5.27}$$

After all, momentum equation is

$$\frac{\partial}{\partial t}\rho d\xi^k + J\frac{\partial}{\partial \xi^l}\left(J^{-1}\rho d\xi^k d\xi^l\right) + \rho d\xi^l d\xi^m \Gamma^k_{lm} + \epsilon^{klm}\frac{1}{h_k h_l h_m}\hat{f}^l \rho d\xi^m$$

$$= -\frac{1}{h_k^2}\frac{\partial p}{\partial \xi^k} + \rho g^p \frac{\partial \xi^k}{\partial x^p}. \tag{5.28}$$

5.3 Map factor

We introduce Map factor m, n.

$$\frac{1}{m}\frac{a+z}{a} = h_1, \tag{5.29}$$

$$\frac{1}{n}\frac{a+z}{a} = h_2, \tag{5.30}$$

$$1 = h_3, \tag{5.31}$$

where is a is radius of the planet. Assuming shallow atmospher,

$$m = h_1^{-1}, \tag{5.32}$$

$$n = h_2^{-1}. \tag{5.33}$$

Normalized velocity is defined as

$$\hat{u} = h_1\frac{d\xi}{dt} = \frac{1}{m}\frac{d\xi}{dt}, \tag{5.34}$$

$$\hat{v} = h_2\frac{d\eta}{dt} = \frac{1}{n}\frac{d\eta}{dt}, \tag{5.35}$$

$$\hat{w} = h_3\frac{d\zeta}{dt} = \frac{d\zeta}{dt}. \tag{5.36}$$

The continuous equation becomes

$$\frac{\partial \rho}{\partial t} + mn\frac{\partial}{\partial \xi}\frac{\rho\hat{u}}{n} + mn\frac{\partial}{\partial \eta}\frac{\rho\hat{v}}{m} + \frac{\partial}{\partial \zeta}\rho\hat{w} = 0 \tag{5.37}$$

The momentum equations are

$$\frac{\partial \rho\hat{u}^k}{\partial t} + mn\frac{\partial}{\partial \xi}\frac{\rho\hat{u}\hat{u}^k}{n} + mn\frac{\partial}{\partial \eta}\frac{\rho\hat{v}\hat{u}^k}{m} + \frac{\partial}{\partial \zeta}\rho\hat{w}\hat{u}^k$$

$$+ mm_k\rho\hat{u}\hat{u}^k\frac{\partial}{\partial \xi}\frac{1}{m_k} + nm_k\rho\hat{v}\hat{u}^k\frac{\partial}{\partial \eta}\frac{1}{m_k}$$

$$- mm_k\rho\hat{u}^2\frac{\partial}{\partial \xi^k}\frac{1}{m} - nm_k\rho\hat{v}^2\frac{\partial}{\partial \xi^k}\frac{1}{n} + \epsilon^{klm}m_l\hat{f}^l\rho\hat{u}^m$$

$$= -m_k\frac{\partial p}{\partial \zeta^k} + \rho g\delta_{3k}. \tag{5.38}$$

This equation can also be written as

$$\frac{\partial \rho u}{\partial t} + mn \frac{\partial}{\partial \xi} \frac{\rho u u}{n} + mn \frac{\partial}{\partial \eta} \frac{\rho u v}{m} + \frac{\partial}{\partial \zeta} \rho u w$$

$$- f\rho v - mn\rho v \left\{ v \frac{\partial}{\partial \xi} \left(\frac{1}{n} \right) - u \frac{\partial}{\partial \eta} \left(\frac{1}{m} \right) \right\} = -m \frac{\partial p}{\partial \xi}, \qquad (5.39)$$

$$\frac{\partial \rho v}{\partial t} + mn \frac{\partial}{\partial \xi} \frac{\rho u v}{n} + mn \frac{\partial}{\partial \eta} \frac{\rho v v}{m} + \frac{\partial}{\partial \zeta} \rho v w$$

$$+ f\rho u + mn\rho u \left\{ v \frac{\partial}{\partial \xi} \left(\frac{1}{n} \right) - u \frac{\partial}{\partial \eta} \left(\frac{1}{m} \right) \right\} = -n \frac{\partial p}{\partial \eta}, \qquad (5.40)$$

$$\frac{\partial \rho w}{\partial t} + mn \frac{\partial}{\partial \xi} \frac{\rho u w}{n} + mn \frac{\partial}{\partial \eta} \frac{\rho v w}{m} + \frac{\partial}{\partial \zeta} \rho w w = -\frac{\partial p}{\partial \zeta} - \rho g. \qquad (5.41)$$

The thermodynamic and tracer equations

$$\frac{\partial \rho \phi}{\partial t} + mn \frac{\partial}{\partial \xi} \frac{\rho \hat{u} \phi}{n} + mn \frac{\partial}{\partial \eta} \frac{\rho \hat{v} \phi}{m} + \frac{\partial \rho \hat{w} \phi}{\partial \zeta} = 0. \qquad (5.42)$$

Chapter 6

Horizontal explicit vertical implicit

Corresponding author : Seiya Nishizawa

6.1   Equations

$$\frac{\partial G^{\frac{1}{2}}\rho}{\partial t} = -\frac{\partial J_{33}G^{\frac{1}{2}}\rho w}{\partial \xi} + G^{\frac{1}{2}}S_\rho, \tag{6.1}$$

$$\frac{\partial G^{\frac{1}{2}}\rho w}{\partial t} = -\frac{\partial J_{33}G^{\frac{1}{2}}p}{\partial \xi} - G^{\frac{1}{2}}\rho g + G^{\frac{1}{2}}S_{\rho w}, \tag{6.2}$$

$$\frac{\partial G^{\frac{1}{2}}\rho\theta}{\partial t} = -\frac{\partial J_{33}G^{\frac{1}{2}}\rho w\theta}{\partial \xi} + G^{\frac{1}{2}}S_{\rho\theta}, \tag{6.3}$$

$$p = P_{00}\left(\frac{R\rho\theta}{P_{00}}\right)^{c_p/c_v}, \tag{6.4}$$

where

$$
\begin{aligned}
G^{\frac{1}{2}}S_\rho &= -G^{\frac{1}{2}}\frac{\partial \rho u}{\partial x} - G^{\frac{1}{2}}\frac{\partial \rho v}{\partial y} \\
&= -\frac{\partial G^{\frac{1}{2}}\rho u}{\partial x^*} - \frac{\partial G^{\frac{1}{2}}\rho v}{\partial y^*} - \frac{\partial J_{13}G^{\frac{1}{2}}\rho u + J_{23}G^{\frac{1}{2}}\rho v}{\partial \xi},
\end{aligned} \tag{6.5}
$$

$$
\begin{aligned}
G^{\frac{1}{2}}S_{\rho w} &= -G^{\frac{1}{2}}\frac{\partial u\rho w}{\partial x} - G^{\frac{1}{2}}\frac{\partial v\rho w}{\partial y} - G^{\frac{1}{2}}\frac{\partial w\rho w}{\partial z} \\
&= -\frac{\partial G^{\frac{1}{2}}u\rho w}{\partial x^*} - \frac{\partial G^{\frac{1}{2}}v\rho w}{\partial y^*} - \frac{\partial}{\partial \xi}(J_{13}G^{\frac{1}{2}}u\rho w + J_{23}G^{\frac{1}{2}}v\rho w + J_{33}G^{\frac{1}{2}}w\rho w),
\end{aligned} \tag{6.6}
$$

$$
\begin{aligned}
G^{\frac{1}{2}}S_{\rho\theta} &= -G^{\frac{1}{2}}\frac{\partial u\rho\theta}{\partial x} - G^{\frac{1}{2}}\frac{\partial v\rho\theta}{\partial y} \\
&= -\frac{\partial G^{\frac{1}{2}}u\rho\theta}{\partial x^*} - \frac{\partial G^{\frac{1}{2}}v\rho\theta}{\partial y^*} - \frac{\partial J_{13}G^{\frac{1}{2}}u\rho\theta + J_{23}G^{\frac{1}{2}}v\rho\theta}{\partial \xi}.
\end{aligned} \tag{6.7}
$$

6.2 Discretization

For the temporal discretization, backward temporal integrations are employed for the terms related to acoustic wave in vertical direction.

$$\frac{\rho^{n+1} - \rho^n}{\Delta t} = -G^{-\frac{1}{2}} \frac{\partial}{\partial \xi} \{ J_{33} G^{\frac{1}{2}} (\rho w)^{n+1} \} + S_\rho^n, \tag{6.8}$$

$$\frac{(\rho w)^{n+1} - (\rho w)^n}{\Delta t} = -G^{-\frac{1}{2}} \frac{\partial}{\partial \xi} (J_{33} G^{\frac{1}{2}} p^{n+1}) - g\rho^{n+1} + S_{\rho w}^n, \tag{6.9}$$

$$\frac{p^{n+1} - p^n}{\Delta t} = \frac{c_p^n}{c_v^n} \frac{p^n}{(\rho\theta)^n} \frac{\partial \rho\theta}{\partial t}, \tag{6.10}$$

$$\frac{\partial \rho\theta}{\partial t} = -G^{-\frac{1}{2}} \frac{\partial}{\partial \xi} \{ J_{33} G^{\frac{1}{2}} \theta^n (\rho w)^{n+1} \} + S_{\rho\theta}^n. \tag{6.11}$$

Note that the potential temperature at previous step, θ^n, is used.

Eliminating p^{n+1}, $(\rho\theta)^{n+1}$, and ρ^{n+1}, the Helmholtz equation for $(\rho w)^{n+1}$ is obtained:

$$(\rho w)^{n+1} - \frac{\Delta t^2 g}{G^{\frac{1}{2}}} \frac{\partial}{\partial \xi} \{ J_{33} G^{\frac{1}{2}} (\rho w)^{n+1} \} - \frac{\Delta t^2}{G^{\frac{1}{2}}} \frac{\partial}{\partial \xi} \left(J_{33} \frac{c_p^n p^n}{c_v^n (\rho\theta)^n} \frac{\partial J_{33} G^{\frac{1}{2}} \theta^n (\rho w)^{n+1}}{\partial \xi} \right)$$

$$= (\rho w)^n - \frac{\Delta t}{G^{\frac{1}{2}}} \frac{\partial}{\partial \xi} \left\{ J_{33} G^{\frac{1}{2}} p^n \left(1 + \frac{\Delta t c_p^n S_{\rho\theta}^n}{c_v^n (\rho\theta)^n} \right) \right\} - \Delta t g(\rho^n + \Delta t S_\rho^n) + \Delta t S_{\rho w}^n. \tag{6.12}$$

Vertical differentials are discretized as follows:

$$(\rho w)_{k+1/2}^{n+1} - \frac{\Delta t^2 g}{(\Delta z_{k+1} + \Delta z_k) G_{k+1/2}^{\frac{1}{2}}} \left\{ J_{33} G^{\frac{1}{2}} (\rho w)_{k+3/2}^{n+1} - J_{33} G^{\frac{1}{2}} (\rho w)_{k-1/2}^{n+1} \right\}$$

$$- \frac{\Delta t^2}{\Delta z_{k+1/2} G_{k+1/2}^{\frac{1}{2}}} \left\{ \left(J_{33} \frac{c_p p}{c_v \rho\theta} \right)_{k+1} \frac{J_{33} G^{\frac{1}{2}} (\rho w)_{k+3/2} \hat{\theta}_{k+3/2} - J_{33} G^{\frac{1}{2}} (\rho w)_{k+1/2} \hat{\theta}_{k+1/2}}{\Delta z_{k+1}} \right.$$

$$\left. - \left(J_{33} \frac{c_p p}{c_v \rho\theta} \right)_k \frac{J_{33} G^{\frac{1}{2}} (\rho w)_{k+1/2} \hat{\theta}_{k+1/2} - J_{33} G^{\frac{1}{2}} (\rho w)_{k-1/2} \hat{\theta}_{k-1/2}}{\Delta z_k} \right\}$$

$$= (\rho w)_{k+1/2}^n$$

$$- \frac{\Delta t}{\Delta z_{k+1/2} G_{k+1/2}^{\frac{1}{2}}} \left\{ J_{33} G^{\frac{1}{2}} p_{k+1} \left(1 + \frac{\Delta t c_p S_{\rho\theta}}{c_v \rho\theta} \right)_{k+1} - J_{33} G^{\frac{1}{2}} p_k \left(1 + \frac{\Delta t c_p S_{\rho\theta}}{c_v \rho\theta} \right)_k \right\}$$

$$- \frac{\Delta t g}{2} \{ (\rho + \Delta t S_\rho)_{k+1} + (\rho + \Delta t S_\rho)_k \} + \Delta t S_{\rho w}, \tag{6.13}$$

where

$$\hat{\theta}_{k+1/2} = \frac{1}{12} \left(-\theta_{k+2} + 7\theta_{k+1} + 7\theta_k - \theta_{k-1} \right). \tag{6.14}$$

Finally, we obtained

$$-\frac{1}{G_{k+1/2}^{\frac{1}{2}}}\left\{\frac{\hat{\theta}_{k+3/2}}{\Delta z_{k+1/2}}A_{k+1}+B_{k+1/2}\right\}(\rho w)_{k+3/2}^{n+1} \tag{6.15}$$

$$+\left\{1+\frac{\hat{\theta}_{k+1/2}}{\Delta z_{k+1/2}G_{k+1/2}^{\frac{1}{2}}}(A_{k+1}+A_k)\right\}(\rho w)_{k+1/2}^{n+1} \tag{6.16}$$

$$-\frac{1}{G_{k+1/2}^{\frac{1}{2}}}\left\{\frac{\hat{\theta}_{k-1/2}}{\Delta z_{k+1/2}}A_k-B_{k+1/2}\right\}(\rho w)_{k-1/2}^{n+1} \tag{6.17}$$

$$=C_{k+1/2}, \tag{6.18}$$

where

$$A_k=\frac{\Delta t^2 J_{33}G^{\frac{1}{2}}}{\Delta z_k}\left(J_{33}\frac{c_p p}{c_v \rho \theta}\right)_k, \tag{6.19}$$

$$B_{k+1/2}=\frac{\Delta t^2 g J_{33}G^{\frac{1}{2}}}{\Delta z_{k+1}+\Delta z_k}, \tag{6.20}$$

$$C_{k+1/2}=(\rho w)_{k+1/2}^n$$

$$-\Delta t\frac{J_{33}G^{\frac{1}{2}}p_{k+1}\left(1+\Delta t\frac{c_p S_{\rho\theta}}{c_v \rho\theta}\right)_{k+1}-J_{33}G^{\frac{1}{2}}p_k\left(1+\Delta t\frac{c_p S_{\rho\theta}}{c_v \rho\theta}\right)_k}{\Delta z_{k+1/2}G_{k+1/2}^{\frac{1}{2}}}$$

$$-\Delta tg\frac{(\rho+\Delta t S_\rho)_{k+1}+(\rho+\Delta t S_\rho)_k}{2}+\Delta t S_{\rho w}. \tag{6.21}$$

41

Chapter 7

Horizontally and vertically implicit

| Corresponding author : Seiya Nishizawa |

7.1 Equations

The governing equation is the followings:

$$\frac{\partial G^{\frac{1}{2}}\rho'}{\partial t} = -\frac{\partial G^{\frac{1}{2}}\rho u}{\partial x^*} - \frac{\partial G^{\frac{1}{2}}\rho v}{\partial y^*} - \frac{\partial J_{33}G^{\frac{1}{2}}\rho w}{\partial \xi} + G^{\frac{1}{2}}S_\rho, \tag{7.1}$$

$$\frac{\partial G^{\frac{1}{2}}\rho u}{\partial t} = -\frac{\partial G^{\frac{1}{2}}p'}{\partial x^*} + G^{\frac{1}{2}}S_{\rho u}, \tag{7.2}$$

$$\frac{\partial G^{\frac{1}{2}}\rho v}{\partial t} = -\frac{\partial G^{\frac{1}{2}}p'}{\partial y^*} + G^{\frac{1}{2}}S_{\rho v}, \tag{7.3}$$

$$\frac{\partial G^{\frac{1}{2}}\rho w}{\partial t} = -\frac{\partial J_{33}G^{\frac{1}{2}}p'}{\partial \xi} - G^{\frac{1}{2}}\rho'g + G^{\frac{1}{2}}S_{\rho w}, \tag{7.4}$$

$$\frac{\partial G^{\frac{1}{2}}\rho\theta}{\partial t} = -\frac{\partial G^{\frac{1}{2}}u\rho\theta}{\partial x^*} - \frac{\partial G^{\frac{1}{2}}v\rho\theta}{\partial y^*} - \frac{\partial J_{33}G^{\frac{1}{2}}w\rho\theta}{\partial \xi} + G^{\frac{1}{2}}S_{\rho\theta}, \tag{7.5}$$

$$p = P_{00}\left(\frac{R\rho\theta}{P_{00}}\right)^{c_p/c_v}, \tag{7.6}$$

where

$$G^{\frac{1}{2}}S_\rho = -\frac{\partial J_{13}G^{\frac{1}{2}}\rho u + J_{23}G^{\frac{1}{2}}\rho v}{\partial \xi}, \tag{7.7}$$

$$G^{\frac{1}{2}}S_{\rho u} = -\frac{\partial G^{\frac{1}{2}}u\rho u}{\partial x^*} - \frac{\partial G^{\frac{1}{2}}v\rho u}{\partial y^*} - \frac{\partial}{\partial \xi}(J_{13}G^{\frac{1}{2}}u\rho u + J_{23}G^{\frac{1}{2}}v\rho u + J_{33}G^{\frac{1}{2}}w\rho u)$$
$$- \frac{\partial}{\partial \xi}(J_{13}G^{\frac{1}{2}}p'), \tag{7.8}$$

$$G^{\frac{1}{2}}S_{\rho v} = -\frac{\partial G^{\frac{1}{2}}u\rho v}{\partial x^*} - \frac{\partial G^{\frac{1}{2}}v\rho v}{\partial y^*} - \frac{\partial}{\partial \xi}(J_{13}G^{\frac{1}{2}}u\rho v + J_{23}G^{\frac{1}{2}}v\rho v + J_{33}G^{\frac{1}{2}}w\rho v),$$
$$- \frac{\partial}{\partial \xi}(J_{23}G^{\frac{1}{2}}p'), \tag{7.9}$$

$$G^{\frac{1}{2}}S_{\rho w} = -\frac{\partial G^{\frac{1}{2}}u\rho w}{\partial x^*} - \frac{\partial G^{\frac{1}{2}}v\rho w}{\partial y^*} - \frac{\partial}{\partial \xi}(J_{13}G^{\frac{1}{2}}u\rho w + J_{23}G^{\frac{1}{2}}v\rho w + J_{33}G^{\frac{1}{2}}w\rho w), \tag{7.10}$$

$$G^{\frac{1}{2}}S_{\rho\theta} = -\frac{\partial J_{13}G^{\frac{1}{2}}u\rho\theta + J_{23}G^{\frac{1}{2}}v\rho\theta}{\partial \xi}. \tag{7.11}$$

Prime describes deviation from a reference state, and the reference state depends only z and satisfies in hydrostatic barance:

$$p' = p - \bar{p}, \tag{7.12}$$
$$\rho' = \rho - \bar{\rho}, \tag{7.13}$$
$$\frac{d\bar{p}(z)}{dz} = -\bar{\rho}(z)g. \tag{7.14}$$

7.2   Descritization

For the temporal discritization, backward temporal integrations are employed for the terms related to acoustic wave.

$$\frac{\rho'^{n+1} - \rho'^n}{\Delta t} = -G^{-\frac{1}{2}}\frac{\partial}{\partial x^*}\{G^{\frac{1}{2}}(\rho u)^{n+1}\} - G^{-\frac{1}{2}}\frac{\partial}{\partial y^*}\{G^{\frac{1}{2}}(\rho v)^{n+1}\}$$
$$- G^{-\frac{1}{2}}\frac{\partial}{\partial \xi}\{J_{33}G^{\frac{1}{2}}(\rho w)^{n+1}\} + S_\rho^n, \tag{7.15}$$

$$\frac{(\rho u)^{n+1} - (\rho u)^n}{\Delta t} = -G^{-\frac{1}{2}}\frac{\partial}{\partial x^*}(G^{\frac{1}{2}}p'^{n+1}) + S_{\rho u}^n, \tag{7.16}$$

$$\frac{(\rho v)^{n+1} - (\rho v)^n}{\Delta t} = -G^{-\frac{1}{2}}\frac{\partial}{\partial y^*}(G^{\frac{1}{2}}p'^{n+1}) + S_{\rho v}^n, \tag{7.17}$$

$$\frac{(\rho w)^{n+1} - (\rho w)^n}{\Delta t} = -G^{-\frac{1}{2}}\frac{\partial}{\partial \xi}(J_{33}G^{\frac{1}{2}}p'^{n+1}) - g\rho'^{n+1} + S_{\rho w}^n, \tag{7.18}$$

$$\frac{p'^{n+1} - p'^n}{\Delta t} = P_{00}\left(\frac{R}{P_{00}}\right)^{\kappa^n}\kappa^n(\rho\theta)^{n^{\kappa^n-1}}\frac{\partial \rho\theta}{\partial t} = \kappa^n\frac{p^n}{(\rho\theta)^n}\frac{\partial \rho\theta}{\partial t}, \tag{7.19}$$

$$\frac{\partial \rho\theta}{\partial t} = -G^{-\frac{1}{2}}\frac{\partial}{\partial x^*}\{G^{\frac{1}{2}}\theta^n(\rho u)^{n+1}\} - G^{-\frac{1}{2}}\frac{\partial}{\partial y^*}\{G^{\frac{1}{2}}\theta^n(\rho v)^{n+1}\}$$
$$- G^{-\frac{1}{2}}\frac{\partial}{\partial \xi}\{J_{33}G^{\frac{1}{2}}\theta^n(\rho w)^{n+1}\} + S_{\rho\theta}^n, \tag{7.20}$$

where $\kappa = c_p/c_v$. Note that the potential temperature at previous step, θ^n, is used.

In order to obtain Helmholtz equation, a linearized equation for the density is used instead of Eq. 7.15.

$$\rho'^{n+1} \sim \rho'^n + \frac{1}{\kappa^n} \frac{\rho^n}{p^n} \left\{ p'^{n+1} - p'^n \right\}. \tag{7.21}$$

Here we assume that the potential temperature does not change during a temporal step due to acoustic wave.

Eliminating $(\rho u)^{n+1}, (\rho v)^{n+1} (\rho w)^{n+1}$,, and ρ'^{n+1}, the Helmholtz equation for p'^{n+1} is obtained.

$$\frac{\partial}{\partial x^*} \left(\theta^n \frac{\partial G^{\frac{1}{2}} p'^{n+1}}{\partial x^*} \right) + \frac{\partial}{\partial y^*} \left(\theta^n \frac{\partial G^{\frac{1}{2}} p'^{n+1}}{\partial y^*} \right) + \frac{\partial}{\partial \xi} \left(J_{33} \theta^n \frac{\partial J_{33} G^{\frac{1}{2}} p'^{n+1}}{\partial \xi} \right)$$

$$+ g \frac{\partial}{\partial \xi} \left(\frac{J_{33} G^{\frac{1}{2}} \theta^n p'^{n+1}}{C_s^{2n}} \right) - \frac{G^{\frac{1}{2}} \theta^n p'^{n+1}}{\Delta t^2 C_s^{2n}}$$

$$= \frac{1}{\Delta t} \left[\frac{\partial G^{\frac{1}{2}} \theta^n \left\{ (\rho u)^n + \Delta t S_{\rho u}^n \right\}}{\partial x^*} + \frac{\partial G^{\frac{1}{2}} \theta^n \left\{ (\rho v)^n + \Delta t S_{\rho v}^n \right\}}{\partial y^*} + \frac{\partial J_{33} G^{\frac{1}{2}} \theta^n \left\{ (\rho w)^n + \Delta t S_{\rho w}^n \right\}}{\partial \xi} \right]$$

$$+ g \frac{\partial}{\partial \xi} \left\{ \frac{J_{33} G^{\frac{1}{2}} \theta^n p'^n}{C_s^{2n}} - J_{33} G^{\frac{1}{2}} (\rho' \theta)^n \right\} + \frac{G^{\frac{1}{2}} S_{\rho \theta}}{\Delta t} - \frac{G^{\frac{1}{2}} \theta^n p'^n}{\Delta t^2 C_s^{2n}}, \tag{7.22}$$

where

$$C_s^2 = \kappa \frac{p}{\rho}. \tag{7.23}$$

Spatial differentials are discretized.

$$\frac{1}{\Delta x_i}\left(\hat{\theta}_{i+1/2}\frac{(G^{\frac{1}{2}}p'^{n+1})_{i+1} - G^{\frac{1}{2}}p'^{n+1}}{\Delta x_{i+1/2}} - \hat{\theta}_{i-1/2}\frac{G^{\frac{1}{2}}p'^{n+1} - (G^{\frac{1}{2}}p'^{n+1})_{i-1}}{\Delta x_{i-1/2}}\right)$$

$$+ \frac{1}{\Delta y_j}\left(\hat{\theta}_{j+1/2}\frac{(G^{\frac{1}{2}}p'^{n+1})_{j+1} - G^{\frac{1}{2}}p'^{n+1}}{\partial y_{j+1/2}} - \hat{\theta}_{j-1/2}\frac{G^{\frac{1}{2}}p'^{n+1} - (G^{\frac{1}{2}}p'^{n+1})_{j-1}}{\partial y_{j-1/2}}\right)$$

$$+ \frac{1}{\Delta z_k}\left\{(J_{33})_{k+1/2}\hat{\theta}_{k+1/2}\frac{J_{33}G^{\frac{1}{2}}p'^{n+1}_{k+1} - J_{33}G^{\frac{1}{2}}p'^{n+1}}{\Delta z_{k+1/2}} - (J_{33})_{k-1/2}\hat{\theta}_{k-1/2}\frac{J_{33}G^{\frac{1}{2}}p'^{n+1} - J_{33}G^{\frac{1}{2}}p'^{n+1}_{k-1}}{\Delta z_{k-1/2}}\right)$$

$$+ g\frac{1}{\Delta_{k+1/2} + \Delta z_{k-1/2}}\left\{\frac{J_{33}G^{\frac{1}{2}}\theta p'^{n+1}_{k+1}}{C^2_{sk+1}} - \frac{J_{33}G^{\frac{1}{2}}\theta p'^{n+1}_{k-1}}{C^2_{sk-1}}\right\} - \frac{G^{\frac{1}{2}}\theta p'^{n+1}}{\Delta t^2 C^2_s}$$

$$= \frac{1}{\Delta t}\left[\frac{G^{\frac{1}{2}}_{i+1/2}\hat{\theta}_{i+1/2}\left\{(\rho u)_{i+1/2} + \Delta t(S_{\rho u})_{i+1/2}\right\} - G^{\frac{1}{2}}_{i-1/2}\hat{\theta}_{i-1/2}\left\{(\rho u)_{i-1/2} + \Delta t(S_{\rho u})_{i-1/2}\right\}}{\Delta x_i}\right.$$

$$+ \frac{G^{\frac{1}{2}}_{j+1/2}\hat{\theta}_{j+1/2}\left\{(\rho v)_{j+1/2} + \Delta t(S_{\rho v})_{j+1/2}\right\} - G^{\frac{1}{2}}_{j-1/2}\hat{\theta}_{j-1/2}\left\{(\rho v)_{j-1/2} + \Delta t' S_{\rho v})_{j-1/2}\right\}}{\Delta y_j}$$

$$+ \left.\frac{J_{33}G^{\frac{1}{2}}\hat{\theta}_{k+1/2}\left\{(\rho w)_{k+1/2} + \Delta t(S_{\rho w})_{k+1/2}\right\} - J_{33}G^{\frac{1}{2}}\hat{\theta}_{k-1/2}\left\{(\rho w)_{k-1/2} + \Delta t(S_{\rho w})_{k-1/2}\right\}}{\Delta z_k}\right]$$

$$+ g\frac{1}{\Delta z_{k+1/2} + \Delta z_{k-1/2}}\left\{\frac{J_{33}G^{\frac{1}{2}}\theta p'^{n}_{k+1}}{C^2_{sk+1}} - \frac{J_{33}G^{\frac{1}{2}}\theta p'^{n}_{k-1}}{C^2_{sk-1}} - J_{33}G^{\frac{1}{2}}\{(\rho'\theta)_{k+1} - (\rho'\theta)_{k-1}\}\right\}$$

$$+ \frac{G^{\frac{1}{2}}S_{\rho\theta}}{\Delta t} - \frac{G^{\frac{1}{2}}\theta p'^{n}}{\Delta t^2 C^2_s}. \tag{7.24}$$

Chapter 8

Physical parameterization

8.1 Turbulence

Corresponding author : Seiya Nishizawa

8.1.1 Spatial filter

The governing equations are the following:

$$\frac{\partial \rho}{\partial t} + \frac{\partial u_i \rho}{\partial x_i} = 0 \tag{8.1}$$

$$\frac{\partial \rho u_i}{\partial t} + \frac{\partial u_j \rho u_i}{\partial x_j} = -\frac{\partial p}{\partial x_i} + g\rho\delta_{i3} \tag{8.2}$$

$$\frac{\partial \rho\theta}{\partial t} + \frac{\partial u_i \rho\theta}{\partial x_i} = Q \tag{8.3}$$

Spatially filtering the continuity equation yields:

$$\frac{\partial \overline{\rho}}{\partial t} + \frac{\partial \overline{u_i \rho}}{\partial x_i} = 0, \tag{8.4}$$

where $\overline{\phi}$ indicates the spatially filtered quantity of an arbitrary variable ϕ. Favre filtering (Favre, 1983), defined by:

$$\widetilde{\phi} = \frac{\overline{\rho\phi}}{\overline{\rho}} \tag{8.5}$$

renders the equation (8.4):

$$\frac{\partial \overline{\rho}}{\partial t} + \frac{\partial \widetilde{u_i}\overline{\rho}}{\partial x_i} = 0. \tag{8.6}$$

The momentum equations become:

$$\frac{\partial \overline{\rho u_i}}{\partial t} + \frac{\partial \overline{u_j \rho u_i}}{\partial x_j} = -\frac{\partial \overline{p}}{\partial x_i} + \overline{\rho}g\delta_{i3} \tag{8.7}$$

$$\frac{\partial \overline{\rho}\widetilde{u_i}}{\partial t} + \frac{\partial \widetilde{u_j}\,\overline{\rho}\widetilde{u_i}}{\partial x_j} = -\frac{\partial \overline{p}}{\partial x_i} + g\overline{\rho}\delta_{i3} - \frac{\partial}{\partial x_j}\left(\overline{u_i \rho u_j} - \widetilde{u_j}\overline{\rho}\widetilde{u_i}\right) \tag{8.8}$$

$$\frac{\partial \overline{\rho}\widetilde{u_i}}{\partial t} + \frac{\partial \widetilde{u_j}\,\overline{\rho}\widetilde{u_i}}{\partial x_j} = -\frac{\partial \overline{p}}{\partial x_i} + g\overline{\rho}\delta_{i3} - \frac{\partial}{\partial x_j}\overline{\rho}\left(\widetilde{u_i u_j} - \widetilde{u_j}\widetilde{u_i}\right). \tag{8.9}$$

As the same matter, the thermal equation becomes:

$$\frac{\partial \overline{\rho}\widetilde{\theta}}{\partial t} + \frac{\partial \widetilde{u_i}\overline{\rho}\widetilde{\theta}}{\partial x_i} = Q - \frac{\partial}{\partial x_i}\overline{\rho}\left(\widetilde{u_i\theta} - \widetilde{u_i}\widetilde{\theta}\right). \tag{8.10}$$

The governing equations for the prognostic variables $(\overline{\rho}, \overline{\rho}\widetilde{u_i}, \text{ and } \overline{\rho}\widetilde{\theta})$ are:

$$\frac{\partial \overline{\rho}}{\partial t} + \frac{\partial \widetilde{u_i}\overline{\rho}}{\partial x_i} = 0, \tag{8.11}$$

$$\frac{\partial \overline{\rho}\widetilde{u_i}}{\partial t} + \frac{\partial \widetilde{u_j}\overline{\rho}\widetilde{u_i}}{\partial x_j} = -\frac{\partial \overline{p}}{\partial x_i} + g\overline{\rho}\delta_{i3} - \frac{\partial \overline{\rho}\tau_{ij}}{\partial x_j}, \tag{8.12}$$

$$\frac{\partial \overline{\rho}\widetilde{\theta}}{\partial t} + \frac{\partial \widetilde{u_i}\overline{\rho}\widetilde{\theta}}{\partial x_i} = Q - \frac{\partial \overline{\rho}\tau_i^D}{\partial x_i}, \tag{8.13}$$

where:

$$\tau_{ij} = \widetilde{u_i u_j} - \widetilde{u_i}\widetilde{u_j}, \tag{8.14}$$

$$\tau_i^D = \widetilde{u_i\theta} - \widetilde{u_i}\widetilde{\theta}. \tag{8.15}$$

Hereafter, we omit the overline and tilde representing the spatial and Favre filters.

8.1.2 SGS model

Smagorinsky-Lilly model

The eddy momentum flux is:

$$\tau_{ij} - \frac{1}{3}\tau_{kk}\delta_{ij} = -2\nu_{SGS}\left(S_{ij} - \frac{1}{3}S_{kk}\delta_{ij}\right), \tag{8.16}$$

where S_{ij} is the strain tensor:

$$S_{ij} = \frac{1}{2}\left(\frac{\partial u_i}{\partial x_j} + \frac{\partial u_j}{\partial x_i}\right), \tag{8.17}$$

and:

$$\nu_{SGS} = (C_s\lambda)^2 |S|. \tag{8.18}$$

C_s is the Smagorinsky constant, λ is a characteristic SGS length scale, and $|S|$ is scale of the tensor S,

$$|S| = \sqrt{2S_{ij}S_{ij}}. \tag{8.19}$$

The eddy momentum flux is then:

$$\tau_{ij} = -2\nu_{SGS}\left(S_{ij} - \frac{1}{3}S_{kk}\delta_{ij}\right) + \frac{2}{3}TKE\delta_{ij}, \tag{8.20}$$

where:

$$TKE = \frac{1}{2}\tau_{ii} = \left(\frac{\nu_{SGS}}{C_k\lambda}\right)^2, \tag{8.21}$$

where C_k is a SGS constant and assumed to be 0.1, following Deardorff (1980) and Moeng and Wyngaard (1988).

The eddy heat flux is:

$$\tau_i^D = -D_{SGS}\frac{\partial \theta}{\partial x_i}, \tag{8.22}$$

where:

$$D_{SGS} = \frac{1}{Pr}\nu_{SGS}. \tag{8.23}$$

Pr is the turbulent Prandtl number. For other scalar constants such as water vapor, D_{SGS} is also used as their diffusivity.

To include buoyancy effects, the extension of the basic Smagorinsky constant developed by Brown et al. (1994) is used.

$$\nu_{SGS} = (C_s\lambda)^2|S|\sqrt{1-Rf}, \tag{8.24}$$

where Rf is the flux Richardson number ($Rf = Ri/Pr$). Ri is the local (pointwise) gradient Richardson number,

$$Ri = \frac{N^2}{|S|^2}, \tag{8.25}$$

and N^2 is the Brunt-Visala frequency,

$$N^2 = \frac{g}{\theta}\frac{\partial \theta}{\partial z}. \tag{8.26}$$

The Prandtl number is an unknown parameter that depends on the Richardson number, though it is often assumed to have a constant value. For unstable conditions ($Ri < 0$),

$$\nu_{SGS} = (C_s\lambda)^2\,|S|\sqrt{1-cRi}, \tag{8.27}$$

$$D_{SGS} = \frac{1}{Pr_N}\,(C_s\lambda)^2\,|S|\sqrt{1-bRi}, \tag{8.28}$$

where Pr_N is the Prandtl number for neutral conditions. The values of c, b, Pr_N are set to 16, 40, and 0.7, respectively. The Prandtl number is then:

$$Pr = Pr_N\sqrt{\frac{1-cRi}{1-bRi}}. \tag{8.29}$$

For stable conditions, when the Richardson number is smaller than the critical Richardson number, $Ri_c(= 0.25)$,

$$\nu_{SGS} = (C_s\lambda)^2\,|S|\left(1-\frac{Ri}{Ri_c}\right)^4, \tag{8.30}$$

$$D_{SGS} = \frac{1}{Pr_N}\,(C_s\lambda)^2\,|S|\left(1-\frac{Ri}{Ri_c}\right)^4(1-gRi). \tag{8.31}$$

The constant g is determined as the Prandtl number becomes 1 in the limit of $Ri \to Ri_C$ and is then $(1 - Pr_N)/Ri_c$. The Prandtl number is

$$Pr = Pr_N\left\{1-(1-Pr_N)\frac{Ri}{Ri_c}\right\}^{-1}. \tag{8.32}$$

For strongly stable conditions ($Ri > Ri_c$), eddy viscosity and diffusivity for scalars are 0;

$$\nu_{SGS} = 0, \tag{8.33}$$

$$D_{SGS} = 0. \tag{8.34}$$

The Prandtl number is $Pr = 1$.

Scotti et al. (1993) suggested that the length scale should depend on the grid aspect ratio. Under equilibrium conditions with the universal Kolmogorov spectrum, energy cascaded to the SGS turbulence, which is equal to SGS dissipation, must not depend on the grid aspect ratio. The energy flux or dissipation can be written as function of S_{ij} and the length scale, λ. The S_{ij} depends on the grid aspect ratio, so the length scale should have dependency on the aspect ratio, cancelling the dependency of S_{ij}. With some approximations, the authors obtained an approximate function of the length scale [1]:

$$\lambda = f(a)\Delta, \tag{8.35}$$

where $f(a)$ is a function of grid aspect ratio, a, and

$$
\begin{aligned}
f(a) = 1.736 a^{1/3} \{ & \\
& 4P_1(b_1)a^{1/3} + 0.222P_2(b_1)a^{-5/3} + 0.077P_3(b_1)a^{-11/3} \\
& - 3b_1 + 4P_1(b_2) + 0.222P_2(b_2) + 0.077P_3(b_2) - 3b_2 \\
\}^{-3/4}. &
\end{aligned} \tag{8.36}
$$

Here $b_1 = \arctan(1/a), b_2 = \arctan(a) = \pi/2 - b_1$, and

$$P_1(z) = 2.5P_2(z) - 1.5(\cos(z))^{2/3}\sin(z), \tag{8.37}$$

$$P_2(z) = 0.98z + 0.073z^2 - 0.418z^3 + 0.120z^4, \tag{8.38}$$

$$P_3(z) = 0.976z + 0.188z^2 + 1.169z^3 + 0.755z^4 - 0.151z^5. \tag{8.39}$$

For instance, $f(2) = 1.036, f(5) = 1.231, f(10) = 1.469$, and $f(20) = 1.790$. Δ is the filter length, and is here defined to be proportional to $(\Delta x \Delta y \Delta z)^{1/3}$. In this model, we introduce a numerical filter to reduce two-grid noise discussed above. This filter also reduces two-grid scale physical variability. This means that two-grid scale would be preferred for the filter length in this model rather than grid spacing itself; that is:

$$\Delta = 2(\Delta x \Delta y \Delta z)^{1/3}. \tag{8.40}$$

---

[1]They considered two grid aspect ratios, while we consider only one, i.e. $\Delta x = \Delta y$.

Terrain-following coordinates

Tendencies representing effect of sub-grid scale turbulence with terrain-following coordinates are as follows: [2];

$$\frac{\partial G^{\frac{1}{2}}\rho u}{\partial t} = -\frac{\partial G^{\frac{1}{2}}\rho\tau_{11}}{\partial x^*} - \frac{\partial G^{\frac{1}{2}}\rho\tau_{12}}{\partial y^*} - \frac{\partial J_{13}G^{\frac{1}{2}}\rho\tau_{11} + J_{23}G^{\frac{1}{2}}\rho\tau_{12} + J_{33}G^{\frac{1}{2}}\rho\tau_{13}}{\partial \xi},$$
(8.41)

$$\frac{\partial G^{\frac{1}{2}}\rho v}{\partial t} = -\frac{\partial G^{\frac{1}{2}}\rho\tau_{21}}{\partial x^*} - \frac{\partial G^{\frac{1}{2}}\rho\tau_{22}}{\partial y^*} - \frac{\partial J_{13}G^{\frac{1}{2}}\rho\tau_{21} + J_{23}G^{\frac{1}{2}}\rho\tau_{22} + J_{33}G^{\frac{1}{2}}\rho\tau_{23}}{\partial \xi},$$
(8.42)

$$\frac{\partial G^{\frac{1}{2}}\rho w}{\partial t} = -\frac{\partial G^{\frac{1}{2}}\rho\tau_{31}}{\partial x^*} - \frac{\partial G^{\frac{1}{2}}\rho\tau_{32}}{\partial y^*} - \frac{\partial J_{13}G^{\frac{1}{2}}\rho\tau_{31} + J_{23}G^{\frac{1}{2}}\rho\tau_{32} + J_{33}G^{\frac{1}{2}}\rho\tau_{33}}{\partial \xi},$$
(8.43)

$$\frac{\partial G^{\frac{1}{2}}\rho\theta}{\partial t} = -\frac{\partial G^{\frac{1}{2}}\rho\tau_1^D}{\partial x^*} - \frac{\partial G^{\frac{1}{2}}\rho\tau_2^D}{\partial y^*} - \frac{\partial J_{13}G^{\frac{1}{2}}\rho\tau_1^D + J_{23}G^{\frac{1}{2}}\rho\tau_2^D + J_{33}G^{\frac{1}{2}}\rho\tau_3^D}{\partial \xi}$$
(8.44)

$$G^{\frac{1}{2}}S_{11} = \frac{\partial G^{\frac{1}{2}}u}{\partial x^*} + \frac{\partial J_{13}G^{\frac{1}{2}}u}{\partial \xi},$$
(8.45)

$$G^{\frac{1}{2}}S_{22} = \frac{\partial G^{\frac{1}{2}}v}{\partial y^*} + \frac{\partial J_{23}G^{\frac{1}{2}}v}{\partial \xi},$$
(8.46)

$$G^{\frac{1}{2}}S_{33} = \frac{\partial J_{33}G^{\frac{1}{2}}w}{\partial \xi},$$
(8.47)

$$G^{\frac{1}{2}}S_{12} = \frac{1}{2}\left(\frac{\partial G^{\frac{1}{2}}u}{\partial y^*} + \frac{\partial G^{\frac{1}{2}}v}{\partial x^*} + \frac{\partial J_{23}G^{\frac{1}{2}}u + J_{13}G^{\frac{1}{2}}v}{\partial \xi}\right),$$
(8.48)

$$G^{\frac{1}{2}}S_{23} = \frac{1}{2}\left(\frac{\partial G^{\frac{1}{2}}w}{\partial y^*} + \frac{\partial J_{33}G^{\frac{1}{2}}v + J_{23}G^{\frac{1}{2}}w}{\partial \xi}\right),$$
(8.49)

$$G^{\frac{1}{2}}S_{31} = \frac{1}{2}\left(\frac{\partial G^{\frac{1}{2}}w}{\partial x^*} + \frac{\partial J_{13}G^{\frac{1}{2}}w + J_{33}G^{\frac{1}{2}}u}{\partial \xi}\right),$$
(8.50)

$$G^{\frac{1}{2}}\tau_1^D = -D_{SGS}\left(\frac{\partial G^{\frac{1}{2}}\theta}{\partial x^*} + \frac{\partial J_{13}G^{\frac{1}{2}}\theta}{\partial \xi}\right),$$
(8.51)

$$G^{\frac{1}{2}}\tau_2^D = -D_{SGS}\left(\frac{\partial G^{\frac{1}{2}}\theta}{\partial y^*} + \frac{\partial J_{23}G^{\frac{1}{2}}\theta}{\partial \xi}\right),$$
(8.52)

$$G^{\frac{1}{2}}\tau_3^D = -D_{SGS}\frac{\partial J_{33}G^{\frac{1}{2}}\theta}{\partial \xi},$$
(8.53)

$$G^{\frac{1}{2}}N^2 = \frac{g}{\theta}\frac{\partial J_{33}G^{\frac{1}{2}}\theta}{\partial \xi}.$$
(8.54)

---

[2]Equations that are not changed in the terrain-following coordinates are omitted.

8.1.3 Discretization

Spatial discretization

We use the 4th order difference scheme for the advection term, as mentioned in the chapter 3. The τ_{ij} and τ_i^D are proportional to the square of the grid spacing (Δ^2). Due to consistency with the advection term in terms of order for spatial difference, the second order central difference scheme is used for terms of sub-grid scale turbulence. In the following part of this sub-section, overline, and i, j, k have the same meaning as in the chapter 3.

Momentum equation   The tendencies in the momentum equation related to the sub-grid scale mode are:

$$
\left.\frac{\partial G^{\frac{1}{2}} \rho u}{\partial t}\right|_{i+\frac{1}{2},j,k} = -\frac{(G^{\frac{1}{2}}\rho\tau_{11})_{i+1,j,k} - (G^{\frac{1}{2}}\rho\tau_{11})_{i,j,k}}{\Delta x}
$$
$$
-\frac{(G^{\frac{1}{2}}\overline{\rho}\tau_{12})_{i+\frac{1}{2},j+\frac{1}{2},k} - (G^{\frac{1}{2}}\overline{\rho}\tau_{12})_{i+\frac{1}{2},j-\frac{1}{2},k}}{\Delta y}
$$
$$
-\frac{\{G^{\frac{1}{2}}\overline{\rho}(J_{13}\tau_{11} + J_{23}\tau_{12} + J_{33}\tau_{13})\}_{i+\frac{1}{2},j,k+\frac{1}{2}} - \{G^{\frac{1}{2}}\overline{\rho}(J_{13}\tau_{11} + J_{23}\tau_{12} + J_{33}\tau_{13})\}_{i+\frac{1}{2},j,k-\frac{1}{2}}}{\Delta z},
$$
$$
\tag{8.55}
$$

$$
\left.\frac{\partial G^{\frac{1}{2}} \rho v}{\partial t}\right|_{i,j+\frac{1}{2},k} = -\frac{(G^{\frac{1}{2}}\overline{\rho}\tau_{21})_{i+\frac{1}{2},j+\frac{1}{2},k} - (G^{\frac{1}{2}}\overline{\rho}\tau_{21})_{i-\frac{1}{2},j+\frac{1}{2},k}}{\Delta x}
$$
$$
-\frac{(G^{\frac{1}{2}}\rho\tau_{22})_{i,j+1,k} - (G^{\frac{1}{2}}\rho\tau_{22})_{i,j,k}}{\Delta y}
$$
$$
-\frac{\{G^{\frac{1}{2}}\overline{\rho}(J_{13}\tau_{21} + J_{23}\tau_{22} + J_{33}\tau_{23})\}_{i,j+\frac{1}{2},k+\frac{1}{2}} - \{G^{\frac{1}{2}}\overline{\rho}(J_{13}\tau_{21} + J_{23}\tau_{22} + J_{33}\tau_{23})\}_{i,j+\frac{1}{2},k-\frac{1}{2}}}{\Delta z},
$$
$$
\tag{8.56}
$$

$$
\left.\frac{\partial G^{\frac{1}{2}} \rho w}{\partial t}\right|_{i,j,k+\frac{1}{2}} = -\frac{(G^{\frac{1}{2}}\overline{\rho}\tau_{31})_{i+\frac{1}{2},j,k+\frac{1}{2}} - (G^{\frac{1}{2}}\overline{\rho}\tau_{31})_{i-\frac{1}{2},j,k+\frac{1}{2}}}{\Delta x}
$$
$$
-\frac{(G^{\frac{1}{2}}\overline{\rho}\tau_{32})_{i,j+\frac{1}{2},k+\frac{1}{2}} - (G^{\frac{1}{2}}\overline{\rho}\tau_{32})_{i,j-\frac{1}{2},k+\frac{1}{2}}}{\Delta y}
$$
$$
-\frac{\{(G^{\frac{1}{2}}\rho(J_{13}\tau_{31} + J_{23}\tau_{32} + J_{33}\tau_{33})\}_{i,j,k+1} - \{(G^{\frac{1}{2}}\rho(J_{13}\tau_{31} + J_{23}\tau_{32} + J_{33}\tau_{33})\}_{i,j,k}}{\Delta z}.
$$
$$
\tag{8.57}
$$

The $\overline{\rho}$ is:

$$
\overline{\rho}_{i,j+\frac{1}{2},k+\frac{1}{2}} = \frac{\rho_{i,j+1,k+1} + \rho_{i,j+1,k} + \rho_{i,j,k+1} + \rho_{i,j,k}}{4}, \tag{8.58}
$$

$$
\overline{\rho}_{i+\frac{1}{2},j,k+\frac{1}{2}} = \frac{\rho_{i+1,j,k+1} + \rho_{i+1,j,k} + \rho_{i,j,k+1} + \rho_{i,j,k}}{4}, \tag{8.59}
$$

$$
\overline{\rho}_{i+\frac{1}{2},j+\frac{1}{2},k} = \frac{\rho_{i+1,j+1,k} + \rho_{i+1,j,k} + \rho_{i,j+1,k} + \rho_{i,j,k}}{4}. \tag{8.60}
$$

Thermal equation   The tendency in the thermal equation related to the sub-grid scale model is:

$$\frac{\partial G^{\frac{1}{2}}\rho\theta}{\partial t}\Bigg|_{i,j,k} = -\frac{(G^{\frac{1}{2}}\overline{\rho}\tau_1^D)_{i+\frac{1}{2},j,k} - (G^{\frac{1}{2}}\overline{\rho}\tau_1^D)_{i-\frac{1}{2},j,k}}{\Delta x}$$

$$-\frac{(G^{\frac{1}{2}}\overline{\rho}\tau_2^D)_{i,j+\frac{1}{2},k} - (G^{\frac{1}{2}}\overline{\rho}\tau_2^D)_{i,j-\frac{1}{2},k}}{\Delta y}$$

$$-\frac{\{G^{\frac{1}{2}}\overline{\rho}(J_{13}\tau_1^D + J_{23}\tau_2^D + J_{33}\tau_3^D)\}_{i,j,k+\frac{1}{2}} - \{G^{\frac{1}{2}}\overline{\rho}(J_{13}\tau_1^D + J_{23}\tau_2^D + J_{33}\tau_3^D)\}_{i,j,k-\frac{1}{2}}}{\Delta z}.$$

$$(8.61)$$

The $\overline{\rho}$ at half-level is eq.(3.81)-(3.83).

The eddy diffusion flux, τ^D, at half-level is:

$$(G^{\frac{1}{2}}\tau_1^D)_{i+\frac{1}{2},j,k} = -D_{SGS,i+\frac{1}{2},j,k}\left\{\frac{(G^{\frac{1}{2}}\theta)_{i+1,j,k} - (G^{\frac{1}{2}}\theta)_{i,j,k}}{\Delta x} + \frac{(J_{13}G^{\frac{1}{2}}\overline{\theta})_{i+\frac{1}{2},j,k+\frac{1}{2}} - (J_{13}G^{\frac{1}{2}}\overline{\theta})_{i+\frac{1}{2},j,k-\frac{1}{2}}}{\Delta z}\right\},$$

$$(8.62)$$

$$(G^{\frac{1}{2}}\tau_2^D)_{i,j+\frac{1}{2},k} = -D_{SGS,i,j+\frac{1}{2},k}\left\{\frac{(G^{\frac{1}{2}}\theta)_{i,j+1,k} - (G^{\frac{1}{2}}\theta)_{i,j,k}}{\Delta y} + \frac{(J_{23}G^{\frac{1}{2}}\overline{\theta})_{i,j+\frac{1}{2},k+\frac{1}{2}} - (J_{23}G^{\frac{1}{2}}\overline{\theta})_{i,j+\frac{1}{2},k-\frac{1}{2}}}{\Delta z}\right\},$$

$$(8.63)$$

$$(G^{\frac{1}{2}}\tau_3^D)_{i,j,k+\frac{1}{2}} = -D_{SGS,i,j,k+\frac{1}{2}}\frac{J_{33}G^{\frac{1}{2}}\theta_{i,j,k+1} - J_{33}G^{\frac{1}{2}}\theta_{i,j,k}}{\Delta z}. \qquad (8.64)$$

Strain tensor   All the strain tensors, eq.(8.17), have to be calculated at full-level (grid cell center), and some are at cell edges.

- cell center (i, j, k)

$$(G^{\frac{1}{2}}S_{11})_{i,j,k} = \frac{(G^{\frac{1}{2}}\overline{u})_{i+\frac{1}{2},j,k} - (G^{\frac{1}{2}}\overline{u})_{i-\frac{1}{2},j,k}}{\Delta x} + \frac{(J_{13}G^{\frac{1}{2}}\overline{u})_{i+\frac{1}{2},j,k+\frac{1}{2}} - (J_{13}G^{\frac{1}{2}}\overline{u})_{i+\frac{1}{2},j,k-\frac{1}{2}}}{\Delta z},$$
(8.65)

$$(G^{\frac{1}{2}}S_{22})_{i,j,k} = \frac{(G^{\frac{1}{2}}\overline{v})_{i,j+\frac{1}{2},k} - (G^{\frac{1}{2}}\overline{v})_{i,j-\frac{1}{2},k}}{\Delta y} + \frac{(J_{23}G^{\frac{1}{2}}\overline{v})_{i,j+\frac{1}{2},k+\frac{1}{2}} - (J_{23}G^{\frac{1}{2}}\overline{v})_{i,j+\frac{1}{2},k-\frac{1}{2}}}{\Delta z},$$
(8.66)

$$(G^{\frac{1}{2}}S_{33})_{i,j,k} = \frac{J_{33}G^{\frac{1}{2}}\overline{w}_{i,j,k+\frac{1}{2}} - J_{33}G^{\frac{1}{2}}\overline{w}_{i,j,k-\frac{1}{2}}}{\Delta z},$$
(8.67)

$$(G^{\frac{1}{2}}S_{12})_{i,j,k} = \frac{1}{2}\left\{ \frac{(G^{\frac{1}{2}}\overline{u})_{i,j+\frac{1}{2},k} - (G^{\frac{1}{2}}\overline{u})_{i,j-\frac{1}{2},k}}{\Delta y} + \frac{(G^{\frac{1}{2}}\overline{v})_{i+\frac{1}{2},j,k} - (G^{\frac{1}{2}}\overline{v})_{i-\frac{1}{2},j,k}}{\Delta x} \right.$$
$$\left. + \frac{(J_{23}G^{\frac{1}{2}}\overline{u})_{i,j,k+\frac{1}{2}} - (J_{23}G^{\frac{1}{2}}\overline{u})_{i,j,k-\frac{1}{2}} + (J_{13}G^{\frac{1}{2}}\overline{v})_{i,j,k+\frac{1}{2}} - (J_{13}G^{\frac{1}{2}}\overline{v})_{i,j,k-\frac{1}{2}}}{\Delta z} \right\},$$
(8.68)

$$(G^{\frac{1}{2}}S_{23})_{i,j,k} = \frac{1}{2}\left\{ \frac{(G^{\frac{1}{2}}\overline{w})_{i,j+\frac{1}{2},k} - (G^{\frac{1}{2}}\overline{w})_{i,j-\frac{1}{2},k}}{\Delta y} \right.$$
$$\left. + \frac{J_{33}G^{\frac{1}{2}}\overline{v}_{i,j,k+\frac{1}{2}} - J_{33}G^{\frac{1}{2}}\overline{v}_{i,j,k-\frac{1}{2}} + (J_{23}G^{\frac{1}{2}}\overline{w})_{i,j,k+\frac{1}{2}} - (J_{23}G^{\frac{1}{2}}\overline{w})_{i,j,k-\frac{1}{2}}}{\Delta z} \right\},$$
(8.69)

$$(G^{\frac{1}{2}}S_{31})_{i,j,k} = \frac{1}{2}\left\{ \frac{(G^{\frac{1}{2}}\overline{w})_{i+\frac{1}{2},j,k} - (G^{\frac{1}{2}}\overline{w})_{i-\frac{1}{2},j,k}}{\Delta x} \right.$$
$$\left. + \frac{J_{33}G^{\frac{1}{2}}\overline{u}_{i,j,k+\frac{1}{2}} - J_{33}G^{\frac{1}{2}}\overline{u}_{i,j,k-\frac{1}{2}} + (J_{13}G^{\frac{1}{2}}\overline{w})_{i,j,k+\frac{1}{2}} - (J_{13}G^{\frac{1}{2}}\overline{w})_{i,j,k-\frac{1}{2}}}{\Delta z} \right\}.$$
(8.70)

- z edge $(i + \frac{1}{2}, j + \frac{1}{2}, k)$

$$(G^{\frac{1}{2}}S_{12})_{i+\frac{1}{2},j+\frac{1}{2},k} = \frac{1}{2}\left\{ \frac{(G^{\frac{1}{2}}\overline{u})_{i+\frac{1}{2},j+1,k} - (G^{\frac{1}{2}}\overline{u})_{i+\frac{1}{2},j,k}}{\Delta y} + \frac{(G^{\frac{1}{2}}\overline{v})_{i+1,j+\frac{1}{2},k} - (G^{\frac{1}{2}}\overline{v})_{i,j+\frac{1}{2},k}}{\Delta x} \right.$$
$$\left. + \frac{(J_{23}G^{\frac{1}{2}}\overline{u})_{i+\frac{1}{2},j+\frac{1}{2},k+\frac{1}{2}} - (J_{23}G^{\frac{1}{2}}\overline{u})_{i+\frac{1}{2},j+\frac{1}{2},k-\frac{1}{2}} + (J_{13}G^{\frac{1}{2}}\overline{v})_{i+\frac{1}{2},j+\frac{1}{2},k+\frac{1}{2}} - (J_{13}G^{\frac{1}{2}}\overline{v})}{\Delta z} \right.$$
(8.71)

- x edge $(i, j + \frac{1}{2}, k + \frac{1}{2})$

$$(G^{\frac{1}{2}}S_{23})_{i,j+\frac{1}{2},k+\frac{1}{2}} = \frac{1}{2}\left\{ \frac{(G^{\frac{1}{2}}\overline{w})_{i,j+1,k+\frac{1}{2}} - (G^{\frac{1}{2}}\overline{w})_{i,j,k+\frac{1}{2}}}{\Delta y} \right.$$
$$\left. + \frac{J_{33}G^{\frac{1}{2}}\overline{v}_{i,j+\frac{1}{2},k+1} - J_{33}G^{\frac{1}{2}}\overline{v}_{i,j+\frac{1}{2},k} + (J_{23}G^{\frac{1}{2}}\overline{w})_{i,j+\frac{1}{2},k+1} - (J_{23}G^{\frac{1}{2}}\overline{w})_{i,j+\frac{1}{2},k}}{\Delta z} \right\}.$$
(8.72)

- y edge $(i+\frac{1}{2}, j, k+\frac{1}{2})$

$$(G^{\frac{1}{2}}S_{31})_{i+\frac{1}{2},j,k+\frac{1}{2}} = \frac{1}{2}\left\{ \frac{(G^{\frac{1}{2}}\overline{w})_{i+1,j,k+\frac{1}{2}} - (G^{\frac{1}{2}}\overline{w})_{i,j,k+\frac{1}{2}}}{\Delta x} \right.$$
$$\left. + \frac{J_{33}G^{\frac{1}{2}}\overline{u}_{i+\frac{1}{2},j,k+1} - J_{33}G^{\frac{1}{2}}\overline{u}_{i+\frac{1}{2},j,k} + (J_{13}G^{\frac{1}{2}}\overline{w})_{i+\frac{1}{2},j,k+1} - (J_{13}G^{\frac{1}{2}}\overline{w})_{i+\frac{1}{2},j,k}}{\Delta z} \right\}.$$
$$(8.73)$$

velocity   Calculation of the strain tensor requires velocity value at cell center, plane center, edge center, and vertex. The velocities at cell center (full-level) are eq.(3.87-3.89):

- x-y plane center $(i, j, k+\frac{1}{2})$

$$\overline{u}_{i,j,k+\frac{1}{2}} = \frac{\overline{u}_{i,j,k+1} + \overline{u}_{i,j,k}}{2}, \tag{8.74}$$

$$\overline{v}_{i,j,k+\frac{1}{2}} = \frac{\overline{v}_{i,j,k+1} + \overline{v}_{i,j,k}}{2}, \tag{8.75}$$

$$\overline{w}_{i,j,k+\frac{1}{2}} = \frac{(\rho w)_{i,j,k+\frac{1}{2}}}{\overline{\rho}_{i,j,k+\frac{1}{2}}}. \tag{8.76}$$

- y-z plane center $(i+\frac{1}{2}, j, k)$

$$\overline{u}_{i+\frac{1}{2},j,k} = \frac{(\rho u)_{i+\frac{1}{2},j,k}}{\overline{\rho}_{i+\frac{1}{2},j,k}}, \tag{8.77}$$

$$\overline{v}_{i+\frac{1}{2},j,k} = \frac{\overline{v}_{i+1,j,k} + \overline{v}_{i,j,k}}{2}, \tag{8.78}$$

$$\overline{w}_{i+\frac{1}{2},j,k} = \frac{\overline{w}_{i+1,j,k} + \overline{w}_{i,j,k}}{2}. \tag{8.79}$$

- z-x plane center $(i, j+\frac{1}{2}, k)$

$$\overline{u}_{i,j+\frac{1}{2},k} = \frac{\overline{u}_{i,j+1,k} + \overline{u}_{i,j,k}}{2}, \tag{8.80}$$

$$\overline{v}_{i,j+\frac{1}{2},k} = \frac{(\rho v)_{i,j+\frac{1}{2},k}}{\overline{\rho}_{i,j+\frac{1}{2},k}}, \tag{8.81}$$

$$\overline{w}_{i,j+\frac{1}{2},k} = \frac{\overline{w}_{i,j+1,k} + \overline{w}_{i,j,k}}{2}. \tag{8.82}$$

- x edge center $(i, j+\frac{1}{2}, k+\frac{1}{2})$

$$\overline{u}_{i,j+\frac{1}{2},k+\frac{1}{2}} = \frac{\overline{u}_{i,j+1,k+1} + \overline{u}_{i,j+1,k} + \overline{u}_{i,j,k+1} + \overline{u}_{i,j,k}}{4}, \tag{8.83}$$

$$\overline{v}_{i,j+\frac{1}{2},k+\frac{1}{2}} = \frac{\overline{v}_{i,j+\frac{1}{2},k+1} + \overline{v}_{i,j+\frac{1}{2},k}}{2}, \tag{8.84}$$

$$\overline{w}_{i,j+\frac{1}{2},k+\frac{1}{2}} = \frac{\overline{w}_{i,j+1,k+\frac{1}{2}} + \overline{w}_{i,j,k+\frac{1}{2}}}{2}. \tag{8.85}$$

- y edge center $(i + \frac{1}{2}, j, k + \frac{1}{2})$

$$\overline{u}_{i+\frac{1}{2},j,k+\frac{1}{2}} = \frac{\overline{u}_{i+\frac{1}{2},j,k+1} + \overline{u}_{i+\frac{1}{2},j,k}}{2}, \tag{8.86}$$

$$\overline{v}_{i+\frac{1}{2},j,k+\frac{1}{2}} = \frac{\overline{v}_{i+1,j,k+1} + \overline{v}_{i+1,j,k} + \overline{v}_{i,j,k+1} + \overline{v}_{i,j,k}}{4}, \tag{8.87}$$

$$\overline{w}_{i+\frac{1}{2},j,k+\frac{1}{2}} = \frac{\overline{w}_{i+1,j,k+\frac{1}{2}} + \overline{w}_{i,j,k+\frac{1}{2}}}{2}. \tag{8.88}$$

- z edge center $(i + \frac{1}{2}, j + \frac{1}{2}, k)$

$$\overline{u}_{i+\frac{1}{2},j+\frac{1}{2},k} = \frac{\overline{u}_{i+\frac{1}{2},j+1,k} + \overline{u}_{i+\frac{1}{2},j,k}}{2}, \tag{8.89}$$

$$\overline{v}_{i+\frac{1}{2},j+\frac{1}{2},k} = \frac{\overline{v}_{i+1,j+\frac{1}{2},k} + \overline{v}_{i,j+\frac{1}{2},k}}{2}, \tag{8.90}$$

$$\overline{w}_{i+\frac{1}{2},j+\frac{1}{2},k} = \frac{\overline{w}_{i+1,j+1,k} + \overline{w}_{i+1,j,k} + \overline{w}_{i,j+1,k} + \overline{w}_{i,j,k}}{4}. \tag{8.91}$$

- vertex $(i + \frac{1}{2}, j + \frac{1}{2}, k + \frac{1}{2})$

$$\overline{u}_{i+\frac{1}{2},j+\frac{1}{2},k+\frac{1}{2}} = \frac{\overline{u}_{i+\frac{1}{2},j+1,k+1} + \overline{u}_{i+\frac{1}{2},j+1,k} + \overline{u}_{i+\frac{1}{2},j,k+1} + \overline{u}_{i+\frac{1}{2},j,k}}{4}, \tag{8.92}$$

$$\overline{v}_{i+\frac{1}{2},j+\frac{1}{2},k+\frac{1}{2}} = \frac{\overline{v}_{i+1,j+\frac{1}{2},k+1} + \overline{v}_{i+1,j+\frac{1}{2},k} + \overline{v}_{i,j+\frac{1}{2},k+1} + \overline{v}_{i,j+\frac{1}{2},k}}{4}, \tag{8.93}$$

$$\overline{w}_{i+\frac{1}{2},j+\frac{1}{2},k+\frac{1}{2}} = \frac{\overline{w}_{i+1,j+1,k+\frac{1}{2}} + \overline{w}_{i+1,j,k+\frac{1}{2}} + \overline{w}_{i,j+1,k+\frac{1}{2}} + \overline{w}_{i,j,k+\frac{1}{2}}}{4}. \tag{8.94}$$

Eddy viscosity/diffusion coefficient The eddy viscosity/diffusion coefficient, ν_{SGS} / D_{SGS}, is calculated at full-level with S and Ri at full-level; at half-level, it is interpolated to full-level.

Brunt-Visala frequency The Brunt-Visala frequency, N^2 is required to calculate the Richardson number at full-level.

$$(G^{\frac{1}{2}} N^2)_{i,j,k} = \frac{g}{\theta_{i,j,k}} \frac{J_{33} G^{\frac{1}{2}} \theta_{i,j,k+1} - J_{33} G^{\frac{1}{2}} \theta_{i,j,k-1}}{2\Delta z}. \tag{8.95}$$

8.2 Boundary layer turbulence model

Corresponding author : Seiya Nishizawa

8.2.1 Mellor-Yamada Nakanishi-Niino model

level 2.5

$$\frac{\partial \rho u}{\partial t} = -\frac{\partial}{\partial z} \rho \overline{u'w'}, \tag{8.96}$$

$$\frac{\partial \rho v}{\partial t} = -\frac{\partial}{\partial z} \rho \overline{v'w'}, \tag{8.97}$$

$$\frac{\partial \rho \theta_l}{\partial t} = -\frac{\partial}{\partial z} \rho \overline{\theta'_l w'}, \tag{8.98}$$

$$\frac{\partial \rho q_a}{\partial t} = -\frac{\partial}{\partial z} \rho \overline{q'_a w'}, \tag{8.99}$$

$$\frac{\partial}{\partial t} \rho q^2 = -2\left(\rho \overline{u'w'}\frac{\partial u}{\partial z} + \rho \overline{v'w'}\frac{\partial v}{\partial z}\right) + 2\frac{g}{\theta_0} \rho \overline{\theta'_v w'} - \frac{\partial}{\partial z} \rho \overline{q^2 w'} - 2\rho\epsilon, \tag{8.100}$$

where:

$$q_a = q_v + q_c + q_r + q_i + q_s + q_g, \tag{8.101}$$

and q^2 is doubled turbulence kinetic energy:

$$q^2 = u'^2 + v'^2 + w'^2. \tag{8.102}$$

The higher order moments and the dissipation term are parameterized as follows:

$$\overline{u'w'} = -LqS_M \frac{\partial u}{\partial z}, \tag{8.103}$$

$$\overline{v'w'} = -LqS_M \frac{\partial v}{\partial z}, \tag{8.104}$$

$$\overline{\theta'_l w'} = -LqS_H \frac{\partial \theta_l}{\partial z}, \tag{8.105}$$

$$\overline{q'_a w'} = -LqS_H \frac{\partial q_a}{\partial z}, \tag{8.106}$$

$$\overline{q^2 w'} = -3LqS_M \frac{\partial q^2}{\partial z}, \tag{8.107}$$

$$\overline{\theta'_v w'} = \beta_\theta \overline{\theta'_l w'} + \beta_q \overline{q'_a w'}, \tag{8.108}$$

$$\epsilon = \frac{q^3}{B_1 L}, \tag{8.109}$$

where:

$$S_M = \alpha_c A_1 \frac{\Phi_3 - 3C_1 \Phi_4}{D_{2.5}}, \tag{8.110}$$

$$S_H = \alpha_c A_2 \frac{\Phi_2 + 3C_1 \Phi_5}{D_{2.5}}, \tag{8.111}$$

$$\beta_\theta = 1 + 0.61q_a - 1.61Q_l - \tilde{R}abc, \tag{8.112}$$

$$\beta_q = 0.61\theta + \tilde{R}ac. \tag{8.113}$$

$$D_{2.5} = \Phi_2\Phi_4 + \Phi_5\Phi_3, \tag{8.114}$$

$$\Phi_1 = 1 - 3\alpha_c^2 A_2 B_2 (1 - C_3) G_H, \tag{8.115}$$

$$\Phi_2 = 1 - 9\alpha_c^2 A_1 A_2 (1 - C_2) G_H, \tag{8.116}$$

$$\Phi_3 = \Phi_1 + 9\alpha_c^2 A_2^2 (1 - C_2)(1 - C_5) G_H, \tag{8.117}$$

$$\Phi_4 = \Phi_1 - 12\alpha_c^2 A_1 A_2 (1 - C_2) G_H, \tag{8.118}$$

$$\Phi_5 = 6\alpha_c^2 A_1^2 G_M, \tag{8.119}$$

$$\alpha_c = \begin{cases} q/q_2, & q < q_2 \\ 1, & q \geq q_2 \end{cases}, \tag{8.120}$$

$$G_M = \frac{L^2}{q^2} \left\{ \left(\frac{\partial u}{\partial z} \right)^2 + \left(\frac{\partial v}{\partial z} \right)^2 \right\}, \tag{8.121}$$

$$G_H = -\frac{L^2}{q^2} N^2, \tag{8.122}$$

$$R = \frac{1}{2} \left\{ 1 + \mathrm{erf} \left(\frac{Q_1}{\sqrt{2}} \right) \right\}, \tag{8.123}$$

$$\tilde{R} = R - \frac{Q_l}{2\sigma_s} \frac{1}{\sqrt{2\pi}} \exp \left(-\frac{q_1^2}{2} \right), \tag{8.124}$$

$$Q_l = 2\sigma_s \left\{ RQ_1 + \frac{1}{\sqrt{2\pi}} \exp \left(-\frac{Q_1^2}{2} \right) \right\}, \tag{8.125}$$

$$Q_1 = \frac{a}{2\sigma_s} (q_a - Q_{sl}), \tag{8.126}$$

$$\sigma_s^2 = \frac{1}{4} a^2 L^2 \alpha_c B_2 S_H \left(\frac{\partial q_a}{\partial z} - b \frac{\partial \theta_l}{\partial z} \right)^2, \tag{8.127}$$

$$\delta Q_{sl} = \left. \frac{\partial Q_s}{\partial T} \right|_{T=T_l}, \tag{8.128}$$

$$a = \left(1 + \frac{L}{C_p} \delta Q_{sl} \right)^{-1}, \tag{8.129}$$

$$b = \frac{T}{\theta} \delta Q_{sl}, \tag{8.130}$$

$$c = (1 + 0.61q_a - 1.61Q_l) \frac{\theta}{T} \frac{L_v}{C_p} - 1.61\theta, \tag{8.131}$$

and Q_{sl} is the saturation-specific humidity at temperature $T_l(= \theta_l T/\theta)$.

The buoyancy flux term, which is the third term on the left hand side of eq. 8.100 is:

$$\begin{aligned} 2\frac{g}{\theta_0}\overline{\theta'_v w'} &= 2\frac{g}{\theta_0} \left(-\beta_\theta L q S_H \frac{\partial \theta_l}{\partial z} - \beta_q L q S_H \frac{\partial q_a}{\partial z} \right) \\ &= -2LqS_H \frac{g}{\theta_0} \left(\beta_\theta \frac{\partial \theta_l}{\partial z} + \beta_q \frac{\partial q_a}{\partial z} \right) \\ &= -2LqS_H \frac{g}{\theta_0} \frac{\partial \theta_v}{\partial z} \\ &= -2LqS_H N^2, \end{aligned} \tag{8.132}$$

where N^2 is the square of the Brunt-Vaisala frequency.

$$\frac{\partial}{\partial t}\rho q^2 = 2\rho LqS_M\left\{\left(\frac{\partial u}{\partial z}\right)^2 + \left(\frac{\partial v}{\partial z}\right)^2\right\}$$

$$- 2\rho LqS_H N^2 + \frac{\partial}{\partial z}\left(3\rho LqS_M\frac{\partial}{\partial z}q^2\right) - 2\rho\frac{q^3}{B_1 L} \quad (8.133)$$

S_{M2}, S_{H2}, and q_2 are for level 2 schemes corresponding to S_M, S_H, and q, respectively:

$$S_{M2} = \frac{A_1 F_1}{A_2 F_2}\frac{R_{f1} - Rf}{R_{f2} - Rf}S_{H2}, \quad (8.134)$$

$$S_{H2} = 3A_2(\gamma_1 + \gamma_2)\frac{Rf_c - Rf}{1 - Rf}, \quad (8.135)$$

$$q_2^2 = B_1 L^2 S_{M2}(1 - Rf)\left\{\left(\frac{\partial u}{\partial z}\right)^2 + \left(\frac{\partial v}{\partial z}\right)^2\right\}. \quad (8.136)$$

Rf and Rf_c are the flux Richardson number and the critical flux Richardson number, respectively. The gradient Richardson number, Ri, is:

$$Ri = Rf\frac{S_{M2}}{S_{H2}}. \quad (8.137)$$

Rf is then:

$$Rf = \frac{1}{2}\frac{A_2 F_2}{A_1 F_1}\left\{Ri + \frac{A_1 F_1}{A_2 F_2}R_{f1} - \sqrt{Ri^2 + 2\frac{A_1 F_1}{A_2 F_2}(R_{f1} - 2R_{f2})Ri + \left(\frac{A_1 F_1}{A_2 F_2}R_{f1}\right)^2}\right\}, \quad (8.138)$$

$$Rf_C = \frac{\gamma_1}{\gamma_1 + \gamma_2}, \quad (8.139)$$

$$(8.140)$$

where:

$$R_{f1} = B_1\frac{\gamma_1 - C_1}{F_1}, \quad (8.141)$$

$$R_{f2} = B_1\frac{\gamma_1}{F_2}. \quad (8.142)$$

The turbulent length scale, L, is determined by the smallest length scale among three scales:

$$\frac{1}{L} = \frac{1}{L_s} + \frac{1}{L_T} + \frac{1}{L_B}. \quad (8.143)$$

the surface layer scale, L_s, the boundary layer scale, L_T, and buoyancy length

scale, T_B:

$$L_S = \begin{cases} kz/3.7, & \zeta \geq 1 \\ kz/(1+2.7\zeta), & 0 \leq \zeta < 1 \\ kz(1-100\zeta)^{0.2}, & \zeta < 0 \end{cases} , \tag{8.144}$$

$$L_T = 0.23 \frac{\int_0^\infty qz dz}{\int_0^\infty q dz}, \tag{8.145}$$

$$L_B = \begin{cases} q/N, & \partial\theta_v/\partial z > 0 \text{ and } \zeta \geq 0 \\ \{1+5(q_c/L_T N)^{1/2}\}q/N, & \partial\theta_v/\partial z > 0 \text{ and } \zeta < 0 \\ \infty, & \partial\theta_v/\partial z \leq 0 \end{cases} , \tag{8.146}$$

where ζ is the dimensionless height:

$$\zeta = \frac{z}{L_M}. \tag{8.147}$$

L_M is the Monin-Obukhov length:

$$L_M = -\frac{\theta_0 u_*^3}{kg\overline{\theta'_v w'}_g}, \tag{8.148}$$

where u_* is the friction velocity, and the subscript g denotes the ground surface. q_c is a velocity scale defined in a similar manner to convective velocity w_*, except that the depth z_i of the convective boundary layer is replaced by L_t:

$$q_c = \left\{ \frac{g}{\theta_0}\overline{\theta'_v w'}_g L_T \right\}^{1/3} \tag{8.149}$$

$$A_1 = B_1 \frac{1-3\gamma_1}{6}, \tag{8.150}$$

$$A_2 = \frac{1}{3\gamma_1 B_1^{1/3} Pr_N}, \tag{8.151}$$

$$B_1 = 24.0, \tag{8.152}$$

$$B_2 = 15.0, \tag{8.153}$$

$$C_1 = \gamma_1 - \frac{1}{3A_1 B_1^{1/3}}, \tag{8.154}$$

$$C_2 = 0.75, \tag{8.155}$$

$$C_3 = 0.352, \tag{8.156}$$

$$C_5 = 0.2, \tag{8.157}$$

$$\gamma_1 = 0.235, \tag{8.158}$$

$$\gamma_2 = \frac{2A_1(3-2C_2)+B_2(1-C_3)}{B_1}, \tag{8.159}$$

$$F_1 = B_1(\gamma_1 - C_1) + 2A_1(3-2C_2) + 3A_2(1-C_2)(1-C_5), \tag{8.160}$$

$$F_2 = B_1(\gamma_1 + \gamma_2) - 3A_1(1-C_2), \tag{8.161}$$

$$Pr_N = 0.74. \tag{8.162}$$

Discretization

The diffusion equations for $q^2 a$ are solved implicitly:

$$\rho_k \frac{(q_k^2)^{n+1} - (q_k^2)^n}{\Delta t} = 2\rho_k \left[(LqS_M)_k \left\{ \left(\frac{\partial u}{\partial z}\right)^2 + \left(\frac{\partial v}{\partial z}\right)^2 \right\} + (LqS_H N^2)_k \right]$$

$$+ \frac{1}{\Delta z_k} \left\{ (3\rho LqS_M)_{k+\frac{1}{2}} \frac{(q_{k+1}^2)^{n+1} - (q_k^2)^{n+1}}{\Delta z_{k+\frac{1}{2}}} - (3\rho LqS_M)_{k-\frac{1}{2}} \frac{(q_k^2)^{n+1} - (q_{k-1}^2)^{n+1}}{\Delta z_{k-\frac{1}{2}}} \right\}$$

$$- \frac{2\rho_k q_k}{B_1 L_k} (q_k^2)^{n+1}. \tag{8.163}$$

$$a_k (q_{k+1}^2)^{n+1} + b_k (q_k^2)^{n+1} + c_k (q_{k-1}^2)^{n+1} = d_k, \tag{8.164}$$

where:

$$a_k = -\frac{\Delta t}{\Delta z_{k+\frac{1}{2}} \Delta z_k \rho_k} (3\rho LqS_M)_{k+\frac{1}{2}}, \tag{8.165}$$

$$b_k = -a_k - c_k + 1 + \frac{2\Delta t q_k}{B_1 L}, \tag{8.166}$$

$$c_k = -\frac{\Delta t}{\Delta z_k \Delta z_{k-\frac{1}{2}} \rho_k} (3\rho LqS_M)_{k-\frac{1}{2}}, \tag{8.167}$$

$$d_k = (q_k^2)^n + 2\Delta t \left[LqS_M \left\{ \left(\frac{\partial u}{\partial z}\right)^2 + \left(\frac{\partial v}{\partial z}\right)^2 \right\} - LqS_H N^2 \right] \tag{8.168}$$

$$(q_k^2)^{n+1} = e_k (q_{k+1}^2)^{n+1} + f_k, \tag{8.169}$$

where:

$$e_k = -\frac{a_k}{b_k + c_k e_{k-1}}, \tag{8.170}$$

$$f_k = \frac{d_k - c_k f_{k-1}}{b_k + c_k e_{k-1}}. \tag{8.171}$$

Vertical fluxes for $\rho u, \rho v, \rho \theta, \rho q_x$ are also solved implicitly. For instance, the flux for ρu, F_u is calculated by:

$$F_{u,k+\frac{1}{2}} = (\rho LqSM)_{k+\frac{1}{2}} \frac{u_{k+1}^{n+1} - u_k^{n+1}}{\Delta z_{k+\frac{1}{2}}}. \tag{8.172}$$

u^{n+1} is calculated as the same way with q^2, but:

$$a_k = -\frac{\Delta t}{\Delta z_{k+\frac{1}{2}} \Delta z_k \rho_k} (\rho LqS_M)_{k+\frac{1}{2}}, \tag{8.173}$$

$$b_k = -a_k - c_k + 1, \tag{8.174}$$

$$c_k = -\frac{\Delta t}{\Delta z_k \Delta z_{k-\frac{1}{2}} \rho_k} (\rho LqS_M)_{k-\frac{1}{2}}, \tag{8.175}$$

$$d_k = u_k^n. \tag{8.176}$$

8.3 Microphysics

Corresponding author	:	Yousuke Sato,
		Kenta Sueki, and
		Toshiki Matsushima

8.3.1 Kessler Parameterization

SCALE implements a one-moment bulk microphysical scheme, which treats only warm clouds (cloud and rain). This scheme predicts the mixing ratio of cloud (Q_{cloud}) and rain (Q_{rain}). Cloud microphysical processes treated in this scheme are saturation adjustment (corresponding to nucleation, evaporation, and cloud condensation), evaporation, auto-conversion, accretion, and sedimentation. The tendency of Q_{cloud}, Q_{rain}, and Q_v (vapor mixing ratio) is as follows:

$$\frac{\partial Q_{cloud}}{\partial t} = dQ|_{sat} - dQ|_{auto} - dQ|_{acc} \tag{8.177}$$

$$\frac{\partial Q_{rain}}{\partial t} = dQ|_{auto} + dQ|_{acc} - dQ|_{evap} - F_{Q_r}|_{sed} \tag{8.178}$$

$$\frac{\partial Q_v}{\partial t} = dQ|_{evap} - dQ|_{sat} \tag{8.179}$$

where $dQ|_{sat}$, $dQ|_{auto}$, $dQ|_{acc}$, and $dQ|_{evap}$ represent the mixing ratio tendency by saturation adjustment, auto-conversion, accretion, and evaporation, respectively. $F_{Q_r}|_{sed}$ represents flux of Q_r by sedimentation.
$dQ|_{auto}$, $dQ|_{acc}$, and $dQ|_{evap}$ are given as:

$$dQ_{auto} = \begin{cases} Q_{cloud} * 10^{-3} & (Q_{cloud} > 10^{-3}) \\ 0 & (else) \end{cases} \tag{8.180}$$

$$dQ_{acc} = 2.2 \times Q_{cloud} \times Q_{rain}^{0.875} \tag{8.181}$$

$$dQ_{evap} = \begin{cases} f_{vent} \frac{q_s - Q_{cloud}}{q_s \rho} \frac{(\rho * Q_{rain})^{0.525}}{5.4 \times 10^5 + \frac{2.55 \times 10^8}{p q_s}} & (q_s > Q_{cloud}) \\ 0 & (else) \end{cases} \tag{8.182}$$

where f_{vent} is the ventilation factor ($f_{vent} = 1.6 + 124.9(\rho Q_{rain})^{0.2046}$), and the unit of dQ_{***} is [kg/kg/s]. p, q_s, and ρ are pressure, saturation vapor mixing ratio, and total density, respectively.
$dQ|_{sat}$ is given as:

$$dQ|_{sat} = Q_v - q_s. \tag{8.183}$$

Terminal velocities of cloud ($V_{t,c}$) and rain ($V_{t,r}$) are given as:

$$V_{t,c} = 0 \tag{8.184}$$

$$V_{t,r} = 36.34(\rho Q_{rain})^{0.1364}[m/s] \tag{8.185}$$

8.3.2 Six-class Single-moment Bulk Scheme (Tomita 2008)

Six-class single-moment bulk scheme in the SCALE was developed by Tomita (2008). This scheme predicts mass exchange among six categories of water substances (water vapor, cloud water, rain, cloud ice, snow, and graupel), which is largely based on the method of Lin et al. (1983). However, there are some modifications from the original method of Lin et al. (1983): Both cloud water and cloud ice are generated only by a saturation adjustment process, and wet growth process of graupel is omitted. According to Tomita (2008), these modifications result in 20% reduction in computational cost compared to Lin et al. (1983) without significant changes on physical performance. In this subsection, the formulations of the microphysical scheme of Tomita (2008) are described. Mass concentrations of water vapor, cloud water, rain, cloud ice, snow, and graupel are indicated by q_v, Q_W, Q_R, Q_I, Q_S, and Q_G respectively.

In Tomita (2008), cloud microphysics processes except for the saturation adjustment process consist of auto-conversion, accretion, evaporation, sublimation, deposition, melting, freezing, and Bergeron process. When $T < T_0$ ($= 273.15$ K), the tendency of each water substance by these processes can be written as follows:

$$\frac{\partial Q_W}{\partial t} = -P_{RAUT} - P_{RACW} - P_{SACW} - P_{GACW} - P_{SFW}, \tag{8.186}$$

$$\frac{\partial Q_I}{\partial t} = -P_{SAUT} - P_{RACI} - P_{SACI} - P_{GACI} - P_{SFI}, \tag{8.187}$$

$$\frac{\partial Q_R}{\partial t} = P_{RAUT} + P_{RACW} - P_{IACR} - P_{SACR} - P_{GACR} - P_{GFRZ} - P_{REVP}, \tag{8.188}$$

$$\begin{aligned}\frac{\partial Q_S}{\partial t} = &\ P_{SAUT} - P_{GAUT} \\ &+ P_{SACW} + P_{SACI} + (1-\delta_1)P_{RACI} + (1-\delta_1)P_{IACR} + \delta_2 P_{SACR} - (1-\delta_2)P_{RACS} - P_{GACS} \\ &- (1-\delta_3)P_{SSUB} + \delta_3 P_{SDEP} + P_{SFW} + P_{SFI}, \end{aligned} \tag{8.189}$$

$$\begin{aligned}\frac{\partial Q_G}{\partial t} = &\ P_{GAUT} \\ &+ P_{GACW} + P_{GACI} + P_{GACR} + P_{GACS} + \delta_1 P_{RACI} + \delta_1 P_{IACR} + (1-\delta_2)P_{SACR} + (1-\delta_2)P_{RACS} \\ &- (1-\delta_3)P_{GSUB} + \delta_3 P_{GDEP} + P_{GFRZ}, \end{aligned} \tag{8.190}$$

$$\frac{\partial q_v}{\partial t} = P_{REVP} + (1-\delta_3)P_{SSUB} + (1-\delta_3)P_{GSUB} - \delta_3 P_{SDEP} - \delta_3 P_{GDEP}, \tag{8.191}$$

where P_* in the right hand sides are conversion terms listed in Table 8.1, and δ_1, δ_2, and δ_3 are defined as

$$\delta_1 = \begin{cases} 1, & \text{for } Q_R \geq 10^{-4} \text{ kg/kg} \\ 0, & \text{otherwise} \end{cases}, \tag{8.192}$$

$$\delta_2 = \begin{cases} 1, & \text{for } Q_R \leq 10^{-4} \text{ kg/kg and } Q_S \leq 10^{-4} \text{ kg/kg} \\ 0, & \text{otherwise} \end{cases}, \tag{8.193}$$

$$\delta_3 = \begin{cases} 1, & \text{for } S_{ice} \geq 1 \\ 0, & \text{otherwise} \end{cases}, \tag{8.194}$$

where S_{ice} is saturation ratio over ice. When $T \geq T_0$, the tendencies of each water substance can be written as follows:

$$\frac{\partial Q_W}{\partial t} = -P_{RAUT} - P_{RACW} - P_{SACW} - P_{GACW}, \tag{8.195}$$

$$\frac{\partial Q_I}{\partial t} = 0, \tag{8.196}$$

$$\frac{\partial Q_R}{\partial t} = P_{RAUT} + P_{RACW} + P_{SACW} + P_{GACW} + P_{SMLT} + P_{GMLT} - P_{REVP}, \tag{8.197}$$

$$\frac{\partial Q_S}{\partial t} = -P_{GACS} - P_{SMLT}, \tag{8.198}$$

$$\frac{\partial Q_G}{\partial t} = P_{GACS} - P_{GMLT}, \tag{8.199}$$

$$\frac{\partial q_v}{\partial t} = P_{REVP}. \tag{8.200}$$

Formulation of each term is described later.

Table 8.1: List of conversion terms used in six-class single-moment bulk scheme of Tomita (2008)

Notation	Description	Direction	Conditions
P_{RAUT}	Auto-conversion rate of cloud water to form rain	$Q_W \longrightarrow Q_R$	
P_{SAUT}	Auto-conversion rate of cloud ice to form snow	$Q_I \longrightarrow Q_S$	$T < T_0$
P_{GAUT}	Auto-conversion rate of snow to form graupel	$Q_S \longrightarrow Q_G$	$T < T_0$
P_{RACW}	Accretion rate of cloud water by rain	$Q_W \longrightarrow Q_R$	
P_{SACW}	Accretion rate of cloud water by snow	$Q_W \longrightarrow Q_S$	$T < T_0$
		$Q_W \longrightarrow Q_R$	$T \geq T_0$
P_{GACW}	Accretion rate of cloud water by graupel	$Q_W \longrightarrow Q_G$	$T < T_0$
		$Q_W \longrightarrow Q_R$	$T \geq T_0$
P_{RACI}	Accretion rate of cloud ice by rain	$Q_I \longrightarrow Q_S$	$T < T_0$ and $Q_R < 10^{-4}$ kg/kg
		$Q_I \longrightarrow Q_G$	$T < T_0$ and $Q_R \geq 10^{-4}$ kg/kg
P_{SACI}	Accretion rate of cloud ice by snow	$Q_I \longrightarrow Q_S$	$T < T_0$
P_{GACI}	Accretion rate of cloud ice by graupel	$Q_I \longrightarrow Q_G$	$T < T_0$
P_{IACR}	Accretion rate of rain by cloud ice	$Q_R \longrightarrow Q_S$	$T < T_0$ and $Q_R < 10^{-4}$ kg/kg
		$Q_R \longrightarrow Q_G$	$T < T_0$ and $Q_R \geq 10^{-4}$ kg/kg
P_{SACR}	Accretion rate of rain by snow	$Q_R \longrightarrow Q_S$	$T < T_0$, $Q_R \leq 10^{-4}$ kg/kg, and $Q_S \leq 10^{-4}$ kg/kg
		$Q_R \longrightarrow Q_G$	$T < T_0$ and (Q_R or Q_S) $> 10^{-4}$ kg/kg
P_{GACR}	Accretion rate of rain by graupel	$Q_R \longrightarrow Q_G$	$T < T_0$
P_{RACS}	Accretion rate of snow by rain	$Q_S \longrightarrow Q_G$	$T < T_0$ and (Q_R or Q_S) $> 10^{-4}$ kg/kg
P_{GACS}	Accretion rate of snow by graupel	$Q_S \longrightarrow Q_G$	
P_{REVP}	Evaporation rate of rain	$Q_R \longrightarrow q_v$	
P_{SSUB}	Sublimation rate of snow	$Q_S \longrightarrow q_v$	$S_{ice} < 1$
P_{GSUB}	Sublimation rate of graupel	$Q_G \longrightarrow q_v$	$S_{ice} < 1$
P_{SDEP}	Deposition rate of water vapor for snow	$q_v \longrightarrow Q_S$	$S_{ice} \geq 1$
P_{GDEP}	Deposition rate of water vapor for graupel	$q_v \longrightarrow Q_G$	$S_{ice} \geq 1$
P_{SMLT}	Melting rate of snow	$Q_S \longrightarrow Q_R$	$T \geq T_0$
P_{GMLT}	Melting rate of graupel	$Q_G \longrightarrow Q_R$	$T \geq T_0$
P_{GFRZ}	Freezing rate of rain to form graupel	$Q_R \longrightarrow Q_G$	$T < T_0$
P_{SFW}	Growth rate of snow by Bergeron process from cloud water	$Q_W \longrightarrow Q_S$	243.15 K $\leq T < T_0$
P_{SFI}	Growth rate of snow by Bergeron process from cloud ice	$Q_I \longrightarrow Q_S$	243.15 K $\leq T < T_0$

The saturation adjustment

Mass exchange among water vapor, cloud water, and cloud ice is controlled by the saturation adjustment. In the SCALE, the saturation adjustment is

calculated after the aforementioned conversion processes of the microphysics. To calculate the adjustment process, saturated mass concentration of water vapor is defined as follows:

$$q_v^*(T) = q_{vl}^*(T) + [1 - \alpha(T)]q_{vi}^*(T), \qquad (8.201)$$

where $q_{vl}^*(T)$ is saturated mass concentration of water vapor against liquid phase, $q_{vi}^*(T)$ is that for ice phase, and $\alpha(T)$ is a continuous function which satisfies

$$\begin{cases} \alpha(T) = 1, & \text{for } T \geq 273.15 \text{ K}, \\ \alpha(T) = \frac{T - 233.15}{40.0}, & \text{for } 233.15 \text{ K} < T < 273.15 \text{ K}, \\ \alpha(T) = 0, & \text{for } T \leq 233.15 \text{ K}. \end{cases} \qquad (8.202)$$

If it is supersaturated, water vapor is converted into cloud water and cloud ice. If it is unsaturated, cloud water and cloud ice are converted into water vapor. As a conserved quantity for the adjustment process, the moist internal energy is also defined as follows:

$$U_0 = [q_d c_{vd} + q_v c_{vv} + (Q_W + Q_R)c_l + (Q_I + Q_S + Q_G)c_s]T$$
$$+ q_v L_v - (Q_I + Q_S + Q_G)L_f, \qquad (8.203)$$

where L_v is the latent heat between water vapor and liquid water, L_f is that between liquid water and solid water. In addition, the sum of the mass concentration of water vapor, cloud water, and cloud ice

$$q_{sum} = q_v + Q_W + Q_I, \qquad (8.204)$$

does not change through the saturation adjustment.

First, it is assumed that all of the cloud water Q_W and cloud ice Q_I evaporate. In this case, the mass concentration of water vapor becomes equal to q_{sum} and the temperature decreases due to the evaporation. The moist internal energy can be written as

$$U_1 = [q_d c_{vd} + q_{sum} c_{vv} + Q_R c_l + (Q_S + Q_G)c_s]T_1$$
$$+ q_{sum} L_v - (Q_S + Q_G)L_f. \qquad (8.205)$$

Since the moist internal energy does not change through the saturation adjustment, we can obtain the new temperature value T_1 easily by solving $U_0 = U_1$. Then, if q_{sum} is less than saturated mass concentration of water vapor at this temperature (i.e. $q_{sum} < q_v^*(T_1)$), no saturation occurs and the new values of water vapor q_v', cloud water Q_W', cloud ice Q_I', and temperature T' are determined as

$$\begin{cases} q_v' & = q_{sum}, \\ Q_W' & = 0, \\ Q_I' & = 0, \\ T' & = T_1. \end{cases} \qquad (8.206)$$

If q_{sum} exceeds $q_v^*(T_1)$, saturation occurs. In this case, new temperature value T_2 should be determined by satisfying the equations of

$$U_0 = [q_d c_{vd} + q_v^*(T_2)c_{vv} + (Q_{W2} + Q_R)c_l + (Q_{I2} + Q_S + Q_G)c_s]T_2$$
$$+ q_v^*(T_2)L_v - (Q_{I2} + Q_S + Q_G)L_f, \tag{8.207}$$
$$Q_{W2} = [q_{sum} - q_v^*(T_2)]\alpha(T_2), \tag{8.208}$$
$$Q_{I2} = [q_{sum} - q_v^*(T_2)](1 - \alpha(T_2)). \tag{8.209}$$

Eqs. (8.201) and (8.207-8.209) are solved numerically and the new values are determined as

$$
\begin{cases}
q_v' & = q_v^*(T_2), \\
Q_W' & = Q_{W2}, \\
Q_I' & = Q_{I2}, \\
T' & = T_2.
\end{cases} \tag{8.210}
$$

Fundamental characteristics of precipitation particles

In the reminder of this subsection, the formulations of all conversion terms listed in Table 8.1 are shown. Before that, however, it is necessary to clarify assumptions about the characteristics of precipitation particles (rain, snow, and graupel). In Tomita (2008), it is assumed that seizes of precipitation particles obey the Marshall-Palmer exponential size distribution:

$$n_{[R,S,G]}(D) = N_{0[R,S,G]} \exp(-\lambda_{[R,S,G]}D), \tag{8.211}$$

where D is the diameter of particle, N_0 is an intercept parameter, and λ is a slope parameter. The subscriptions of R, S, and G denote rain, snow, and graupel, respectively. In the SCALE, each intercept parameter has values of

$$
\begin{cases}
N_{0R} & = 8.0 \times 10^6 \text{ m}^{-4}, \\
N_{0S} & = 3.0 \times 10^6 \text{ m}^{-4}, \\
N_{0G} & = 4.0 \times 10^6 \text{ m}^{-4}.
\end{cases} \tag{8.212}
$$

The mass and terminal velocity of each particle are described as

$$m_{[R,S,G]}(D) = a_{[R,S,G]}D^{b_{[R,S,G]}} \tag{8.213}$$

$$v_{t[R,S,G]}(D) = c_{[R,S,G]}D^{d_{[R,S,G]}}\left(\frac{\rho_0}{\rho}\right)^{1/2} \tag{8.214}$$

where ρ_0 (= 1.28 kg/m³) is a reference density, and a, b, c, and d are coefficients depending on the particle shape. All precipitation particles are treated as spherical, thus

$$a_R = \pi\rho_w/6, \quad a_S = \pi\rho_S/6, \quad a_G = \pi\rho_G/6, \tag{8.215}$$
$$b_R = b_S = b_G = 3, \tag{8.216}$$

where $\rho_w = 1000$ kg/m³, $\rho_S = 100$ kg/m³, $\rho_G = 400$ kg/m³. The coefficients c and d are determined empirically. In the SCALE, their values are

$$c_R = 130.0, \quad c_S = 4.84, \quad c_G = 82.5, \tag{8.217}$$
$$d_R = 0.5, \quad d_S = 0.25, \quad d_G = 0.5, \tag{8.218}$$

The slope parameters are determined from Eqs. (8.211) and (8.213) as

$$\lambda = \left[\frac{a N_0 \Gamma(b+1)}{\rho Q} \right]^{1/(b+1)}, \tag{8.219}$$

where Γ is the gamma function. The bulk terminal velocities are derived as

$$V_T = c \left(\frac{\rho_0}{\rho} \right)^{1/2} \frac{\Gamma(b+d+1)}{\Gamma(b+1)\lambda^d}. \tag{8.220}$$

Note that subscription R, S, and G in Eqs. (8.219) and (8.220) are omitted for simplicity.

Auto-conversion terms

The auto-conversion rate of cloud water to form rain (P_{RAUT}) is given as

$$P_{RAUT} = \frac{1}{\rho} \left[16.7 \times (\rho Q_W)^2 \left(5 + \frac{3.6 \times 10^{-5} N_d}{D_d \rho Q_W} \right)^{-1} \right], \tag{8.221}$$

where N_d is the number concentration of cloud water ($N_d = 50$ cm^{-3} in the SCALE) and D_d is given as

$$D_d = 0.146 - 5.964 \times 10^{-2} \ln \frac{N_d}{2000}. \tag{8.222}$$

The auto-conversion rate of cloud ice to form snow (P_{SAUT}) is given as

$$P_{SAUT} = \beta_1 (Q_I - Q_{I0}), \tag{8.223}$$

where Q_{I0} is set to 0 kg/kg and β_1 is formulated as

$$\beta_1 = \beta_{10} \exp[\gamma_{SAUT}(T - T_0)]. \tag{8.224}$$

β_{10} and γ_{SAUT} are set to 0.001 and 0.025, respectively, in Tomita (2008). In the SCALE, however, they are set to 0.006 and 0.06 as default settings. The auto-conversion rate of snow to form graupel (P_{GAUT}) is given as

$$P_{GAUT} = \beta_2 (Q_S - Q_{S0}), \tag{8.225}$$

where Q_{S0} is set to 6×10^{-4} kg/kg and β_2 is formulated as

$$\beta_2 = \beta_{20} \exp[\gamma_{GAUT}(T - T_0)]. \tag{8.226}$$

β_{20} and γ_{GAUT} are set to 0.001 and 0.09, respectively, in Tomita (2008). In the SCALE, however, $\beta_{20} = 0$ as a default setting, which means that auto-conversion of snow to graupel is turned off.

Accretion terms

Accretion of cloud particles by precipitation particles (P_{RACW}, P_{SACW}, P_{GACW}, P_{RACI}, P_{SACI}, and P_{GACI}) can be derived as

$$
\begin{aligned}
P_{RACW} &= E_{RW}Q_W \int_0^\infty \frac{\pi}{4}D^2 v_{tR}(D)n_R(D)dD \\
&= \frac{\pi E_{RW}N_{0R}c_R Q_W \Gamma(3+d_R)}{4\lambda_R^{3+d_R}}\left(\frac{\rho_0}{\rho}\right)^{1/2},
\end{aligned} \tag{8.227}
$$

$$
P_{SACW} = \frac{\pi E_{SW}N_{0S}c_S Q_W \Gamma(3+d_S)}{4\lambda_S^{3+d_S}}\left(\frac{\rho_0}{\rho}\right)^{1/2}, \tag{8.228}
$$

$$
P_{GACW} = \frac{\pi E_{GW}N_{0G}c_G Q_W \Gamma(3+d_G)}{4\lambda_G^{3+d_G}}\left(\frac{\rho_0}{\rho}\right)^{1/2}, \tag{8.229}
$$

$$
P_{RACI} = \frac{\pi E_{RI}N_{0R}c_R Q_I \Gamma(3+d_R)}{4\lambda_R^{3+d_R}}\left(\frac{\rho_0}{\rho}\right)^{1/2}, \tag{8.230}
$$

$$
P_{SACI} = \frac{\pi E_{SI}N_{0S}c_S Q_I \Gamma(3+d_S)}{4\lambda_S^{3+d_S}}\left(\frac{\rho_0}{\rho}\right)^{1/2}, \tag{8.231}
$$

$$
P_{GACI} = \frac{\pi E_{GI}N_{0G}c_G Q_I \Gamma(3+d_G)}{4\lambda_G^{3+d_G}}\left(\frac{\rho_0}{\rho}\right)^{1/2}, \tag{8.232}
$$

where E_{RW}, E_{SW}, E_{GW}, E_{RI}, E_{SI}, and E_{GI} are collection efficiency of each accretion process. In the SCALE, $E_{RW} = E_{SW} = E_{GW} = E_{RI} = 1$, $E_{GI} = 0.1$, and E_{SI} is formulated as

$$
E_{SI} = \exp[\gamma_{SACI}(T - T_0)], \tag{8.233}
$$

where γ_{SACI} is set to 0.025. When the accretion of cloud ice by rain occurs, rain freezes to become snow or graupel. Thus, the conversion term from rain to these particles (P_{IACR}) should be considered. It is derived as

$$
\begin{aligned}
P_{IACR} &= \frac{1}{\rho}\int_0^\infty N_I E_{RI}\frac{\pi}{4}D^2 v_{tR}(D)m_R(D)n_R(D)dD \\
&= \frac{\pi a_R E_{RI}Q_I N_{0R}c_R \Gamma(6+d_R)}{4M_I \lambda_R^{6+d_R}}\left(\frac{\rho_0}{\rho}\right)^{1/2},
\end{aligned} \tag{8.234}
$$

where N_I is the number concentration of cloud ice, and M_I ($= 4.19 \times 10^{-13}$ kg) is mass of cloud ice particle.

Accretion of precipitation particles (P_{SACR}, P_{GACR}, and P_{GACS}) can be

derived as

$$P_{SACR} = \frac{1}{\rho} \int_0^\infty E_{SR} m_R(D_R) n_R(D_R) \left[\int_0^\infty \frac{\pi}{4} (D_S + D_R)^2 |V_{TS} - V_{TR}| n_S(D_S) dD_S \right] dD_R$$

$$= \frac{\pi a_R |V_{TS} - V_{TR}| E_{SR} N_{0S} N_{0R}}{4\rho}$$

$$\times \left[\frac{\Gamma(b_R + 1)\Gamma(3)}{\lambda_R^{b_R+1} \lambda_S^3} + 2 \frac{\Gamma(b_R + 2)\Gamma(2)}{\lambda_R^{b_R+2} \lambda_S^2} + \frac{\Gamma(b_R + 3)\Gamma(1)}{\lambda_R^{b_R+3} \lambda_S} \right], \qquad (8.235)$$

$$P_{GACR} = \frac{\pi a_R |V_{TG} - V_{TR}| E_{GR} N_{0G} N_{0R}}{4\rho}$$

$$\times \left[\frac{\Gamma(b_R + 1)\Gamma(3)}{\lambda_R^{b_R+1} \lambda_G^3} + 2 \frac{\Gamma(b_R + 2)\Gamma(2)}{\lambda_R^{b_R+2} \lambda_G^2} + \frac{\Gamma(b_R + 3)\Gamma(1)}{\lambda_R^{b_R+3} \lambda_G} \right], \qquad (8.236)$$

$$P_{GACS} = \frac{\pi a_S |V_{TG} - V_{TS}| E_{GS} N_{0G} N_{0S}}{4\rho}$$

$$\times \left[\frac{\Gamma(b_S + 1)\Gamma(3)}{\lambda_S^{b_S+1} \lambda_G^3} + 2 \frac{\Gamma(b_S + 2)\Gamma(2)}{\lambda_S^{b_S+2} \lambda_G^2} + \frac{\Gamma(b_S + 3)\Gamma(1)}{\lambda_S^{b_S+3} \lambda_G} \right], \qquad (8.237)$$

where E_{SR}, E_{GR}, and E_{GS} are collection efficiency of each accretion process. Note that terminal velocity for each particle size is approximated by the bulk terminal velocity (e.g. $|v_{tS}(D_S) - v_{tR}(D_R)| \simeq |V_{TS} - V_{TR}|$). In the SCALE, $E_{SR} = E_{GR} = 1$, and E_{GS} is formulated as

$$E_{GS} = \min(1, \exp[\gamma_{GACS}(T - T_0)]), \qquad (8.238)$$

where γ_{GACS} is set to 0.09. When the accretion of rain by snow occurs under the condition of $Q_R > 10^{-4}$ kg/kg or $Q_S > 10^{-4}$ kg/kg, graupel particle is generated. Thus, the conversion term from snow to graupel (P_{RACS}) should be also considered. It can be written as

$$P_{RACS} = \frac{\pi a_S |V_{TR} - V_{TS}| E_{SR} N_{0R} N_{0S}}{4\rho}$$

$$\times \left[\frac{\Gamma(b_S + 1)\Gamma(3)}{\lambda_S^{b_S+1} \lambda_R^3} + 2 \frac{\Gamma(b_S + 2)\Gamma(2)}{\lambda_S^{b_S+2} \lambda_R^2} + \frac{\Gamma(b_S + 3)\Gamma(1)}{\lambda_S^{b_S+3} \lambda_R} \right]. \qquad (8.239)$$

Evaporation, sublimation, and deposition

Evaporation rate of rain (P_{REVP}) is described as

$$P_{REVP} = \frac{2\pi N_{0R}(1 - \min(S_{liq}, 1)) G_w(T)}{\rho}$$

$$\times \left[f_{1R} \frac{\Gamma(2)}{\lambda_R^2} + f_{2R} c_R^{1/2} \left(\frac{\rho_0}{\rho} \right)^{1/4} \nu^{-1/2} \frac{\Gamma(\frac{5+d_R}{2})}{\lambda_R^{\frac{5+d_R}{2}}} \right], \qquad (8.240)$$

where S_{liq} is saturation ratio over liquid, coefficients f_{1R} and f_{2R} are 0.78 and 0.27 respectively, ν is the kinematic viscosity of air, and $G_w(T)$ is the thermodynamic function for liquid water given as

$$G_w(T) = \left[\frac{L_v}{K_a T} \left(\frac{L_v}{R_v T} - 1 \right) + \frac{1}{\rho q_{vl}^*(T) K_d} \right]^{-1}, \qquad (8.241)$$

where K_a is the thermal diffusion coefficient of air and K_d is the diffusion coefficient of water vapor in air. P_{REVP} works only when S_{liq} is less than 1 (i.e. unsaturated condition).

Sublimation and deposition rates for snow (P_{SSUB} and P_{SDEP}) are described by the same equation:

$$P^*_{SSUB,SDEP} = \frac{2\pi N_{0S}(1 - S_{ice})G_i(T)}{\rho}$$
$$\times \left[f_{1S}\frac{\Gamma(2)}{\lambda_S^2} + f_{2S}c_S^{1/2}\left(\frac{\rho_0}{\rho}\right)^{1/4}\nu^{-1/2}\frac{\Gamma(\frac{5+d_S}{2})}{\lambda_S^{\frac{5+d_S}{2}}} \right], \qquad (8.242)$$

where coefficients f_{1S} and f_{2S} are 0.65 and 0.39 respectively, and $G_i(T)$ is the thermodynamic function for ice water given as

$$G_i(T) = \left[\frac{L_s}{K_a T}\left(\frac{L_s}{R_v T} - 1\right) + \frac{1}{\rho q^*_{vi}(T) K_d} \right]^{-1}, \qquad (8.243)$$

where L_s is the latent heat between water vapor and solid water. If it is unsaturated ($S_{ice} < 1$), the sublimation rate of snow is given as

$$P_{SSUB} = P^*_{SSUB,SDEP}. \qquad (8.244)$$

If it is supersaturated ($S_{ice} \geq 1$), the deposition rate of water vapor for snow is given as

$$P_{SDEP} = -P^*_{SSUB,SDEP}. \qquad (8.245)$$

Also sublimation and deposition rates for graupel (P_{GSUB} and P_{GDEP}) are described by

$$P^*_{GSUB,GDEP} = \frac{2\pi N_{0G}(1 - S_{ice})G_i(T)}{\rho}$$
$$\times \left[f_{1G}\frac{\Gamma(2)}{\lambda_G^2} + f_{2G}c_G^{1/2}\left(\frac{\rho_0}{\rho}\right)^{1/4}\nu^{-1/2}\frac{\Gamma(\frac{5+d_G}{2})}{\lambda_G^{\frac{5+d_G}{2}}} \right], \qquad (8.246)$$

where coefficients f_{1G} and f_{2G} are 0.78 and 0.27 respectively. If it is unsaturated ($S_{ice} < 1$), the sublimation rate of graupel is given as

$$P_{GSUB} = P^*_{GSUB,GDEP}. \qquad (8.247)$$

If it is supersaturated ($S_{ice} \geq 1$), the deposition rate of water vapor for graupel is given as

$$P_{GDEP} = -P^*_{GSUB,GDEP}. \qquad (8.248)$$

Melting and freezing

When $T \geq T_0$, snow particle melts to become rain. The melting rate of snow is described as

$$P_{SMLT} = \frac{2\pi K_a(T - T_0)N_{0S}}{\rho L_f}$$

$$\times \left[f_{1S}\frac{\Gamma(2)}{\lambda_S^2} + f_{2S}c_S^{1/2}\left(\frac{\rho_0}{\rho}\right)^{1/4}\nu^{-1/2}\frac{\Gamma\left(\frac{5+d_S}{2}\right)}{\lambda_S^{\frac{5+d_S}{2}}} \right]$$

$$+ \frac{c_l(T - T_0)}{L_f}(P_{SACW} + P_{SACR}). \qquad (8.249)$$

The last term indicates that the accretions of cloud water and rain promote snow melting. Similarly, the melting rate of graupel is described as

$$P_{GMLT} = \frac{2\pi K_a(T - T_0)N_{0G}}{\rho L_f}$$

$$\times \left[f_{1G}\frac{\Gamma(2)}{\lambda_G^2} + f_{2G}c_G^{1/2}\left(\frac{\rho_0}{\rho}\right)^{1/4}\nu^{-1/2}\frac{\Gamma\left(\frac{5+d_G}{2}\right)}{\lambda_G^{\frac{5+d_G}{2}}} \right]$$

$$+ \frac{c_l(T - T_0)}{L_f}(P_{GACW} + P_{GACR}). \qquad (8.250)$$

When $T < T_0$, rain particle freezes to become graupel. The freezing rate of rain is described as

$$P_{GFRZ} = 20\pi^2 B' N_{0R}\frac{\rho_w}{\rho}\frac{\exp[A'(T_0 - T)] - 1}{\lambda_R^7}, \qquad (8.251)$$

where $A' = 0.66$ K^{-1} and $B' = 100$ m^{-3} s^{-1}.

Bergeron process

When cloud water and cloud ice coexist under the condition of $T < T_0$, supercooled cloud water evaporates and diffuses to cloud ice because the saturated vapor pressure over liquid water is higher than that for solid water. This process is called Bergeron process. Through this process, cloud ice particle grows to become precipitating snow particle. Thus, mass conversion from cloud water and cloud ice to snow occurs. Conversion rates of cloud water (P_{SFW}) and cloud ice (P_{SFI}) are formulated as

$$P_{SFW} = N_{I50}(a_1 m_{I50}^{a_2} + \pi E_{IW}\rho Q_W R_{I50}^2 U_{I50}), \qquad (8.252)$$
$$P_{SFI} = Q_I/\Delta t_1, \qquad (8.253)$$

where m_{I50} ($= 4.8 \times 10^{-10}$ kg) and U_{I50} ($= 1$ m/s) denotes mass and terminal velocity of ice particle having a radius of 50 μm ($\equiv R_{I50}$), and $E_{IW} = 1$ is collection efficiency of cloud ice for cloud water. The values of a_1 and a_2 is determined from a laboratory experiment by Koenig (1971). Δt_1 is the time during which an ice particle of 40 μm grows to 50 μm, which is formulated as

$$\Delta t_1 = \frac{1}{a_1(1 - a_2)}\left[m_{I50}^{1-a_2} - m_{I40}^{1-a_2} \right], \qquad (8.254)$$

where $m_{I40} = 2.46 \times 10^{-10}$ kg. N_{I50} is the number concentration of 50 μm ice particle which is formulated as

$$N_{I50} = q_{I50}/m_{I50} = \frac{Q_I \Delta t}{m_{I50} \Delta t_1}. \tag{8.255}$$

In the SCALE, the Bergeron process occurs only when 243.15 K $\leq T < T_0$.

Optional schemes in the SCALE

There are some optional schemes which can be applied to the six-class single-moment bulk microphysics. Cloud ice generation can be explicitly solved as the original method of Lin et al. (1983), instead of the saturation adjustment process. Conversion terms of cloud water to rain (P_{RAUT} and P_{RACW}) can be replaced with those used in Khairoutdinov and Kogan (2000). Intercept parameters of particle size distribution (N_{0R}, N_{0S}, N_{0G}) can be diagnostically derived by using the equation of Wainwright et al. (2014), instead of the constant values. Bimodal particle size distribution can be applied to snow following Roh and Satoh (2014), instead of the Marshall-Palmer exponential size distribution.

8.3.3 Double-Moment Bulk scheme

SCALE implements a double-moment bulk microphysical scheme with six categories (cloud water, rain, cloud ice, snow, and graupel) based on Seiki and Nakajima (2014) (hereafter SN14). SN14 is designed to maintain the self consistency of the assumptions regarding particle mass distribution and the shapes of ice particles throughout cloud microphysical process. In this scheme, particle mass distributions of each category are expressed as a generalized gamma function and 0-th moments (number density) and 1-th moments (mass concentration) of the distributions are predicted. SN14 calculates microphysical process for nucleation of cloud droplets and cloud ice, phase change (condensation/evaporation, deposition/sublimation, freezing, melting), and collection (self-collection, auto-conversion, accretion and breakup). Precipitation process for SN14 is separated from other microphysical process and calculated using terminal velocity in SCALE. More details are described in Appendix B.

8.3.4 Spectral Bin Model(SBM)

The Spectral Bin Model (SBM) was developed by Suzuki (2006) and Suzuki et al. (2010). The model forecasts the Size Distribution Function (SDF) of seven types of hydrometeors (liquid, plate-ice, columnar-ice, dendritic-ice, snow, graupel, and hail).
The SBM calculates mass density of the seven types of hydrometeor and one type of aerosol as their SDFs. The SDF of aerosol can be changed by advection and activation (i.e., nucleation from aerosol to cloud) processes. The SDF of hydrometeors can be changed by several growth processes (i.e., activation from aerosol to cloud, condensation/evaporation, collision/coagulation, freezing/melting, ice nucleation, riming, aggregation, advection, and gravitational falling).
The time evolution of SDF (number density) of aerosol ($f_a(m,t)$) and SDF (number density) of hydrometeor ($f_c(m,t)$) are shown as:

$$\frac{\partial f_c^{(\mu)}(m,t)}{\partial t} = Adv\big[f_c^{(\mu)}(m,t)\big] + Grav\big[f_c^{(\mu)}(m,t)\big] + \Big[\frac{\partial f_c^{(\mu)}(m,t)}{\partial t}\Big]_{cloud\ microphysics} \quad (8.256)$$

$$\frac{\partial f_a(m_a,t)}{\partial t} = Adv\big[f_a(m_a,t)\big] + Grav\big[f_a(m_a,t)\big] + \Big[\frac{\partial f_a(m_a,t)}{\partial t}\Big]_{cloud\ microphysics} \quad (8.257)$$

where μ shows type of hydrometeor (the seven types), and $Adv[]$, $Grav[]$ show change of SDF by advection and gravitational falling. $\big[\ \big]_{cloud\ microphysics}$ shows SDF changes by cloud microphysical processes.

The time evolution of $f_c^{(\mu)}(m,t)$, and $f_a(m,t)$ are shown as:

$$\Big[\frac{\partial f_c^{(\mu)}(m,t)}{\partial t}\Big]_{cloud\ microphysics} = \Big[\frac{\partial f_c^{(\mu)}(m,t)}{\partial t}\Big]_{activation} + \Big[\frac{\partial f_c^{(\mu)}(m,t)}{\partial t}\Big]_{cond/evap}$$

$$+ \Big[\frac{\partial f_c^{(\mu)}(m,t)}{\partial t}\Big]_{coll/coag/rim/agg}$$

$$+ \Big[\frac{\partial f_c^{(\mu)}(m,t)}{\partial t}\Big]_{frz} + \Big[\frac{\partial f_c^{(\mu)}(m,t)}{\partial t}\Big]_{melt}$$

$$\Big[\frac{\partial f_a(m_a,t)}{\partial t}\Big]_{cloud\ microphysics} = \Big[\frac{\partial f_a(m_a,t)}{\partial t}\Big]_{activation}$$

where $\big[\ \big]_{***}$ show change of SDF by each cloud growth process. The detail of these processes will be provided later.

The change of SDFs by advection and gravitational falling (i.e., first and second terms of eq.(8.256), and (8.257)) are calculated by dynamical core of SCALE-RM shown in section 3.

Discretization of Size Distribution Function(SDF)

The SDF of aerosol and cloud is predicted as mass density of each particle size $(g_a(m_a),\ g_c^{(\mu)}(m))$. However most equations are given as equations of number density of cloud/aerosol $(f_c^{(\mu)}(m,t),\ f_a(m_a,t))$; the mass density of cloud/aerosol is transferred to the number density of cloud/aerosol $(g_a(m_a,t) = m_a g_a(m_a,t),\ g_c^{(\mu)}(m,t) = m^{(\mu)} f_c^{(\mu)}(m,t))$.

To cover a wide size range (i.e., $2\ \mu m \sim 3\ mm$), a logarithmically uniform grid system $(log(m) \equiv \eta,\ log(m_a) \equiv \eta_a)$ is used. In this system, the relationship, $\frac{m_{i+1}}{m_i} = const.$ is satisfied.

Activation from aerosol to cloud particles (nucleation process)

The change of SDFs by activation from aerosol to cloud particles is calculated based on Kohler theory Kohler (1936). Through this process, aerosols with radii larger than the aerosol critical radius $(r_{a,crit})$ are activated to clouds. The critical radius is given as:

$$r_{a,crit} = \Big(\frac{4}{27}\frac{A^3}{B}\frac{1}{S_w}\Big)^{1/3}, \quad A = \frac{2\sigma}{R_v \rho_L T}, \quad B = i_v \frac{M_v}{M_s}\frac{\rho_s}{\rho_L}. \quad (8.258)$$

where S_w, σ, R_v, ρ_L, T, i_v, M_v, M_s, and ρ_s show supersaturation of water, surface tension of water, vapor gas constant, temperature, van't Hoff factor (= 2), molecular weight of water, molecular weight of aerosol, and density of aerosol, respectively.

At each time step, $r_{a,crit}$ is calculated using temperature, and masses of aerosols with radii $¿$ $r_{a,crit}$ are removed from SDF of aerosol and transferred to SDF of cloud as newly generated cloud particles.

The radii of newly generated clouds correspond to those of aerosols, but if the radii of aerosols are smaller than the lower limit of cloud SDF, the radii of newly generated clouds are set to the smallest size of cloud SDF ($\sim 2\mu m$).

The changes in aerosol and hydrometeor SDF are shown as:

$$\left[\frac{\partial f_a}{\partial t}\right]_{activation} = -\int_{m_{a,crit}}^{\infty} f_a(m_a, t)dm_a \qquad (8.259)$$

$$\left[\frac{\partial f_c^{(\mu)}}{\partial t}\right]_{activation} = -\left[\frac{\partial f_a}{\partial t}\right]_{activation} \qquad (8.260)$$

where $m_{a,crit} = (= \frac{4\pi}{3}r_a^3\rho_a$ is mass of aerosol particles with radii the same as critical radii, $r_{a,crit}$. When there is not enough vapor to activate all aerosol particles with radii larger than the critical radius, i.e.,

$$\int_{m_{a,crit}}^{\infty} m_a f_a(m_a, t)dm_a > q_v\rho, \qquad (8.261)$$

only the aerosol particles with radii $¿$ than $r_{a0,crit}$, given as:

$$\int_{m_{a0,crit}}^{\infty} m_a f_a(m_a, t)dm_a = q_v\rho, \qquad (8.262)$$

are transferred to cloud particles as:

$$\left[\frac{\partial f_a}{\partial t}\right]_{activation} = -\int_{m_{a0,crit}}^{\infty} f_a(m_a, t)dm_a, \qquad (8.263)$$

$$\left[\frac{\partial f_c^{(\mu)}}{\partial t}\right]_{activation} = -\left[\frac{\partial f_a}{\partial t}\right]_{activation}. \qquad (8.264)$$

where q_v and ρ is the mixing ratio of water vapor and density.

Condensation/evaporation

Calculation of condensation and evaporation processes is based on an equation. The mass change by these two process is given by an equation (e.g., Rogers and Yau (1989)):

$$\frac{dm}{dt} = C^{(\mu)}(m)G^{(\mu)}(T)S^{(\mu)} \tag{8.265}$$

$$G^{(\mu)}(T) = \begin{cases} G_w(T) & (\mu : liquid) \\ G_i(T) & (\mu : ice) \end{cases}$$

$$G_w(T) = \frac{4\pi}{\frac{R_v T}{e_w(T)D_v} + \frac{L_w}{KT}\left(\frac{L_w}{R_v T} - 1\right)}$$

$$G_i(T) = \frac{4\pi}{\frac{R_v T}{e_i(T)D_v} + \frac{L_i}{KT}\left(\frac{L_i}{R_v T} - 1\right)}$$

$$S^{(\mu)} = \begin{cases} S_w & (\mu : liquid) \\ S_i & (\mu : ice) \end{cases}$$

where $C^{(\mu)}(m)$ is capacitance, which depends on the shape of each type of hydrometeor, S_w, S_i are super saturation of water and ice, L_w, L_i are sensible heat of evaporation, sublimation, D_v is diffusion constant of vapor, K is conductivity of air, and e_w, e_i are saturation vapor pressure and saturation ice pressure, respectively. Condensation (evaporation) occur when $S^{(\mu)}$ is positive (negative).

To calculate change of SDF by condensation/evaporation, mass flux ($F^{(\mu)}_{cond/evap}$) on each bin is given by using number density ($f_c^{(\mu)}$) and $\frac{dm}{dt}$ as:

$$F^{(\mu)}_{cond/evap} = f^{(\mu)}(m)\frac{dm}{dt} = f^{(\mu)}(m)C^{(\mu)}G^{(\mu)}(T)S^{(\mu)}. \tag{8.266}$$

Using this equation, time evolution of SDF ($f^{(\mu)}$) is given as

$$\left[\frac{\partial f^{(\mu)}(m,t)}{\partial t}\right]_{cond/evap} = -\frac{\partial}{\partial m}F^{(\mu)}_{cond/evap}(m)$$

$$= -\frac{\partial}{\partial m}\left(f^{(\mu)}(m)C^{(\mu)}\right)G^{(\mu)}(T)S^{(\mu)}. \tag{8.267}$$

By using the $\eta(= \log(m))$, eq.(8.267) is transferred to the advection equation:

$$\frac{\partial f^{(\mu)}(\eta)}{\partial t} = -\frac{\partial}{\partial \eta}\left(f^{(\mu)}(\eta)U^{(\mu)}(\eta)\right) \tag{8.268}$$

$$U^{(\mu)}(\eta) = \frac{C^{(\mu)}(\eta)}{\exp(\eta)}G^{(\eta)}(T)S^{(\eta)}.$$

To solve eq.(8.268), a scheme developed by Bott (1989) is used. The number density of the i-th bin after Δt ($f_i(t + \Delta t)$) is given as follows:

$$f_i(t + \Delta t) = f_i(t) - \frac{\Delta t}{\Delta \eta}\big[F_{cond/evap,i+1/2} - F_{cond/evap,i-1/2}\big].$$

$$F_{cond/evap,i+1/2} = \frac{\Delta \eta}{\Delta t}\Big[\frac{i^{+}_{l,i+1/2}}{i_{l,j}}f_i(t) - \frac{i^{-}_{l,i+1/2}}{i_{l,i+1}}f_{i+1}(t)\Big]$$

$$i^{+}_{l,i+1/2} = max\big(0, I^{+}_l(c_{i+1/2})\big)$$

$$i^{-}_{l,i+1/2} = max\big(0, I^{-}_l(c_{i+1/2})\big)$$

$$i^{+}_{l,i} = max\big(I_{l,i}, i^{+}_{l,i+1/2} + i^{-}_{l,i+1/2}\big)$$

$$I^{+}_l(c_{i+1/2}) = \sum_{k=0}^{2}\frac{a_{i,k}}{(k+1)2^{k+1}}\big[1 - (1 - 2c^{+}_j)^{k+1}\big]$$

$$I^{-}_l(c_{i+1/2}) = \sum_{k=0}^{2}\frac{a_{i+1,k}}{(k+1)2^{k+1}}(-1)^k\big[1 - (1 - 2c^{-}_j)^{k+1}\big]$$

$$a_{i,0} = -\frac{1}{24}\big(f_{i+1}(t) - 26f_i(t) + f_{i-1}(t)\big)$$

$$a_{i,1} = \frac{1}{2}\big(f_{i+1}(t) - f_{i-1}(t)\big)$$

$$a_{i,2} = \frac{1}{2}\big(f_{i+1}(t) - 2f_i(t) + f_{i-1}(t)\big)$$

$$c^{\pm}_i = \pm\big(c^n_{i+1/2} \pm |c^n_{i+1/2}|\big)/2$$

$$c^n_{i+1/2} = U^n_{i+1/2}\frac{\Delta t}{\Delta \eta} \tag{8.269}$$

Since super saturation ($S^{(\mu)}$) can change during time step (Δt), we apply a method shown below to reflect the change of supersaturation during Δt.
Time evolution of supersaturation can be given by equations:

$$\frac{d}{dt}\left(\begin{array}{c} S_w \\ S_i \end{array}\right) = \left(\begin{array}{cc} a_{c/e} & b_{c/e} \\ c_{c/e} & d_{c/e} \end{array}\right)\left(\begin{array}{c} S_w \\ S_i \end{array}\right) = A\left(\begin{array}{c} S_w \\ S_i \end{array}\right) \tag{8.270}$$

$$a_{c/e} = -(S_w + 1)\Big(\frac{1}{q_v} + \frac{L_w}{R_v T^2}\frac{L_w}{C_p}\Big)\int f^{(w)}(m)C^{(w)}(m)dmG_w(t)$$

$$b_{c/e} = -(S_w + 1)\Big(\frac{1}{q_v} + \frac{L_w}{R_v T^2}\frac{L_i}{C_p}\Big)\sum_{\mu \in ice}\int f^{(\mu)}(m)C^{(\mu)}(m)dmG_i(t)$$

$$c_{c/e} = -(S_i + 1)\Big(\frac{1}{q_v} + \frac{L_i}{R_v T^2}\frac{L_w}{C_p}\Big)\int f^{(w)}(m)C^{(w)}(m)dmG_w(t)$$

$$d_{c/e} = -(S_i + 1)\Big(\frac{1}{q_v} + \frac{L_i}{R_v T^2}\frac{L_i}{C_p}\Big)\sum_{\mu \in ice}\int f^{(\mu)}(m)C^{(^m u)}(m)dmG_i(t)$$

where q_v is the mixing ratio of vapor.
Using eigen value of A (Λ_+, Λ_- ($\Lambda_+ > \Lambda_-$)), and assuming $a_{c/e}, b_{c/e}, c_{c/e}, d_{c/e}$ are constant during Δt, average value of super saturation ($\bar{S}_{w,i}(t)$) during Δt is given as:

$$\bar{S}_w(t) = \frac{1}{\Delta t} \int_t^{t+\Delta t} S_w(\tau)d\tau = b\frac{e^{\Lambda_+ \Delta t} - 1}{\Lambda_+ \Delta t}S_+(t) + b\frac{e^{\Lambda_- \Delta t} - 1}{\Lambda_- \Delta t}S_-(t)$$

$$\bar{S}_i(t) = \frac{1}{\Delta t} \int_t^{t+\Delta t} S_i(\tau)d\tau = (\Lambda_+ - a)\frac{e^{\Lambda_+ \Delta t} - 1}{\Lambda_+ \Delta t}S_+(t) + (\Lambda_- - a)\frac{e^{\Lambda_- \Delta t} - 1}{\Lambda_- \Delta t}S_-(t)$$

$$S_+(t) = \frac{(\Lambda_- - a)S_w(t) - bS_i(t)}{b(\Lambda_- - \Lambda_+)}$$

$$S_+(t) = \frac{(a - \Lambda_+)S_w(t) + bS_i(t)}{b(\Lambda_- - \Lambda_+)}$$

The averaged super saturation $(\bar{S}_{w,i}(t))$ is used to solve the eq.(8.270).

Collision/coagulation/riming/aggregation

Collision/coagulation processes are calculated by solving stochastic collision equations (e.g., Pruppacher and Klett (1997)):

$$\frac{\partial f(m)}{\partial t} = \int_0^{m/2} f(m')f(m - m')K(m', m - m')dm'$$
$$- f(m)\int_0^\infty f(m'')K(m, m'')dm'' \tag{8.271}$$

where $K(m, m')$ is collection kernel function. Three types of kernel function, i.e., Long type kernel (Long (1974)), Golovin type kernel (Golovin (1963)), and Hydro-dynamic dynamic kernel as shown in eq.(8.272), are implemented into the SCALE-RM.

$$K(m, m') = \pi(r(m) - r(m'))\,|V(m) - V(m')|\, E_{col}(m, m')E_{coag}(m, m') \tag{8.272}$$

where $r(m)$ is radius of hydrometeors with mass m and $V(m)$ is terminal velocity of hydrometeors. The terminal velocity of each species of hydrometeor and each size are shown in Figure 8.1 E_{col}, and E_{coag} are collision efficiency and coagulation efficiency, respectively.

Although the stochastic collision equation can be applied for collision/coagulation of one type of hydrometeor (i.e., liquid water), SCALE-RM predicts seven types of hydrometeors and interactions of these types (i.e., riming/aggregation) must be calculated. To calculate the interaction of all seven types of hydrometeors, the extended stochastic collision equation:

$$\left[\frac{\partial f^{(\mu)}(m)}{\partial t}\right]_{coll/coag/rim/agg} =$$
$$\sum_\lambda \sum_\nu \int_0^{m/2} f^{(\lambda)}(\quad m')f^{(\nu)}(m - m')K_{\lambda\nu}(m', m - m')dm'$$
$$-f^{(\mu)}(m)\sum_\kappa \int_0^\infty f^{(\kappa)}(\quad m'')K_{\kappa\mu}(m, m'')dm'' \tag{8.273}$$
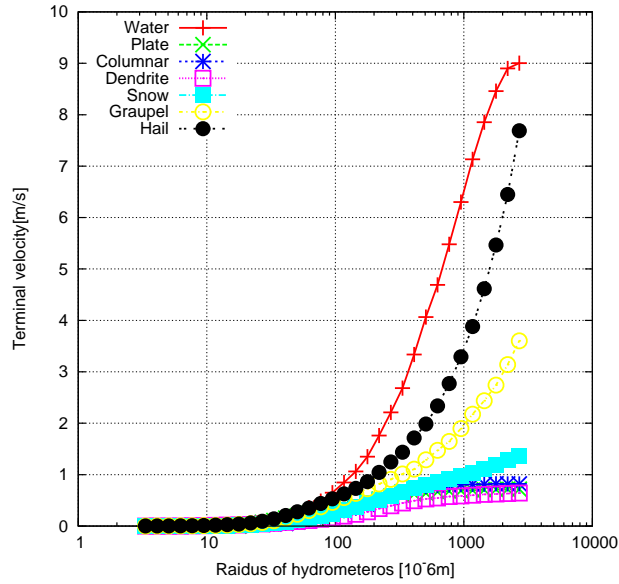
Figure 8.1: Terminal velocity of Water (Plus), plate-type ice (cross), columnar-type ice (asterisk), dendritic-type ice (open square), snow (closed square), graupel (open circle), and hail (closed circle). Cited from Figure A3 of Suzuki (2006) and rearranged.

is applied (where μ, ν, λ, κ represent species of hydrometeor). The combinations of μ, ν, λ are shown in table 8.2.

Table 8.2: Catalog of interaction between seven species. W, I, S, G, and H show water, ice, snow, graupel, and hail, respectively. G/H shows graupel(hail) generated when T is lower(higher) than 270.15 K

	W	I	S	G	H
W	W	G/H	G/H	G/H	G/H
I	I	S	S	I	I
S	S	S	S	S	S
G	G/H	G/H	G	G	G/H
H	G/H	G/H	G/H	G/H	H

To solve the stochastic collision equation, a scheme developed by Bott (1998) was implemented into SCALE-RM.
The Bott (1998) scheme calculates evolution of mass density distribution ($g(\eta) = mf(\eta)$, $\eta = \log(m)$). The stochastic collision equation can be transferred to:

$$\frac{\partial g(\eta)}{\partial t} = \int_{\eta_0}^{\eta_1} \frac{m^2}{(m-m')^2 m'} g(\eta - \eta') K(\eta - \eta', \eta') g(\eta') d\eta'$$
$$- \int_{\eta_0}^{\infty} g(\eta) \frac{K(\eta, \eta')}{m'} g(\eta') d\eta'. \tag{8.274}$$

where $\eta_1 = \log(m/2)$. Decreases of mass of i-th bin and j-th bin are given by:

$$\frac{\partial g_i^{(\mu)}}{\partial t} = -\Delta g_i^{(\mu)} K_{\mu\nu}(i,j) \frac{g_j^{(\nu)}}{m_j} \Delta\eta \tag{8.275}$$

and

$$\frac{\partial g_j^{(\mu)}}{\partial t} = -\Delta g_j^{(\nu)} K_{\mu\nu}(i,j) \frac{g_i^{(\mu)}}{m_i} \Delta\eta \tag{8.276}$$

respectively. The terms corresponds to the second term of the right-hand side of eq.(8.274). Eqs.(8.275) and (8.276) can transfer to:

$$\Delta g_i^{(\mu)} = g_i^{(\mu)} \left[1 - \exp\left(-K_{\mu\nu}(i,j) \frac{g_j^{(\nu)}}{m_j} \Delta\eta \Delta t \right) \right] \tag{8.277}$$

$$\Delta g_j^{(\nu)} = g_j^{(\nu)} \left[1 - \exp\left(-K_{\mu\nu}(i,j) \frac{g_i^{(\mu)}}{m_i} \Delta\eta \Delta t \right) \right]. \tag{8.278}$$

The sum of $\Delta g_i^{(\mu)}$ and $\Delta g_j^{(\nu)}$ corresponds to newly generated mass by collision of hydrometeors with mass of m_i and m_j. The newly generated mass $(g' = \Delta g_i^{(\mu)} + \Delta g_j^{(\nu)}$, corresponds to the first term of the right-hand side of eq.(8.274)) added k-th bin ($m_k = m_i + m_j$). Since m_k is not always bin center, newly generated mass is divided to the k-th and k+1-th bin, as follows. The production of k-th and k+1-th bin is represented as:

$$\Delta g_k^{(\lambda)} = g_k^\lambda + g' - \zeta \tag{8.279}$$
$$\Delta g_{k+1}^{(\lambda)} = g_{k+1}^\lambda + \zeta \tag{8.280}$$
$$\zeta = \frac{g'}{g_k^{(\lambda)} + g'} \sum_{s=0}^{2} \frac{a_{k,s}}{(s+1)2^{k+1}} [1 - (1-2c_k)^{k+1}]$$
$$c_k = \frac{m' - m_k}{m_{k+1} - m_k}$$
$$a_{k,0} = -\frac{1}{24}(g_{k+1}^{(\lambda)} - 26g_k^{(\lambda)} + g_{k-1}^{(\lambda)})$$
$$a_{k,1} = -\frac{1}{2}(g_{k+1}^{(\lambda)} - g_{k-1}^{(\lambda)})$$
$$a_{k,2} = -\frac{1}{2}(g_{k+1}^{(\lambda)} - 2g_k^{(\lambda)} + g_{k-1}^{(\lambda)})$$

This procedure is applied for all bins of all types of hydrometeors.

In addition, for more rapid calculation, Sato et al. (2009) 's scheme is also implemented into SCALE-RM.

Freezing

The calculation of the freezing process is based on a parameterization by Bigg (1953). The parameterization calculates number density of water ($f_c^{(w)}$) that can be frozen:

$$\frac{\partial}{\partial t} f^{(w)}(m) = -\frac{f^{(w)}(m)}{\tau_{fr}} \tag{8.281}$$

$$\tau_{fr} = \frac{\exp\left[b_{fr}(T_0 - T)\right]}{a_{fr}m}$$

where $a_{fr} = 10^{-4} s^{-1}$, and $b_{fr} = 0.66^o C^{-1}$ are empirical parameters, and T_0 is 273.15 K.

Eq.(8.281) can transfer to:

$$\frac{\partial g^{(w)(m)}}{\partial t} = -\frac{g^{(w)}(m)}{\tau_{fr}(m)} \tag{8.282}$$

$$\tau_{fr,i} = \frac{\exp\left(b_{fr}(T_0 - T)\right)}{a_{fr}m}$$

From this equation, the mass change of i-th bin during Δt is given as:

$$g_i^{(w)}(t + \Delta t) = g_i^{(w)} - Frz_i \tag{8.283}$$

$$\begin{cases} g_i^{(plate)}(t + \Delta t) = g_i^{(plate)} + Frz_i & (r_w < 200\mu m) \\ g_i^{(hail)}(t + \Delta t) = g_i^{(hail)} + Frz_i & (r_w > 200\mu m) \end{cases} \tag{8.284}$$

$$Frz_i = g_i^{(w)}(t)\left[1 - \exp\left(-\frac{\Delta t}{\tau_{fr,i}}\right)\right]$$

As shown in eq.(8.284), the mass of liquid is transferred to plate type ice ($r_w < 200\mu m$) or hail ($r_w > 200\mu m$).

Melting

The calculation of the melting process is too simple, with all ice particles (i.e., plate, columnar, dendritic, snow, graupel and hail) melting immediately when the temperature is ¿ $T_0 = 273.15$ K. This is too simplistic to represent ice phase processes, and we will modify this method in the near future.

8.4   Radiation

Corresponding author   :   Hisashi Yashiro

8.4.1 mstrnX

SCALE implements a broadband atmospheric radiative transfer model named "Model Simulation radiation TRaNsfer code version X (mstrn-X)" developed by Nakajima et al. (2000) and Sekiguchi and Nakajima (2008). `mstrn` is based on the discrete ordinate method with a delta two-stream approximation and the correlated k-distribution method. The model calculates long- and short-wave radiation fluxes using the atmospheric states, the three dimensional distribution of clouds/gases/aerosols, and the property of land/ocean surface. The spectrum between 0.2 and 200 μm is divided into 29 spectral bands and 111 integration points.

The calculation of solar insolation is based on the parameterization of Berger (1978). The expected top of atmosphere in the radiation model is 100 km above sea level. However, it is sometimes higher than the top of the domain used in the limited-area simulations. Thus, SCALE can add the climatological profile to the upper part of the model domain, as needed. The COSPAR International Reference Atmosphere (CIRA-86) (Committee on Space Research; NASA National Space Science Data Center, 2006) is used for the climatological profile of temperature and pressure. The standard profiles of trace gases such as oxygen, carbon dioxide, ozone, water vapor, methane, etc., are referred to the MIPAS reference atmospheres (Remedios et al. (2007)).

8.5 Surface flux

Corresponding author : Seiya Nishizawa

8.5.1 Monin-Obukhov similarity

First of all, we assume that in the boundary layer 1. fluxes are constant, and 2. variables are horizontally uniform.

Relations between flux and vertical gradient are:

$$\frac{kz}{u_*}\frac{\partial u}{\partial z} = \phi_m\left(\frac{z}{L}\right), \tag{8.285}$$

$$\frac{kz}{\theta_*}\frac{\partial \theta}{\partial z} = \phi_h\left(\frac{z}{L}\right), \tag{8.286}$$

$$\frac{kz}{q_*}\frac{\partial q}{\partial z} = \phi_q\left(\frac{z}{L}\right), \tag{8.287}$$

where k is the Von Karman constant. L is the Monin-Obukhov scale height:

$$L = \frac{\theta u_*^2}{kg\theta_*}, \tag{8.288}$$

where g is gravity. The scaling velocity, u_*, temperature, θ_*, and water vapor, q_*, are defined from the vertical eddy fluxes of momentum, sensible heat, and water vapor:

$$\overline{u'w'} = -u_*u_*, \tag{8.289}$$

$$\overline{w'\theta'} = -u_*\theta_*, \tag{8.290}$$

$$\overline{w'q'} = -u_*q_*. \tag{8.291}$$

The integration between roughness length z_0 to height z of the lowest model level, eqs. (8.285) and (8.286) becomes:

$$u(z) = \frac{u_*}{k} \left\{ \ln(z/z_0) - \Phi_m(z/L) + \Phi_m(z_0/L) \right\}, \qquad (8.292)$$

$$\Delta\theta = R\frac{\theta_*}{k} \left\{ \ln(z/z_0) - \Phi_h(z/L) + \Phi_h(z_0/L) \right\}, \qquad (8.293)$$

where $\Delta\theta = \theta - \theta_0$, and

$$\Phi_m(z) = \int^z \frac{1 - \phi_m(z')}{z'} dz', \qquad (8.294)$$

$$\Phi_h(z) = \int^z \frac{R - \phi_h(z')}{Rz'} dz'. \qquad (8.295)$$

8.5.2 Louis′s (1979) Model

Louis (1979) introduced a parametric model of vertical eddy fluxes.

The L becomes:

$$L = \frac{\theta u^2}{g\Delta\theta} \frac{\ln(z/z_0) - \Phi_h(z/L) + \Phi_h(z_0/L)}{\left\{ \ln(z/z_0) - \Phi_m(z/L) + \Phi_m(z/L) \right\}^2}. \qquad (8.296)$$

The bulk Richardson number for the layer Ri_B is:

$$Ri_B = \frac{gz\Delta\theta}{\theta u^2}, \qquad (8.297)$$

and its form implies a relationship with the Monin-Obukhov scale height L. The fluxes can then be written as:

$$u_*^2 = a^2 u^2 F_m \left(\frac{z}{z_0}, Ri_B \right), \qquad (8.298)$$

$$u_* \theta_* = \frac{a^2}{R} u \Delta\theta F_h \left(\frac{z}{z_0}, Ri_B \right), \qquad (8.299)$$

where R is ratio of the drag coefficients for momentum and heat in the neutral limit(the turbulent Prandtl number), and

$$a^2 = \frac{k^2}{\left\{ \ln(z/z_0) \right\}^2} \qquad (8.300)$$

is the drag coefficient under neutral conditions.

For unstable conditions $(Ri_B < 0)$, F_is $(i = m, h)$ could be:

$$F_i = 1 - \frac{bRi_B}{1 + c_i \sqrt{|Ri_B|}}, \qquad (8.301)$$

under the consideration that F_i must behave as $1/u$ (i.e., $\sqrt{|Ri_B|}$) in the free convection limit $(u \to 0)$ and becomes 1 under neutral conditions $(Ri_B \to 0)$. On the other hand, under stable conditions (Ri_b), Louis (1979) adopted the following form for F_i:

$$F_i = \frac{1}{(1 + b'Ri_B)^2}. \qquad (8.302)$$

The constants are estimated as $R = 0.74$ by Businger et al. (1971), and $b = 2b' = 9.4$ by Louis (1979). By dimensional analysis:

$$c_i = C_i^* a^2 b \sqrt{\frac{z}{z_0}}, \tag{8.303}$$

and $C_m^* = 7.4, C_h^* = 5.3$, which result best fits curves.

8.5.3 Uno et al. ′ s (1995) Model

Uno et al. (1995) extended the Louis Model, considering differences in roughness lengths related to momentum and temperature, i.e., z_0 and z_t, respectively.

The potential temperature difference between $z = z$ and $z = z_t$, $\Delta\theta_t$, is:

$$
\begin{aligned}
\Delta\theta_t &= R\frac{\theta_*}{k}\left\{\ln(z_0/z_t) - \Phi_h(z_0/L) + \Phi_h(z_t/L)\right\} + \Delta\theta_0, \\
&= R\frac{\theta_*}{k}\ln(z_0/z_t) + \Delta\theta_0, \\
&= \Delta\theta_0\left\{\frac{R\ln(z_0/z_t)}{\Psi_h} + 1\right\},
\end{aligned} \tag{8.304}
$$

where $\Delta\theta_0 = \theta_z - \theta_{z_0}(= \Delta\theta)$:

$$\Psi_h = \int_{z_0}^{z} \frac{\phi_h}{z'}dz', \tag{8.305}$$

and ϕ_h is assumed to be R in the range $z_t < z < z_0$. Thus:

$$\Delta\theta_0 = \Delta\theta_t\left\{\frac{R\ln(z_0/z_t)}{\Psi_h} + 1\right\}^{-1}, \tag{8.306}$$

or equivalently,

$$Ri_{B0} = Ri_{Bt}\left\{\frac{R\ln(z_0/z_t)}{\Psi_h} + 1\right\}^{-1}. \tag{8.307}$$

From eqs. (8.298) and (8.299):

$$\Delta\theta_0 = \frac{R\theta_*}{k}\ln\left(\frac{z}{z_0}\right)\frac{\sqrt{F_m}}{F_h}, \tag{8.308}$$

while

$$\Delta\theta_0 = \frac{\theta_*}{k}\Psi_h, \tag{8.309}$$

from eqs. (8.286) and (8.305). Therefore:

$$\Psi_h = R\ln\left(\frac{z}{z_0}\right)\frac{\sqrt{F_m}}{F_h}. \tag{8.310}$$

Because Ψ_h depends on Ri_{B0}, Ri_{B0} cannot be calculated from Ri_{Bt} with eq. (8.307) directly, so numerical iteration is required to obtain Ri_{B0} [3]. Starting

---

[3]In the stable case, it can be solved analytically with eq. (8.302), but the solution is too complicated.

from Ri_{Bt} as the first estimation of Ri_{B0}, the second estimate by the Newton-Raphson iteration becomes:

$$\hat{Ri}_{B0} = Ri_{Bt} - \frac{Ri_{Bt} R \ln(z_0/z_t)}{\ln(z_0/z_t) + \hat{\Psi}_h},\tag{8.311}$$

where $\hat{\Psi}_h$ is the estimate of Ψ_h using Ri_{Bt} instead of Ri_{B0}. Approximate values for F_m, F_h, and Ψ_h are re-calculated based on the $\hat{Ri}_{B0}$, and then $\Delta\theta_0$, and the surface fluxes u_*^2 and $u_*\theta_*$ are calculated from eqs. (8.306), (8.298), and (8.299), respectively.

8.5.4   Discretization

All the fluxes are calculated based on the velocity at the first full-level (k=1) ($z = \Delta z/2$). The absolute velocities U are:

$$U^2_{i+\frac{1}{2},j,1} = \left\{ \frac{2(\rho u)_{i+\frac{1}{2},j,1}}{\rho_{i,j,1} + \rho_{i+1,j,1}} \right\}^2 + \left\{ \frac{(\rho v)_{i,j-\frac{1}{2},1} + (\rho v)_{i,j+\frac{1}{2},1} + (\rho v)_{i+1,j-\frac{1}{2},1} + (\rho v)_{i+1,j+\frac{1}{2},1}}{2(\rho_{i,j,1} + \rho_{i+1,j,1})} \right\}^2$$

$$+ \left\{ \frac{(\rho w)_{i,j,1+\frac{1}{2}} + (\rho w)_{i+1,j,1+\frac{1}{2}}}{2(\rho_{i,j,1} + \rho_{i+1,j,1})} \right\}^2,\tag{8.312}$$

$$U^2_{i,j+\frac{1}{2},1} = \left\{ \frac{(\rho u)_{i-\frac{1}{2},j,1} + (\rho u)_{i+\frac{1}{2},j,1} + (\rho u)_{i-\frac{1}{2},j+1,1} + (\rho u)_{i+\frac{1}{2},j+1,1}}{2(\rho_{i,j,1} + \rho_{i,j+1,1})} \right\}^2$$

$$+ \left\{ \frac{2(\rho v)_{i,j+\frac{1}{2},1}}{\rho_{i,j,1} + \rho_{i,j+1,1}} \right\}^2 + \left\{ \frac{(\rho w)_{i,j,1+\frac{1}{2}} + (\rho w)_{i,j+1,1+\frac{1}{2}}}{2(\rho_{i,j,1} + \rho_{i,j+1,1})} \right\}^2,\tag{8.313}$$

$$U^2_{i,j,1} = \left\{ \frac{(\rho u)_{i-\frac{1}{2},j,1} + (\rho u)_{i+\frac{1}{2},j,1}}{2\rho_{i,j,1}} \right\}^2 + \left\{ \frac{(\rho v)_{i,j-\frac{1}{2},1} + (\rho v)_{i,j+\frac{1}{2},1}}{2\rho_{i,j,1}} \right\}^2 + \left\{ \frac{(\rho w)_{i,j,1+\frac{1}{2}}}{2\rho_{i,j,1}} \right\}^2,\tag{8.314}$$

It is here of note that $(\rho w)_{i,j,\frac{1}{2}} = 0$. The potential temperatures θ are:

$$\theta_{i,j,1} = \frac{(\rho\theta)_{i,j,1}}{\rho_{i,j,1}},\tag{8.315}$$

$$\bar{\theta}_{i+\frac{1}{2},j,1} = \frac{\theta_{i,j,1} + \theta_{i+1,j,1}}{2},\tag{8.316}$$

$$\bar{\theta}_{i,j+\frac{1}{2},1} = \frac{\theta_{i,j,1} + \theta_{i,j+1,1}}{2}.\tag{8.317}$$

The roughness lengths, z_0, z_t, and z_q are calculated from eqs. (8.360), (8.361), and (8.362), in which the friction velocity u_* is estimated as:

$$u_* = \sqrt{C_{m0}}U,\tag{8.318}$$

where C_{m0} is a constant bulk coefficient, and we use 1.0×10^{-3} as its value.

From eq. (8.307), the Ri_{Bt}, which is the first guess of the Ri_{B0}, is:

$$Ri_{Bt} = \frac{gz_1(\theta_1 - \theta_{sfc})}{\bar{\Theta}U^2},\tag{8.319}$$

with the assumption that $\theta_{z_t} = \theta_{sfc}$. The estimation of $\hat{\Psi}_h$ is calculated with Ri_{Bt} from eqs. (8.310), (8.301), and (8.302). The final estimation of Ri_{B0} is obtained from eq. (8.311),and the final estimation of Ψ_h is obtained with Ri_{B0}.

Now we can calculate the bulk coefficients, C_m, C_h, and C_e for moments, heat, and vapor:

$$C_m = \frac{k^2}{\ln(z_1/z_0)} F_m(Ri_{B0}), \tag{8.320}$$

$$C_h = \frac{k^2}{R\ln(z_1/z_0)} F_h(Ri_{B0}) \left\{ \frac{R\ln(z_0/z_t)}{\Psi_h} + 1 \right\}^{-1}, \tag{8.321}$$

$$C_e = \frac{k^2}{R\ln(z_1/z_0)} F_h(Ri_{B0}) \left\{ \frac{R\ln(z_0/z_e)}{\Psi_h} + 1 \right\}^{-1}. \tag{8.322}$$

The fluxes are:

$$\overline{\rho u'w'} = -C_m U \rho u, \tag{8.323}$$

$$\overline{\rho v'w'} = -C_m U \rho v, \tag{8.324}$$

$$\overline{\rho w'w'} = -C_m U \rho w, \tag{8.325}$$

$$\overline{\rho \theta'w'} = -C_h U \{\rho\theta - \rho\theta_{sfc}\}, \tag{8.326}$$

$$\overline{\rho q'w'} = -C_e U \rho (q - q_{evap}), \tag{8.327}$$

where q_{evap} is the saturation value at the surface.

8.6   Ocean

Corresponding author   :   Tsuyoshi Yamaura

8.6.1   Ocean physics: slab model

The ocean slab model estimates sea temperature tendencies using a single-layered model. The governing equations of the internal energy E (J/m^2) and mass of ocean M (kg/m^2) are

$$\frac{\partial E}{\partial t} = G + e_{prec} - e_{evap} + Q_{ext}, \tag{8.328}$$

$$\frac{\partial M}{\partial t} = F_{prec} - F_{evap}, \tag{8.329}$$

where G is the downward surface heat flux (J/m^2/s); e_{prec} and e_{evap} are the downward surface internal energy flux (J/m^2/s) of the precipitation and evaporation, respectively; Q_{ext} is external heat source (J/m^2/s); and F_{prec} and F_{evap} are the surface mass flux (kg/m^2/s) of the precipitation and evaporation, respectively.

The internal energy E (J/m^2) is

$$E = c_l M T, \tag{8.330}$$

where M and T are total mass of water (kg/m^2) and temperature, and c_l is the specific heat capacity of water (J/K/kg),

The surface preciptaion flux is

$$F_{prec} = F_{rain} + F_{snow}, \tag{8.331}$$

where F_{rain} and F_{snow} are the surface flux of rain and snow, respectively. The internal energy fluxes are

$$e_{prec} = c_l T_{rain} F_{rain} + (c_i T_{snow} - L_f) F_{snow}, \tag{8.332}$$

$$e_{evap} = c_l T_{evap} F_{evap}, \tag{8.333}$$

where c_i is the specific heat capacity of ice (J/K/kg); T_{rain}, T_{snow} and T_{evap} are the temperature of rain, snow, and evaporated water, respectively; Note that the fluxes of the rain and snow are positive for the downward direction and that of the evapolation is positive for the upward. These ground surface fluxes are calculated in the surface scheme.

In the calculation of change of temperature, the mass change is taken into the account. However, the mass change is ignored after the calculation and then $M = \rho_w D$, where ρ_w is the water density (kg/m^3), and D is the water depth of the slab model.

Eq. (8.328) is discretized as follows:

$$\begin{aligned}
T^{n+1} &= \frac{C_w T^n + \Delta t(G + e_{prec} - e_{evap} + Q_{ext})}{C_w + \Delta t c_l(F_{prec} - F_{evap})}, \\
&= T^n + \Delta t \frac{G + e_{prec} - e_{evap} + Q_{ext} - c_l(F_{prec} - F_{evap})T^n}{C_w + \Delta t c_l(F_{prec} - F_{evap})},
\end{aligned} \tag{8.334}$$

where C_w is the heat capacity of the slab layer (J/K/m^2) and $C_w = \rho_w c_l D$.

Note that the internal energy is not conserved, since the mass change is ignored.

8.6.2 Sea ice

Governing equation

The equations of budget of the mass (kg/m^2) and internal energy (J/m^2) in the ocean and sea ice are

$$\frac{\partial M_i}{\partial t} = f_i(F_{prec} - F_{subl}) - m_{mlt} + m_{frz}, \tag{8.335}$$

$$\frac{\partial E_i}{\partial t} = f_i(G_i - G_{oi} + e_{prec} - e_{subl}) - c_l T_0 m_{mlt} + (c_i T_0 - L_f)m_{frz}, \tag{8.336}$$

$$\frac{\partial M}{\partial t} = (1 - f_i)(F_{prec} - F_{evap}) + m_{mlt} - m_{frz}, \tag{8.337}$$

$$\frac{\partial E}{\partial t} = (1 - f_i)(G_o + e_{prec} - e_{evap}) + f_i G_{oi} + c_l T_0 m_{mlt} - (c_i T_0 - L_f)m_{frz}, \tag{8.338}$$

where f_i is the fraction of the sea ice; m_{mlt} and m_{frz} are the mass change (kg/m^2/s) by melting of ice and freezing of sea water; and G_i, G_o and G_{oi} are the heat flux (J/m^2/s) at the ice-atmosphere, ocean-atmosphere, and ice-ocean surfaces, respectively; F_{subl} is the upward mass flux due to the sublimation of ice

$(\mathrm{kg/m^2/s})$; and e_{subl} is the upward internal energy flux at the surface $(\mathrm{J/m^2/s})$ of the sublimated ice as

$$e_{subl} = (c_i T_{subl} - L_f) F_{subl}. \tag{8.339}$$

As noted in the previous section, the mass change in the sea water is ignored after the calculation of change in the ocean temperature.

The G_{oi} is estimated by the diffusion equation

$$G_{oi} = \nu_i \frac{T_i - T}{D_i/2}, \tag{8.340}$$

$$D_i = \frac{M_i}{\rho_i f_i}, \tag{8.341}$$

where T_i is the temperature of the sea ice; ν_i and D_i are the thermal conductivity of ice $(\mathrm{J/K/m^3/s})$ and depth of the sea ice (m).

The fraction is estimated as

$$f_i = \sqrt{\frac{M_i}{M_c}}, \tag{8.342}$$

where M_c is the critical ice mass $(\mathrm{kg/m^2})$.

The amount of the melting during a time step is estimated to satisfy the conservation of mass and internal energy of the sea ice as

$$M_{mlt} = \int_t^{t+\Delta t} m_{mlt} dt$$
$$= \min \left\{ \max \left\{ \frac{c_i(T_i - T_0)}{(c_w - c_i)T_0 + L_f} M_i, 0 \right\}, M_i \right\}. \tag{8.343}$$

The amount of the freezing is estimated to satisfy the conservation of mass and internal energy of the ocean as

$$M_{frz} = \int_t^{t+\Delta t} m_{frz} dt$$
$$= \min \left\{ \max \left\{ \frac{c_l \rho_w D(T_0 - T)}{(c_l - c_i)T_0 + L_f}, 0 \right\}, \rho_w D \right\}, \tag{8.344}$$

where T_0 is the freezing tempearture.

Time integration

The governing equation is solved by a spliting method. In the first step, the mass and internal energy budgets of the ice without the phase change is solved. In the second step, the melting of sea ice is estimated by the mass and internal energy conservation. In the next step, then the temperature change of ocean is calculated in the ocean scheme. In the last step, the freezing ocean water is estimated and the mass and temperature of ice and ocean is updated.

The followings are the summary of the sequence of calculation. Here, the superscript "n" indicates the quantites at the time step n, and "n_1", "n_2", "n_3", and "$n + 1$" are those after calculation of the first, seccond, third and the last step, respectively.

First step

$$\Delta M_i^{n_1} = \Delta t f_i^n (F_{prec} - F_{subl}), \tag{8.345}$$

$$\Delta E_i^{n_1} = \Delta t f_i (G_i - G_{oi} + e_{prec} - e_{subl}), \tag{8.346}$$

$$M_i^{n_1} = M_i^n + \Delta M_i^{n_1}, \tag{8.347}$$

$$T_i^{n_1} = T_i^n + \frac{\Delta E_i^{n_1} - (c_i T_i^n - L_f)\Delta M_i^{n_1}}{c_i M_i^{n_1}}. \tag{8.348}$$

Second step

$$M_{mlt} = \min \left\{ \max \left\{ \frac{c_i (T_i^{n_1} - T_0) M_i^{n_1}}{(c_w - c_i)T_0 + L_f}, 0 \right\}, M_i^{n_1} \right\}, \tag{8.349}$$

$$M_i^{n_2} = M_i^{n_1} - M_{mlt}, \tag{8.350}$$

$$T_i^{n_2} = T_i^{n_1} + \frac{-c_l T_0 + (c_i T_i^{n_1} - L_f)}{c_i M_i^{n_2}} M_{mlt}. \tag{8.351}$$

Third step (Ocean model)

$$\Delta E^{n_3} = \Delta t \{(1 - f_i)(G_o + e_{prec} - e_{evap}) + f_i G_{oi}\} + c_l T_0 M_{mlt}, \tag{8.352}$$

$$\Delta M^{n_3} = \Delta t (1 - f_i)(F_{prec} - F_{evap}) + M_{mlt}, \tag{8.353}$$

$$T^{n_3} = T^n + \frac{\Delta E^{n_3} - c_l T^n \Delta M^{n_3}}{c_l \{\rho_w D + \Delta M^{n_3}\}}. \tag{8.354}$$

Forth step

$$M_{frz} = \min \left\{ \max \left\{ \frac{c_l \rho_w D(T_0 - T^{n_3})}{(c_l - c_i)T_0 + L_f}, 0 \right\}, \rho_w D \right\}, \tag{8.355}$$

$$M_i^{n+1} = M_i^{n_2} + M_{frz}, \tag{8.356}$$

$$T_i^{n+1} = T_i^{n_3} + (T_0 - T_i^{n_3})\frac{M_{frz}}{M_i^{n+1}}, \tag{8.357}$$

$$T^{n+1} = T^{n_3} + \frac{-(c_i T_0 - L_f) + c_l T^{n_3}}{c_l(\rho_w D - M_{frz})} M_{frz}. \tag{8.358}$$

8.6.3 Sea surface albedo

Nakajima et al. (2000) model

Nakajima et al. (2000) provided the albedo for the short wave on the sea surface A:

$$A = \exp \left[\Sigma_{i=1}^3 \Sigma_{j=1}^5 C_{ij} t^{j-1} \mu_0^{i-1} \right], \tag{8.359}$$

where C_{ij} is the empirical optical parameters, t is the flux transmissivity for short-wave radiation, and μ_0 is cosine of the solar zenith angle.

8.6.4 Roughness length

Miller et al. (1992) model

Miller et al. (1992) provides the roughness length over the tropical ocean, based on numerical calculations by combining smooth surface values with the

Charnock relation for aerodynamic roughness length and constant values for heat and moisture in accordance with Smith (1988, 1989) suggestions:

$$z_0 = 0.11u/\nu_* + 0.018u_*^2/g, \tag{8.360}$$

$$z_t = 0.40u/\nu_* + 1.4 \times 10^{-5}, \tag{8.361}$$

$$z_q = 0.62u/\nu_* + 1.3 \times 10^{-4}, \tag{8.362}$$

where ν_* is the kinematic viscosity of air ($\sim 1.5 \times 10^{-5}$), and z_0, z_t, and z_q are the roughness length for momentum, heat, and vapor, respectively.

Moon et al. (2007) model

Moon et al. (2007) provides the air–sea momentum flux at high wind speeds based on the coupled wave–wind model simulations for hurricanes. At first, the wind speed U at 10-m height is estimated from the previous roughness length z_0, as follows:

$$U = \frac{u_*}{\kappa} \ln \frac{10}{z_0}, \tag{8.363}$$

where u_* is friction velocity (m/s) and κ is von Kalman constant. And then, new roughness length z_0 is iteratively estimated from the wind speed:

$$z_0 = \begin{cases} \frac{0.0185}{g}u_*^2 & \text{for} \quad U < 12.5, \\ \left[0.085\left(-0.56u_*^2 + 20.255u_* + 2.458\right) - 0.58\right] \times 10^{-3} & \text{for} \quad U \geq 12.5. \end{cases} \tag{8.364}$$

Furthermore, Fairall et al. (2003) provides the roughness length for the heat and vapor using that for momentum, as follows:

$$z_t = \frac{5.5 \times 10^{-5}}{(z_0 u_*/\nu_*)^{0.6}}, \tag{8.365}$$

$$z_q = z_t. \tag{8.366}$$

8.7 Land

Corresponding author   :
Tsuyoshi Yamaura and Seiya Nishizawa

8.7.1 Bucket model

The land bucket model estimates the soil temperature and soil moisture tendencies using a multi-layered bucket model.

Soil moisture equation

The conservation equations of the specific mass of the liquid and ice water (kg/m^3), M_w and M_i, respectively, are

$$\frac{\partial M_w}{\partial t} = -\frac{\partial}{\partial z}\left(F_w + F_{rain} - F_{evap}\right) - m_{frz} - m_{ro,w}, \tag{8.367}$$

$$\frac{\partial M_i}{\partial t} = -\frac{\partial}{\partial z}\left(F_{snow} - F_{subl}\right) + m_{frz} - m_{ro,i}, \tag{8.368}$$

where ν_w is the constant water diffusivity (m^2/s); ρ_w and ρ_i are the dencity of liquid and ice water (kg/m^3), respectively; $F_{rain}, F_{snow}, F_{evap}$ and F_{subl} are the surface flux of rain, snow, evapolation, and sublimation (kg/m^2/s), respectively; m_{frz} and m_{ro} are the mass change by freezing and the runoff of the water from the system (kg/m^3/s), respectively. Note that the F_{rain} and F_{snow} are positive for the downward direction and the F_{evap} and F_{subl} are positive for the upward. F_w is the vertical flux due to the diffusion, and

$$F_w = -\rho_w \nu_w \frac{\partial W}{\partial z}. \tag{8.369}$$

W and I are the soil moisture content (m^3/m^3) of liquid and ice water, respectively, and are

$$W = \frac{M_w}{\rho_w}, \tag{8.370}$$

$$I = \frac{M_i}{\rho_i}. \tag{8.371}$$

The bucket model has the maximum soil mositure content $W_{\max}$, so if the moisture content is larger than the maximum, the moisuter runs off to the out of the system:

$$W + I \leq W_{\max}. \tag{8.372}$$

Therefore, The amount of the runoff (kg/m^3) is estimated as

$$M_{ro} = M_{ro,w} + M_{ro,i}, \tag{8.373}$$

where

$$M_{ro,w} = \int_t^{t+\Delta t} m_{ro,w} dt = \rho_w \min\{W_{ro}, W\}, \tag{8.374}$$

$$M_{ro,i} = \int_t^{t+\Delta t} m_{ro,i} dt = \rho_i (W_{ro} - \min\{W_{ro}, W\}), \tag{8.375}$$

and $W_{ro} = \max\{W + I - W_{\max}, 0\}$.

Thermodynamical equation

The total internal energy is the sum of that of the soil, liquid water and ice water, U_s, U_w and U_i, respectively:

$$U = U_s + U_w + U_i, \tag{8.376}$$
$$U_s = C_s T, \tag{8.377}$$
$$U_w = c_l T \rho_w W, \tag{8.378}$$
$$U_i = (c_i T - L_f) \rho_i I, \tag{8.379}$$

where T is the soil temperature (K). Note that, the temperature is

$$T = \frac{U + L_f \rho_i I}{C_L}, \tag{8.380}$$

where C_L is the total heat capacity (J/K/m^3) and

$$C_L = C_s + c_l\rho_w W + c_i\rho_i I. \tag{8.381}$$

The conservation equation of the total internal energy is

$$\frac{\partial U}{\partial t} = -\frac{\partial}{\partial z}\left[-\kappa\frac{\partial T}{\partial z} + c_l T F_w + F_{surf}\right]$$
$$- c_l T M_{ro,w} - (c_i T - L_f)M_{ro,i}, \tag{8.382}$$

where κ is the thermal conductivity (J/K/m/s). F_{surf} is the ground surface flux, and

$$F_{surf} = G + c_l T_{rain}F_{rain} - c_l T_{evap}F_{evap}$$
$$+ (c_i T_{snow} - L_f)F_{snow}, -(c_i T_{subl} - L_f)F_{subl}, \tag{8.383}$$

where G is the downward ground heat flux (J/m^2/s); and $T_{rain}, T_{evap}, T_{snow}$ and T_{subl} are the temperature of the rain, evaporation water, snow, and sublimation ice, respectively. These ground surface fluxes are calculated in the surface scheme.

The thermal conductivity depends on the moisture content, and Kondo and Saigusa 1994) gived it empirically as

$$\kappa = \kappa_s + 0.5W^{\frac{1}{3}}, \tag{8.384}$$

where κ_s is the thermal conductivity of the soil particle.

Phase change

The liquid water and ice water can exist instantenously only at the temperature T_0. If the internal energy is lower than $C_s T_0 + (c_i T_0 - L_f)M$, all the moisutre is ice, where M is the total moisture $M = M_w + M_i$. On the other hand, the internal energy is larther than $C_s T_0 + c_l T_0 M$, all the moisture is liquid. Otherwize,

$$M_i = \frac{U - (C_s + c_l M)T_0}{(c_i - c_l)T_0 - L_f}, \tag{8.385}$$

$$M_w = M - M_i. \tag{8.386}$$

That is,

$$M_i = \min\left\{\max\left\{\frac{U - (C_s + c_l M)T_0}{(c_i - c_l)T_0 - L_f}, 0\right\}, M\right\}, \tag{8.387}$$

$$M_w = M - M_i. \tag{8.388}$$

Temporal integration

Eqs. (8.367, 8.368 and 8.382) are solved by a splitting method. In the first step, the moisture mass and internal energy changes are calculated without the diffusion, runoff, and phase change. In the second step, the phase change is calculated. In the third step, the moisture diffusion equation is solved. In the fouth step, the temperature diffusion is calculated with the thermal conductivity

with the moisture content obtained in the second step. At the last step, the runoff is calculated.

The followings are the summary of the sequence of calculation. Here, the superscript "n" indicates the quantites at the time step n, "n_1", "n_2", "n_3", "n_4", and "$n+1$" are those after calculation of the first, seccond, third, fourth, and the last steps, respectively. The vertical diffusion terms are calculated by the implicit scheme for numerical stability.

First step

$$M^{n_1} = \rho_w W^n + \rho_i I^n + \Delta t \frac{\partial}{\partial z}(F_{rain} + F_{snow} - F_{evap} - F_{subl}), \quad (8.389)$$

$$U^{n_1} = C_L^n T^n - L_f \rho_i I^n + \Delta t \frac{\partial F_{surf}}{\partial z}, \quad (8.390)$$

where M is the total moisture mass (kg/m^3) and $M = M_w + M_i$.

Second step

$$M_i^{n_2} = \min\left\{\max\left\{\frac{U^{n_1} - (C_s + c_l M^{n_1})T_0}{(c_i - c_l)T_0 - L_f}, 0\right\}, M^{n_1}\right\}, \quad (8.391)$$

$$M_w^{n_2} = M^{n_1} - M_i^{n_2}, \quad (8.392)$$

$$W^{n_2} = \frac{M_w^{n_2}}{\rho_w}, \quad (8.393)$$

$$I^{n_2} = \frac{M_i^{n_2}}{\rho_i}, \quad (8.394)$$

$$T^{n_2} = \frac{U^{n_1} + L_f M_i^{n_2}}{C_s + c_l M_w^{n_2} + c_i M_i^{n_2}}. \quad (8.395)$$

Third step

$$F_w = -\rho_w \nu_w \frac{\partial W^{n_3}}{\partial z}, \quad (8.396)$$

$$W^{n_3} = W^{n_2} - \frac{\Delta t}{\rho_w}\frac{\partial F_w}{\partial z}, \quad (8.397)$$

$$U^{n_3} = U^{n_1} - \Delta t \frac{\partial c_l F_w T^{n_2}}{\partial z}, \quad (8.398)$$

$$C_L^{n_3} = C_s + c_l \rho_w W^{n_3} + c_i M_i^{n_2}. \quad (8.399)$$

Fourth step

$$\kappa = \kappa_s + 0.5(W^{n_3})^{\frac{1}{3}}, \quad (8.400)$$

$$C_L^{n_3} T^{n+1} = U^{n_3} + L_f M_i^{n_2} - \Delta t \frac{\partial}{\partial z}\left(-\kappa \frac{\partial T^{n+1}}{\partial z}\right). \quad (8.401)$$

Fifth step

$$I^{n+1} = \min\{I^{n_2}, W_{\max}\}, \quad (8.402)$$

$$W^{n+1} = \min\{W_{\max} - I^{n+1}, W^{n_3}\}, \quad (8.403)$$

$$M_{ro,w} = \rho_w(W^{n+1} - W^{n_3}), \quad (8.404)$$

$$M_{ro,i} = \rho_i(I^{n+1} - I^{n_2}) \quad (8.405)$$

Descretization

The moisture diffusion in the third step is solved as

$$W_1^{n_3} = W_1^{n_2} + \frac{2\Delta t \nu_w}{\Delta z_1} \frac{W_2^{n_3} - W_1^{n_3}}{\Delta z_2 + \Delta z_1}, \tag{8.406}$$

$$W_k^{n_3} = W_k^{n_2} + \frac{2\Delta t \nu_w}{\Delta z_k} \left(\frac{W_{k+1}^{n_3} - W_k^{n_3}}{\Delta z_{k+1} + \Delta z_k} - \frac{W_k^{n_3} - W_{k-1}^{n_3}}{\Delta z_k + \Delta z_{k-1}} \right), \tag{8.407}$$

$$W_m^{n_3} = W_m^{n_2} - \frac{2\Delta t \nu_w}{\Delta z_m} \left(\frac{W_m^{n_3} - W_{m-1}^{n_3}}{\Delta z_m + \Delta z_{m-1}} \right), \tag{8.408}$$

where the subscription k represents that W_k is the moisture content in the k-layer, and $k = 1, \cdots, m$, where m is the number of the layers. This can be written in the matrix form as

$$\begin{pmatrix} c_1 & b_1 & & & \\ \ddots & \ddots & \ddots & & \\ & a_k & c_k & b_k & \\ & & \ddots & \ddots & \ddots \\ & & & a_m & c_m \end{pmatrix} \begin{pmatrix} W_1^{n_1} \\ \vdots \\ W_k^{n_1} \\ \vdots \\ W_m^{n_1} \end{pmatrix} = \begin{pmatrix} V_1 \\ \vdots \\ V_k \\ \vdots \\ V_m \end{pmatrix}, \tag{8.409}$$

where

$$V_k = W_k^{n_2}, \tag{8.410}$$

$$a_k = -\frac{2\Delta t \nu_w}{\Delta z_k (\Delta z_k + \Delta z_{k-1})}, \tag{8.411}$$

$$b_k = -\frac{2\Delta t \nu_w}{\Delta z_k (\Delta z_{k+1} + \Delta z_k)}, \tag{8.412}$$

$$c_k = 1 - a_k - b_k. \tag{8.413}$$

This matrix can be solved by the Thomas algorithm (tridiagonal matrix algorithm).

The thermodynamical diffusion in the fourth step is discretized as

$$\kappa_k = \kappa_s + 0.5(W_k^{n_3})^{\frac{1}{3}}, \tag{8.414}$$

$$(F_w)_{k+\frac{1}{2}} = -2\rho_w \nu_w \frac{W_{k+1}^{n_3} - W_k^{n_3}}{\Delta z_{k+1} + \Delta z_k}, \tag{8.415}$$

$$(C_L^{n_3})_1 T_1^{n+1} = U_1^{n_3} + L_f (M_i)_1^{n_2} + \frac{\Delta t}{\Delta z_1} (\kappa_2 + \kappa_1) \frac{T_2^{n+1} - T_1^{n+1}}{\Delta z_2 + \Delta z_1}, \tag{8.416}$$

$$(C_L^{n_3})_k T_k^{n+1} = U_k^{n_3} + L_f (M_i)_k^{n_2}$$
$$+ \frac{\Delta t}{\Delta z_k} \left((\kappa_{k+1} + \kappa_k) \frac{T_{k+1}^{n+1} - T_k^{n+1}}{\Delta z_{k+1} + \Delta z_k} - (\kappa_k + \kappa_{k-1}) \frac{T_k^{n+1} - T_{k-1}^{n+1}}{\Delta z_k + \Delta z_{k-1}} \right), \tag{8.417}$$

$$(C_L^{n_3})_m T_m^{n+1} = U_m^{n_3} + L_f (M_i)_m^{n_2} - \frac{\Delta t}{\Delta z_m} (\kappa_m + \kappa_{m-1}) \frac{T_m^{n+1} - T_{m-1}^{n+1}}{\Delta z_m + \Delta z_{m-1}}. \tag{8.418}$$

As in the case of the soil moisture, the tendency equations can be solved

using the Thomas algorithm.

$$V_k = U_k^{n_3} + L_f(M_i)_k^{n_2}, \tag{8.419}$$

$$a_k = -\frac{\Delta t(\kappa_k + \kappa_{k-1})}{\Delta z_k(\Delta z_k + \Delta_{k-1})}, \tag{8.420}$$

$$b_k = -\frac{\Delta t(\kappa_{k+1} + \kappa_k)}{\Delta z_k(\Delta z_{k+1} + \Delta_k)}, \tag{8.421}$$

$$c_k = (C_L^{n_1})_k - a_k - b_k. \tag{8.422}$$

8.8 Urban

Corresponding author : Sachiho A. Adachi

Urban models calculate energy exchanges between the urban surface (urban canopy) and atmosphere. In paricular, the model estimates sensible and latent heat fluxes and momentum flux from urban surface to atmosphere. SCALE-RM has two options for calculation in urban areas: LAND and KUSAKA01. In LAND option, fluxes over urban subtile are calculated by the land model you chose for your experiment. Please refer to Section 8.7.

8.8.1 KUSAKA01: Single layer urban canopy model

KUSAKA01 is the single layer urban canopy model (UCM) by Kusaka et al. (2001) and Kusaka and Kimura (2004). The UCM of KUSAKA01 assumes street canyons as the urban geometry.

The model has the prognostic variables at the roof, wall, and road: the surface tempeature and near-surface temparature of artificial construction. The near-surface temparature is calculated by dividing facets of artificial construction into a number of thickness layers. The rain amount remaining over the roof, wall, and road are also calculated to evaluate evaporation efficiency. And then, it also calculates the the heat fluxes from their facets. The fluxes from urban subtile are estimated by weighted avrage of fluxes from roof, wall, and road.

The model assumes that the urban canopy layer is located lower than the 1st layer of the atmospheric model. Therefore, there is a restriction that a sum of the displacement height of the canopy and roughness length must be two meters lower than the center level of the 1st layer of the atmosphere.

In this version, only single urban type can be considered. Several parameters are prepared to specify the urban geometry and anthropogenic heat.

8.9 Large scale sinking

Corresponding author : Seiya Nishizawa

In the DYCOMS01 experiment, large scale sinking is added to express large scale downward motion corresponding to the Hadley circulation. There is virtual convergence of motion, resulting in mass escape out of the system.

The density loss rate is constant L:

$$L = -\frac{\partial \rho w_L}{\partial z},\tag{8.423}$$

where w_l is vertical velocity corresponding to large scale sinking. Vertical momentum with sinking is defined as follows:

$$\rho w_L = -Lz.\tag{8.424}$$

The continuous equation is now:

$$\frac{\partial \rho}{\partial t} + \frac{\partial \rho u}{\partial x} + \frac{\partial \rho v}{\partial y} + \frac{\partial \rho(w + w_L)}{\partial z} = -L.\tag{8.425}$$

The Lagrangian conservation equation for scalar quantities is:

$$\rho\frac{\partial \phi}{\partial t} + \rho u\frac{\partial \phi}{\partial x} + \rho v\frac{\partial \phi}{\partial y} + \rho(w + w_L)\frac{\partial \phi}{\partial z} = 0,\tag{8.426}$$

When combined with eq. (8.425), this becomes:

$$\frac{\partial \rho\phi}{\partial t} + \frac{\partial \rho u\phi}{\partial x} + \frac{\partial \rho v\phi}{\partial y} + \frac{\partial \rho(w + w_L)\phi}{\partial z} = -L\phi.\tag{8.427}$$

The equation for the mixing ratio is:

$$\frac{\partial \rho Q}{\partial t} + \frac{\partial \rho Q u}{\partial x} + \frac{\partial \rho Q v}{\partial y} + \frac{\partial \rho Q(w + w_L)}{\partial z} = -LQ.\tag{8.428}$$

Note that this is identical to that for scalar quantities.

The w_L at the top boundary is not zero, while w is zero. The vertical flux $\rho w_L \phi$ at the top layer interface could be determined as that convergence of the flux canceled with $L\phi$.

Bibliography

AndréL. Berger. Long-term variations of daily insolation and quaternary climatic changes. *Journal of the Atmospheric Sciences*, 35(12):2362–2367, 1978. doi: 10.1175/1520-0469(1978)035⟨2362:LTVODI⟩2.0.CO;2.

E. K. Bigg. The formation of atmospheric ice crystals by the freezing of droplets. *Quarterly Journal of the Royal Meteorological Society*, 79:510–519, 1953.

A. Bott. A positive definite advection scheme obtained by nonlinear renormalization of the advective fluxes. *Monthly Weather Review*, 117:833–853, 1989.

A. Bott. A flux method for the numerical solution of the stochastic collection equation. *Journal of the Atmospheric Sciences*, 55:2284–2293, 1998.

A. R. Brown, S. H. Derbyshire, and P. J. Mason. Large-eddy simulation of stable atmospheric boundary layers with a revised stochastic subgrid model. *Quarterly Journal of the Royal Meteorological Society*, 120:1485–1512, 1994.

Committee on Space Research; NASA National Space Science Data Center. COSPAR International Reference Atmosphere (cira-86): Global climatology of atmospheric parameters, 2006.

J. W. Deardorff. Stratocumulus-capped mixed layers derived from a three-dimensional model. *Boundary-Layer Meteorology*, 18:495–527, 1980.

C. W. Fairall, E. F. Bradley, J. E. Hare, A. A. Grachev, and J. B. Edson. Bulk parameterization of air–sea fluxes: Updates and verification forthe COARE algorithm. *J. Climate*, 16:571–591, 2003.

A. Favre. Turbulence: Spacetime statistical properties and behavior in supersonic flows. *Physics of Fluids*, 26:2851–2863, 1983.

A. M. Golovin. The solution of the coagulation equation for cloud droplets in a rising air current. *Izv. Geophys. Ser*, 5:482–487, 1963.

M. Khairoutdinov and Y. Kogan. A new cloud physics parameterization in a large-eddy simulation model of marine stratocumulus. *Monthly Weather Review*, 128:229–243, 2000.

L. R. Koenig. Numerical modeling of ice deposition. *Journal of the Atmospheric Sciences*, 28:226–237, 1971.

H. Kohler. The nucleus in and the growth of hygroscopic droplets. *Transactions of the Faraday Society*, 32:1152–1161, 1936.

H. Kusaka and F. Kimura. Coupling a single-layer urban canopy model with a simple atmospheric model: Impact on urban heat island simulation for an idealized case. *J. Meteor. Soc. Japan*, 82(1):67–80, 2004.

H. Kusaka, H. Kondo, Y. Kikegawa, and F. Kimura. A simple single-layer urban canopy model for atmospheric models: comparison with multi-layer and slab models. *Boundary-Layer Meteorol.*, 101:329–358, 2001.

Y.-L. Lin, R. D. Farley, and H. D. Orville. Bulk parameterization of the snow field in a cloud model. *Journal of Climate and Applied Meteorology*, 22:1065–1092, 1983.

A. Long. Solutions to the droplet collection equation for polynomial kernels. *Journal of the Atmospheric Sciences*, 31:1041–1052, 1974.

M. J. Miller, A. C. M. Beljaars, and T. N. Palmer. The sensitivity of the ecmwf model to the parameterization of evaporation from the tropical oceans. *Journal of Climate*, 5(5):418–434, 1992.

C.-H. Moeng and J. C. Wyngaard. Spectral analysis of large-eddy simulation of the convective boundary layer. *Journal of the Atmospheric Sciences*, 45: 3573–3587, 1988.

I.-J. Moon, I. Ginis, T. Hara, and B. Thomas. A physics-based parameterization of air-sea momentum flux at high wind speeds and its impact on hurricane intensity predictions. *Mon. Weather Rev.*, 135:2869–2878, 2007. doi: 10.1175/MWR3432.1.

T. Nakajima, M. Tsukamoto, Y. Tsushima, A. Numaguti, and T. Kimura. Modeling of the radiative process in an atmospheric general circulation model. *Applied Optics*, 39:4869–4878, 2000. doi: 10.1364/AO.39.004869.

H. R. Pruppacher and J. D. Klett. *Microphysics of Clouds and Precipitation, 2nd edition*. Lkuwer Academic Publishers, 1997.

J. J. Remedios, R. J. Leigh, A. M. Waterfall, D. P. Moore, H. Sembhi, I. Parkes, J. Greenhough, M. P. Chipperfield, and D. Hauglustaine. Mipas reference atmospheres and comparisons to v4.61/v4.62 mipas level 2 geophysical data sets. *Atmos. Chem. Phys. Discuss.*, 7:9973–10017, 2007. doi: doi:10.5194/acpd-7-9973-2007.

R. R. Rogers and M. K. Yau. *Short Course in Cloud Physics, 3rd edition*. Butterworth-Heinemann, Elsevier, Unitate States, 1989.

W. Roh and M. Satoh. Evaluation of precipitating hydrometeor parameterizations in a single-moment bulk microphysics scheme for deep convective systems over the tropical central pacific. *Journal of the Atmospheric Sciences*, 71:2654–2673, 2014.

Y. Sato, T. Nakajima, K. Suzuki, and T. Iguchi. Application of a monte carlo integration method to collision and coagulation growth processes of hydrometeors in a bin-type model. *Journal of Geophysical Research*, 114(D9):D09215, 2009. doi: 10.1029/2008JD011247.

A. Scotti, C. Meneveau, and D. K. Lilly. Generalized smagorinsky model for anisotropic grids. *Physics of Fluids A*, 5:2306–2308, 1993.

T. Seiki and T. Nakajima. Aerosol effects of the condensation process on a convective cloud simulation. *Journal of the Atmospheric Sciences*, 71:833–853, 2014.

M. Sekiguchi and T. Nakajima. A k-distribution-based radiation code and its computational optimization for an atmospheric general circulation model. *J. of Quantitative Spectroscopy and Radiative Transfer*, 109:2779—-2793, 2008.

S. D. Smith. Coefficients for sea surface wind stress, heat flux and wind profiles as a function of wind speed and temperature. *J. Geophys. Res.*, 93:15467–15472, 1988.

S. D. Smith. Water vapor flux at the sea surface. *Boundary-Layer Meteorology*, 47:277–293, 1989.

K. Suzuki. *A study on numerical modeling of cloud microphysics for calculating the particle growth process (in Japanese)*. PhD thesis, The University of Tokyo, 2006.

K. Suzuki, T. Nakajima, T. Y. Nakajima, and A. P. Khain. A study of microphysical mechanisms for correlation patterns between droplet radius and optical thickness of warm clouds with a spectral bin microphysics cloud model. *Journal of the Atmospheric Sciences*, 67(4):1126–1141, 2010.

H. Tomita. New microphysical schemes with five and six categories by diagnostic generation of cloud ice. *Journal of the Meteorological Society of Japan*, 86:121–142, 2008.

C. E. Wainwright, D. T. Dawson II, M. Xue, and G. Zhang. Diagnosing the intercept parameters of the exponential drop size distributions in a single-moment microphysics scheme and impact on supercell storm simulations. *Journal of Applied Meteorology and Climatology*, 53:2072–2090, 2014.

Louis J Wicker and William C Skamarock. Time-splitting methods for elastic models using forward time schemes. *Monthly Weather Review*, 130(8):2088–2097, 2002.

Appendix A

The detail numerics

A.1   4th order central difference

The 4th order central difference is given by

$$\frac{\partial \phi}{\partial x} = \frac{-\phi_{i+2} + 8\phi_{i+1} - 8\phi_{i-1} + \phi_{i+2}}{12\Delta x} = 0 \tag{A.1}$$

where

$$\phi_{i+2} = \phi_i + 2\Delta x \left(\frac{\partial \phi}{\partial x}\right)_i + 2\Delta x^2 \left(\frac{\partial^2 \phi}{\partial x^2}\right)_i + \frac{4\Delta x^3}{3}\left(\frac{\partial^3 \phi}{\partial x^3}\right)_i + \frac{2\Delta x^4}{3}\left(\frac{\partial^3 \phi}{\partial x^4}\right)_i + O(\Delta x^5) \tag{A.2}$$

$$\phi_{i+1} = \phi_i + \Delta x \left(\frac{\partial \phi}{\partial x}\right)_i + \frac{\Delta x^2}{2}\left(\frac{\partial^2 \phi}{\partial x^2}\right)_i + \frac{\Delta x^3}{6}\left(\frac{\partial^3 \phi}{\partial x^3}\right)_i + \frac{\Delta x^4}{24}\left(\frac{\partial^3 \phi}{\partial x^4}\right)_i + O(\Delta x^5) \tag{A.3}$$

$$\phi_i = \phi_i \tag{A.4}$$

$$\phi_{i-1} = \phi_i - \Delta x \left(\frac{\partial \phi}{\partial x}\right)_i + \frac{\Delta x^2}{2}\left(\frac{\partial^2 \phi}{\partial x^2}\right)_i - \frac{\Delta x^3}{6}\left(\frac{\partial^3 \phi}{\partial x^3}\right)_i + \frac{\Delta x^4}{24}\left(\frac{\partial^3 \phi}{\partial x^4}\right)_i + O(\Delta x^5) \tag{A.5}$$

$$\phi_{i+2} = \phi_i - 2\Delta x \left(\frac{\partial \phi}{\partial x}\right)_i + 2\Delta x^2 \left(\frac{\partial^2 \phi}{\partial x^2}\right)_i - \frac{4\Delta x^3}{3}\left(\frac{\partial^3 \phi}{\partial x^3}\right)_i + \frac{2\Delta x^4}{3}\left(\frac{\partial^3 \phi}{\partial x^4}\right)_i + O(\Delta x^5) \tag{A.6}$$

Therefore,

$$\frac{-\phi_{i+2} + 8\phi_{i+1} - 8\phi_{i-1} + \phi_{i+2}}{12\Delta x} = \left(\frac{\partial \phi}{\partial x}\right)_i + O(\Delta x^4) \tag{A.7}$$

$$\frac{(-\phi_{i+2} + 7\phi_{i+1} + 7\phi_i - \phi_{i-1}) - (-\phi_{i+1} + 7\phi_i + 7\phi_{i-1} - \phi_{i-2})}{12\Delta x} = \left(\frac{\partial \phi}{\partial x}\right)_i + O(\Delta x^4) \tag{A.8}$$

A.2 Flux Corrected Transport scheme

Equation (3.106) can be written as

$$
\begin{aligned}
(\rho q)_{i,j,k}^{n+1} &= (\rho q)_{i,j,k}^{n} - \frac{1}{\Delta x \Delta y \Delta z} \Big[\\
&+ \left[C_{i+\frac{1}{2},j,k} F_{i+\frac{1}{2},j,k}^{high} + \left(1 - C_{i+\frac{1}{2},j,k}\right) F_{i+\frac{1}{2},j,k}^{low} \right] \\
&- \left[C_{i-\frac{1}{2},j,k} F_{i-\frac{1}{2},j,k}^{high} + \left(1 - C_{i-\frac{1}{2},j,k}\right) F_{i-\frac{1}{2},j,k}^{low} \right] \\
&+ \left[C_{i,j+\frac{1}{2},k} F_{i,j+\frac{1}{2},k}^{high} + \left(1 - C_{i,j+\frac{1}{2},k}\right) F_{i,j+\frac{1}{2},k}^{low} \right] \\
&- \left[C_{i,j-\frac{1}{2},k} F_{i,j-\frac{1}{2},k}^{high} + \left(1 - C_{i,j-\frac{1}{2},k}\right) F_{i,j-\frac{1}{2},k}^{low} \right] \\
&+ \left[C_{i,j,k+\frac{1}{2}} F_{i,j,k+\frac{1}{2}}^{high} + \left(1 - C_{i,j,k+\frac{1}{2}}\right) F_{i,j,k+\frac{1}{2}}^{low} \right] \\
&- \left[C_{i,j,k-\frac{1}{2}} F_{i,j,k-\frac{1}{2}}^{high} + \left(1 - C_{i,j,k-\frac{1}{2}}\right) F_{i,j,k-\frac{1}{2}}^{low} \right] \\
&\Big]
\end{aligned} \tag{A.9}
$$

where

$$
F_{i+\frac{1}{2},j,k}^{high,low} = \Delta t \Delta y \Delta z (\rho u)_{i+\frac{1}{2},j,k} q_{i+\frac{1}{2},j,k}^{high,low} \tag{A.10}
$$

$$
F_{i,j+\frac{1}{2},k}^{high,low} = \Delta t \Delta z \Delta x (\rho u)_{i,j+\frac{1}{2},k} q_{i,j+\frac{1}{2},k}^{high,low} \tag{A.11}
$$

$$
F_{i,j,k+\frac{1}{2}}^{high,low} = \Delta t \Delta x \Delta y (\rho u)_{i,j,k+\frac{1}{2}} q_{i,j,k+\frac{1}{2}}^{high,low} \tag{A.12}
$$

The anti-diffusive flux are defined as

$$
A_{i+\frac{1}{2},j,k} = F_{i+\frac{1}{2},j,k}^{high} - F_{i+\frac{1}{2},j,k}^{low} \tag{A.13}
$$

$$
A_{i,j+\frac{1}{2},k} = F_{i,j+\frac{1}{2},k}^{high} - F_{i,j+\frac{1}{2},k}^{low} \tag{A.14}
$$

$$
A_{i,j,k+\frac{1}{2}} = F_{i,j,k+\frac{1}{2}}^{high} - F_{i,j,k+\frac{1}{2}}^{low} \tag{A.15}
$$

Equation (A.9) can be rewritten as

$$
\begin{aligned}
(\rho q)_{i,j,k}^{n+1} &= (\rho q)_{i,j,k}^{n} - \frac{1}{\Delta x \Delta y \Delta z} \Big[\\
&+ \left[F_{i+\frac{1}{2},j,k}^{low} + C_{i+\frac{1}{2},j,k} A_{i+\frac{1}{2},j,k} \right] \\
&- \left[F_{i-\frac{1}{2},j,k}^{low} + C_{i-\frac{1}{2},j,k} A_{i-\frac{1}{2},j,k} \right] \\
&+ \left[F_{i,j+\frac{1}{2},k}^{low} + C_{i,j+\frac{1}{2},k} A_{i,j+\frac{1}{2},k} \right] \\
&- \left[F_{i,j-\frac{1}{2},k}^{low} + C_{i,j-\frac{1}{2},k} A_{i,j-\frac{1}{2},k} \right] \\
&+ \left[F_{i,j,k+\frac{1}{2}}^{low} + C_{i,j,k+\frac{1}{2}} A_{i,j,k+\frac{1}{2}} \right] \\
&- \left[F_{i,j,k-\frac{1}{2}}^{low} + C_{i,j,k-\frac{1}{2}} A_{i,j,k-\frac{1}{2}} \right] \\
&\Big]
\end{aligned} \tag{A.16}
$$

In practice, we calculate Eq.(A.16) by the following steps:

1. The tentative values are calculated by using the low order flux:

$$
\begin{aligned}
(\rho q)_{i,j,k}^{\dagger} &= (\rho q)_{i,j,k}^{n} \\
&- \frac{1}{\Delta x \Delta y \Delta z} \left[+F_{i+\frac{1}{2},j,k}^{low} - F_{i-\frac{1}{2},j,k}^{low} + F_{i,j+\frac{1}{2},k}^{low} - F_{i,j-\frac{1}{2},k}^{low} + F_{i,j,k+\frac{1}{2}}^{low} - F_{i,j,k-\frac{1}{2}}^{low} \right]
\end{aligned} \tag{A.17}
$$

2. Allowable maximum and minimum values are calculated:

$$
\begin{aligned}
(\rho q)_{i,j,k}^{\max} \;=\; \max[\\
\max((\rho q)_{i,j,k}^{\dagger}, (\rho q)_{i,j,k}^{n}), \\
\max((\rho q)_{i-1,j,k}^{\dagger}, (\rho q)_{i-1,j,k}^{n}), \\
\max((\rho q)_{i+1,j,k}^{\dagger}, (\rho q)_{i+1,j,k}^{n}), \\
\max((\rho q)_{i,j-1,k}^{\dagger}, (\rho q)_{i,j-1,k}^{n}), \\
\max((\rho q)_{i,j+1,k}^{\dagger}, (\rho q)_{i,j+1,k}^{n}), \\
\max((\rho q)_{i,j,k-1}^{\dagger}, (\rho q)_{i,j,k-1}^{n}), \\
\max((\rho q)_{i,j,k+1}^{\dagger}, (\rho q)_{i,j,k+1}^{n}) \\
]
\end{aligned}
\tag{A.18}
$$

$$
\begin{aligned}
(\rho q)_{i,j,k}^{\min} \;=\; \min[\\
\min((\rho q)_{i,j,k}^{\dagger}, (\rho q)_{i,j,k}^{n}), \\
\min((\rho q)_{i-1,j,k}^{\dagger}, (\rho q)_{i-1,j,k}^{n}), \\
\min((\rho q)_{i+1,j,k}^{\dagger}, (\rho q)_{i+1,j,k}^{n}), \\
\min((\rho q)_{i,j-1,k}^{\dagger}, (\rho q)_{i,j-1,k}^{n}), \\
\min((\rho q)_{i,j+1,k}^{\dagger}, (\rho q)_{i,j+1,k}^{n}), \\
\min((\rho q)_{i,j,k-1}^{\dagger}, (\rho q)_{i,j,k-1}^{n}), \\
\min((\rho q)_{i,j,k+1}^{\dagger}, (\rho q)_{i,j,k+1}^{n}) \\
]
\end{aligned}
\tag{A.19}
$$

3. Several values for the flux limiter are calculated:

$$
\begin{aligned}
P_{i,j,k}^{+} \;=\; & -\min(0, A_{i+\frac{1}{2},j,k}) + \max(0, A_{i-\frac{1}{2},j,k}) \\
& -\min(0, A_{i,j+\frac{1}{2},k}) + \max(0, A_{i,j-\frac{1}{2},k}) \\
& -\min(0, A_{i,j,k+\frac{1}{2}}) + \max(0, A_{i,j,k-\frac{1}{2}})
\end{aligned}
\tag{A.20}
$$

$$
\begin{aligned}
P_{i,j,k}^{-} \;=\; & -\max(0, A_{i+\frac{1}{2},j,k}) + \min(0, A_{i-\frac{1}{2},j,k}) \\
& -\max(0, A_{i,j+\frac{1}{2},k}) + \min(0, A_{i,j-\frac{1}{2},k}) \\
& -\max(0, A_{i,j,k+\frac{1}{2}}) + \min(0, A_{i,j,k-\frac{1}{2}})
\end{aligned}
\tag{A.21}
$$

$$
\tag{A.22}
$$

$$
Q_{i,j,k}^{+} \;=\; \left[(\rho q)_{i,j,k}^{\max} - (\rho q)_{i,j,k}^{\dagger} \right] \Delta x \Delta y \Delta z
\tag{A.23}
$$

$$
Q_{i,j,k}^{-} \;=\; \left[(\rho q)_{i,j,k}^{\dagger} - (\rho q)_{i,j,k}^{\min} \right] \Delta x \Delta y \Delta z
\tag{A.24}
$$

$$
R_{i,j,k}^{+} \;=\;
\begin{cases}
\min(1, Q_{i,j,k}^{+}/P_{i,j,k}^{+}) & \text{if } P_{i,j,k}^{+} > 0 \\
0 & \text{if } P_{i,j,k}^{+} = 0
\end{cases}
\tag{A.25}
$$

$$
R_{i,j,k}^{-} \;=\;
\begin{cases}
\min(1, Q_{i,j,k}^{-}/P_{i,j,k}^{-}) & \text{if } P_{i,j,k}^{-} > 0 \\
0 & \text{if } P_{i,j,k}^{-} = 0
\end{cases}
\tag{A.26}
$$

100

4. The flux limiters at the cell wall are calculated:

$$C_{i+\frac{1}{2},j,k} \quad = \quad \begin{cases} \min(R^+_{i+1,j,k}, R^-_{i,j,k}) & \text{if } A^-_{i+\frac{1}{2},j,k} \geq 0 \\ \min(R^+_{i,j,k}, R^-_{i+1,j,k}) & \text{if } A^-_{i+\frac{1}{2},j,k} < 0 \end{cases} \qquad (A.27)$$

$$C_{i,j+\frac{1}{2},k} \quad = \quad \begin{cases} \min(R^+_{i,j+1,k}, R^-_{i,j,k}) & \text{if } A^-_{i,j+\frac{1}{2},k} \geq 0 \\ \min(R^+_{i,j,k}, R^-_{i,j+1,k}) & \text{if } A^-_{i,j+\frac{1}{2},k} < 0 \end{cases} \qquad (A.28)$$

$$C_{i,j,k+\frac{1}{2}} \quad = \quad \begin{cases} \min(R^+_{i,j,k+1}, R^-_{i,j,k}) & \text{if } A^-_{i,j,k+\frac{1}{2}} \geq 0 \\ \min(R^+_{i,j,k}, R^-_{i,j,k+1}) & \text{if } A^-_{i,j,k+\frac{1}{2}} < 0 \end{cases} \qquad (A.29)$$

Appendix B

Details of Seiki and Nakajima (2014)

B.1 Treatment of hydrometeors

Generally, characteristics of cloud particles are determined by their size, shape, and the chemical properties of solute within them. Representation of these characteristics requires a multi-dimensional parameter space of size, shape, and chemical compositions. Since development of a cloud resolving model (CRM) coupled with an aerosol transport model is beyond the scope of this study, we consider a two-dimensional parameter space of size and shape of cloud particles. We then categorize cloud models into two major groups, according to their representation of cloud particles. One is the bin method, using discretized particle size bins and predicting the population density of particles in each bin. The other is the bulk method, in which particle size distributions are approximated by several prescribed modes, predicting the total populations of particles of each mode. The treatment of hydrometeors adopted in this study is described in the following sections.

B.1.1 Droplet Size Distribution

Seiki and Nakajima (2014) scheme is designed to maintain the self-consistency of assumptions regarding droplet size distribution (DSD) and the shapes of ice particles among cloud microphysical processes. Following Seifert and Beheng (2006; hereafter, SB06), Seiki and Nakajima (2014) predict the moments of the DSD of each hydrometeor, assuming generalized gamma distribution to analytically formulate cloud microphysics, as follows:

$$f_a(r) = \alpha_a x^{\nu_a} \exp(-\lambda x) \tag{B.1}$$

where the index a $\in$ (c,r,i,s,g) represents cloud water, rain, cloud ice, snow, and graupel. For a given DSD, the k-th moment can be defined as follows:

$$M_a^{(k)} \equiv \int_0^\infty x^k f_a(r) dx, \quad (k \in \mathbf{R}) \tag{B.2}$$

For example, the 0-th moment of a DSD is the number concentration N_a, and the 1st moment is the mass concentration $L_a = \rho q_a$. The evolution of DSD is represented by updating α_a and λ_a using N_a and L_a with two fixed parameters, ν_a and μ_a, respectively. The diagnostic parameters α_a and λ_a are calculated as follows:

$$\alpha_a = \frac{\mu_a \lambda_a}{\Gamma\left(\frac{\nu_a+1}{\mu_a}\right)} \lambda_a^{\frac{\nu_a+1}{\mu_a}} \tag{B.3}$$

$$\lambda_a = \Big[\frac{\Gamma\left(\frac{\nu_a+1}{\mu_a}\right)}{\Gamma\left(\frac{\nu_a+2}{\mu_a}\right)}\Big]^{-\nu_a}$$

with mean particle mass $\bar{x} \equiv L_a/N_a$. We maintain the self-consistency of the shape of ice particles by assuming power law relationships between: 1) particle mass and maximum dimension D, and 2) particle mass and projected area to flow A, as follows:

$$D = a_m x^{b_m} \tag{B.4}$$

$$A = a_{ax} x^{b_m} \tag{B.5}$$

where a_m, b_m, a_{ax}, and b_{ax} are constant coefficients. We chose to use constant parameters for DSD representation, following SB06 for cloud water, cloud ice, snow, and graupel, and following Seifert (2008) for rain (assuming collisional-breakup equilibrium conditions). The shapes of ice particles are those given by Mitchell (1996), assuming cloud ice as hexagonal plates, snow as assemblages of planar polycrystals in cirrus clouds, and graupel as lump graupel. The above-mentioned constant parameters for each hydrometeor are summarized in Table B.1.

Table B.1: Constant parameters chosen for the generalized gamma distribution; power law coefficients used for maximum dimensions and projected area, and ranges of lower- and upper limits of mean mass.

	cloud water	rain	cloud ice	snow	graupel
ν	1	-1/3	1	1	1
μ	1	1/3	1/3	1/3	1/3
$a_m[\text{m } kg^{-bm}]$	0.124	0.124	1.24	1.24	0.346
b_m	1/3	1/3	0.408	0.408	0.357
$a_{ax}[m^2 kg^{-bA}]$	0.0121	0.0121	0.178	0.196	0.0599
b_{ax}	2/3	2/3	0.755	0.768	0.714
$x_{min}^-[kg]$	4.2×10^{-12}	4.2×10^{-12}	4.2×10^{-12}	4.2×10^{-12}	4.2×10^{-12}
$x_{max}^-[kg]$	2.6×10^{-10}	2.6×10^{-10}	2.6×10^{-10}	2.6×10^{-10}	2.6×10^{-10}

B.1.2 Terminal velocity of hydrometeors

In the same manner as Seifert and Beheng (2006a), the terminal velocities of particles are formulated in power laws, except for gravitational sedimentation, which is described using an accurate formula because it is directly compared with precipitation data. The terminal velocities of hydrometeors are determined by the balance between drag and gravitational forces. Traditionally, the terminal velocities for small spherical particles with small Reynolds number (N_{Re}) are described by Stokes' Law:

$$\nu_{t,stokes}(r) = \frac{2g(\rho_w - \rho)}{9\eta_a}r^2 \tag{B.6}$$

where $g = 9.80616 \ [ms^{-2}]$ is gravitational acceleration, $\rho w = 1000 \ kgm^{-3}$ is the density of liquid water, ρ is the density of air, and η_a is the dynamic viscosity of air. Laboratory experiments have shown that terminal velocity departs from Stokes' Law as the Reynolds number increases (Gunn and Kinzer, 1948; Beard and Pruppacher, 1969). Other formulas are thus required for larger droplets, such as rain droplets and ice crystals.

In the case of liquid water droplets, terminal velocity can be determined well by laboratory experiments because of the simplicity of shape. In contrast, there are many observed terminal velocities of ice particles for various shapes of ice crystals. Bohm (1989), Bohm (1992), and Mitchell (1996) proposed general formulations of the terminal velocities of ice particles based on the boundary layer theory, with their studies showing good agreement with observational data. In this study, we calculated terminal velocities for each ice particle based on Mitchell (1996) and then created a fitting curve using a power law within a suitable diameter range.

In theoretical formulas, the terminal velocities of hydrometeors are dependent on diameter, shape, the Reynolds number, and the Best (or Davies) number (N_X). Applying these to cloud microphysics is extremely complicated; here, we therefore apply a simplified approach suggested by Beard (1980):

1. The terminal velocity is calculated for the reference atmosphere.

2. The terminal velocity in the atmosphere is adjusted from the reference value.
In the following paragraphs, we describe terminal velocities for the reference atmosphere and the adjustment technique.

B.1.3 Terminal velocity of liquid water droplets for the reference atmosphere

In the case of liquid water droplets, absence of shape variability makes formulation easier than in the case of ice particles. Here, we only consider dependency on the diameter of droplets. Seifert and Beheng (2006) applied the formulation of Rogers et al. (1993), the analytical approximation of Gunn and Kinzer ' s (1948) observation data:

$$\nu_t(D) = \begin{cases} a_{R_s}D(1 - exp(-b_{R_s}D)), & (D < D_{0,r}) \\ a_{R_l} - b_{R_l}exp(-c_{R_l}D), & (D > D_{0,r}) \end{cases} \tag{B.7}$$

where $a_{R_s} = 4000s^{-1}$, $b_{R_s} = 12000m^{-1}$, $a_{R_l} = 9.65ms^{-1}$, $b_{R_l} = 10.43ms^{-1}$, $c_{R_l} = 600m^{-1}$, and $D_0, r = 7.45 \times 10^{-4}$ m. This formulation approaches the quadratic form of Stokes ' Law in the limit for small diameters. In addition, Gunn and Kinzer ' s (1948) data agrees well with the terminal velocities calculated via theoretical formulation based on the boundary layer theory (Bohm, 1992). We therefore applied eq.B.7 for rain sedimentation (Fig. B.12 11). Here, the reference atmosphere of the formulation is $T = 293K$, $p = 1000hPa$, and relative humidity is 0.5 (Gunn and Kinzer, 1948).

B.1.4 Terminal velocity of solid water particles for the reference atmosphere

In the case of ice particles, we derive the theoretical formulation of the terminal velocity based on Mitchell (1996). In general the aerodynamic drag force F_D on a particle is expressed as follows:

$$F_D \equiv \frac{1}{2}\rho\nu_t^2 A C_D \tag{B.8}$$

where C_D is the drag coefficient. Terminal velocity is determined by the equilibrium condition between the drag force and gravitational acceleration:

$$\nu_t = \left(\frac{2xg}{\rho A C_D}\right)^{1/2} \tag{B.9}$$

The problem of derivation of the terminal velocity is reduced to derivation of the drag coefficient, independent of the terminal velocity. In practice, Mitchell (1996) and many other researchers calculated the terminal velocity by defining the Best number (N_X), as follows:

$$N_x \equiv C_D N_{R_e}^2 = \frac{2xg\rho D^2}{A\eta_a^2} \tag{B.10}$$

where N_{R_e} is the Reynolds number. The terminal velocity can be calculated after the relationship between Best and Reynolds numbers is determined. In the relationship, it is convenient for the drag coefficient to be determined by the Reynolds number, although the dependency of the former is complicated. A theoretical formulation of the drag coefficient was proposed by Abraham (1970). The drag coefficient is the dimensionless number defined by the drag force, the dynamic pressure, and the projection area of the particle (see eq.B.8). Abraham (1970) assumed that the effective projection area of the particle contained the projection area of the particle itself and also the boundary layer surrounding the particle, as follows:

$$F_D = \frac{1}{2}\rho\nu_t^2 C_0 A\left(1 + \frac{\delta_b}{r_A}\right)^2 \tag{B.11}$$

where C_0 is the drag coefficient due to the pressure of the fluid and should be determined independently of the shape, δ_b is the boundary layer depth, and r_A is the radius of a circle

with the equivalent projection area. Furthermore, the ratio of boundary layer depth to radius is expressed as follows:

$$\frac{\delta_b}{r_A} = \frac{\delta_0}{N_{R_e}^{1/2}} \tag{B.12}$$

where δ_0 is a non-dimensional constant. Substituting eq.B.12 into eq.B.11, the drag coefficient, which also includes the effect of the boundary layer, corresponds to the following:

$$C_D = C_0 \left(1 + \frac{\delta_0}{N_{R_e}^{1/2}}\right)^2 \tag{B.13}$$

The drag coefficient is thus expressed by the Reynolds number. The relationship between Reynolds and Best numbers is derived by substituting eq.B.13 into eq.B.10:

$$N_{R_e} = \frac{\delta_0^2}{4} \left[\left(1 + \frac{4N_X^{1/2}}{\delta_0^2 C_0^{1/2}}\right)^{1/2} - 1\right]^2 \tag{B.14}$$

Here we use $C_0 = 0.6$ and $\delta_0 = 5.83$, as provided by Bohm (1989). Finally the terminal velocity of ice particles is calculated by substituting eq.B.10 and eq.B.14 into the definition of the Reynolds number:

$$
\begin{aligned}
\nu_t &= \frac{N_{Re}\eta_a}{D\rho} \\
&= \frac{\eta_a}{D\rho}\frac{\delta_0^2}{4}\left[\left[1 + \frac{4}{\delta_0^2 C_0^{1/2}}\left(\frac{2xg\rho D^2}{A\eta_a^2}\right)^{1/2}\right]^{1/2} - 1\right]^2
\end{aligned} \tag{B.15}
$$

In this formulation, required variables are mass, projection area, maximum dimension of ice particles, and thermodynamical variables. Here we use several piecewise-constant mass-maximum dimension, and projection area-maximum dimension relationships provided by Mitchell (1996). The terminal velocities of various ice particles are plotted in Fig.B.2. As shown in Fig.B.1, there is less difference between hexagonal plates and stellar crystals with broad arms with diameter less than a few hundred micrometers. We therefore only consider hexagonal columns and hexagonal plates as representative of the ice category.

B.1.5 Adjustment factor of terminal velocity

Beard (1980) suggested that calculation of the terminal velocity using the Best number could be simplified with use of an adjustment factor (f_{vt}), defined as:

$$\nu_t = \nu_{t0} f_{vt} \tag{B.16}$$

where v_{t0} is a reference terminal velocity. He demonstrated that f_{vt} was not sensitive to the shape of hydrometeors. When electrical force is not considered in cloud microphysics, formulas of f_{vt} are as follows:

$$
\begin{aligned}
f_{vt} &= f_{vt0} \ \ (N_{Re_0} \leq 0.2) \tag{B.17}\\
f_{vt} &= f_{vt\infty} \ \ (N_{Re_0} \geq 1000) \tag{B.18}\\
f_{vt} &= f_{vt0} \\
&+ (f_{vt\infty} - f_{vt0})(1.61 + lnN_{Re_0})/8.52 \ \ (N_{Re_0} < 1000) \tag{B.19}\\
f_{vt0} &\equiv (\eta_0/\eta) \tag{B.20}\\
f_{vt\infty} &\equiv (\rho_0/\rho)^{0.5} \tag{B.21}\\
N_{Re_0} &\equiv \rho_0 D v_{t0}/\eta_0 \tag{B.22}
\end{aligned}
$$

The upper ($N_{R_e} = 1000$) and lower ($N_{R_e} = 0.2$) limits of the Reynolds number correspond to diameters of several millimeters and tens of micrometers, respectively. Seifert and Beheng (2006) applied a further simplified adjustment factor based on eqs.B.20 and B.21, as follows:

$$f_{vt,n} = (\rho_0/\rho)^{\gamma_n}, \quad (n = c, r, i, s, g) \tag{B.23}$$

where $\gamma_c = 1.0$ and $\gamma_r = \gamma_i = \gamma_s = \gamma_g = 0.5$ This simplified formula of the adjustment factor is intended to avoid dependency on the Reynolds number. However, $\gamma_n = 0.5$ is only valid for high Reynolds number particles with diameters > several millimeters, as shown in eq.B.15. The above formula therefore always underestimates the terminal velocity of cirrus clouds. Another simplified formula for cirrus clouds was suggested by Heymsfield and Iaquinta (2000), as follows:

$$f_{vt} = (p/p_0)^{-0.178}(T/T_0)^{-0.394} \tag{B.24}$$

where $T_0 = 233$ K and $p_0 = 300$ hPa. By using these adjustment factors, we can only consider the terminal velocity for the reference atmosphere. Adjustment factors used for each hydrometeor in this study are summarized in Table B.2:

Table B.2: Adjustment factor for the reference terminal velocity.

	cloud	rain	ice	snow	graupel
f_{vt}	1	$(\rho_0/\rho)^{0.5}$	$(p/p_0)^{-0.178}(T/T_0)^{-0.394}$	$(p/p_0)^{-0.178}(T/T_0)^{-0.394}$	$(p/p_0)^{-0.178}(T/T_0)^{-0.394}$

B.1.6 Weighted mean terminal velocity

In gravitational sedimentation, mean terminal velocity weighted by the k-th moments of DSD ($\bar{v_{k,nq}}$) is calculated in a straightforward manner, as follows:

$$v_{k,nq}^- = \int_0^\infty x^k f_{nq}(x)v_{t,nq}(x)dx \tag{B.25}$$

However, the terminal velocity formulas, eqs.B.8 and B.15, are too complicated to analytically integrate eq.B.25. Seifert and Beheng (2006) and Seifert (2008) used the large branch of eq.B.8 for rain droplets and simple power laws derived by observation for other hydrometeors. Here, we provide more accurate formulations to calculate weighted terminal velocities.

As shown above, dependency of the terminal velocity on diameter varies across aerodynamical regimes. In other words, dependency varies with diameter range. We therefore first prepared two branches of the terminal velocities of hydrometeors (except for cloud droplets) so as to integrate DSDs analytically. For cloud droplets, we used the same power law provided by Seifert and Beheng (2006), based on Stokes' law. For rain droplets, we directly used the formulation of eq.B.8, which allows analytical integration of each branch. In contrast, we need to derive two fitting curves for ice particles. The formulation of the terminal velocity of ice particles is described as a power law of the diameter using the least-square method, as follows:

$$v_{t,js} = a_{v,js}x^{b_{v,js}}, \quad (js = i, s, g) \tag{B.26}$$

$$(RMSE)_{k,js} = \sum_{id=1}^{id_{max}} \left(lnv_{k,js,true}^-(\bar{D_{id}}) - lnv_{k,js}^-(\bar{D_{id}})\right)^2 \tag{B.27}$$

$$\frac{\partial(RMSE)_{k,js}}{\partial a_{v,js}} = 0, \frac{\partial(RMSE)_{k,js}}{\partial b_{v,js}} = 0$$

$$v_{k,js}^-(\bar{D_{id}}) = \int_0^\infty a_{v,js}x^{b_{v,js}+k}f(x,\bar{D_{id}},L)dx/L$$

$$= a_{v,js}\frac{\Gamma\left(\frac{v_{js}+b_{v,js}+k+1}{\mu_{js}}\right)}{\Gamma\left(\frac{v_{js}+k+1}{\mu_{js}}\right)}\left[\frac{\Gamma\left(\frac{v_{js}+1}{\mu_{js}}\right)}{\Gamma\left(\frac{v_{js}+2}{\mu_{js}}\right)}\right]^{b_{v,js}}x_{id,js}^{\bar{b_{v,js}}} \tag{B.28}$$

$$v_{k,js,true}^-(\bar{D_{id}}) = \sum_{i=1}^{imax} x^k v_{t,js,true}f_{logD}(lnD_i,\bar{D_{id}},L)\Delta lnD/L$$

where $D_1 = 10\mu m$, $D_{imax} = 10mm$, $i_{max} = 1000$, and L is an arbitrary constant. The fitting ranges of the mean volume diameter in eq.B.27 are from 20 to 400 μm for the small branch and from 200 to 2000 μm for the large branch. The derived parameters are summarized in Table B.3.

Second, the terminal velocity with a certain mean diameter is calculated by interpolating between the two branches in the logarithmic scale of the diameter. We use the mean diameter weighted by the kth moments of DSD in the interpolation. The formulation of weighted terminal velocities of rain droplets and solid particles are as shown below:

$$v_{k,nq}^- = w_{k,nq}v_{k,lrg,nq}^- + (1 - w_{k,nq})v_{k,lrg,nq}^-, \quad (nq = r,i,s,g) \tag{B.29}$$

$$w_{k,r} = 0.5(1 + tanh(\pi ln(D_{k,r}^-/D_{0,k,r})))$$

$$w_{k,js} = max(0.0, \ min(1.0, 0.5(1 + ln(D_{k,js}^-/D_{0,k,js})))) \quad (js = i,s,g)$$

$$D_{k,nq}^- = \frac{\int_0^\infty D_{nq}(x)x^k f_{nq}(x)dx}{\int_0^\infty x^k f_{nq}(x)dx}$$

$$= D_{nq}^- \frac{\Gamma(\frac{v_{nq}+b_{m,nq}+k+1}{\mu_{nq}})}{\Gamma(\frac{v_{nq}+k+1}{\mu_{nq}})} \Big[\frac{\Gamma(\frac{v_{nq}+1}{/mu_{nq}})}{\Gamma(\frac{v_{nq}+2}{\mu_{nq}})}\Big]^{b_{m,nq}} \tag{B.30}$$

$$v_{k,sml,r}^- = \frac{f_{vt,r}}{M_r^k} \int_0^\infty \big[a_{R_s}D(1 - exp(-b_{R_s}D))\big]x^k N_r(D)dD$$

$$= a_{R_s}\frac{(1 + \mu_{D,r} + 3k)}{\lambda_{D,r}}$$

$$\times \ \Big[1 - \big(1 + \frac{b_{R_s}}{\lambda_{D,r}}\big)^{-2-\mu_{D,r}-3k}\Big]\big(\frac{\rho_0}{\rho}\big)^{1/2} \tag{B.31}$$

$$v_{k,lrg,r}^- = \frac{f_{vt,r}}{M_r^k} \int_0^\infty \big[a_{Rl} - b_{Rl}exp(-c_{Rl}D)\big]x^k N_r(D)dD$$

$$= a_{Rl} - b_{Rl}\big(1 + \frac{c_{Rl}}{\lambda_{D,r}}\big)^{-1-\mu_{D,r}-3k}\big(\frac{\rho_0}{\rho}\big)^{1/2} \tag{B.32}$$

$$N_r(D) = N_{0,r}D^{-\mu_{D,r}}exp(-\lambda_{D,r}D) \tag{B.33}$$

where $D_{0,r}$ and $D_{0,js}$ are the branch points of the fitting curves (see Table B.4). Here we apply the form of the modified gamma distribution for diameter as a DSD of rain droplets. Derivation and correspondences of the coefficient $N_{0,r}$, the slope parameter λ_D,r, and shape parameter μD appearing in the modified gamma distribution are described in Appendix B. Weighted terminal velocities of ice particles for two branches are calculated by eq.B.28. Fig.B.3 shows the terminal velocity of rain droplets weighted by number and mass concentration. Our method gives better results than those obtained using the approximated method adopted by Seifert and Beheng (2006) in the range within their upper and lower limits. Fig.B.4 shows terminal velocities of ice particles weighted by number and mass concentration.

Table B.3: Coefficients and exponents of the relationship between mass and terminal velocity of each hydrometeor used in gravitational sedimentation and other processes.

Hydrometeors	Sedimentation of mass	Sedimentation of mass	Sedimentation of number	Sedimentation number	other process
	Small	Large	Small	Large	
Cloud	$a_v = 3.75 \times 10^5, b_v = 2/3$	$a_v = 3.75 \times 10^5, b_v = 2/3$	$a_v = 3.75 \times 10^5, b_v = 2/3$	$a_v = 3.75 \times 10^5, b_v = 2/3$	$a_v = 3.75 \times 10^5, b_v = 2/3$
Rain	B.8	B.8	B.8	B.8	B.8
Hexagonal plate	$a_v = 5800, b_v = 0.505$	$a_v = 167, b_v = 0.325$	$a_v = 1.24 \times 10^5, b_v 0.549$	$a_v = 422, b_v = 0.385$	$a_v = 5800, b_v = 0.505$
Hexagonal columns	$a_v = 2900, b_v = 0.466$	$a_v = 32.2, b_v = 0.224$	$a_v = 9698, b_v 0.531$	$a_v = 64.2, b_v = 0.274$	$a_v = 2900, b_v = 0.466$
Aggregates of planar polycrystals	$a_v = 1.52 \times 10^5, b_v = 0.528$	$a_v = 306.0, b_v = 0.330$	$a_v = 2.93 \times 10^5, b_v 0.567$	$a_v = 818, b_v = 0.394$	$a_v = 1.52 \times 10^5 b_v = 0.528$
Lump graupel	$a_v = 1.55 \times 10^5, b_v = 0.535$	$a_v = 312.0, b_v = 0.330$	$a_v = 2.76 \times 10^5, b_v 0.571$	$a_v = 698, b_v = 0.387$	$a_v = 1.55 \times 10^5 b_v = 0.535$

B.2 Detailed description of cloud microphysics

Cloud microphysics is mainly subdivided into two. One is phase change among gas, liquid, and solid phases, while the other is the collection process among all particles. In addition,
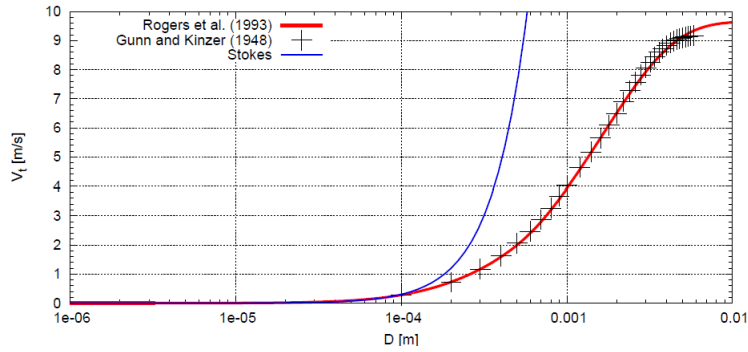
Figure B.1: Dependency of terminal velocity of liquid water droplet on diameter. Marks are from Gunn and Kinzer (1948), red line is from Rogers et al. (1993), and blue line is calculated by Stokes' law (eq.B.6) under the condition T=293K, p=1000hPa.
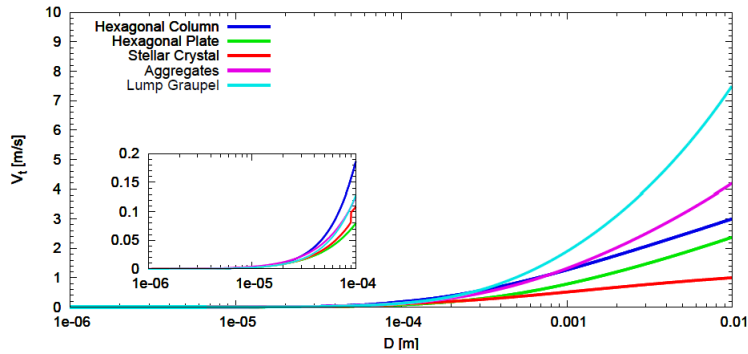

Figure B.2: Dependency of terminal velocity of liquid water droplet in maximum dimension. Each solid line color corresponds to different ice particle types, based on Mitchell (1996). Hexagonal columns are blue, hexagonal plates are green, stellar crystals with broad arms are red, aggregates of planar polycrystals in cirrus clouds are purple, and lump graupel is light blue.
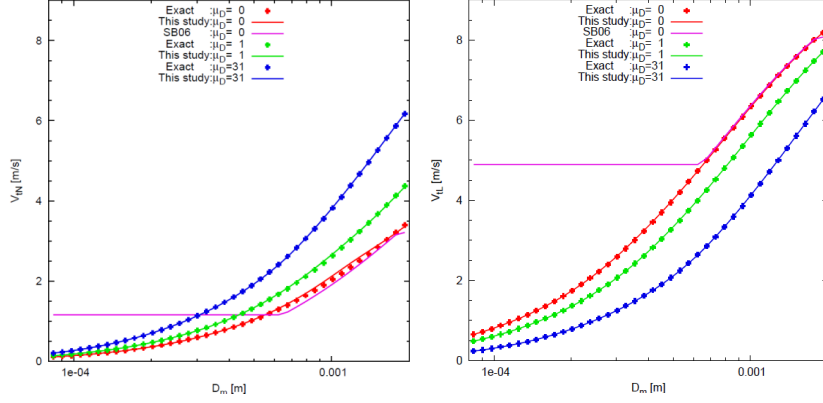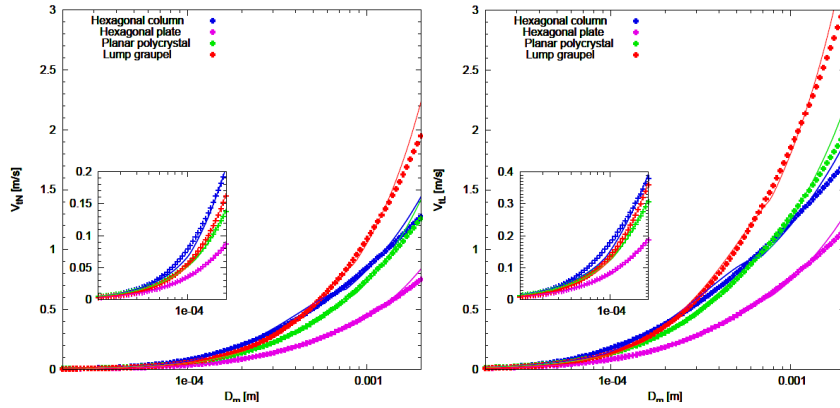
Figure B.3: Dependencies of number weighted terminal velocity (v_{tN}) (left) and mass weighted terminal velocity (v_{tL}) (right) of rain droplets on mean volume diameter (D_m). Abscissa is the mean volume diameter and vertical axis is the terminal velocity. Dots show exactly integrated values and solid lines show approximated values obtained in this study (red, green, and blue) and by Seifert and Beheng (2006) (purple). Red and purple lines are calculated with $\mu D = 0$, green lines are calculated with $\mu D = 1$, and blue lines are calculated with $\mu D = 31$.

Figure B.4: Dependencies of number weighted terminal velocity (v_{tN}) (left) and mass weighted terminal velocity (v_{tL}) (right) of ice particles on mean volume diameter (D_m). Abscissa is the mean volume diameter and vertical axis is the terminal velocity. Dots show the exact value calculated by Mitchell (1996) and solid lines show the fitting curves. Red, green, blue, and purple denote lump graupels, assemblages of planar polycrystals, hexagonal columns, and hexagonal plates, respectively.

109

Table B.4: Branch points of the weighted terminal velocity.

Hydrometeors	branch points of weighted terminal velocity [m]
Cloud	Not used
Rain	$D_{0,r} = 7.45 \times 10^{-4}$
Hexagonal plates	$D_{0,0,i} = 262 \times 10^{-6}, D_{0,1,i} = 399 \times 10^{-6}$
Hexagonal columns	$D_{0,0,i} = 240.5 \times 10^{-6}, D_{0,1,i} = 330 \times 10^{-6}$
Aggregates of planar polycrystals	$D_{0,0,s} = 270 \times 10^{-6}, D_{0,1,s} = 270 \times 10^{-6}$
Lump graupel	$D_{0,0,g} = 269 \times 10^{-6}, D_{0,1,g} = 376 \times 10^{-6}$

all hydrometeors are vertically transported by gravitational sedimentation. Phase change depends on the thermodynamics of environment air and itself affects thermodynamics through latent heat release. In contrast, collection is an internal growth process with less interaction with the atmosphere. Since the growth speed of the collection process is much faster than that of phase change, the role of the collection process is key to determining the lifetime of clouds (e.g., lifetime effect). Finally, gravitational sedimentation determines the removal rate of clouds from the atmosphere. It removes cloud directly by transportation, and indirectly by the collection process via collision volume (swept volume).

The cloud microphysics scheme developed in this study basically follows Seifert and Beheng (2006). Their two-moment bulk cloud microphysics scheme is remarkable in improvement of the collection process by using a bin cloud microphysics scheme. Based on their work, we modify the cloud nucleation process (Twomey 1959; and Lohmann 2002), the condensation process (Morrison et al. 2005), and the formulation of terminal velocities (Mitchell, 1996) with expectation of the application to global cloud resolving simulations. We describe production and reduction terms of mass concentration and number concentration in the following subsections.

B.2.1 Phase change

Condensation/evaporation

Theoretical formulation of condensation or evaporation is basically derived by balance equation of vapor and thermal diffusion above the surface of a single particle (Rogers and Yau, 1989; Pruppacher and Klett, 1997). The growth rate of liquid droplet mass $x_i l$ is described as follows:

$$\frac{dx_{jl}}{d} = 2\pi D(x_{jl})G_{lv}(T,p)F_{vf}(x_{(jl)})S_w, \ (jl = c, r) \tag{B.34}$$

$$G_{lv} = \Big[\frac{R_v T}{p_{sw}(T)D_v} + \frac{L_{v0}}{K_T T}\Big(\frac{L_{v0}}{R_v}T - 1\Big)\Big]^{-1} \tag{B.35}$$

$$F_{vf}(x_r) = a_{vf,r} + b_{vf,r}N_{S_c}^{1/3}N_{R_e}^{1/2} \tag{B.36}$$

Here G_{lv} is a coefficient related to vapor and thermal diffusion, D_v is diffusivity of water vapor and K_T is thermal conductivity, and F_{vf} is the so-called ventilation coefficient. This is a correction factor for the assumption that the water vapor field surrounding each droplet is spherically symmetrical. Formulation of Fvf was experimentally determined by Pruppacher and Klett (1997) and it depends on the Schmidt (N_{S_c}) and Reynolds (N_{R_e}) numbers. This formulation for single droplets is transformed into one for moments following Seifert and Beheng (2006). Assuming DSD as a generalized Gamma distribution and neglecting change in DSD caused by other processes in a time step, we can derive the growth rate of moments:

$$\frac{\partial M_{jl}^k}{\partial t}\Big|_{cnd,evp} \cong \int_0^\infty f_{jl}(x)x^{k-1}\frac{\partial x}{\partial t}\Big|_{cnd,evp}dx \tag{B.37}$$

We can consider eq.B.37 from a different view point, as follows:

$$\begin{aligned}
\frac{\partial M_{jl}^k}{\partial t}\Big|_{cnd,evp} &\cong \int_0^\infty f_{jl}(x)x^k\Big[\frac{1}{x}\frac{\partial x}{\partial t}\Big|_{cnd,evp}\Big]dx \\
&= \int_0^\infty \frac{f_{jl}(x)x^k}{\tau}dx, \ \tau \equiv \frac{x}{\frac{\partial x}{\partial t}}\Big|_{cnd,evp} \tag{B.38}
\end{aligned}$$

Here, we note that theoretical treatment of condensation or evaporation only changes droplet mass. We then diagnose the growth rates of other moments using the change ratio of droplet mass with time scale τ. We can thus derive the growth equation for arbitrary moments, as follows:

$$
\begin{aligned}
\frac{\partial M_{jl}^k}{\partial t}\Big|_{cnd,evp} &= 2\pi G_{lv} S_w \int_0^\infty D_{jl}(x) F_{vf,jl}(x) f_{jl}(x) x^{k-1} dx \\
&= 2\pi G_{lv} S_w N_{jl} D_{jl}(\bar{x}_{jl}) \bar{F}_{vf,k,jl}(\bar{x}_{jl}) \bar{x}_{jl}^{k-1}
\end{aligned}
\tag{B.39}
$$

where $\bar{F}_{vf,k,il}$ is an averaged ventilation factor for the k-th moment of DSD. This formulation seems to be valid unless reduction of number concentration occurs. Because reduction of number concentration occurs only in the case of the smallest droplet being completely dissipated by evaporation, the formulation by change ratio is not suitable for complete dissipation. This formulation is therefore incomplete to derive the reduction tendency of number concentration by evaporation (condensation never changes number concentration). Temporarily, we assumed that the number concentration of cloud droplets never declines unless the mean mass of cloud ($\bar{x}_c$) falls below the lower limit $\bar{x}_{c,min}$. The treatment of rain droplets is discussed in the following section.

Evaporation of rain droplets

Only in the case of rain droplets, Seifert (2008) attempted to overcome incompleteness for the reduction of number concentration in evaporation. He reformulated eq.B.39 as follows:

$$
\frac{\partial N_r}{\partial t}\Big|_{evp} \equiv \gamma_{evp} \frac{N_r}{L_r} \frac{\partial L_r}{\partial t} = \frac{\gamma_{evp}}{\bar{x}} 2\pi G_{lv} S_w N_r D_r(\bar{x}_r) \bar{F}_{vf,l}(\bar{x}_r)
\tag{B.40}
$$

Here, evaporation parameter γ_{evp} means the evaporation efficiency of number concentration towards mean mass $\bar{x}_r$. According to Seifert (2008), γ_{evp} and $\mu_{m,r}$ are parameterized as follows:

$$
\gamma_{evp} = \frac{D_{eq}}{D(\bar{x}_r)} exp(-0.2\mu_{m,r})
\tag{B.41}
$$

$$
\mu_{m,r} = \begin{cases} 6tauh[c_{evp,1}(D(\bar{x}_r) - D_{eq})^2] + 1 & (D(\bar{x}_r) \leq D_{eq}) \\ 30tauh[c_{evp,2}(D(\bar{x}_r) - D_{eq})^2] + 1 & (D(\bar{x}_r) \leq D_{eq}) \end{cases}
\tag{B.42}
$$

where $D_{eq} = 1.1 \times 10^{-3} m$ is the equilibrium diameter in breakup-coalescence processes, and $c_{evp,1}$ and $c_{evp,2}$ are set to 4000 m^{-1} and 1000 m^{-1}, respectively. In this study, we apply eq.B.39 for mass and eq.B.40 with $\gamma_{evp} = 1$ for number concentration as a default setting (refer to SB06-run).

Deposition/sublimation for solid water

Theoretical formulation of deposition or sublimation is the same as that of condensation or evaporation, except for the definition of surface area. The shape of ice particles is not spherical and varies widely, as shown in section 2.1.2. Vapor and thermal transfer over the particle surface are therefore expressed by the analogy between the diffusion equation and equations in electrostatics (Pruppacher and Klett, 1997). Replacing diameter D_{js} by capacitance $C_{js} \equiv Djs/c_{js}$, we can derive the growth equation of a single particle, as follows:

$$
\frac{dx_{js}}{dt}\Big|_{dep,sbl} = 4\pi C_{js} G_{sv}(T,p) F_{vf}(x_{js}) S_i, \quad (js = i, s, g)
\tag{B.43}
$$

$$
G_{sv} = \Big[\frac{R_v T}{p_{si}(T) D_v} + \frac{L_{s,0}}{K_T T}\Big(\frac{L_{s0}}{R_v T} - 1\Big)\Big]^{-1}
\tag{B.44}
$$

Here $C_{js} = D_{js}/2$ for sphere, $C_{js} = D_{js}/\pi$ for circular plate, and capacitance of other typical shapes (such as oblate spheroid crystals and columnar crystals) are expressed by:

$$
C_{js} = \frac{D_{js}\varepsilon}{2sin^{-1}\varepsilon}, \quad \varepsilon \equiv \Big(1 - \frac{b^2}{a^2}\Big), \ (for \ spheroid)
\tag{B.45}
$$

$$
C_{js} = \frac{A}{ln[(a+A)/b]}, \quad A \equiv = (a^2 - b^2)^{1/2}, \ (for \ columnar)
\tag{B.46}
$$

where a is the semi-major axis and b is the semi-minor axis. For simplification, cloud, rain, snow, and graupel are assumed to be spherical, and hexagonal plate ice is assumed to be a circular plate. In the same manner as condensation (evaporation), we can derive the growth equation of arbitrary moments, as follows:

$$\frac{\partial M_{js}^k}{\partial t}\Big|_{dep,sbl} = \frac{4\pi}{c_{js}} G_{sv} S_i N_{js} D_{js}(\bar{x}_{js}) \bar{F}_{vf,k}(\bar{x}_{js}) \bar{x}_{js}^{k-1} \tag{B.47}$$

The discussion concerning the reduction term of number concentration is the same as for rain droplets. We therefore applied eq.B.47 for mass concentration of solid particles. For snow and graupel, the reduction rate of number concentration is as follows:

$$\begin{aligned} \frac{\partial N_{js}^k}{\partial t}\Big|_{sbl} &\equiv \frac{N_{js}}{L_{js}} \frac{\partial L_{js}}{\partial t}\Big|_{sbl} \\ &= \frac{1}{\bar{x}_{js}} \frac{4\pi}{c_{js}} G_{sv} S_i N_{js} D_{js}(\bar{x}_{js}) \bar{F}_{vf,1}(\bar{x}_{js}) (js = s, g) \end{aligned} \tag{B.48}$$

This formulation corresponds to $\gamma_{evp} = 1$ in the reduction term for rain droplets. This means that sublimation occurs so as not to change the mean mass of DSD ($\bar{x}_{js}$). Number concentration of ice never reduces in sublimation unless the mean mass of ice ($\bar{x}_i$) falls below the lower limit. The formulations of the reduction rate for the number concentration of ice particles are somewhat temporary and will be improved based on insights drawn from the results of microphysics bin schemes and observations in future.

Accurate integration method to solve condensation/evaporation and deposition/sublimation

The condensation/evaporation process for cloud droplets usually requires a smaller time step than rain droplets or other particles because of its timescale. When we apply time integration with the first-ordered Euler method, the accuracies of condensation/evaporation and deposition/sublimation processes are poor unless we resolve their timescale. We initially estimate the timescale with the exact thermodynamic definition in NICAM and then formulate an accurate method to apply the condensation and evaporation processes for cloud droplets, similar to Khvorostyanov and Sassen (1998) and Morrison et al., (2005). Since the supersaturated condition is achieved by updraft of air mass, we consider a Lagrangian parcel model with constant updraft velocity and no mixing with external air mass. Basic formulation is based on the Lagrangian change rate of supersaturation ($\delta_{sw} = q_v - q_{sw}$), as follows:

$$\frac{d\delta_{sw}}{dt} = \left(\frac{dq_v}{dt} - \frac{dq_{sw}}{dt} \right) \tag{B.49}$$

Hereafter, we consider the tendency of specific humidity and saturation, specific humidity by dynamics, cloud microphysics, and radiative heating.
At first, assuming an adiabatically ascending/descending parcel with no phase change ($q_v/dt = 0$), eq.(B.49) becomes:

$$\frac{d\delta_{sw}}{dt} = -\left(\frac{\partial q_{sw}}{\partial T} \right)_p \frac{dT}{dt} - \left(\frac{\partial q_{sw}}{\partial p} \right)_T \frac{dp}{dt} \tag{B.50}$$

Here, the tendencies of temperature and pressure are described as follows:

$$\frac{dT}{dt} = \frac{1}{\rho \bar{c}_p} \frac{dp}{dt}, \quad \frac{dp}{dt} \approx -\rho g w \tag{B.51}$$

where $\bar{c}_p \equiv q_d c_{pd} + q_v c_{pv} + q_{liq} c_l + q_{sol} c_i$ is the mean specific heat at constant pressure. We can derive the dynamic component of the tendency of δ_{sw} by substituting eq. B.51 into eq.B.50, as follows:

$$\frac{d\delta_{sw}}{dt}\Big|_{DYN} = wg\left(\frac{1}{\bar{c}_p} \left(\frac{\partial q_{sw}}{\partial T} \right)_p + \rho \left(\frac{\partial q_{sw}}{\partial p} \right)_T \right) \tag{B.52}$$

Assuming an air parcel with only cooling/heating by latent heat release, eq. B.49 becomes:

$$\frac{d\delta_{sw}}{dt} = \frac{dq_v}{dt} - \left(\frac{\partial q_{sw}}{\partial T}\right)\frac{dT}{dt} \tag{B.53}$$

The tendency of temperature is caused by latent heat release with condensation/evaporation and deposition/sublimation:

$$
\begin{aligned}
\frac{dT}{dt} &= \frac{L_{v,00} + (c_{vv} - c_l)T}{\bar{c}_{va}}\frac{dq_{liq}}{dt} + \frac{L_{v,00} + L_{f,00} + (c_v - c_i)T}{\bar{c}_{va}}\frac{dq_{sol}}{dt} \\
&= \frac{L_{v,00} + (c_{vv} - c_l)T}{\bar{c}_{va}}\sum_{jl=1}^{jl_{max}}\left.\frac{dq_{jl}}{dt}\right|_{cnd,evp} \\
&+ \frac{L_{v,00} + L_{f,00} + (c_{vv} - c_i)T}{\bar{c}_{va}}\sum_{js=1}^{js_{max}}\left.\frac{dq_{js}}{dt}\right|_{dep,sbl}
\end{aligned} \tag{B.54}
$$

The tendency of specific humidity is caused by condensation/evaporation and deposition/sublimation:

$$\frac{dq_v}{dt} = -\sum_{jl=1}^{jl_{max}}\left.\frac{dq_{jl}}{dt}\right|_{cnd,evp} - \sum_{js=1}^{js_{max}}\left.\frac{dq_{js}}{dt}\right|_{dep,sbl} \tag{B.55}$$

We can then derive the cloud microphysics component of the tendency of δ_{sw} by substituting eqs.B.54 and B.55 into eq.B.53:

$$
\begin{aligned}
\left.\frac{d\delta_{sw}}{dt}\right|_{MP} &= -\left(1 + \frac{L_{v,00} + (c_{vv} - c_l)T}{\bar{c}_v}\left(\frac{\partial q_{sw}}{\partial T}\right)_p\right)\sum_{jl=1}^{jl_{max}}\left.\partial dq_{jl}dt\right|_{cnd,evp} \\
&- \left(1 + \frac{L_{v,00} + L_{f,00} + (c_{vv} - c_i)T}{\bar{c}_v}\left(\frac{\partial q_{sw}}{\partial T}\right)_p\right)\sum_{js=1}^{js_{max}}\left.\frac{dq_{js}}{dt}\right|_{dep,sbl}
\end{aligned} \tag{B.56}
$$

By replacing the source term of the mixing ratio of hydrometeors in eq.B.56 with eqs.B.39 and B.47:

$$
\begin{aligned}
\left.\frac{dq_{jl}}{dt}\right|_{cnd,evp} &= \frac{\delta_{sw}}{\tau_{cnd,jl}}, \text{ or} \\
\left.\frac{dq_{jl}}{dt}\right|_{cnd,evp} &= \frac{\delta_{si}}{\tau_{cnd,jl}} - \frac{q_{sw} - q_{si}}{\tau_{cnd,jl}}, \quad (jl = c, r) \tag{B.57}
\end{aligned}
$$

$$
\begin{aligned}
\left.\frac{dq_{js}}{dt}\right|_{de,sbl} &= \frac{\delta_{si}}{\tau_{dep,js}}, \text{ or} \\
\left.\frac{dq_{js}}{dt}\right|_{dep,sbl} &= \frac{\delta_{sw}}{\tau_{dep,js}} + \frac{q_{sw} - q_{si}}{\tau_{dep,js}}, \quad (js = i, s, g) \tag{B.58}
\end{aligned}
$$

$$\tau_{cnd,jl} \equiv \left(\frac{1}{\rho q_{sw}}2\pi G_{lv}D_{jl}(\bar{x}_{jl})N_{jl}\bar{F}_{vf,1}\right)^{-1} \tag{B.59}$$

$$\tau_{dep,js} \equiv \left(\frac{1}{\rho q_{si}}\frac{4\pi}{c_{js}}G_{sv}D_{js}(\bar{x}_{js})N_{js}\bar{F}_{vf,1}\right)^{-1} \tag{B.60}$$

We can rewrite eq.B.56 as a function of super saturation itself:

$$
\begin{aligned}
\left.\frac{\partial\delta_{sw}}{\partial t}\right|_{MP} &= -\left(\frac{a_{liq,liq}}{\tau_{cnd,c}} + \frac{a_{liq,liq}}{\tau_{cnd,r}} + \frac{a_{sol,liq}}{\tau_{dep}} + \frac{a_{sol,liq}}{\tau_{dep,s}} + \frac{a_{sol,liq}}{\tau_{dep,g}}\right)\delta_{sw} \\
&- \left(\frac{1}{\tau_{dep,i}} + \frac{1}{\tau_{dep,s}} + \frac{1}{\tau_{dep,g}}\right)(q_{sw} - q_{si})
\end{aligned} \tag{B.61}
$$

$$a_{liq,liq} \equiv 1 + \frac{L_{v00} + (c_{vv} - c_l)T}{\bar{c}_v}\left(\frac{\partial q_{sw}}{\partial T}\right)_p \tag{B.62}$$

$$a_{sol,liq} \equiv 1 + \frac{L_{v00} + L_{f00} + (c_{vv} - c_i)T}{\bar{c}_v}\left(\frac{\partial q_{sw}}{\partial T}\right)_p \tag{B.63}$$

Here, we can find that $\tau_{cnd,jl}$ and $\tau_{dep,js}$ in eq.B.61 are considered as the characteristic time scale for relaxation of the super saturation condition by condensation/evaporation and deposition/sublimation processes. The timescale of each hydrometeor is modified by coefficient $a_{liq,liq}$ or $a_{sol,liq}$, indicating the effect of latent heat release. The second term on the right hand side in eq.B.61 means the transfer of vapor from liquid droplets to solid particles. The Bergeron-Findeisen process is implicitly formulated by the difference of saturation vapor pressure between liquid and solid.

Finally, assuming an air parcel with radiative heating (cooling), eq.B.49 becomes

$$\frac{d\delta_{sw}}{dt}\Big|_{RAD} = -\left(\frac{\partial q_{sw}}{\partial T}\right)_\rho \left(\frac{dT}{dt}\right)_{RAD} \tag{B.64}$$

All the components in the Lagrangian ascending/descending parcel model are described by eqs.B.52, B.61, and B.64:

$$\frac{d\delta_{sw}}{dt} = A_{cnd} - \frac{\delta_{sw}}{\tau_{cnd}} \tag{B.65}$$

$$A_{cnd} \equiv \frac{d\delta_{sw}}{dt}\Big|_{DYN} + \frac{d\delta_{sw}}{dt}\Big|_{RAD}$$
$$- \left(\frac{1}{\tau_{dep,i}} + \frac{1}{\tau_{dep,s}} + \frac{1}{\tau_{dep,g}}\right)(q_{sw} - q_{si}) \tag{B.66}$$

$$\tau_{cnd} \equiv \left(\frac{a_{liq,liq}}{\tau_{cnd,c}} + \frac{a_{liq,liq}}{\tau_{cnd,r}} + \frac{a_{sol,liq}}{\tau_{dep,i}} + \frac{a_{sol,liq}}{\tau_{dep,s}} + \frac{a_{sol,liq}}{\tau_{dep,g}}\right)^{-1} \tag{B.67}$$

Here, we can see that A_{cnd} is a production term of super saturation and cnd is a characteristic timescale of all phase changes. From formulations of eqs.B.59 and B.60), we find that the timescale of each hydrometeor is in inverse proportion to its number concentration. Therefore, the timescale of cloud droplets is the shortest one in all hydrometeors because the typical numbers of cloud droplets are about 10,000 times more than any others. The timescales under various conditions are shown in Fig.B.7.

Assuming that time variance of the production term and the timescale in a simulation time step do not vary much within a model timestep, we can analytically solve eq.B.65:

$$\delta_{sw}(t) = A_{cnd}\tau_{cnd} + (\delta_{sw}(t_0) - A_{cnd}\tau_{cnd})exp\left(-\frac{t}{\tau_{cnd}}\right) \tag{B.68}$$

where $t = t_0 + \Delta t$ and $t_0 = 0$. Then, the condensation (evaporation) rates of cloud and rain are reformulated by substituting eq.B.68 into eq.B.39 and integrating these:

$$\frac{\Delta L_{jl}}{\Delta t}\Big|_{cnd,evp} = \rho A_{cnd}\frac{\tau_{cnd}}{\tau_{cnd,jl}}$$
$$- \rho\frac{(\delta_{sw}(t_0) - A_{cnd}\tau_{cnd})}{\Delta t}\frac{\tau_{cnd}}{\tau_{cnd,jl}}\left[exp\left(-\frac{\Delta t}{\tau_{cnd}}\right) - 1\right] \tag{B.69}$$

This semi-analytical formulation takes time variability of super saturation into condensation (evaporation) growth. It is therefore better than direct time integration with a first-order Euler method.

In the same manner, we can also derive the semi-analytical formulation for deposition (sublimation) with super saturation for solid water: (δ_{si}),

$$\delta_{si}(t) = A_{dep}\tau_{dep} + (\delta_{si}(t_0) - A_{dep}\tau_{dep})exp\left(-\frac{t}{\tau_{dep}}\right) \tag{B.70}$$

$$\frac{\Delta L_{js}}{\Delta t}\Big|_{dep,sbl} = \rho A_{dep}\frac{\tau_{dep}}{\tau_{dep,js}}$$
$$- \rho\frac{(\delta_{si}(t_0) - A_{dep}\tau_{dep})}{\Delta t}\frac{\tau_{dep}}{\tau_{dep,js}}\left[exp\left(-\frac{\Delta t}{\tau_{dep}}\right) - 1\right] \tag{B.71}$$

where:

$$A_{dep} \equiv \left.\frac{d\delta_{si}}{dt}\right|_{DYN} + \left.\frac{d\delta_{si}}{dt}\right|_{RAD}$$
$$+ \left(\frac{1}{\tau_{cnd,c}} + \frac{1}{\tau_{cnd,r}}\right)(q_{sw} - q_{si}) \tag{B.72}$$

$$\tau_{dep} \equiv \left(\frac{a_{liq,sol}}{\tau_{cnd,c}} + \frac{a_{liq,sol}}{\tau_{cnd,r}} + \frac{a_{sol,sol}}{\tau_{dep,i}} + \frac{a_{sol,sol}}{\tau_{dep,s}} + \frac{a_{sol,sol}}{\tau_{dep,g}}\right)^{-1} \tag{B.73}$$

$$a_{liq,sol} \equiv 1 + \frac{L_{v00} + (c_{vv} - c_l)T}{\bar{c}_v}\left(\frac{\partial q_{si}}{\partial T}\right)_p$$

$$a_{sol,sol} \equiv 1 + \frac{L_{v00} + L_{f00} + (c_{vv} - c_i)T}{\bar{c}_v}\left(\frac{\partial q_{si}}{\partial T}\right)_p$$

$$\left.\frac{d\delta_{si}}{dt}\right|_{DYN} = wg\left(\frac{1}{\bar{c}_p}\left(\frac{\partial q_{si}}{\partial T}\right)_p + \rho\left(\frac{\partial q_{si}}{\partial p}\right)_T\right)$$

$$\left.\frac{d\delta_{si}}{dt}\right|_{RAD} = -\left(\frac{\partial q_{si}}{\partial T}\right)_\rho\left(\frac{dT}{dt}\right)_{RAD}$$

Finally, we applied eqs.B.69 and B.71 for prediction of mass concentration and eqs.B.40 and B.48 for prediction of number concentrations of rain, snow, and graupel. Number concentrations of cloud and ice are assumed not to change by evaporation and sublimation.

Nucleation of cloud droplets

Seifert and Beheng (2006) applied a traditional empirical formulation as an aerosol activation spectrum, as follows:

$$N_c(S_{w,100}) = C_{ccn}S_{w,100}^{\kappa_{ccn}} \tag{B.74}$$

where the super saturation ratio $S_{w,100}$ is in   . They use $C_{ccn} = 1.26 \times 10^9 m^{-3}$ and $\kappa_{ccn} = 0.308$ in continental conditions and $C_{ccn} = 1.0 \times 10^8 m^{-3}$ and $\kappa_{ccn} = 0.462$ in maritime conditions. Further, Seifert and Beheng (2006) transformed eq.B.74 into a tendency formulation by time differentiation of the activation spectrum:

$$\frac{\partial N_c}{\partial t} = \begin{cases} C_{ccn}\kappa_{ccn}S_{w,100}^{\kappa_{ccn}-1}\frac{\partial S_{w,100}}{\partial z}w \\ (S_{w,100} > 0, \ w\frac{\partial S_{w,100}}{\partial z} > 0, \ and \ S_{w,100} < 1.1) \\ 0, \ (else) \end{cases}$$

$$\left.\frac{\partial L_c}{\partial t}\right|_{nuc} = x_{c,nuc}\left.\frac{\partial N_c}{\partial t}\right|_{nuc} \tag{B.75}$$

where $x_{c,nuc} = 10^{-12}kg$ is an arbitrary mass of nucleated droplets. Because the aerosol activity spectrum is a function of supersaturation and is unbounded by total aerosol number concentration, we chose an upper limit of activated aerosols as $1.5 \times C_{ccn}$, as similarly chosen by SB06. The maximum activated aerosol number concentration is 1.5 times the activated aerosol number concentration at $ssw = 1 \ ^o/_o$. It should be noted that this formulation depends on the grid value of super saturation ratio, vertical velocity, and vertical derivation of the super saturation ratio. Since super saturation significantly varies with tens of meters above the cloud base (see Fig.B.9), accurate prediction of super saturation and its vertical derivation is quite difficult. In this study, we applied a traditional nucleation scheme (Twomey, 1959; Rogers and Yau, 1989) following Morrison et al. (2005):

$$N_{c,nuc}(w_{eff}) = 0.88C_{ccn}^{2/(\kappa_{ccn}+2)}(0.07w_{eff}^{3/2})^{\kappa_{ccn}/(\kappa_{ccn}+2)} \tag{B.76}$$

$$w_{eff} \equiv w + w_{TB} - \frac{\bar{c}_p}{g}\left(\frac{dT}{dt}\right)_{RAD} \tag{B.77}$$

where w_{eff} is effective vertical velocity for nucleation and w_{TB} is the sub-grid variability of terminal velocity. This is an analytical formulation of maximum number concentration around the cloud base for the Twomey equation, with aerosol activated spectrum by eq.B.74 (see Fig.B.6). Using this scheme, we do not have to resolve the vertical variability of super saturation around the cloud base. Furthermore, applying sub-grid turbulence effects on vertical velocity reduces under-estimation of nucleated cloud number concentration caused by low

horizontal resolution (Ghan et al., 1997; Lohmann, 2002; Morrison and Pinto, 2005). In this study, implementation of the sub-grid turbulence effect follows Lohmann (2002):

$$w_{TB} = c_{TB}\left(\frac{2}{3}TKE\right)^{1/2} \tag{B.78}$$

$$\bar{N}_{c,nucl} = 0.1 \times N_{c,nuc}(w_{eff})^{1.27} \tag{B.79}$$

where $c_{TB} = 1$ is used in this study, $\bar{N}_{c,nuc}$ cm^{-3} is a grid-averaged nucleated cloud number concentration, and $N_{c,nuc}(w_{eff})cm^{-3}$ is maximum cloud number concentration in turbulent air. By substituting eqs.B.76, B.77, and B.78 into eq.B.79, the tendency of cloud number concentration is calculated as follows:

$$\left.\frac{\partial N_c}{\partial t}\right|_{nucl} = \begin{cases} \frac{N_{c,nu}(w_{eff})-N_c}{\Delta t}, & (S_w > 0, \ \bar{N}_{c,nuc} > N_c \ and \ at \ cloud \ base) \\ 0, & (else) \end{cases} \tag{B.80}$$

$$\left.\frac{\partial L_c}{\partial t}\right|_{nuc} = min\left(x_{c,min}\left.\frac{\partial N_c}{\partial t}\right|_{nuc}, \frac{\delta_{sw}}{\Delta t}\right) \tag{B.81}$$

Since nucleation is usually limited around the cloud base within several tens of meters (see Fig.B.9), we define the cloud base layer (k_{cbase}) where the nucleation scheme works as follows:

$$1.5 \times C_{ccn} > \bar{N}_{c,nu}(k_{cbase}) > 0, \ and \ \bar{N}_{c,nu}(k_{cbase} - 1) < 10^6 \tag{B.82}$$

In addition, we prepare the option (NO-TB) to switch off the effect of turbulence by substituting eqs.B.76 and B.77 with $w_{TB} = 0$ into eq.B.80. However, there remain some problems to be solved in future:
1.Definition of cloud base is empirical and arbitrary.
2.Implementation of sub-grid scale is empirical and c_{TB} is a kind of tuning parameter. In particular, the TKE approach only considers isotropic eddies. Sub-grid should be expressed as sub-grid cloud dynamics.
3.Formulation of eq.B.79 does not converge with the NO-TB option when TKE = 0.
We need to investigate the above problems by using a large eddy simulation (LES) cloud model.

Nucleation of cloud ice

This study employed two simple ice nucleation schemes, which do not require the properties of ice nuclei. One is the depositional and condensational freezing nucleation scheme parameterized by Meyers et al. (1992):

$$N_{IN} = 10^3 exp(-0.639 + 12.96S_{sol})$$

where N_{IN} is nucleated ice nuclei and S_{sol} is supersaturation for solid water. While this scheme is widely used in CRMs (e.g., Walko et al. 1995; Khain et al., 2000; Seifert and Beheng, 2006), it is not acceptable for temperature conditions < -20 °C or supersaturation > 0.25, where observational data were not available in their study. For simulating cirrus clouds around the tropopause, application of this scheme to CRMs may cause significant error. Phillips et al. (2007) proposed an alternative scheme to modify Meyers's scheme by fitting observational data at temperatures between -30 °C and -80 °C obtained by Demott et al. (2003):

$$N_{IN} = 10^3 exp[0.3 \times 12.96(S_i - 0.1)] \tag{B.83}$$

In this study, the nucleation rate is formulated by newly nucleated ice nuclei with supersaturation tendency in the same manner as Murakami (1990):

$$\frac{\Delta N_i}{\Delta t} = \begin{cases} \frac{\partial N_{IN}}{\partial S_{sol}}\frac{\partial S_{sol}}{\partial t}, & (S_{sol} > 0 \ and \ \frac{\partial S_{sol}}{\partial t} > 0) \\ 0, & (else) \end{cases} \tag{B.84}$$

$$\frac{\partial S_{sol}}{\partial t} \approx \left[\frac{\partial S_{sol}}{\partial z}w + \left(\frac{\partial S_{sol}}{\partial T}\right)\left(\frac{\partial T}{\partial t}\right)_{RAD}\right]$$

$$\left.\frac{\Delta L_i}{\Delta t}\right|_{nuc} = \left.\frac{\Delta N_i}{\Delta t}\right|_{nuc} x_{IN} \tag{B.85}$$

where $x_{IN} = 10^{-12} kg$ is an arbitrary parameter for a nucleated ice nuclei mass. Here, we assume the change of supersaturation comes from the vertical motion of air masses and radiative cooling. Meyers's scheme better reflects the number concentration of cloud ice than Phillips's scheme, and the divergence becomes larger as supersaturation increases. This difference stems from the sampled air masses used in observational data that the schemes referred to and from implicit dependencies of the schemes on temperature and aerosol species. It is expected that Phillips's scheme is appropriate for simulation of mid-latitude cirrus clouds because it is based on air masses sampled in the free troposphere in mid-latitudes, while Meyers's scheme is based on air masses sampled in the atmospheric boundary layer, which is rich in ice nuclei.

Freezing

The freezing process involves two types of mechanisms. One is homogenous freezing, i.e., freezing of supercooled water droplets without other agents. Another is heterogeneous freezing, i.e., freezing of supercooled water droplets with insoluble parts of aerosols dissolved in cloud droplets. We apply the same parameterizations for both homogeneous and heterogeneous freezing as Seifert and Beheng (2006a). Cotton and Field (2002) parameterized the homogeneous freezing rate for a single droplet by fitting to the theoretical estimation of Jeffery and Austin (1997). We apply their parameterization as per Seifert and Beheng (2006a):

$$\frac{1}{f_c(x)} \frac{\partial f_c(x)}{\partial t}\Big|_{hom} = -x J_{hom}(T_c) \tag{B.86}$$

where J_{hom} is a homogeneous freezing rate ($kg^{-1}s^{-1}$) and T_c is centigrade temperature. J_{hom} is formulated as a function of temperature, as follows:

$$log_{10}(10^{-3} J_{hom}) = \begin{cases} 25.63 - 243.4 - 14.75 T_c - 0.307 T_c^2, & (-65^o C > T_c) \\ -0.00287 T_c^3 - 0.0000102 T_c^4, & (-65^o C \le T_c < -30^o C) \\ -7.63 - 2.996(T_c + 30), & (-30^o C < T_c) \end{cases}$$

Based on the equation for a single droplet, we can derive the equation for moments by integrating eq.B.86, as follows:

$$\frac{\partial N_c}{\partial t}\Big|_{hom} = -L_c J_{hom} = -N_c \bar{x}_c J_{hom} \tag{B.87}$$

$$\frac{\partial L_c}{\partial t}\Big|_{hom} = -Z_c J_{hom} = -\frac{\Gamma\left(\frac{\nu_c+3}{\mu_c}\right)\Gamma\left(\frac{\nu_c+1}{\mu_c}\right)}{\Gamma\left(\frac{\nu_c+2}{\mu_c}\right)^2} L_c \bar{x}_c J_{hom} \tag{B.88}$$

Here, we mention that eqs.B.87 and B.88 are expressed via filtered $\bar{x}_c$ in order to avoid artificial values of the prognostic variables. Homogeneous freezing for rain is not considered because it is negligible compared with heterogeneous freezing, given the large size. Although Cotton and Field (2002) also considered freezing point depression due to soluble aerosols, we do not consider the effect because Seiki and Nakajima (2014)'s approach is not yet coupled with aerosol transport models. Heterogeneous freezing is based on Bigg's (1953) empirical formulation, which is widely used in CRMs:

$$\frac{1}{f(x)} \frac{\partial f(x)}{\partial t} = -x J_{het}(T_c) \tag{B.89}$$

where J_{het} is the heterogeneous freezing rate. J_{het} is formulated as a function of temperature, as follows:

$$J_{het} = A_{het}(exp(-B_{het} T_c) - 1) \tag{B.90}$$

where $A_{het} = 0.2 kg^{-1}s^{-1}$ and $B_{het} = 0.65 K^{-1}$ are empirically determined parameters. Similar to homogeneous freezing, we can derive the equation for moments, as follows:

$$\frac{\partial N_{il}}{\partial t}\Big|_{het} = -N_{il} \bar{x}_{il} J_{het} \quad (il = c, r) sn126) \tag{B.91}$$

$$\frac{\partial L_{il}}{\partial t}\Big|_{het} = -\frac{\Gamma\left(\frac{\nu_{il}+3}{\mu_{il}}\right)\Gamma\left(\frac{\nu_{il}+1}{\mu_{il}}\right)}{\Gamma\left(\frac{\nu_{il}L2}{\mu_{il}}\right)^2} L_{il} \bar{x}_{il} J_{het} \quad (il = c, r) \tag{B.92}$$

117

Although heterogeneous freezing should also be formulated as a function of aerosol concentration, here we apply a simple formulation because our model is not yet coupled with an aerosol transport model.

These parameterizations thus do not include aerosol information and are considered to assume background aerosols. The validity of parameterization was demonstrated by Khain et al. (2001). Nevertheless their model also applied the same simple freezing parameterizations, representing observational features of supercooled liquid water as per Rosenfeld and Woodley (2000). Both freezing rates are shown in Fig. B.10. Heterogeneous freezing is dominant at temperatures > -35 °C. At these temperatures, supercooled liquid water is mixed with ice particles. In contrast, the homogeneous freezing rate suddenly increases < -35 °C. Liquid water droplets have hardly been observed < -40 °C (Rosenfeld and Woodley, 2000). This can be represented by using the parameterization.

Melting

The melting process is the same as that of Seifert and Beheng (2006a), based on Pruppacher and Klett (1997). Theoretical treatment of this process is similar to that of the condensation process. The differences are:

1. Time scale of evaporation of a single particle is replaced by that of fusion of a single particle.
2. Vaporization of melted particle is considered in a balance equation of vapor and thermal diffusion.

As a result, the melting rate of a single ice particle is described as follows:

$$
\begin{aligned}
\frac{dx_{js}}{dt}\Big|_{mlt} = & - \frac{2\pi D_{js}}{L_{f0}} \Big[K_T(T - T_0)\frac{D_T}{D_v}F_{vf}(x_{js}) \\
& + \frac{D_v L_{v0}}{R_v}\Big(\frac{p_v}{T} - \frac{p_{sw}(T_0)}{T}\Big)F_{vf}(x_{js}) \Big] \quad (js = i, s, g) \qquad \text{(B.93)}
\end{aligned}
$$

where D_T is diffusivity of heat and $T_0 = 273.15K$ is melting point. The growth rate of moments can be formulated by using a melting time scale τ_{mlt}, defined as follows:

$$
\begin{aligned}
\tau_{mlt} & \equiv \frac{x_{js}}{\left(\frac{dx_{js}}{dt}\right)_{mlt}} \qquad\qquad\qquad\qquad\qquad\qquad \text{(B.94)} \\
\frac{\partial M_{js}^k}{\partial t}\Big|_{mlt} & = -\int_0^\infty \frac{x^k f_{js}(x)}{\tau_{mlt}}dx \\
& = -\frac{2\pi}{L_{f0}}\Big[\frac{K_T D_T}{D_v}(T - T_0) + \frac{D_v L_{v0}}{R_v}\Big(\frac{p_v}{T} - \frac{p_{sw}(T_0)}{T_0}\Big) \Big] \\
& \times \; N_{js}D_{js}(\bar{x}_{js})x_{js}^{n-1}\bar{F}_{vf,js} \qquad\qquad\qquad \text{(B.95)}
\end{aligned}
$$

We mention that this scheme allows the existence of ice particles over the melting point $(T > 273.15K)$ since the melting time scale of large particles can be longer than a simulation time step. Actually, ice particles are transitionally converted into liquid droplets and the type of hydrometeor is not changed in the transition. However, here we assume that ice water mass is converted into liquid water mass over a certain melting time scale and the liquid water component is categorized as other hydrometeors. Here, graupel and snow are converted into rain, and ice is converted into cloud. This formulation may cause artificial production of cloud or rain in melting. Validation experiments and impact assessment are therefore necessary in future.

B.2.2 Collection process

The collection processes are the same as Seifert and Beheng (2001), Seifert and Beheng (2006a), and Seifert (2008). The collection processes among hydrometeors are summarized in Table B.5. In this section, the formulations of the collection processes, auto-conversion, accretion, aggregation, riming, and related processes are described.

Self-collection, auto-conversion, and accretion

With a few assumptions and a little algebra, Seifert and Beheng (2001) derived the analytical formulations of self-collection, auto-conversion, and accretion processes, as follows:

Table B.5: Hydrometeors that result from binary collision. Collecting hydrometeors are written in the 1st row and collected hydrometeors are written in the 1st column.

	cloud water	rain	cloud ice	snow	graupel
cloud water	rain	-	-	-	-
rain	rain	rain	rain($T > 273K$), graupel($T < 273K$)	rain($T > 273K$), graupel($T < 273K$)	rain($T > 273K$)
cloud ice	cloud ice	-	snow	-	-
snow	snow	-	-	snow	-
graupel	graupel	graupel($T < 273K$)	graupel	graupel	-

$$\frac{\partial N_c}{\partial t}\Big|_{aut+sle} = -k_{cc}\frac{(\nu_c+2)}{(\nu_c+1)}\frac{\rho_0}{\rho}L_c^2 \tag{B.96}$$

$$\frac{\partial L_c}{\partial t}\Big|_{aut} = -\frac{k_{cc}}{20x^*}\frac{(\nu_c+2)(\nu_c+4)}{(\nu_c+1)^2}\frac{\rho_0}{\rho}L_c^2 x_c^2 \tag{B.97}$$

$$\frac{\partial N_c}{\partial t}\Big|_{aut} = \frac{2}{x^*}\frac{\partial L_c}{\partial t}\Big|_{aut} \tag{B.98}$$

$$\frac{\partial N_r}{\partial t}\Big|_{aut} = -\frac{1}{2}\frac{\partial N_c}{\partial t}\Big|_{aut} = -\frac{1}{x^*}\frac{\partial L_c}{\partial t}\Big|_{aut} \tag{B.99}$$

$$\frac{\partial N_c}{\partial t}\Big|_{acc} = -k_{cr}N_c L_r \big(\frac{\rho_0}{\rho}\big)^{1/2} \tag{B.100}$$

$$\frac{\partial L_c}{\partial t}\Big|_{acc} = -k_{cr}L_c L_r \big(\frac{\rho_0}{\rho}\big)^{1/2} \tag{B.101}$$

$$\frac{\partial N_r}{\partial t}\Big|_{slc} = -k_{rr}L_r L_r \big(\frac{\rho_0}{\rho}\big)^{1/2} \tag{B.102}$$

with $k_{rr} = 4.33 m^3 kg^{-1} s^{-1}$, and where density factors are introduced by Seifert and Beheng (2006a) in order to correct the effect of terminal velocity on collision efficiency. In addition to the analytical derivation, Seifert and Beheng (2001) made corrections depending on the development stage by using the dimensionless internal time scale. Since moment bulk methods cannot represent complicated changes of high-order moments, corrections are necessary as DSD undergoes evolution by collection processes. First, the auto-conversion rate is represented by τ by substituting eq.**??** with eq.B.97:

$$\frac{\partial \tau}{\partial t}\Big|_{aut} = \frac{k_{cc}}{20x^*}\frac{(\nu_c+2)(\nu_c+4)}{(\nu_c+1)^2}\frac{\rho_0}{\rho}x_c^2 L(1-\tau^2) \tag{B.103}$$

The assumptions used in the derivation of eq.B.103 are valid for the initial stage of collisional growth. Additional collection by a universal function ϕ_{aut} was therefore introduced by Seifert and Beheng (2001), as follows:

$$\frac{\partial \tau}{\partial t}\Big|_{aut} = \frac{k_{cc}}{20x^*}\frac{(\nu_c+2)(\nu_c+4)}{(\nu_c+1)^2}\frac{\rho_0}{\rho}x_c^2 L_c^2 x_c^2 \big[(1-\tau^2) + \phi_{aut}(\tau)\big] \tag{B.104}$$

Similarly, the correction for the accretion rate is also made by a universal function ϕ_{acc}:

$$\frac{\partial \tau}{\partial t}\Big|_{acc} = k_{cr}L\big(\frac{\rho_0}{\rho}\big)^{1/2}(1-\tau)\tau\phi_{acc}(\tau) \tag{B.105}$$

In contrast to the correction for the auto-conversion rate, the assumptions used in the derivation of the accretion rate are valid for the mature stage of collisional growth. A correction function is therefore multiplied so that ϕ_{aut} becomes zero for the beginning of collisional growth and one for the mature stage of collisional growth. Here, it is recognized that the growth rate of the dimensional internal time scale is proportional to LWC in eqs.B.104 and B.105. The parameterizations developed by Seifert and Beheng (2001) therefore satisfy the similarity included in the SCE. Finally, the universal functions are derived by fitting to results by a bin cloud microphysics model:

$$\phi_{aut}(\tau) = 400\tau^{0.7}(1-\tau^{0.7})^3 \tag{B.106}$$

$$\phi_{acc}(\tau) = \big(\frac{\tau}{\tau + 5 \times 10^{-5}}\big)^4 \tag{B.107}$$

These functions are shown in Fig.B.9.

Here, we mention that the fitting curves of the universal functions highly depend on calculation by a bin cloud microphysics model. In fact, the functions proposed by Seifert and Beheng (2006a) were modified from the original functions by Seifert and Beheng (2001), with progress in the estimation of the collection kernel. We will have to update the parameterizations when more sophisticated collection kernels than the one used by Seifert and Beheng (2006a) become available.

Break-up

Large rain droplets are not always stable in the collision process. It was observed that large rain droplets could break up into many small droplets after the collision (Low and Lists, 1982). Collisional break-up sustains mean droplet size so as not to grow extremely large and cause strong precipitation. As discussed by Hu and Srivastava (1995), the system of collision, coalescence, and break-up reaches the equilibrium condition between coalescence and break-up after a sufficiently long time. Consequently the DSD form of rain is led to the self-similar equilibrium DSD with equilibrium mean diameter $\bar{D}_{eq}$. Seifert and Beheng (2006a) simply parameterized the break-up process as a relaxation of DSD with mean diameter $> \bar{D}_{eq}$ to the self-similar equilibrium DSD.

$$\frac{\partial N_r}{\partial t}\Big|_{brk} = -\big[\phi_{brk}(\Delta \bar{D}_r) + 1\big]\frac{\partial N_r}{\partial t}\Big|_{slc} \tag{B.108}$$

where ϕ_{brk} is a universal function of break-up, and $\Delta \bar{D}_r \equiv \bar{D}_r - \bar{D}_{eq}$, $\bar{D}_r$ is the mean volume diameter of rain, with $\bar{D}_{eq} = 1.1mm$ according to Seifert (2008). The universal function was derived by fitting to the results by a bin cloud microphysics model based on (Seifert et al. 2005), formulated as follows:

$$\phi_{brk}(\Delta \bar{D}_r) = \begin{cases} exp(\kappa_{brk}\Delta \bar{D}_r) - 1, & (\bar{D}_r > \bar{D}_{eq}) \\ k_{brk}\Delta \bar{D}_r, & (\bar{D}_{eq} \geq \bar{D}_r > 0.35 \times 10^{-3}m) \\ -1, & (0.35 \times 10^{-3} > \bar{D}_r) \end{cases} \tag{B.109}$$

with $\kappa_{brk} = 2.3 \times 10^3 m^{-1}$, and $k_{brk} = 1000 m^{-1}$. For mean volume diameter $< 0.35 \times 10^{-3}m$, break-up is neglected.

Mixed-phase collection

In the previous sections, collection processes are limited for warm clouds. In this section, we describe the collection processes for mixed phase clouds. In contrast to warm clouds, there exist many kinds of particles in cold clouds, as discussed in section 2.1. Since the variety of shapes and their coexistence conditions differ case by case, there are no systematized theories, observations, and experiments for mixed phase collection processes. Seifert and Beheng (2006a) therefore proposed a general formulation of collisional interactions among hydrometeors starting from simplification of the SCE. Due to the variety of hydrometeor types, the patterns of interaction are categorized into the following five cases.

1.A particle of hydrometeor " a " collects " b " and then the collecting particle " a " grows. This pattern corresponds to the collision between ice and cloud (ic), snow and cloud (sc), graupel and cloud (gc), snow and ice (si), graupel and rain (gr), and graupel and snow (gs).

2.A particle of hydrometeor " a " collects " b " and then another particle " c " is produced. This pattern corresponds to the collision between rain and ice (ri), and rain and snow (rs).

3.A particle of hydrometeor " a " collects " a " and another particle " b " is produced. This pattern corresponds to the collision between ice and ice (ii).

4.A particle of hydrometeor " a " collects " a " and then the collecting particle " a " grows. This pattern corresponds to the collision between snow and snow (ss).

In the following sections, we introduce the derivation of mixed phase collection corresponding to the five cases.

Collision case 1: a+b → a

In contrast to the SCE for warm cloud, the production and reduction terms are slightly different in binary collision between two types of hydrometeors. The reduction term of the hydrometeor " b " and the production term of the hydrometeor " a " are described as follows:

$$\frac{\partial f_b(y)}{\partial t}\bigg|_{col,ab} = -\int_0^\infty f_b(y)f_a(x)K_{ab}(x,y)dx \tag{B.110}$$

$$\frac{\partial f_b(y)}{\partial t}\bigg|_{col.ab} = \int_0^\infty f_a(x-y)f_b(x)K_{ab}(x-y,y)dx$$
$$- \int_0^\infty f_a(x)f_b(y)K_{ab}(x,y)dy \tag{B.111}$$

Here, the formulation of the collection kernel is often described by the swept volume of large particle, as follows:

$$K_{ab}(x,y) \equiv E_{ab}(x,y)\frac{\pi}{4}\big[D_a(x)+D_b(y)\big]^2\big[v_{t,a}(x)-v_{t,b}(y)\big] \tag{B.112}$$

where E_{ab} is collection efficiency, and D_i and $v_{t,i}$ are diameter and terminal velocity respectively. We can derive the growth rate of the kth moments by integrating eqs.B.110 and B.111:

$$\frac{\partial M_b^k}{\partial t}\bigg|_{col,ab} = \frac{\pi}{4}\int_0^\infty\int_0^\infty f_b(y)f_a(x)\big[D_a(x)+D_b(y)\big]^2$$
$$\times \big|v_{t,a}(x)-v_{t,b}(y)\big|E_{ab}(x,y)y^k dxdy \tag{B.113}$$

$$\frac{\partial M_a^k}{\partial t}\bigg|_{col,ab} = \frac{\pi}{4}\int_0^\infty\int_0^\infty f_a(x)f_b(y)\big[D_a(x)+D_b(y)\big]^2$$
$$\times \big|v_{t,a}(x)-v_{t,b}(y)\big|E_{ab}(x,y)\big[(x+y)^k-x^k\big]dxdy \tag{B.114}$$

Here, the difference of the terminal velocities and the collection efficiency in the integrand make analytical integration of eqs.B.113 and B.114 impossible. In the past, many researchers have tried to express integration by approximation. Seifert and Beheng (2006a) achieved integration by using the approximation proposed by Wisner et al. (1972), with some improvements. Hereafter, we only demonstrate the equations for the 0th moment N and the 1st moment L.

$$\frac{\partial L_b}{\partial t}\bigg|_{col,ab} \cong -\frac{\pi}{4}\bar{E}_{ab}\Delta\bar{v}_{t,ab}^1$$
$$\times \int_0^\infty\int_0^\infty f_a(x)f_b(y)\big[D_a(x)+D_b(y)\big]^2ydxdy \tag{B.115}$$

$$\frac{\partial L_a}{\partial t}\bigg|_{col,ab} \cong \frac{\pi}{4}\bar{E}_{ab}\Delta\bar{v}_{t,ab}^1\int_0^\infty\int_0^\infty f_a(x)f_b(y)\big[D_a(x)+D_b(y)\big]^2ydxdy$$
$$= -\frac{\partial L_b}{\partial t} \tag{B.116}$$

$$\frac{\partial N_b}{\partial t}\bigg|_{col,ab} \cong -\frac{\pi}{4}\bar{E}_{ab}\Delta\bar{v}_{t,ab}^0\int_0^\infty$$
$$\times \int_0^\infty f_a(x)f_b(y)\big[D_a(x)+D_b(y)\big]^2dxdy \tag{B.117}$$

$$\frac{\partial N_a}{\partial t}\bigg|_{col,ab} = 0 \tag{B.118}$$

where $\bar{E}_{ab}$ is the mean collection efficiency and $\Delta\bar{v}_{t,ab}^k$ is a characteristic velocity difference. Thus, the integrands are transformed so as to be integrated analytically and the problems result in the evaluation of $\bar{E}_{ab}$ and $\Delta\bar{v}_{t,ab}^k$. Some cloud microphysics schemes evaluate $\Delta\bar{v}_{t,ab}^k$ as the approximation proposed by Wisner (1972):

$$\Delta\bar{v}_{t,ab}^k = \big|\bar{v}_{M_a^k}(\bar{x}_a)-\bar{v}_{M_b^k}(\bar{y}_b)\big| \tag{B.119}$$

The characteristic velocity difference is simply approximated by the difference between mass weighted mean terminal velocity of the hydrometeors. This is equivalent to the physical assumption that all particles are falling with the same terminal velocity equal to the mass weighted mean terminal velocity. However, as pointed out by Seifert and Beheng (2006a), the

formulation underestimates the term for similar mass weighted mean terminal velocities, even though larger particles preferentially collect smaller particles due to their different terminal velocities. Seifert and Beheng (2006a) applied an alternate approximation in order to avoid the abovementioned problem, as follows:

$$\Delta \bar{v}_{t,ab}^k = \left[\frac{\int_0^\infty \int_0^\infty v_{t,a}(x) - v_{t,b}(y)^2 D_a^2 D_b^2 f_a(x) f_b(y) y^k dx dy}{\int_0^\infty \int_0^\infty D_a^2 D_b^2 f_a(x) f_b(y) y^k dx dy} \right]^{1/2} \tag{B.120}$$

The integrand can be integrated straightforwardly assuming diameter and terminal velocity follow power laws given in section 2.1. Here, we apply the equivalent projected area diameter, in contrast to the maximum dimension applied by Seifert and Beheng (2006a):

$$D = D_C(x) = \left(\frac{4}{\pi} A\right)^{1/2} = a_C x^{b_C} \tag{B.121}$$

$$a_C = \left(\frac{4}{\pi} a_{ax}\right)^{1/2}, \quad b_C = \frac{b_{ax}}{2}$$

Since diameter is used in the calculation of collisional cross section, maximum dimension overestimates collisional cross section for needle or column-like crystals. First, the denominator in eq.B.120 is transformed as follows:

$$\int_0^\infty \int_0^\infty D_{C,a}^2 D_{C,b}^2 f_a(x) f_b(y) y^k dx dy$$

$$= a_{C_a}^2 a_{C_b}^2 M_a^{2b_{C,a}} M_b^{2b_{C,b}+k}$$

$$= D_{C,a}^2(\bar{x}) D_{C,b}^2(\bar{y}) \bar{y}^k$$

$$\times \frac{\Gamma\left(\frac{2b_{C,a}+\nu_a+1}{\mu_a}\right)}{\Gamma\left(\frac{\nu_a+1}{\mu_a}\right)} \frac{\Gamma\left(\frac{2b_{C,b}+k+\nu_a+1}{\mu_a}\right)}{\Gamma\left(\frac{\nu_a+1}{\mu_a}\right)}$$

$$\times \left[\frac{\Gamma\left(\frac{\nu_a+1}{\mu_a}\right)}{\Gamma\left(\frac{\nu_a+1}{\mu_a}\right)}\right]^{2b_{C,a}} \left[\frac{\Gamma\left(\frac{\nu_b+1}{\mu_b}\right)}{\Gamma\left(\frac{\nu_b+1}{\mu_b}\right)}\right]^{2b_{C,b}+k} \tag{B.122}$$

Second, the numerator in eq.B.120 is transformed as follows:

$$\int_0^\infty \int_0^\infty \left[v_{t,a}(x) - v_{t,b}(y)\right]^2 D_{C,b}^2 D_{C,b}^2 f_a(x) f_b(y) y^k dx dy$$

$$= a_{C_a}^2 a_{C_b}^2 [a_{v,a}^2 M_a^{2b_{C,a}+2b_{v,a}}$$

$$+ M_b^{2b_{C,b}+k} - 2a_{v,a} a_{v,b} M_a^{2b_{C,a}+b_{v,a}} M_b^{2b_{C,b}+b_{v,b}+k} + a_{v,b}^2 M_a^{2b_{C,a}} M_b^{2b_{C,b}+2b_{v,b}+k}]$$

$$= D_{C,a}^2(\bar{x}) D_{C,b}^2(\bar{y}) \bar{y}^k$$

$$+ v_{t,a}^2(\bar{x}) \frac{\Gamma\left(\frac{2b_{C,a}+2b_{v,a}+\nu_a+1}{\mu_a}\right)}{\Gamma\left(\frac{\nu_a+1}{\mu_a}\right)} \frac{\Gamma\left(\frac{2b_{C,b}+k+\nu_a+1}{\mu_a}\right)}{\Gamma\left(\frac{\nu_a+1}{\mu_a}\right)} \left[\frac{\Gamma\left(\frac{\nu_a+1}{\mu_a}\right)}{\Gamma\left(\frac{\nu_a+2}{\mu_a}\right)}\right]^{2b_{C,a}+2b_{v,a}} \left[\frac{\Gamma\left(\frac{\nu_b+1}{\mu_b}\right)}{\Gamma\left(\frac{\nu_b+2}{\mu_b}\right)}\right]^{2b_{C,a}+k}$$

$$= 2v_{t,a}(\bar{x}) v_{t,b}(\bar{y}) \frac{\Gamma\left(\frac{2b_{C,a}+b_{v,a}+\nu_a+1}{\mu_a}\right)}{\Gamma\left(\frac{\nu_a+1}{\mu_a}\right)} \frac{\Gamma\left(\frac{2b_{C,b}+b_{v,a}+k+\nu_a+1}{\mu_a}\right)}{\Gamma\left(\frac{\nu_a+1}{\mu_a}\right)}$$

$$\times \left[\frac{\Gamma\left(\frac{\nu_a+1}{\mu_a}\right)}{\Gamma\left(\frac{\nu_a+2}{\mu_a}\right)}\right]^{2b_{C,a}+b_{v,a}} \left[\frac{\Gamma\left(\frac{\nu_b+1}{\mu_b}\right)}{\Gamma\left(\frac{\nu_b+2}{\mu_b}\right)}\right]^{2b_{C,a}+b_{v,b}+k}$$

$$+ v_{t,b}^2(\bar{y}) \frac{\Gamma\left(\frac{2b_{C,a}+\nu_a+1}{\mu_a}\right)}{\Gamma\left(\frac{\nu_a+1}{\mu_a}\right)} \frac{\Gamma\left(\frac{2b_{C,b}+2b_{v,a}+k+\nu_a+1}{\mu_a}\right)}{\Gamma\left(\frac{\nu_a+1}{\mu_a}\right)} \left[\frac{\Gamma\left(\frac{\nu_a+1}{\mu_a}\right)}{\Gamma\left(\frac{\nu_a+2}{\mu_a}\right)}\right]^{2b_{C,a}}$$

$$\times \left[\frac{\Gamma\left(\frac{\nu_b+1}{\mu_b}\right)}{\Gamma\left(\frac{\nu_b+2}{\mu_b}\right)}\right]^{2b_{C,a}+2b_{v,b}+k} \tag{B.123}$$

Finally, the characteristic velocity differences are derived by substituting eqs.B.122 and B.123 into B.120:

$$\Delta \bar{v}^k_{t,ab} = \left[\theta^0_a v^2_{t,a}(\bar{x}) - \theta^k_{ab} v_{t,a}(\bar{x}) v_{t,b}(\bar{y}) + \theta^k_b v^2_{t,b}\right]^{1/2} \tag{B.124}$$

$$\theta^k_a = \frac{\Gamma\left(\frac{2b_{C,a}+2b_{v,a}+k+v_a+1}{\mu_a}\right)}{\Gamma\left(\frac{2b_{C,a}+k+v_a+1}{\mu_a}\right)} \left[\frac{\Gamma\left(\frac{v_a+1}{\mu_a}\right)}{\Gamma\left(\frac{v_b+2}{\mu_b}\right)}\right] \{2b_{v,a+k} \tag{B.125}$$

$$\theta^k_{ab} = 2\frac{\Gamma\left(\frac{2b_{C,a}+b_{v,a}+v_a+1}{\mu_a}\right)}{\Gamma\left(\frac{2b_{C,a}+v_a+1}{\mu_a}\right)} \frac{\Gamma\left(\frac{2b_{C,b}+b_{v,b}+k+v_b+1}{\mu_b}\right)}{\Gamma\left(\frac{2b_{C,b}+k+v_b+1}{\mu_b}\right)}$$

$$\times \left[\frac{\Gamma\left(\frac{v_a+1}{\mu_a}\right)}{\Gamma\left(\frac{v_a+2}{\mu_a}\right)}\right]^{b_{v,a}} \left[\frac{\Gamma\left(\frac{v_b+1}{\mu_b}\right)}{\Gamma\left(\frac{v_b+2}{\mu_b}\right)}\right]^{b_{v,b}} \tag{B.126}$$

Here, it can be noted that the notation " ab " in θ^k_{ab} is not symmetrical because θ^k_{ab} is weighted by the mass of collected particle to the power of " k ". Integrations in eqs.B.115 and B.117 are similarly calculated as follows:

$$\int_0^\infty \int_0^\infty f_a(x) f_b(y) D_a(x) + D_b(y)^2 y^k dx$$

$$= a^2_{C_a} M^{2b_{C,a}}_a M^k_b + 2a_{C_a} a_{C_b} M^{b_{C,a}}_a M^{b_{C,b}+k}_b + a^2_{C_b} M^0_a M^{2b_{C,b}+k}_b$$

$$= \delta^0_a D^2_{C,a}(\bar{x}) N_a M^k_b + \delta^k_{ab} D_{C,a}(\bar{x}) D_{C,b}(\bar{y}) N_a N_b \bar{y}^k$$

$$+ \delta^k_b D^2_{C,b}(\bar{y}) N_a N_b \bar{y}^k \tag{B.127}$$

$$\delta^k_a = \frac{\Gamma\left(\frac{2b_{C,b}+k+v_a+1}{\mu_a}\right)}{\Gamma\left(\frac{\mu_a+1}{\mu_a}\right)} \left[\frac{\Gamma\left(\frac{v_a+1}{\mu_a}\right)}{\Gamma\left(\frac{v_a+2}{\mu_a}\right)}\right]^{2b_{C,a}+k} \tag{B.128}$$

$$\delta^k_{ab} = 2\frac{\Gamma\left(\frac{b_{C,a}+v_a+1}{\mu_a}\right)}{\Gamma\left(\frac{v_a+1}{\mu_a}\right)} \frac{\Gamma\left(\frac{b_{C,b}+k+v_b+1}{\mu_b}\right)}{\Gamma\left(\frac{v_b+1}{\mu_b}\right)} \left[\frac{\Gamma\left(\frac{v_a+1}{\mu_a}\right)}{\Gamma\left(\frac{v_a+2}{\mu_a}\right)}\right]^{b_{C,a}} \left[\frac{\Gamma\left(\frac{v_b+1}{\mu_b}\right)}{\Gamma\left(\frac{v_b+2}{\mu_b}\right)}\right]^{b_{C,b}+k} \tag{B.129}$$

Here, δ^k_{ab} is also asymmetrical in " ab " as θ^k_{ab}. Finally, the growth rates of the prognostic moments are represented as follows:

$$\frac{\partial L_a}{\partial}\bigg|_{col,ab} = \frac{\pi}{4} \bar{E}_{ab} N_a L_b \delta^0_a D^2_{C,a}(\bar{x}_a) + \delta^1_{ab} D_{C,a}(\bar{x}_a) D_{C,b}(\bar{x}_b) + \delta^1_b D^2_{C,b}(\bar{x}_b)$$

$$\times \left[\theta^0_a v^2_{t,a}(\bar{x}_a) - \theta^1_{ab} v_{t,a}(\bar{x}_a) v_{t,b}(\bar{x}_b) + \theta^1_b v^2_{t,b}(\bar{x}_b) + \sigma_a + \sigma_b\right]^{1/2} \tag{B.130}$$

$$\frac{\partial L_b}{\partial t}\bigg|_{col,ab} = -\frac{\partial L_a}{\partial t}\bigg|_{col,ab} \tag{B.131}$$

$$\frac{\partial N_b}{\partial}\bigg|_{col,ab} = \frac{\pi}{4} \bar{E}_{ab} N_a N_b \delta^0_a D^2_{C,a}(\bar{x}_a) + \delta^0_{ab} D_{C,a}(\bar{x}_a) D_{C,b}(\bar{x}_b) + \delta^0_b D^2_{C,b}(\bar{x}_b)$$

$$\times \left[\theta^0_a v^2_{t,a}(\bar{x}_a) - \theta^0_{ab} v_{t,a}(\bar{x}_a) v_{t,b}(\bar{x}_b) + \theta^0_b v^2_{t,b}(\bar{x}_b) + \sigma_a + \sigma_b\right]^{1/2} \tag{B.132}$$

$$\frac{\partial N_b}{\partial t}\bigg|_{col,ab} = 0 \tag{B.133}$$

where σ_a and σ_b are constant variances due to the probabilities of the terminal velocity of particles. Seifert and Beheng (2006a) proposed the concept to mimic an introduction of the effect of turbulence on the collection kernel with the use of constant variances. The constant variances are only applied to ice and snow with $\sigma_i = \sigma_s = 0.2 ms^{-1}$; no variances are assumed for other particles.

Collection efficiencies of ice particles

The collection efficiencies of ice particles are poorly understood due to their varieties and to the lack of systematic observations. In addition, efficiencies cannot be approximated by power laws. Seifert and Beheng (2006a) therefore described them in a simple way. The collection efficiency E_{ab} can be decomposed into two components of efficiency: the collision efficiency E_{col} and the sticking efficiency E_{stick}. This means that two particles stochastically collide with each other with E_{col}, and then stick to each other with E_{stick}. It is considered that the mean possibility of collection $\bar{E}_{ab}$ is parameterized by multiplying $\bar{E}_{col}$ by $\bar{E}_{stick}$:

$$\bar{E}_{ab} = \bar{E}_{col,ab} \times \bar{E}_{stick,ab} \tag{B.134}$$

The mean collision efficiencies of each hydrometeor are given as follows:

$$\bar{E}_{col,ab} = \bar{E}_{col,a} \times \bar{E}_{colk,b} \tag{B.135}$$

$$\bar{E}_{col,c} = \begin{cases} 0, & (\bar{D}_c < \bar{D}_{c,0}) \\ \frac{\bar{D}_c - \bar{D}_{c,0}}{\bar{D}_{c,1} - \bar{D}_{c,0}}, & (\bar{D}_{c,0} \leq \bar{D}_c \leq \bar{D}_{c,1}) \\ 1, & (\bar{D}_{c,1} < \bar{D}_c) \end{cases} \tag{B.136}$$

$$\bar{E}_{col,r} = 1 \tag{B.137}$$

$$\bar{E}_{col,js} = \begin{cases} 0, & (\bar{D}_{js} < 150nm) \\ \bar{E}_{col,max,js}, & (\bar{D}_{js} > 150nm), \quad (js = i, s, g) \end{cases} \tag{B.138}$$

with $\bar{D}_{c,0} = 15\mu m$, $\bar{D}_{c,1} = 40\mu m$, $\bar{E}_{col,max,i} = \bar{E}_{col,max,s} = 0.8$, and $\bar{E}_{col,max,g} = 1.0$. Furthermore, the mean collision efficiency of one is assumed in the collision between rain droplets and ice particles, and between ice particles. These values are so empirical that further investigations and assessments are required.

Sticking efficiency is considered only in the case of the collision between ice particles. Otherwise, efficiency is assumed to be one. It is known that sticking efficiency depends on environmental conditions and on the shape of ice particles (Pruppacher and Klett, 1997). Ice crystals with many branches are likely to stick each other. In wet conditions, ice particles are also likely to coalescence because of their surface condition. Since these dependencies of sticking efficiency are poorly understood, some simple formulations have been proposed by past researchers. Lin et al. (1983) proposed the following:

$$\bar{E}_{stick}(T) = \begin{cases} exp[0.09 \times T_c], & (T_c \leq 0^oC) \\ 1, & (T_c > 0^oC) \end{cases} \tag{B.139}$$

In contrast, Cotton et al. (1986), proposed an alternative formulation based on observations (Hallgren and Hosler, 1960), as follows:

$$\bar{E}_{stick}(T_p) = min(10^{0.035(T_p - 273.15) - 0.7}, 0.2) \tag{B.140}$$

where T_p is particle surface temperature. They also diagnosed the departure of particle surface temperature from the environment due to phase changes in the calculation. In addition, their formulation has an upper limit to reduce efficiency, based on observations. Similarly, Khain and Sednev (1996) proposed a formulation based on other observations (Hosler et al., 1957; Rogers et al., 1974). Their formulation also depends on vapor pressure, as follows:

$$\bar{E}_{stick} = min\left(\delta E \frac{p_v}{p_{si}}, 1\right) \tag{B.141}$$

$$\delta E = max(a_\delta + b_\delta T_c + c_\delta T_c^2 + d_\delta T_c^3, 0) \tag{B.142}$$

with $a_\delta = 0.883$, $b_\delta = 0.093$, $c_\delta = 0.00348$, and $d_\delta = 4.5185 \times 10^{-5}$. In this study, the formulation proposed by Lin et al. (1983) is applied following Seifert and Beheng (2006a). These efficiencies are shown in Fig.B.10, with various observational data from Pruppacher and Klett (1997). Further investigations and assessments are necessary to determine which is better, although there is limited information.

Collision case 2: a+b → c

The case is the same as case 1, except for growing particles.

$$\frac{\partial f_b(y)}{\partial t}\bigg|_{col,abs} = -\int_0^\infty f_b(y)f_a(x)K_{ab}(x,y)dx \tag{B.143}$$

$$\frac{\partial f_a(x)}{\partial t}\bigg|_{col,abs} = -\int_0^\infty f_a(x)f_b(y)K_{ab}(x,y)dy \tag{B.144}$$

The growth rates of prognostic moments are derived as follows:

$$\left.\frac{\partial L_a}{\partial t}\right|_{col,ab} = -\frac{\pi}{4}\bar{E}_{ab}\Delta \overline{v}^1_{t,ab}$$
$$\times \int_0^\infty \int_0^\infty f_a(x)f_b(y)[D_a(x)+D_b(y)]^2 x\,dx\,dy \tag{B.145}$$

$$\left.\frac{\partial L_b}{\partial t}\right|_{col,ab} = -\frac{\pi}{4}\bar{E}_{ab}\Delta \overline{v}^1_{t,ab}$$
$$\times \int_0^\infty \int_0^\infty f_a(x)f_b(y)[D_a(x)+D_b(y)]^2 y\,dx\,dy \tag{B.146}$$

$$\left.\frac{\partial N_a}{\partial t}\right|_{col,ab} = \left.\frac{\partial N_b}{\partial t}\right|_{col,ab} = -\frac{\pi}{4}\bar{E}_{ab}\Delta \overline{v}^0_{t,ab}$$
$$\times \int_0^\infty \int_0^\infty f_a(x)f_b(y)[D_a(x)+D_b(y)]^2 dx\,dy \tag{B.147}$$

$$\left.\frac{\partial N_c}{\partial t}\right|_{col,ab} = -\left.\frac{\partial N_a}{\partial t}\right|_{col,ab} \tag{B.148}$$

Finally, the equations are transformed by using approximations, as follows:

$$\left.\frac{\partial L_b}{\partial t}\right|_{col,ab} = -\frac{\pi}{4}\bar{E}_{ab}N_a L_b$$
$$\times [\delta_a^0 D^2_{C,a}(\bar{x}_a)+\delta_{ab}^1 D_{C,a}(\bar{x}_a)D_{C,b}(\bar{x}_b)+\delta_b^1 D^2_{C,b}(\bar{x}_b)] \tag{B.149}$$
$$\times [\theta_a^0 v^2_{t,a}(\bar{x}_a)-\theta_{ab}^1 v_{t,a}(\bar{x}_a)v_{t,b}(\bar{x}_b)+\theta_b^1 v^2_{t,b}(\bar{x}_b)+\sigma_a+\sigma_b]^{1/2}$$

$$\left.\frac{\partial L_a}{\partial t}\right|_{col,ab} = -\frac{\pi}{4}\bar{E}_{ab}N_b L_a$$
$$\times [\delta_b^0 D^2_{C,b}(\bar{x}_b)+\delta_{ab}^1 D_{C,a}(\bar{x}_a)D_{C,b}(\bar{x}_b)+\delta_a^1 D^2_{C,a}(\bar{x}_b)] \tag{B.150}$$
$$\times [\theta_b^0 v^2_{t,b}(\bar{x}_b)-\theta_{ba}^1 v_{t,a}(\bar{x}_a)v_{t,b}(\bar{x}_b)+\theta_a^1 v^2_{t,a}(\bar{x}_b)+\sigma_a+\sigma_b]^{1/2}$$

$$\left.\frac{\partial N_b}{\partial t}\right|_{col,ab} = -\frac{\pi}{4}\bar{E}_{ab}N_a N_b$$
$$\times [\delta_a^0 D^2_{C,a}(\bar{x}_a)+\delta_{ab}^0 D_{C,a}(\bar{x}_a)D_{C,b}(\bar{x}_b)+\delta_b^0 D^2_{C,a}(\bar{x}_b)] \tag{B.151}$$
$$\times [\theta_a^0 v^2_{t,a}(\bar{x}_a)-\theta_{ab}^0 v_{t,a}(\bar{x}_a)v_{t,b}(\bar{x}_b)+\theta_b^0 v^2_{t,a}(\bar{x}_b)+\sigma_a+\sigma_b]^{1/2}$$

$$\left.\frac{\partial N_a}{\partial t}\right|_{col,ab} = -\frac{\pi}{4}\bar{E}_{ab}N_a N_b$$
$$\times [\delta_a^0 D^2_{C,a}(\bar{x}_a)+\delta_{ab}^0 D_{C,b}(\bar{x}_a)D_{C,b}(\bar{x}_b)+\delta_b^0 D^2_{C,b}(\bar{x}_b)] \tag{B.152}$$
$$\times [\theta_a^0 v^2_{t,a}(\bar{x}_a)-\theta_{ba}^0 v_{t,b}(\bar{x}_a)v_{t,b}(\bar{x}_b)+\theta_b^0 v^2_{t,b}(\bar{x}_b)+\sigma_a+\sigma_b]^{1/2}$$

Collision case 3: a+a → b

In this case, binary collisions between particles in the same hydrometeor are considered. All pairs in the collision turn into the other hydrometeor, as follows:

$$\left.\frac{\partial f_a(x)}{\partial t}\right|_{col,aa} = -\int_0^\infty f_a(x)f_a(y)K_{aa}(x,y)dy \tag{B.153}$$

The growth rate of prognostic moments is as follows:

$$\left. \frac{\partial L_a}{\partial t} \right|_{col,aa} = -\frac{\pi}{4} \bar{E}_{aa} N_a L_a$$
$$\times \quad \delta_a^0 D_{C,a}^2(\bar{x}_a) + \delta_{aa}^1 D_{C,a}^2(\bar{x}_a)$$
$$\times \quad \theta_a^0 v_{t,a}^2(\bar{x}_a) - \theta_{aa}^1 v_{t,a}^2(\bar{x}_a) + 2\sigma_a \qquad (B.154)$$

$$\left. \frac{\partial N_a}{\partial t} \right|_{col,aa} = -\frac{\pi}{4} \bar{E}_{aa} N_a N_a$$
$$\times \quad 2\delta_a^0 D_{C,a}^2(\bar{x}_a) + \delta_{aa}^0 D_{C,a}^2(\bar{x}_a)$$
$$\times \quad 2\theta_a^0 v_{t,a}^2(\bar{x}_a) - \theta_{aa}^0 v_{t,a}^2(\bar{x}_a) + 2\sigma_a \qquad (B.155)$$

$$\left. \frac{\partial L_b}{\partial t} \right|_{col,aa} = -\left. \frac{\partial L_a}{\partial t} \right|_{col,aa} \qquad (B.156)$$

$$\left. \frac{\partial N_b}{\partial t} \right|_{col,aa} = -\frac{1}{2} \left. \frac{\partial N_a}{\partial t} \right|_{col,aa} \qquad (B.157)$$

Collision case 4: a+a → a

In the case, self-aggregational growth is considered. In the aggregation, the number concentration of the hydrometeor " a " decreases under conservation of mass concentration. The basic equation is the same as for case 3, except for the absence of the other hydrometeor:

$$\frac{\partial N_a}{\partial t} = -\frac{1}{2} \frac{\pi}{4} \bar{E}_{aa} N_a N_a$$
$$\times \quad 2\delta_a^0 D_{C,a}^2(\bar{x}_a) + \delta_{aa}^0 D_{C,a}^2(\bar{x}_a)$$
$$\times \quad 2\theta_a^0 v_{t,a}^2(\bar{x}_a) + \theta_{aa}^0 v_{t,a}^2(\bar{x}_a) + 2\sigma_a^{1/2} \qquad (B.158)$$

B.2.3 Secondary processes

There are several secondary processes associated with mixed phase collection. Here, we briefly describe these, following Seifert and Beheng (2006a).

Enhanced melting

We assume that particle temperature is the same as environmental temperature. However, the melting process allows the existence of ice particles under warmer conditions than the melting point. Under these conditions, in the riming process, coalescence of a liquid droplet uniformizes the temperature of two colliding particles. Subsequently, the temperature difference between an ice particle and a liquid droplet are compensated for by latent heat release of the ice particle. In our model framework, since the category of wet ice particles is not considered, the melting part of a riming particle is accounted for as the production of a liquid droplet. The melting rate by the riming process is formulated following Rutledge and Hobbs (1984):

$$\left. \frac{\partial L_{js}}{\partial t} \right|_{eml} = -\frac{c_1 T_c}{L_{f0}} \left. \frac{\partial L_{js}}{\partial t} \right|_{col} \quad (T_c > 0^oC), \ (js = i,s,g) \qquad (B.159)$$

Here, the reduction rate of number concentration is treated similarly to the melting process:

$$\left. \frac{\partial N_{js}}{\partial t} \right|_{eml} = \frac{1}{\bar{x}_{js}} \left. \frac{\partial L_{js}}{\partial t} \right|_{col} \qquad (B.160)$$

Partial conversion

According to Seifert and Beheng (2006a), a riming particle becomes a densely rimed spherical particle as soon as the collected liquid droplet fills up the envelop of the collecting ice particle. The produced densely rimed spherical particle is categorized as graupel. Here, we consider that the volume difference between an ice crystal or a spongy ice particle and its enveloping sphere is filled by the collected liquid droplet. The critical liquid droplet mass $\bar{x}_{crit,pcon}$ is estimated by the geometry of ice, as follows:

$$\bar{x}_{crit,pcon,js} = \alpha_{fill,js}\rho_w\Big(\frac{\pi}{6}\bar{D}_{js}^3 - \frac{\bar{x}_{js}}{\rho_\varepsilon}\Big), \quad (js = i, s) \tag{B.161}$$

where α_{fill} is the so-called filling coefficient, and $\rho_\varepsilon = 900 kg m^{-3}$ is density of ice. The filling coefficient is the criterion used to categorize an ice particle as graupel based on density. Tentatively, $\alpha_{fill}, i = 0.68$ and $\alpha_{fill}, s = 0.01$ are set by Seifert and Beheng (2006a). This means that snow is categorized as almost unrimed ice particles. The characteristic conversion time scale   pcon is estimated by the growth rate of mean particle mass by the riming process, as follows:

$$\tau_{pcon,js} = \frac{\bar{x}_{crit,pcon,js}}{\frac{1}{N_{js}}\frac{\partial L_{js}}{\partial t}\Big|_{rime}} \tag{B.162}$$

Finally, the conversion rates of riming particles into graupel are derived by using the characteristic time scale:

$$\frac{\partial L_g}{\partial t}\Big|_{pcon} = \frac{L_{js}}{\tau_{pcon,js}} = min\Big(\frac{\bar{x}_{js}}{\bar{x}_{crit,pcon,js}}, 1\Big)\frac{\partial L_{js}}{\partial t}\Big|_{rime} \tag{B.163}$$

$$\frac{\bar{x}_{js}}{\bar{x}_{crit,pcon,js}} = \Big[\alpha_{fill,js}\frac{\rho_w}{\rho_\varepsilon}\Big(\frac{\pi}{6}D_i^3\rho_i\frac{1}{\bar{x}_{js}} - 1\Big)\Big]^{-1} \tag{B.164}$$

The conversion rate of number concentration is as follows:

$$\frac{\partial N_g}{\partial t}\Big|_{pcon} = \frac{1}{\bar{x}_{js}}\frac{\partial L_g}{\partial t}\Big|_{pcon} \tag{B.165}$$

The conversion coefficient of riming particle $\bar{x}/\bar{x}_{crit,pconv}$ is shown in Fig.B.11. In this formulation, small ice particles are likely to convert into graupel in riming because small ice particles have simple geometry and are almost spherical. In order to suppress the conversion of small ice particles, partial conversions are limited to ice particles with mean diameter $> 500\mu m$.

Ice multiplication

It has been observed that the number concentration of ice particles can be up to several orders of magnitude larger than ice nuclei in atmospheric clouds (Pruppacher and Klett, 1997). Among the possible mechanisms to explain this, the Hallet-Mossop mechanism has been widely discussed and applied in cloud microphysics schemes. The Hallet-Mossop mechanism is based on the fact that ice splintering occurs when many liquid droplets are collected by graupel. Cotton et al. (1986) applied the formulations based on observations by Hallet and Mossop (1974) and Mossop (1976). Hallet and Mossop (1974) reported that approximately 350 ice splinters were produced for every $10^{-3}g$ of rime accreted by graupel at -5 °C. The parameterization is formulated with the temperature correction f1 in units of mks, as follows:

$$\frac{\partial N_i}{\partial t}\Big|_{spl1,js} = 350 \times 10^6 \times f_1(T) \times \frac{\partial L_{js}}{\partial t}\Big|_{rime,js}, \quad (js = i, s, g) \tag{B.166}$$

$$f_1(T) = \begin{cases} 0, & (T >< 270.16K) \\ \frac{T-268.16}{3}, & (270.16K \geq T \geq 268.16K) \\ \frac{T-268.16}{3}, & (268.16K > T \geq 265.16K) \\ 0, & (265.16K > T) \end{cases} \tag{B.167}$$

The splintering mass concentration is assumed as follows:

$$\frac{\partial L_i}{\partial t}\Big|_{spl1} = \bar{x}_i\frac{\partial N_i}{\partial t}\Big|_{spl1} \tag{B.168}$$

On the other hand, Mossop (1976) reported that approximately one ice crystal was produced per 250 drops $> 12\mu m$ radius accreted onto a graupel at -5 °C. Since it is difficult to calculate the number concentration of riming cloud droplets $> 12\mu m$ ($N_{rime,c}$), here we assume a simple relationship following Cotton et al. (1986), as follows:

$$\frac{N_{rime,c}}{N_{rime,c}} \approx \frac{N_c}{N_c} = Q\left(\frac{\nu_c + 1}{\mu_c}, x_{12}\right) \tag{B.169}$$

where Q is the complement of the incomplete gamma function and x_{12} is droplet mass with radius of $12\mu m$. With the above relation, the parameterization is formulated with the same temperature correction function in units of mks, as follows:

$$\frac{\partial N_i}{\partial t}\bigg|_{spl2,js} = \frac{1}{250} \times f_1 \times Q \times \left(\frac{N_c}{L_c} \frac{\partial L_{js}}{\partial t}\bigg|_{rime,js}\right), \ \ (js = i, s, g) \tag{B.170}$$

In contrast to Cotton et al. (1986), we evaluate the incomplete gamma function with an accurate approximation by Press et al. (2007). The splintering rates of mass concentration are assumed as follows:

$$\frac{\partial L_i}{\partial t}\bigg|_{spl2} = \bar{x}_i \frac{\partial N_i}{\partial t}\bigg|_{spl2} \tag{B.171}$$

Here, it should be noted that we may double-count the ice multiplication process due to the Hallet-Mossop mechanism by using two formulations. Those two formulations may be two independent processes or interpretations of the same process under two different developmental stages. Since the process is poorly understood because of lack of observation, assessment of the process based on sensitivity studies will be necessary in future.
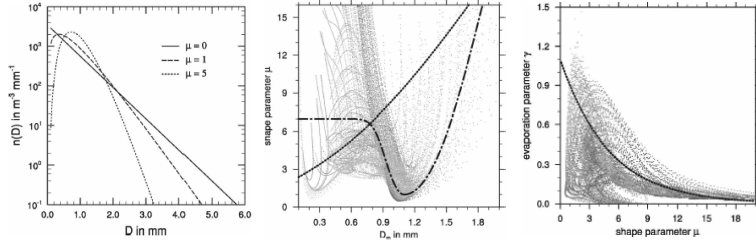

Figure B.5: Left figure shows the modified Gamma distribution for various shape parameters μ m. Center figure shows the scatter plot of shape parameter and mean volume diameter for various initial conditions. Gray dots are from the cloud model, dotted line is parameterization of Milbrandt and Yau (2005), and dashed-dotted line is that of Seifert (2008). Right figure shows the scatter plot of evaporation and shape parameters. These are from Seifert (2008).

B.2.4 The k-th moment of generalized Gamma distribution

The kth moment of the DSD frequently appears in cloud microphysics equations. In this section, we describe derivation of the kth moment of the generalized Gamma distribution. The generalized Gamma distribution is defined as $f(x) = \alpha x \nu exp(-\lambda x \mu)$. There are four parameters in this generalized Gamma distribution but only two prognostic moments in a CRM - the number concentration N and mass concentration L. Hence, μ and ν are set constant parameters so that the other coefficients α and λ can be related to N and L, as follows:

$$
\begin{aligned}
M^0 = N &= \alpha \int_0^\infty x^\nu exp(\lambda x^\mu) dx \\
&= \frac{\alpha}{\lambda^{(\nu+1)/\mu}\mu} \int_0^\infty y^{(\nu+1)/\mu - 1} exp(-y) dy, \ (y \equiv \lambda x^\mu) \\
&= \frac{\alpha}{\lambda^{(\nu+2)/\mu}\mu} \Gamma\left(\frac{\nu+1}{\mu}\right) \\
M^1 = L &= \frac{\alpha}{\lambda^{(\nu+2)/\mu}\mu} \Gamma\left(\frac{\nu+1}{\mu}\right)
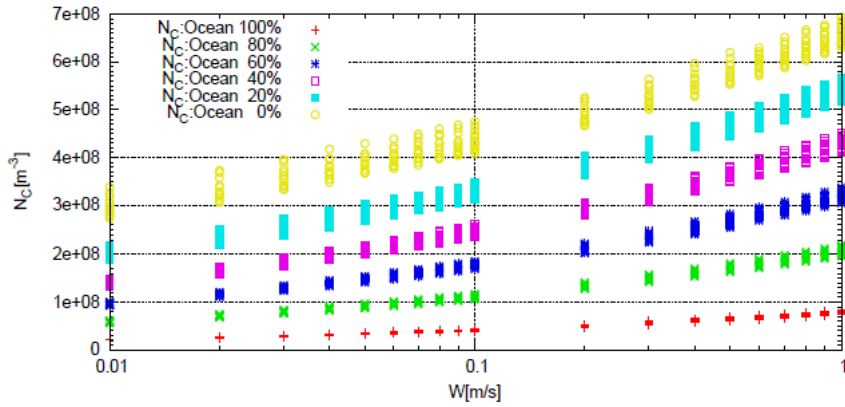\end{aligned}
\tag{B.172}
$$

Figure B.6: Dependency of maximum number concentration on updraft velocity in ascending air parcel. These are based on a Twomey equation with various CCN conditions. Aerosol activation spectrum refers to eq.B.74.
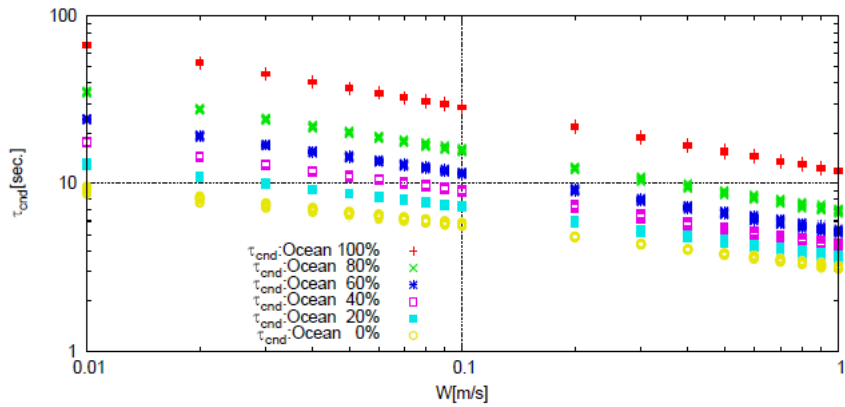

Figure B.7: Timescale of condensation for cloud droplets at maximum number concentration in ascending air parcel. Experimental design is the same as Fig.B.6.
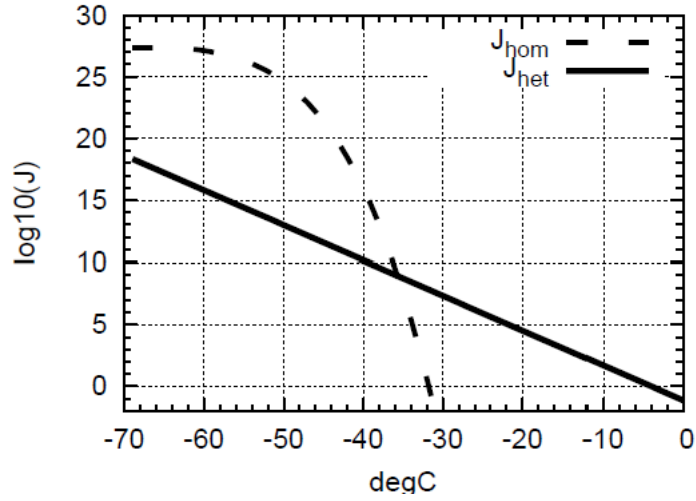
Figure B.8: Dependencies of homogeneous freezing rate (dashed line) and heterogeneous freezing rate (solid line) on centigrade temperature. Freezing rates are in common logarithmic scale.
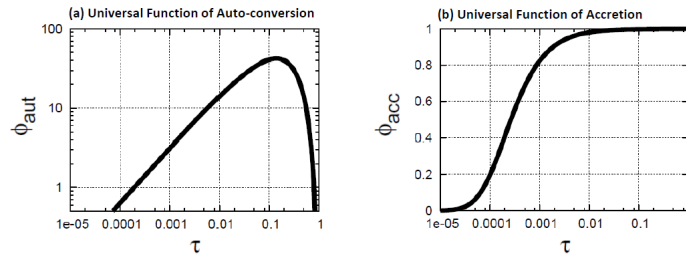

Figure B.9: The universal functions of (a) auto-conversion and (b) accretion as a function of the dimensionless internal time scale.
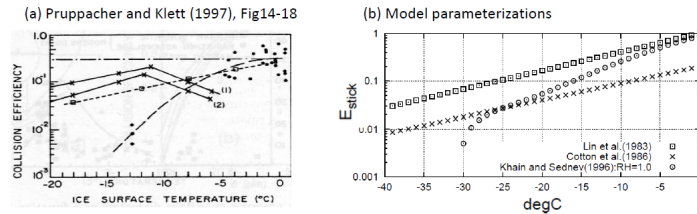

Figure B.10: Dependency of sticking efficiencies on centigrade temperature. Sticking efficiencies based on (a) various observations from Pruppacher and Klett (1997) and (b) model parameterizations.
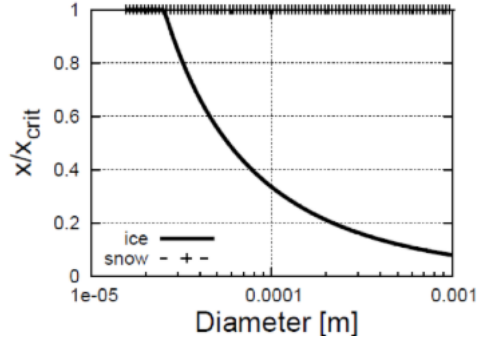
Figure B.11: Coefficients of partial conversion. Solid line shows the coefficient of ice and the line with symbol shows the coefficient of snow.

α is then expressed as:

$$\alpha = \frac{N\mu\lambda^{(\nu+1)/\mu}}{\Gamma\left(\frac{\nu+1}{\mu}\right)} = \frac{L\mu\lambda^{(\nu+2)/\mu}}{\Gamma\left(\frac{\nu+2}{\mu}\right)}$$

and we can derive λ and α:

$$\lambda = \left[\frac{\Gamma\left(\frac{\nu+1}{\mu}\right)}{\Gamma\left(\frac{\nu+2}{\mu}\right)}\right]^{-\mu}\bar{x}^{-\mu} \quad and \quad \alpha = \frac{\nu N}{\Gamma\left(\frac{\nu+1}{\mu}\right)}\lambda^{(\nu+1)/\mu} \tag{B.173}$$

where $\bar{x} = L/N$ defines the mean particle mass. We can rewrite the generalized Gamma distribution by using N and L, in the following form:

$$f(x) = \frac{N}{\bar{x}}\left(\frac{x}{\bar{x}}\right)^{\nu}\frac{\mu}{\Gamma\left(\frac{nu+1}{\mu}\right)}\left[\frac{\Gamma\left(\frac{\nu+2}{\mu}\right)}{\Gamma\left(\frac{\nu+1}{\mu}\right)}\right]^{\nu+1}\exp\left[-\left[\frac{\Gamma((\nu+2)/\mu)}{\Gamma((\nu+1)/\mu)}\frac{x}{\bar{x}}\right]^{\mu}\right] \tag{B.174}$$

The kth moment of DSD is now given by the expansion of eq.B.172 and by using eq.B.173:

$$M^k = \frac{\Gamma\left(\frac{k+\nu+1}{\mu}\right)}{\Gamma\left(\frac{\nu+1}{\mu}\right)}\left[\frac{\Gamma\left(\frac{\nu+1}{\mu}\right)}{\Gamma\left(\frac{\nu+2}{\mu}\right)}\right]^k N\bar{x}^k, \quad (k \in R) \tag{B.175}$$

Appendix C

Notation

Notation of symbols is shown in the Table C.1.

Table C.1: Notation of symbols

variables	description	unit
ρ	total density	kg/m^3
q_d	mass concentration of dry air	kg/kg
q_v	mass concentration of water vapor	kg/kg
q_l	mass concentration of liquid water	kg/kg
q_s	mass concentration of solid water	kg/kg
t	time	s
$\mathbf{u}$	velocity of air flow	m/s
w_l	relative velocity of liquid water to the gas	m/s
w_s	relative velocity of solid water to the gas	m/s
DIFF $[x]$	Diffusion term by turbulene	kg/m^3/s
S_v	source term of water vapor	kg/m^3/s
S_l	source term of liquid water	kg/m^3/s
S_s	source term of solid water	kg/m^3/s
p	pressure	N/m^2
g	gravitational acceraration	9.8 m/s^2
f_l	drag force due to water loading by liquid water	kg /m^2/s^2
f_s	drag force due to water loading by solid water	kg /m^2/s^2
$\mathbf{e_z}$	vertical unit vector (upward)	-
R_d	gas constant for dry air for uint mass	J/kg
R_v	gas constant for water vapor for uint mass	J/kg
T	temperature	K
Q_d	diabatic heating due to physical processes for dry air	J/m^3/s
Q_v	diabatic heating due to physical processes for water vapor	J/m^3/s
Q_l	diabatic heating due to physical processes for liquid water	J/m^3/s
Q_s	diabatic heating due to physical processes for solid water	J/m^3/s
e_d	internal energy for dry air	J/kg
e_v	internal energy for water vapor	J/kg
e_l	internal energy for liquid water	J/kg
e_s	internal energy for solid water	J/kg
e	total internal energy	J/kg
c_{vd}	specific heat at constant volume for dry air	J/kg/K
c_{vv}	specific heat at constant volume for water vapor	J/kg/K
c_{pd}	specific heat at constant pressure for dry air	J/kg/K
c_{pv}	specific heat at constant pressure for water vapor	J/kg/K
c_l	specific heat for liquid water	J/kg/K
c_s	specific heat for solid water	J/kg/K
p_{00}	standard pressure	1000.0 Pa
θ_d	potential temperature for dry air	K
θ	total potential temperature	K

Appendix D

Variables in the source code

The variables used in the model is listed in the Tables D.1 and D.2.

Table D.1: Variables of the dynamics

DENS(k,i,j)	$\rho_{i,j,k}$
MOMZ(k,i,j)	$(\rho w)_{i,j,k+\frac{1}{2}}$
MOMX(k,i,j)	$(\rho u)_{i+\frac{1}{2},j,k}$
MOMY(k,i,j)	$(\rho v)_{i,j+\frac{1}{2},k}$
RHOT(k,i,j)	$(\rho\theta)_{i,j,k}$
QTRC(k,i,j,iq)	$q_{i,j,k}$
PRES(k,i,j)	$p_{i,j,k}$
VELZ(k,i,j)	$\bar{w}_{i,j,k+\frac{1}{2}}$
VELX(k,i,j)	$\bar{u}_{i+\frac{1}{2},j,k}$
VELY(k,i,j)	$\bar{v}_{i,j+\frac{1}{2},k}$
POTT(k,i,j)	$\theta_{i,j,k}$
QDRY(k,i,j)	q_d
Rtot(k,i,j)	R^*
num_diff(k,i,j)	$F_{i+\frac{1}{2}}$
qflx_hi(k,i,j)	$\bar{q}^{high}$
qflx_lo(k,i,j)	$\bar{q}^{low}$
qjpls(k,i,j)	$Q^+_{i,j,k}$
qjmns(k,i,j)	$Q^-_{i,j,k}$
pjpls(k,i,j)	$P^+_{i,j,k}$
pjmns(k,i,j)	$P^-_{i,j,k}$
rjpls(k,i,j)	$R^+_{i,j,k}$
rjmns(k,i,j)	$R^-_{i,j,k}$

Table D.2: Variables of the Smagorinsky scheme.

tke(k,i,j)	TKE
nu(k,i,j), nu_*(k,i,j)	ν_{SGS}
Ri(k,i,j)	Ri
Pr(k,i,j)	Pr
S33_*(k,i,j)	S_{33}
S11_*(k,i,j)	S_{11}
S22_*(k,i,j)	S_{22}
S31_*(k,i,j)	S_{31}
S12_*(k,i,j)	S_{12}
S23_*(k,i,j)	S_{23}
qflx_sgs(k,i,j)	$\bar{\rho}\tau_{ij}$, $\bar{\rho}\tau_{ij}^{*}$